

**A Computational Investigation of Oxaziridine Photoconversion
and *E-Z* Isomerization Processes of Some Acyclic Nitron Systems**

THESIS

Submitted in partial fulfilment
of the requirements for the degree of
DOCTOR OF PHILOSOPHY

by

PRAVEEN SAINI

Under the Supervision of
Dr. Anjan Chattopadhyay



BIRLA INSTITUTE OF TECHNOLOGY AND SCIENCE, PILANI

2016

BIRLA INSTITUTE OF TECHNOLOGY AND SCIENCE, PILANI

CERTIFICATE

This is to certify that the thesis entitled “A Computational Investigation of Oxaziridine Photoconversion and *E-Z* Isomerization Processes of Some Acyclic Nitron Systems”, which is submitted by PRAVEEN SAINI, ID No 2012PHXF012G for award of Ph.D. of the Institute embodies original work done by him under my supervision.

Signature of the Supervisor

Anjan Chattopadhyay

Name in capital letters:

Dr. ANJAN CHATTOPADHYAY

Designation:

Associate Professor,

Department of Chemistry

Date: 13/8/2016

*Dedicated
to
My Parents, Friends and
My Wife*

ACKNOWLEDGEMENTS

First and foremost I would like to express my special gratitude to my PhD advisor *Prof. Anjan Chattopadhyay* for his constant support and valuable guidance throughout my doctoral program. It has been an honor for me to be his first PhD student. He helped me a lot in building by basics of computational chemistry, as I was from different background. He has made himself always available to clarify my doubts despite of his busy schedules. I am thankful for all his contributions in form of time, ideas and guidance to make my PhD experience productive and stimulating. The dedication and passion he has for his research was contagious and motivational for me, even during tough times of my PhD. He had paid attention to my weakness and pushed me hard to bring out the best. His suggestions on both academic as well as on my career have been invaluable.

I extend my sincere thanks to the members of *Doctoral Advisory Committee (DAC)*, Prof. R. N. Behera and Prof. Amrita Chatterjee for their valuable guidance and support at various phases of my research work. I also express my gratitude to the members of *Doctoral Research Committee (DRC)*.

I would like to thanks *Director, BITS, Pilani - K. K. Birla Goa Campus* and *Head of the Chemistry Department*, for providing me all the necessary institute facilities and resources to carry out this research work. I am also thankful to the entire faculty and staff members of *Sponsored Research and Consulting Division and Academic Research Division*, BITS, Pilani- K. K. Birla Goa campus for necessary co-operation in the completion of my research work.

I gratefully acknowledge *Council of Scientific and Industrial Research (CSIR)* New Delhi, India and *BITS Pilani* for providing me financial support as senior research fellowship (SRF) during my PhD programme.

I extend my thanks to my research scholar colleagues and friends *Ajay Ghosh, Angela, Ashu Sharma, Aman Gupta, Arpan Chowdhury, Diprtan Khandare, Meghanath, Omprakash Chauhan, Priyadarshini Parakh, Puneet Khurana, Riddish, Uday K. Padidela, Vikas Gulia, Vikas Kumar, Yogesh and Zigmi Bhutiya* for their support in various ways.

A special thank to my group "The Originals" (*Yogi Bee, Aashu, Maggie, Omi, Angela, Akku and Priya*) to make this journey memorable.

I also thank the *non-teaching staff* of Department of Chemistry, BITS, Pilani-K. K. Birla Goa Campus for their kind help.

I would like again express my sincere thanks to *Prof. Anjan Chattopadhyay, Mrs. Ananya Chattopadhyay* and their son *Aryan* for the affection given by them and always considered me as a family member.

I would like to thank my parents, *Shri Som Datt Saini* and *Smt. Vimal Saini* for all their love and encouragement. My in-laws, *Shri J. P. Saini, Smt. Sadhna Saini, Aditya Saini* and *Apoorva Saini* deserve a special mention for their constant love, support and motivation throughout my PhD.

No words can express my appreciation to my supportive, encouraging, and patient beloved wife *Akanksha*, whose enormous love and continuous moral support kept me focus in my ups and downs.

At the end, thanks to the almighty *God* for his grace and blessings.

PRAVEEN SAINI

ABSTRACT

Computational and theoretical chemistry have reached new heights due to the advancement in the computing methodologies and facilities in the recent years. Nowadays, comprehensive investigations of the mechanisms of unexplored complicated chemical reactions are possible through computational studies which include detection of short-lived transition states in the reaction path, as well. In the last few decades, behavior of the photo-excited organic molecules and their photochemical reaction pathways are thoroughly analyzed by exploring their potential energy surfaces. The radiative and non-radiative decay processes have drawn considerable attention of the computational chemists and their enormous efforts have put forward the explanations of several unanswered questions in photophysics and photochemistry. The huge development in the field of ultrafast non-radiative processes requires a special mention in this regard; they are found to be governed by decay of excited states through radiationless molecular funnels (conical intersections) and their key role in the photochemical reactions of various organic molecules has been widely accepted now. In **Chapter 1** of the present thesis, various important points on the potential energy surfaces and the surface crossing phenomenon have been discussed in detail.

In this thesis work, our targeted molecules for photochemical investigations are different kinds of acyclic nitron systems. *N*-Oxides of imines, commonly known as Nitrones, are well known for their 1,3 dipolar cycloaddition reactions; they are highly photosensitive and on photo-irradiation results in corresponding oxaziridines and other photoproducts, such as amides. The *cis-trans* isomerizations of nitrones were reported to occur thermally or through triplet excited states, in presence of photosensitizers, whereas, their conversion to oxaziridine were found to be a photochemical process and involvement of singlet excited state was suspected in this reaction. These investigations have revealed the fact that the stability of the oxaziridine ring and the nature of its cleavage primarily depend on the types of substituents present on nitrogen and carbon. However, inspite of numerous experimental studies, the photo-conversion mechanism of nitron to oxaziridine had remained an unsolved problem, probably due to the lack of enough information on their excited state characteristics (**Chapter 1**). We have employed rigorous computational studies based on high-level quantum mechanical techniques to explore the exact mechanism for the photo-excitation process of several nitron systems.

In **Chapter 2**, computational investigations on the low-lying singlet states of *N*-alkyl retinyl nitrones and their involvement in oxaziridine formation have been presented. These nitrones are chemopreventive in nature and their oxaziridine photo-conversion process was experimentally reported, long back. The first part of this thesis chapter has focused on the fate of photo-excitation and subsequent non-radiative decay processes of the model compounds of retinyl nitrones at CASSCF/6-31G*, CASMP2/6-31G* and PM3/CI level of theories. A relaxed planar geometry of the first excited singlet state is reached after the initial photo-excitation and it was found to have a mixed ionic-biradical nature. The initial photo-excitation to this state is followed by non-radiative decay processes through conical intersection (S_0/S_1) channels. The lowest-energy intersection point was obtained due to a twist in the terminal part with an out-of-plane CNO-kink ($R_{C-O}=2.12\text{\AA}$, $R_{N-O}=1.38\text{\AA}$) structure. Following its gradient difference (GD) vectors, the oxaziridine geometry ($R_{C-O}=1.38\text{\AA}$, $R_{N-O}=1.44\text{\AA}$, $\angle OCN=62.3^\circ$, $\angle ONC=57.6^\circ$) was obtained. The radiative transition studies of these nitrones at their respective ground state equilibrium geometries have shown allowed $S_0\rightarrow S_1$ transitions with high transition moment values (4.5-5.0 Debye). In the latter section, the 2-layer hybrid ONIOM based QM:QM and QM:MM studies on the 13-*trans* and 13-*cis* isomeric form of the long-chain *N*-methyl retinyl nitrones are discussed. These hybrid studies have revealed the presence of low-lying CNO-kinked conical intersections (65-70 kcal/mol above their ground states) on the nitrone-oxaziridine photo-conversion path, similar to their model compounds. Following the GD vectors of the low-lying conical intersections, optimized oxaziridine structures were obtained at the CASSCF/6-31G*:HF/STO-6G and CASSCF/6-31G*:UFF(with electronic embedding) level, taking the CNO moiety as the high-level part. A transition state ($\Delta E_{\text{activation}}=30\text{ kcal/mol}$) with imaginary frequency of $361i\text{ cm}^{-1}$ was found to be responsible for the thermal *E-Z* isomerization of the 13-*trans* isomer.

In **Chapter 3**, the photo-excitation of the open-chain conjugated nitrone systems having electron-withdrawing groups on nitrogen and their subsequent photoproduct formation through non-radiative deactivation channels have been analyzed. After initial photo-excitation of *N*-trifluoromethyl-substituted conjugated nitrone system (taken as a representative system for the above-mentioned kind of nitrones), a planar singlet excited state geometry was found which is followed by a barrierless non-radiative channel through the lowest-energy conical intersection geometry having a terminal CNO-kink

structure and situated at 30 kcal/mol below the optimized excited state. Following its GD vectors, an oxaziridine-type species ($R_{C-O} = 1.38 \text{ \AA}$, $R_{N-O} = 1.53 \text{ \AA}$, $\angle CNO = 55.8^\circ$) was found on the reaction pathway at 3-6 kcal/mol below the optimized ground state geometry of the parent nitrene. This oxaziridine-type species has an elongated N–O bond and seemed to be heading towards amide geometry. On the other hand, following the opposite direction of the GD vectors, a proper oxaziridine geometry was obtained with a much shorter N–O bond distance ($R_{N-O} = 1.42 \text{ \AA}$). This investigation has justified the possibility reported a few years back by other groups that the unstable oxaziridine-type species obtained from nitrenes having electron withdrawing groups on nitrogen may result in N–O bond cleavage with three electrons on nitrogen and one electron on oxygen, which eventually leads to the product, amide.

In **Chapter 4**, a comprehensive study of the photo-conversion process of α -(2-naphthyl)-*N*-methylnitrene to oxaziridine and its thermal *E-Z* isomerization have been presented. Experimental work related to the photo-irradiation of this fluorescent nitrene was reported almost thirty years back. The involvement of non-radiative decay channels in the nitrene-oxaziridine photochemical conversion was confirmed by both CASSCF and ONIOM-based calculations in our present work. These non-radiative decay channels include biradicaloid conical intersection points, situated at 35-40 kcal/mol below the first excited singlet state. Following the GD vectors, the optimized oxaziridine geometries were obtained. The nature of the low-lying singlet-singlet transitions of these nitrenes was found to be similar to the conjugated non-polar polyenes, and they differ significantly from the long-chain conjugated nitrene systems. At the CASSCF/6-31G* level of calculation the activation energy for the conversion of unstable non-planar *E* isomer to the stable planar *Z*-isomer was found to be 23.7 kcal/mol. A transition state with imaginary frequency of $350i \text{ cm}^{-1}$ was found responsible for this isomerization process.

The computational investigation presented in **Chapter 5** reveals the photochemistry of two small open-chain conjugated *N*-methylnitrene systems with phenyl substitutions at the C-terminal positions. Photo-excitation of α -styryl *N*-methylnitrene populates the first excited singlet state which subsequently follows a reaction path towards the lowest-energy conical intersection geometry (situated 27-30 kcal/mol below) with a terminal CNO-kink. Following the GD vectors of this conical intersection, oxaziridine structure

with its characteristic geometry was obtained at roughly 14 kcal/mol above the ground state. On the other hand, the photo-excitation of the non-planar 3,3-diphenylethylene *N*-methylnitron leads to two strong singlet-singlet absorptions with almost 5 Debye transition moment values. The initially photo-excited S_2 state relaxes to the S_1 state which is further followed by oxaziridine formation through the terminally twisted conical intersection. However, the S_0 - S_1 transition in this nitron is found to follow another route by transfer of huge amount of non-bonding electron cloud of oxygen to the π^* orbital, and thus forming a stable excited state geometry with an elongated N-O bond which gets involved in a sloped conical intersection with the ground state; this can be related to the experimentally observed slow decay of the longer wavelength UV peak of this nitron (Chapter 5).

TABLE OF CONTENTS

	Description	Page No.
Chapter 1: Introduction		1-33
1.1.	Scope of research work	1
1.2.	Introduction to computational photochemistry	1
1.3.	Important points on PES	3
1.3.1.	Stationary points: Minima and Maxima	3
1.3.2.	The Born–Oppenheimer approximation and surface crossings	5
1.4.	Brief background of research based on literature survey	11
1.5.	Gaps in existing research	16
1.6.	Objectives of the research	17
1.7.	Thesis structure	18
1.8	A brief overview of some of the quantum chemical methods used to explore the photochemical reactions in this thesis	20
1.8.1.	Post Hartree-Fock calculations and electron-correlation methods	20
A.	Configuration interaction	21
B.	Multi-Configurational Self Consistent Field (MCSCF)	22
C.	Complete Active Space SCF (CASSCF)	23
D.	Dynamic correlation methods (CASMP2 and CASPT2)	24
1.8.2.	ONIOM	24
1.9.	References	27
Chapter 2: A computational study of the photochemistry of some retinyl nitrones and their model compounds with electron-donating groups on nitrogen		34-69
2.1.	Introduction	34
2.2.	Computational details	36

2.3.	SECTION 1: Model compounds of the <i>N</i> -alkyl retinylnitrone	38
2.3.1.	Results and discussions	39
A)	Important points on the potential energy surface	39
a)	Results of semiempirical-based Configuration Interaction calculations	39
b)	Results of <i>ab initio</i> calculation	41
i)	Optimized ground states and first singlet excited states	41
ii)	Conical intersections at higher energies than planer excited state	42
iii)	Transition states (TS ₁₋₃) at excited state surface	48
iv)	Conical intersections situated at lower energies	50
v)	Optimized oxaziridine geometries	51
B)	Radiative transition properties and vertical excitation energies	51
C)	A complete possible scheme of whole photo-isomerization process	53
2.4.	SECTION 2: <i>N</i> -methyl substituted retinylnitrones	55
2.4.1.	Purpose of studying extended conjugated <i>N</i> -methyl retinylnitrone system using ONIOM methodology	55
2.4.2.	Results and discussions	56
A)	Optimized points on potential energy surface	56
a)	Initial guess from semi-empirical calculations	56
b)	Results of hybrid ONIOM calculations.	56
i)	Optimized ground states geometries	56
ii)	Optimized conical intersection and oxaziridine geometries	59
B)	<i>E-Z</i> isomerization of the 13- <i>trans</i> retinylnitrone system	64
2.5.	Conclusions	66
2.6.	References	67

Chapter 3: A computational investigation of the photochemistry of open-chain conjugated nitrone systems with electron-withdrawing group on nitrogen	70-88	
3.1.	Introduction	70
3.2.	Computational details	72
3.3.	Results and discussions	74
3.3.1.	Important optimized points on potential energy surfaces	74
A)	Ground, vertically excited and optimized excited state geometries	74
B)	Transition states and conical intersections	76
a)	Conical intersection geometries at CAS (4,4) level	77
b)	Conical intersection geometries with larger active spaces	79
C)	Possible photoproducts of system I	80
3.3.2.	A complete possible scheme of the photochemical path of system I	82
3.3.3.	Radiative transition properties	83
3.4.	Possible practical significance of this work	83
3.5.	Conclusions	84
3.6.	References	85
Chapter 4: A computational investigation of the photochemical nitrone-oxaziridine conversion and thermal <i>E-Z</i> isomerization processes of fluorescent α-(2-naphthyl)-<i>N</i>-methylnitrone	89-112	
4.1.	Introduction	89
4.2.	Computational methods	90
4.3.	Results and discussions	93
4.3.1.	Important points on the potential energy surfaces	93
A)	Optimized ground and excited state geometries	93
B)	Optimized conical intersections and oxaziridine geometries	96
C)	Optimized Transition states (TS)	101

	a)	TS geometries on the excited state surface	101
	b)	TS geometries on the ground state surface	102
4.3.2.		<i>E-Z</i> isomerization mechanism of α -(2-naphthyl)- <i>N</i> -methylnitron	104
4.3.3.		Radiative transition studies	105
4.4.		Conclusions	109
4.5.		References	109

Chapter 5: A computational investigation of the photochemical reaction paths of C-terminal aryl substituted small-chain conjugated nitrones 113-130

5.1		Introduction	113
5.2		Computational methods	114
5.3.		Results and discussions	115
	5.3.1.	Photo-irradiation of studied nitron systems	115
	5.3.2.	Important points on the potential energy surface	116
	A)	Ground and excited singlet state	116
	B)	Saddle points and transition states	120
	C)	Optimized conical intersections and oxaziridines	121
5.3.3.		Oxaziridine absorption peaks	126
5.3.4.		Summary of the overall photochemical path	127
5.4.		Conclusions	128
5.5.		References	129

Chapter 6: Conclusions and Future Scope 131-133

List of publications	Appendix I
Bio-data of candidate	Appendix II
Bio-data of supervisor	Appendix III

LIST OF FIGURES

Figure No.	Figures	Page No.
1-1	A schematic representation of a photochemical reaction through conical intersection	3
1-2	A schematic representation of conical intersection with double cone topology	9
1-3	Comparison of (a) transition state (TS) and (b) a conical intersection (CI)	10
1-4	Photoisomerization of a) Bacteriorhodopsin chromophore and b) Rhodopsin chromophore	12
1-5	Different types of conical intersections where a) is sloped type conical intersection, b) and c) are peaked conical intersection	12
1-6	Structure of <i>N</i> -substituted retinyl nitrones	13
1-7	Nitrone to amide conversion via oxaziridine	15
1-8	Excited Slater determinants can be generated by promoting electrons from the $N/2$ occupied to $b-N/2$ virtuals.	21
2-1	Photo-conversion of <i>N</i> -methyl retinyl nitron to oxaziridine and reverse conversion to the parent nitron in dark	35
2-2	Structures of (a) studied model systems of methyl (system I) and isopropyl-substituted (system II) retinyl nitrones, (b) 13- <i>trans</i> and 13- <i>cis</i> isomer of <i>N</i> -methyl retinyl nitron studied at hybrid ONIOM methods	35
2-3	a) Structures of the studied nitrones (13- <i>trans</i> and 13- <i>cis</i>) and b) the different high-level and low-level portions used in the ONIOM calculations. Portions on which high level calculations were carried out are shown in ball-and-stick, and the low level regions are shown in wireframe	38
2-4	Non-planar excited state geometries (B₁ and B₂) of system I and II at the PM3/CI level of calculations	40
2-5	Possible ionic (I-III) and non-ionic (IV-V) canonical forms of nitron systems	41

2-6	Optimized excited state (A) geometries of system I and II at the CASSCF/6-31G* (4,4) ^a and (6,6) ^b level of theories with dominant configurations at the respective geometries.	42
2-7	A possible scheme of nitrene to oxaziridine conversion	43
2-8	Molecular Orbitals involved in the CAS(4,4) active space calculations for the methyl nitrene (system I).	44
2-9	Optimized conical intersection geometries (CI ₁₋₃) for three different types of motions of (a) System I and (b) System II at the CASSCF/6-31G* level with their respective gradient difference and derivative coupling vectors. [$d_{(3-4-5-6)}$ indicates $\angle C3-C4-C5-N$ torsion angle, $d_{(4-5-6-7)}$ indicates $\angle C4-C5-N-C6$ torsion angle]	45
2-10	A schematic representation of the difference in ground and excited singlet state properties of (a) non-polar conjugated hexatriene (b) polar 2,5-pentadien-1-iminium cation and (c) conjugated nitrene systems.	46
2-11	Transition states (a-c) TS ₁₋₃ on the excited state surface with the transition vectors corresponding to their imaginary frequencies and plots of minimum energy path along the intrinsic reaction coordinate from these transition states.	49
2-12	Optimized conical intersections (a) CI ₄ and (b) CI ₅ of system I with their gradient difference and derivative coupling vectors. [$d_{(3-4-5-6)}$ indicates $\angle C3-C4-C5-N$ torsion angle, $d_{(4-5-6-7)}$ indicates $\angle C4-C5-N-C6$ torsion angle]	50
2-13	(a) <i>Trans</i> oxaziridine (Ox ₁) geometry of system I with its HOMO (b) <i>cis</i> oxaziridine (Ox ₂) geometry of system I	51
2-14	A schematic representation of the non-radiative decay processes involving different conical intersections in system I. (Relative energies in kcal/mol with respect to the optimized ground state energy at CASSCF ^a and CASMP2 ^b levels are given in the parentheses)	53
2-15	Planar ground state and non-planar biradical excited state geometries of 13- <i>trans</i> and 13- <i>cis</i> isomers obtained at semi-empirical PM3/CI level	58
2-16	Important molecular orbitals involved in the active space for the	58

	model part of the a) ONIOM (CASSCF (4,4): QM'/MM), b) ONIOM (CASSCF (6,6): RHF) and b) ONIOM (CASSCF (8,8): RHF)	
2-17	Conical intersection (CI) geometries of a) 13- <i>trans</i> isomer and b) 13- <i>cis</i> isomer at ¹ CASSCF(4,4)/6-31G*:HF/STO-6G level and ² CASSCF(4,4)/6-31G*:UFF (with EE) level of ONIOM calculations. Important bond lengths (in angstrom) and dihedral angle (in degrees) are also shown	59
2-18	Gradient difference and derivative coupling vectors of conical intersection geometries of a) 13- <i>trans</i> and b) 13- <i>cis</i> isomer at (I) CASSCF(4,4)/6-31G*:RHF/STO-6G and (II) CASSCF(4,4)/6-31G*:RHF/UFF (with EE) level of ONIOM calculations.	60
2-19	Conical intersection geometry of 13- <i>trans</i> isomer with their gradient difference and derivative coupling vectors at CASSCF(4,4)/6-31G*:RHF/STO-3G. Important bond lengths (in angstrom) and dihedral angle (in degrees) are also shown	60
2-20	Optimized oxaziridine geometries Ox_I and Ox_{II} obtained from a) 13- <i>trans</i> isomer and b) 13- <i>cis</i> isomer of <i>N</i> -methyl retinyl nitron at ¹ CASSCF(4,4)/6-31G*:HF/STO-6G level, ² CASSCF(4,4)/6-31G*:UFF(with EE) level and ³ CASSCF(4,4)/6-31G*:HF/STO-3G of ONIOM calculations. Important bond lengths (in angstrom) and bond angles (in degrees) are also shown	62
2-21	Conical intersection (CI) geometry of 13- <i>trans</i> isomer with their gradient difference (GD) and derivative coupling (DC) vectors at a) CASSCF (6,6)/6-31G*:RHF/STO-6G and b) CASSCF (8,8)/6-31G*:RHF/STO-6G level of of ONIOM calculations.	63
2-22	Schematic representation of <i>E-Z</i> isomerization of 13- <i>trans</i> <i>N</i> -Methyl retinyl nitron	65
2-23	A possible scheme of thermal and photochemical processes occurring in <i>N</i> -Methyl retinyl nitron	65
3-1	Structure of (a) <i>N</i> -substituted retinyl nitron and (b) studied <i>N</i> -trifluoromethyl-substituted (I) and unsubstituted (II) model nitron system.	71

3-2	A possible route of nitron-oxaziridine conversion in conjugated <i>N</i> -alkyl nitrones	73
3-3	Molecular orbitals involved in the CASSCF (4,4) active space calculations	74
3-4	A schematic representation of the possible negative hyper-conjugative effect operating in the excited state (S_1) of the system I	76
3-5	Optimized conical intersection (CI) geometry of system I at the CAS(4,4)/6-31G* level with its gradient difference (GD) and -GD vectors	79
3-6	Optimized conical intersection geometry of system II at the CAS(4,4)/6-31G* level with its corresponding gradient difference (GD) and derivative coupling (DC) vectors	79
3-7	(a) Non-Optimized conical intersection geometry at CASSCF (6,6)/6-31G* level and (b) optimized conical intersection geometry at CASSCF (8,8)/6-31G* level with its GD and DC vectors	80
3-8	(a) Transition state (TS_G) with displacement vectors corresponding to its imaginary frequency (b) Forward and reverse intrinsic reaction coordinate (IRC) path of TS_G	81
3-9	Optimized geometries of Ox₁ and Ox₂ with structural parameters at the CASSCF/6-31G* level of calculation.	81
3-10	A Schematic representation of the non-radiative decay in system I	82
3-11	A summary of the whole photochemical process operating in system I .	83
4-1	The studied <i>Z</i> and <i>E</i> isomers of the α -(2-naphthyl) <i>N</i> -methyl nitron system	90
4-2	Molecular orbitals involved in the active space of CASSCF (4, 4) /6-31G* calculations for the α - (2-naphthyl)- <i>N</i> -methylnitron.	92
4-3	Optimized excited state geometries of <i>E</i> and <i>Z</i> isomers of α -(2-naphthyl)- <i>N</i> -methyl nitron at CASSCF (4,4)/6-31G*, CASSCF (14,12)/ 6-31G* and ONIOM (QM:QM') level of calculations.	94
4-4	i) Ground state ii) Excited state and iii) Biradical excited state geometries of <i>Z</i> and <i>E</i> isomers with important structural parameters	95

	obtained at the PM3/CI level of calculations.	
4-5	Optimized conical intersection geometries (CI₁₋₄) at the CASSCF/6-31G* level. The corresponding gradient difference and derivative coupling vectors are also shown	99
4-6	Optimized geometries of the oxaziridines (Ox₁₋₃) at the CASSCF/6-31G*level. Their corresponding HOMOs are also shown.	101
4-7	Optimized transition states geometries (TS_{ex1-3}) on excited state surface with displacement vectors.	102
4-8	Optimized transition states geometries (TS_{gs1-4}) on ground state surface with their respective displacement vectors.	103
4-9	A) Intrinsic reaction coordinate (IRC) path of TS_{gs5} along forward and reverse directions. B) Schematic representation of <i>E-Z</i> isomerization of α -(2-naphthyl)- <i>N</i> -methylnitron through TS_{gs5}	105
4-10	A Schematic representation of the low-lying singlet-singlet transitions and involvement of some important low-lying conical intersections (<i>S₀/S₁</i>) in α -(2-naphthyl)- <i>N</i> -methylnitron system	107
5-1	Structures of a) nitron A and b) nitron B	113
5-2	Photo-irradiation of a) nitron A and b) nitron B	116
5-3	Optimized saddle point (SP_B) and transition states (TS_A , TS_{B1} and TS_{B2}) with structural parameters	121
5-4	Optimized lowest-energy conical intersection geometries of a) nitron A and b) nitron B with their gradient difference (GD) and derivative coupling (DC) vectors at CASSCF (4,4) level of calculation	123
5-5	Optimized oxaziridine geometries of a) nitron A and b) nitron B with structural parameters at CASSCF (4,4) level of calculation	123
5-6	Conical intersection geometries of nitron A and nitron B at CASSCF (6,6) level of calculations with their gradient difference (GD) and derivative coupling (DC) vectors	124
5-7	Conical intersection geometry (CI_{B2}) with its gradient difference (GD) and derivative coupling (DC) vectors	125
5-8	Comparison of theoretically obtained UV-Visible spectrum with the	126

experimental peaks of **a) OX_A** and **b) OX_B**

- 5-9** Schematic representation of the entire photo-conversion process of **a) nitrone A** and **b) nitrone B**. Energy values are shown in parenthesis (in kcal/ mol) with respect to the optimized ground state geometries of the respective nitrones **127**

LIST OF TABLES

Table No.	Tables	Page No.
2-1	Atomic charges of important atoms determined from the electrostatic potential at PM3/CI level	40
2-2	Structural parameters of the optimized ground state geometries of system I and II at various level of calculations. Reported bond lengths are in angstrom (Å)	42
2-3	Absolute energy values (E) in Hartree and relative energy values (ΔE) in kcal/mol (with respect to the planar excited states) at various important geometries on the potential energy surfaces	44
2-4	Atomic charges determined using Merz-Kollman scheme) at the CASSCF/6-31G* level	48
2-5	Vertical excitation energies (VEE) and radiative transition properties corresponding to the lowest vertical transition ($S_0 \rightarrow S_1$) at the ground state equilibrium geometry. The values in parentheses are the power to base 10.	52
2-6	Structural parameters of optimized ground states of 13- <i>trans</i> and 13- <i>cis</i> isomers at various level of calculations. Bond lengths are in Å and angles are in degrees	57
2-7	Relative energy values (ΔE) in kcal/mol of 13- <i>trans</i> and 13- <i>cis</i> isomers of <i>N</i> -methyl retinyl nitron using method I and method II, without using dynamic correlation ($\Delta E'$) and using dynamic correlation ($\Delta E''$) in the high-level calculations	61
2-8	Structural parameters of optimized oxaziridines of 13- <i>trans</i> and 13- <i>cis</i> isomers. Bond lengths are in Å and angles are in degrees	62
3-1	Structural parameters of optimized ground state (GS) and excited state (ES) geometries at various level of calculations. The bond lengths are in Angstrom (Å)	75
3-2	Absolute (E) and relative (ΔE) energies of ground state (GS), vertically excited state (VEE), and optimized excited state energies(ES) of	76

	system I and II	
3-3	Atomic charges determined from electrostatic potential (using Merz-Kollman scheme) at the CASSCF/6-31G* level of calculation of trifluoromethyl and methyl-substituted model systems of retinyl nitron	77
3-4	Absolute (E) and relative (ΔE) energy values of various important geometries of system I with respect to its relaxed planar excited state (ES)	78
3-5	Radiative transition properties of the studied systems corresponding to the lowest energy ($S_0 \rightarrow S_1$) transitions at their respective ground state equilibrium geometry	83
4-1	Structural parameters of the optimized ground states (GS) of Z and E isomers at various level of calculations. Bond lengths are in Å and angles are in degree	94
4-2	Relative energy values (ΔE) of important excited state geometries of E and Z isomers at different level of calculations; values in parentheses are in nm	96
4-3	Atomic charges of optimized ground state (GS) and excited states (ES) of both the isomers, determined using Merz-Kollman scheme at CASSCF/6-31G*	96
4-4	Structural parameters of some important conical intersections and oxaziridine geometries at CASSCF (I) and 2-layered ONIOM (II) level of calculations	97
4-5	Relative energy (ΔE) values with respect to the relaxed excited state (ES) energy of Z -isomer at various important geometries on the potential energy surfaces	98
4-6	Atomic charges of various important points on potential energy surfaces determined using Merz-Kollman scheme at CASSCF level	100
4-7	Absolute (E) and relative energy values (ΔE) of various transition states geometries with respect to the relaxed excited states (ES). Imaginary frequencies of the corresponding transition states are also reported.	104

4-8	A comparison of radiative transition properties at ground state equilibrium geometries of different systems. The values in parentheses are the powers to base 10.	106
4-9	A comparison of dominant configurations of S_1 and S_2 states at Frank Condon (FC) geometries and at optimized S_1 states of different systems	108
4-10	Important radiative transition properties of the oxaziridine geometries at their respective ground state equilibrium geometries	108
5-1	Structural parameters of optimized ground and excited states of nitrone A and nitrone B at various levels of calculation	117
5-2	Absolute (E ; in hartree) and relative (ΔE ; in kcal/mol) energy values at CASSCF level and with dynamic correlation corrections on the optimized structures of ground and excited states	118
5-3	Radiative transition properties of nitrone A and nitrone B at their optimized ground state geometries using GUGA CI code	119
5-4	Atomic charges determined using Merz-Kollmen scheme at various important geometries on potential energy surface	120
5-5	Absolute and relative energy values at CASSCF (4,4) level and with dynamic correlation corrections on the optimized transition states, conical intersection points and oxaziridine structures	122

LIST OF ABBREVIATIONS

Abbreviation	Description
Å	Angstrom
AM1	Austin Model 1
B3LYP	Becke, three-parameter, Lee-Yang-Parr
BO	Born–Oppenheimer
CASMP2	Complete Active Space Moller-Plesset theory
CASPT2	Complete Active Space Perturbation theory
CASSCF/CAS	Complete Active Space Self-Consistent Field
CI	Conical Intersection
CISD	Configuration Interaction Singles and Doubles
D	Debye
DC	Derivative Coupling
DFT	Density Functional Theory
EDG	Electron-Donating Group
EE	Electronic Embedding
ES	Excited State
ESP	Electrostatic Potential
eV	Electron Volts
EWG	Electron-Withdrawing Groups
FC	Franck-Condon
fs	Femto second
GD	Gradient Difference
GS	Ground State
GUGA	Graphical Unitary Group Approach
HF	Hartree-Fock
HOMO	Highest Occupied Molecular Orbital
HT	Hula Twist
IRC	Intrinsic Reaction Coordinate
LUMO	Lowest Unoccupied Molecular Orbital
MECI	Multielectron Configuration Interaction Technique
MEP	Minimum Energy Path
MK	Merz-Kollman

MM	Molecular Mechanics
MOPAC	Molecular Orbital PACkage
MP2	Moller-Plesset perturbation theory
NDDO	Neglect of Diatomic Differential Overlap
ns	Nano Second
OBF	One-Bond Flip
ONIOM	Our own N-layered Integrated molecular Orbital and Molecular mechanics
Ox	Oxaziridine
PBN	<i>N</i> -tert-butyl- α -phenylnitron
PES	Potential Energy Surface
PM3	Parameterized Model number 3
PM3/CI	Configuration Interaction calculations with PM3 Hamiltonian
ps	Pico second
PSB	Protonated Schiff Base
QM	Quantum Mechanics
QM:MM	Quantum Mechanics/ Molecular mechanics
RHF	Restricted Hartree-Fock
RPSB	Retinal Protonated Schiff Base
s	Second
S ₀	Ground State
S ₁	First singlet excited state
S ₂	Second singlet excited state
SCF	Self-Consistent Field
SP	Saddle Point
STQN	Synchronous Transit-Guided Quasi-Newton Method
TD-DFT	Time Dependent Density Functional Theory
TICT	Twisted Internal Charge Transfer
TICT-CI	Twisted Internal Charge Transfer Conical Intersection
TM	Transition Moment
TS	Transition State
UFF	Universal Force Field
VEE	Vertical Excitation Energies

CHAPTER 1

Introduction

1.1. Scope of research work

In this thesis, we have carried out computational investigations on the low-lying electronic states of some nitrene systems to reveal their so far unexplored photo-induced properties. Open-chain nitrenes with different substitutions on either sides of the C=N bond were studied to propose the mechanism of their photo-excitation processes. High-level computational methodologies were employed to explore their photo-chemical reaction paths which include the involvement of non-radiative decay channels through conical intersections. The photochemical behaviors of the zwitterionic nitrene systems are compared with that of open-chain conjugated polar iminium ions (protonated Schiff bases) and non-polar polyene systems. The proposed nitrene-oxaziridine photoconversion mechanism or the thermal isomerization reaction paths of nitrenes discussed in this thesis work may have far reaching consequences in terms of nitrene chemistry and the effect of substituents on the reaction paths may give valuable information to the experimentalists.

1.2. Introduction to computational photochemistry

Chemistry was primarily known to be an experimental science. However, in recent times the scenario has changed drastically, and now theoretical and computational chemistry has already established its huge importance in several fields; this includes some significant advances in designing drugs to fit with their target molecules to produce therapeutic effects and so on. In 1966, the well-known American chemist, Robert S. Mulliken, stated during his Nobel lecture, “.....*In conclusion, I would like to emphasize strongly my belief that the era of computing chemists, when hundreds if not thousands of chemists will go to the computing machine instead of the laboratory for increasingly many facets of chemical information, is already at hand...*”, and today, probably that era has truly arrived. Modern applications of computational chemistry include complete investigations of the various useful unexplored reaction mechanisms which involve the detection of short lived organic intermediates or transition states, as well. Today with the help of high-level quantum mechanical methods we may get the complete picture of thermal [1,2] and photochemical reactions [3]. Now it is possible to understand at the molecular level about the probable series of events happening during the bond-breaking and bond forming processes. The complete reaction path can be predicted by computing

the minimum energy path (MEP) [4-6] which connects the reactant to the product through a transition state on the $3N-6$ dimensional potential energy surface of the system, where N is the number of atoms. The thermal reaction takes place at the ground state surface or in other words a single potential energy surface is involved in the process. On the contrary, a photochemical reaction involves at least two potential energy surfaces (PES), although the strategy employed to investigate a photochemical pathway is quite similar to that of thermal reactions.

A photochemical reaction is characterized by absorption of light by a ground state chromophore at equilibrium which is subsequently promoted to an electronically excited state. This initially formed excited state has the same nuclear configuration as the ground state as the absorption of light takes place in a much faster time scale ($\sim 10^{-15}$ s) than the molecular vibration ($\sim 10^{-12}$ s). This principle governing the vertical transition is commonly known as the Franck-Condon (FC) principle, and results in the excess vibrational energy of the molecule. The excess vibrational energy of the initially populated FC geometry gets dissipated and vibrational relaxation takes place. This leads to significant changes in the original molecular and electronic structures, and the lowest vibrational level of that excited state is reached thereafter. The absorbed light energy can either be released (via internal conversion/ Fluorescence / Phosphorescence) or can produce a change in geometry (i.e. a photochemical reaction). Nowadays, such photophysical and photochemical events can be examined computationally with the help of effective electronic structure theories; this includes the analysis of the evolution of the chromophore's nuclear coordinates along different and interconnected $3N-6$ dimensional potential energy surfaces. In the last few decades, computational chemistry has successfully explored various photochemical reaction mechanisms in organic chromophores [7,8]. A computational investigation of the photochemical reaction mechanism involves the tracking of the sequence of events starting from the absorption of light by the reactant up to the photoproduct formation. Usually in the photochemical processes, the reactant is first excited from its ground state to the excited state; finally the product accumulates on the ground state. The features of photochemical processes are relatively more complicated in comparison to the thermal processes where the latter involves only the ground state surfaces. The mapping of the complete photochemical reaction path is done by following the minimum energy path (MEP) from the excited state Frank-Condon structure to the ground state photoproduct through slopes, barriers (transition states) and funnels (conical intersection) [9-11]. The conical intersection

processes occur in femto to pico second timescale and makes the reactions ultrafast. These types of photochemical processes have received huge attention in recent times due to the advancement of femtosecond spectroscopy [12-13] and ultrafast techniques [14]. The theoretical background of the ultrafast processes has been discussed in detail in the subsequent sections of this chapter. A general overview of a photo-excitation process followed by the relaxation to a stable minimum and then subsequent decay through the conical intersection to the ground state is shown in Figure 1-1.

Numerous computational investigations have been reported in the last several decades on the behavior of the photo-excited organic molecules [15-16] and their photochemical reaction pathways [17] by exploring their potential energy surfaces (PES). As discussed earlier, studying a photochemical reaction is relatively difficult as it involves at least two PESs; therefore, to understand the complete mechanistic pathway of a photochemical transformation, we should be familiar with the different important geometries (i.e. stationary points, slopes, saddle points, barriers and funnels) and processes occurring along the reaction pathway of that transformation.

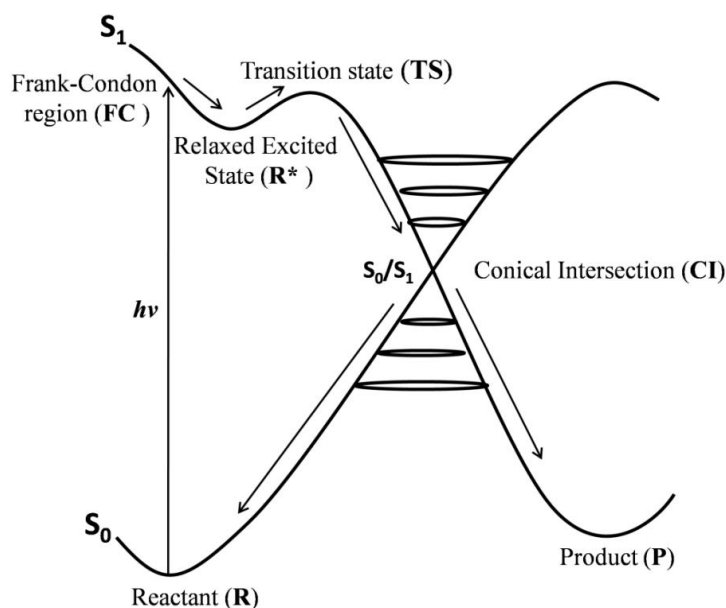


Figure 1-1: A schematic representation of a photochemical reaction through conical intersection

1.3. Important points on PES

1.3.1 Stationary points: Minima and Maxima

Minima on the potential energy surfaces are relatively stable species with a finite lifetime. They are called stationary points, which mathematically means that they have the first derivative of energy (E) with respect to the nuclear coordinates (i.e. the gradient) equal to zero.

$$\frac{\partial E}{\partial q_1} = \frac{\partial E}{\partial q_2} = \frac{\partial E}{\partial q_3} = \dots = 0$$

where, E is a function of q and partial derivatives $\partial E/\partial q$ (rather than dE/dq) indicates that each derivative is with respect to just one of the variables q . On the other hand, the transition states (maxima on the curve) are relatively less stable species and they are experimentally non-isolable.

A stationary point is a minimum or a transition state on the PES and this can be identified by the eigenvalues of the Hessian (second order derivative). Diagonalization of the hessian matrix gives the force constants. To calculate the vibrational frequencies, the Hessian matrix is first mass-weighted or in other words, the vibrational frequencies are calculated after diagonalizing a mass-weighted force constant matrix. The corresponding eigenvalues can be further used to describe the characteristics of a stationary point; if there exists no negative eigenvalue or the vibrational frequencies are all real (positive), the stationary point is a minimum. Either it can be a local minimum (lowest point in a limited region of the PES) or it can also be a global minimum (the lowest energy point on the overall PES). On the other hand, in case of a transition state on the potential energy surface one imaginary frequency exists, which implies a negative force constant. This indicates that in only one direction in nuclear configuration space the energy has a maximum, while in all other (orthogonal) directions the energy is a minimum. A transition state is also known as the first-order saddle point as it has one negative eigenvalue. An n^{th} order saddle point has n negative eigenvalues, which implies that it is a maximum with respect to n mutually perpendicular directions. The first order saddle point usually corresponds to a transition structure connecting the two equilibrium structures. As mentioned, the transition structure is a maximum along the reaction path and a minimum for all displacements perpendicular to the path. Mathematically, at both the maximum and the minimum, the first order derivative is zero:

$$\frac{\partial E}{\partial q} = 0, \text{ For all geometric coordinates } q \text{ (along all directions).}$$

The difference between them lies in the second order derivative. At the transition state,

$$\frac{\partial^2 E}{\partial q^2} < 0, \text{ for } q \text{ along the reaction coordinate and,}$$

$$\frac{\partial^2 E}{\partial q^2} > 0, \text{ for } q \text{ along all other directions}$$

Whereas, at a minimum;

$$\frac{\partial^2 E}{\partial q^2} > 0, \text{ for } q \text{ along all directions}$$

The eigenvector which corresponds to the single negative eigenvalue of a transition state (or a first order saddle point) is known as the transition vector. The reaction path (at least initially) can be found by following the mass weighted steepest descent path from the transition state to either of the two minima by moving along this transition vector. This minimum energy path connecting reactants and products via transition state is known as the Intrinsic Reaction Coordinate (IRC) [18-20]. It must be mentioned here that not all reacting molecules follow the IRC. It is must to have an optimized transition state to compute IRC. This intrinsic reaction coordinate is found in two directions, going forward and reverse from the transition state, following the steepest descent path in mass weighted Cartesian coordinates. With the help of IRC run we can verify whether the optimized transition state actually connects the reactant and products, or not.

1.3.2. The Born–Oppenheimer approximation and surface crossings

The first step in any quantum chemical problem is to solve the Schrödinger equation. As polyatomic molecules have many degrees of freedom, solving the Schrödinger equation for them is a very complicated task. Different mathematical transformation and approximation techniques are used to simplify this complex equation. The Born-Oppenheimer (BO) approximation [21,22] is one of the most fundamental approximations used to simplify the Schrödinger equation. Max Born and J. Robert Oppenheimer [21] in 1927 showed that the complex Schrödinger equation for a molecule can be simplified by separating its nuclear and electronic motions.

$$\Psi(r, R) = \chi^{nucl}(R)\psi^{elec}(r, R)$$

For any molecule, the full Hamiltonian includes terms for kinetic energy of electrons, kinetic energy of the nuclei, electron-nuclear attraction, nuclear repulsion and electronic repulsion. In atomic units it can be written as:

$$\hat{H} = - \sum_i^{elec} \frac{1}{2} \nabla_e^2 - \sum_I^{nucl} \frac{1}{2} \nabla_N^2 - \sum_i^{elec} \sum_I^{nucl} \frac{Z_I}{r_{iI}} + \sum_{I < J}^{nucl} \frac{Z_I Z_J}{r_{IJ}} + \sum_{i < j}^{elec} \frac{1}{r_{ij}}$$

Where, $r_{iI} = |r_i - R_I|$, $R_{IJ} = |R_I - R_J|$, $r_{ij} = |r_i - r_j|$ and ∇^2 is Laplacian operator. Nucleus is characterized by huge mass in comparison to that of an electron; it moves very slowly with respect to the electrons. The electrons can react instantaneously to the change in the nuclear position, which permits an approximate separation of the electronic and nuclear motion and thus allows solving the two parts of the problem independently. Neglecting the nuclear kinetic energy term from the full Hamiltonian (as nuclei can be

considered to be fixed with respect to the electrons), an electronic Hamiltonian (\hat{H}^{elec}) can be expressed as:

$$\hat{H}^{elec} = - \sum_i^{elec} \frac{1}{2} \nabla_e^2 - \sum_i^{elec} \sum_I^{nucl} \frac{Z_I}{r_{iI}} + \sum_{I < J}^{nucl} \frac{Z_I Z_J}{r_{IJ}} + \sum_{i < j}^{elec} \frac{1}{r_{ij}}$$

This \hat{H}^{elec} can be further used to solve the quantum mechanical problem of the electronic motion in the field of fixed nuclei, leading to an effective electronic energy (E^{eff}), which depends on the relative nuclear coordinates (R) and describes the potential energy surface (PES) for the system.

$$\hat{H}^{elec} \psi^{elec}(r, R) = E^{eff}(R) \psi^{elec}(r, R)$$

where, ψ^{elec} is the electronic wavefunction which depends on the electronic (r) and nuclear (R) coordinates.

The potential energy surfaces of a molecule derived by the BO approximation are known as *adiabatic* surfaces. On the other hand, there are some situations where the BO approximation is not valid (i.e. the separation of nuclear and electron motion is not possible). These situations represent *non-adiabatic* or *diabatic* behavior, which indicates break down of BO approximation. The PES in these cases can simply cross over to the other adiabatic surface, adopting its configuration. The non-radiative decays from the excited to ground states are the key processes in photochemistry and were usually assumed to occur via surface crossing points. As the system travels in the vicinity of such crossing points, the BO approximation breaks down and a radiation less decay from the upper to the lower intersecting state occurs within a single vibration period. To have a correct description of such molecular motion at these crossing points, we need to estimate non-adiabatic coupling effects (such as surface hopping probability) along with calculating the potential energy surfaces for the electronic states (by solving the electronic part of the Schrödinger equation). Edward Teller [23] suggested that in polyatomic molecules these types of intersections may provide a very fast decay channel from the lowest excited states to ground states.

Various photochemical processes, such as isomerization of simple dienes [24], cyclohexadienes [25,26], hexatrienes [27], and many other systems lack fluorescence emission from the excited states; they are governed by extremely fast radiationless processes characterized by real crossing (commonly known as conical intersection) where the life time of the excited states are in picoseconds to femtosecond order. The probability of decay from the excited state to a lower state is very high in such surface crossing processes. Conical intersection [9-11] is characterized by the degeneracy of the

two potential energy surfaces where they intersect. It is widely accepted now that conical intersections of the molecular potential energy surfaces play key role in the spectroscopy and photochemistry of numerous polyatomic molecules.

The electronic and the nuclear coordinates can no longer be separated in the vicinity of the conical intersections and the non-adiabatic processes starts happening with the breakdown of BO approximation. These intersection points are also known as photochemical or molecular funnels [28,29]. This is due to the fact that the excited electronic states are “funnelled” through these points to the ground electronic states which subsequently lead to the formation of photoproducts. First we will discuss about the reason behind referring these molecular or photochemical funnels as “conical” intersection. Let us imagine following Neumann & Wigner [30,31] that all but two of the electronic wave equations have been found and suppose ϕ_1 and ϕ_2 are any two functions (states involved in the crossing) which constitute a complete orthonormal set along with the found solutions. In that case it must be possible to express each of the two remaining electronic wave functions in the form,

$$\Psi = c_1\phi_1 + c_2\phi_2$$

The following integral can be written as,

$$\begin{aligned} \int \Psi \hat{H} \Psi d\tau &= \int (c_1\phi_1 + c_2\phi_2) \hat{H} (c_1\phi_1 + c_2\phi_2) d\tau \\ &= c_1^2 \int \phi_1 \hat{H} \phi_1 d\tau + c_1c_2 \int \phi_1 \hat{H} \phi_2 d\tau + c_1c_2 \int \phi_2 \hat{H} \phi_1 d\tau + c_2^2 \int \phi_2 \hat{H} \phi_2 d\tau \\ &= c_1^2 H_{11} + c_1c_2 H_{12} + c_1c_2 H_{21} + c_2^2 H_{22} \end{aligned}$$

where, $H_{11} = \int \phi_1 \hat{H} \phi_1 d\tau$ or $\langle \phi_1 | \hat{H} | \phi_1 \rangle$,

$$H_{12} = \int \phi_1 \hat{H} \phi_2 d\tau \text{ or } \langle \phi_1 | \hat{H} | \phi_2 \rangle,$$

$$H_{21} = \int \phi_2 \hat{H} \phi_1 d\tau \text{ or } \langle \phi_2 | \hat{H} | \phi_1 \rangle,$$

$$H_{22} = \int \phi_2 \hat{H} \phi_2 d\tau \text{ or } \langle \phi_2 | \hat{H} | \phi_2 \rangle$$

The secular equation resulting from the linear variation method can be written as:

$$\begin{bmatrix} H_{11} - E & H_{12} \\ H_{21} & H_{22} - E \end{bmatrix} \begin{bmatrix} c_1 \\ c_2 \end{bmatrix} = 0$$

After solving, the energy values E_1 and E_2 of the two states can be expressed as

$$\begin{aligned} E_1 &= \frac{1}{2} \left[(H_{11} + H_{22}) - \sqrt{(H_{11} - H_{22})^2 + 4H_{12}^2} \right], \\ E_2 &= \frac{1}{2} \left[(H_{11} + H_{22}) + \sqrt{(H_{11} - H_{22})^2 + 4H_{12}^2} \right] \end{aligned}$$

As conical intersections are true crossings between PESs, so they must have degenerate solutions. In order to have such degeneracy, the following two independent conditions must be fulfilled:

$$H_{11} = H_{22}, \text{ and } H_{12} = H_{21} = 0$$

To satisfy these conditions, at least two independently variable nuclear coordinates are required.

Unlike diatomic system (which has only one variable coordinate, i.e. the interatomic distance), polyatomic systems have enough number of degrees of freedom ($n = 3N-6$; N is no. of atoms in system) to simultaneously satisfy the above mentioned two conditions by choosing appropriate values for two independent variables. The remaining $n-2$ (or $3N-8$) degrees of freedom can be varied without leaving the crossing region. These subspaces of remaining $n-2$ dimensions, where all the degenerate points lie are commonly known as the intersection space or seam.

Now, let's take x_1 and x_2 as the two independent coordinates, and assume the origin at the point where $H_{11}=H_{22}, H_{12}=H_{21}=0$, then the secular equations [32] can be written as

$$\begin{bmatrix} W + h_1 x_1 - E & lx_2 \\ lx_2 & W + h_2 x_1 - E \end{bmatrix} \begin{bmatrix} c_1 \\ c_2 \end{bmatrix} = 0$$

where, $H_{11}=W + h_1 x_1, H_{22}=W + h_2 x_1$, etc.

$$\begin{bmatrix} W + (m + k)x_1 - E & lx_2 \\ lx_2 & W + (m - k)x_1 - E \end{bmatrix} \begin{bmatrix} c_1 \\ c_2 \end{bmatrix} = 0$$

where, $m = \frac{1}{2}(h_1 + h_2)$ and $k = \frac{1}{2}(h_1 - h_2)$

Solving the above equation, the eigenvalue (E) will be:

$$E = W + mx_1 \pm \sqrt{k^2 x_1^2 + l^2 x_2^2}$$

The above mentioned equation is an equation of elliptic double cone with vertex at the origin and hence these crossing points are termed as conical intersections. Movement in the plane in the directions of these two dimensions (x_1 and x_2) from the point of intersection, will lift the degeneracy of the system. This two dimensional space is commonly known as the branching space (Figure1-2). On the other hand, as mentioned above, if the movement is from the apex of the cone along the $n-2$ intersection seam, the degeneracy will be maintained. This intersection seam is a hyperline consists of infinite number of conical intersection points.

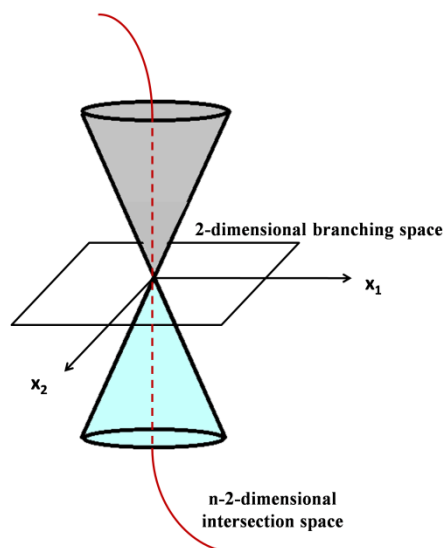


Figure 1-2: A schematic representation of conical intersection with double cone topology

The vectors x_1 and x_2 corresponds to the gradient difference (GD) vector and interstate coupling gradient or derivative coupling (DC) vector, respectively. Mathematically [33], the GD vector x_1 is:

$$x_1 = \frac{\partial(E_1 - E_2)}{\partial Q}$$

and the DC vector x_2 can be expressed as :

$$x_2 = \left\langle c_1^t \left| \frac{\partial H}{\partial Q} \right| c_2 \right\rangle$$

where, c_1 and c_2 are the configuration interaction eigenvectors, H is CI Hamiltonian and Q is the nuclear configuration vector of the system. The role of a transition state in a thermal reaction and a conical intersection in a photochemical reaction can be compared at this point. A transition state forms a bottleneck between product and reactant and spanned by a single reaction coordinate (x_1). A conical intersection also forms a bottleneck which separates the excited state reaction surface from the ground state surface; however, unlike the transition state in a thermal reaction, at a conical intersection in a photochemical reaction, the branching space is spanned by the two coordinate (x_1 and x_2). Consequently, a conical intersection can lead to two or more products on the ground state PES through a branching of the excited reaction path into different ground state relaxation channels; on the other hand, a transition state leads to a single product only (Figure 1-3) [34].

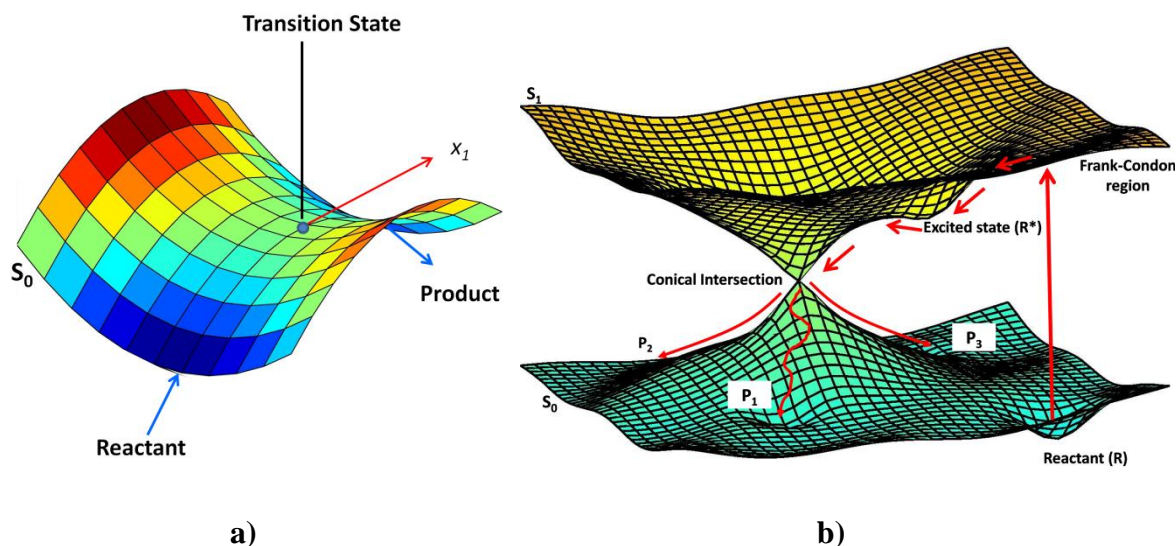


Figure 1-3: Comparison of (a) transition state (TS) and (b) a conical intersection (CI)

Nowadays, femtosecond time-resolved spectroscopy and modern laser experimental techniques [35] have allowed us to study the structures and energetic of important points on excited state surfaces of polyatomic molecules. However, still the experimental analysis of conical intersections on the potential energy surfaces is quite difficult as they are not stationary points. Direct experimental (laboratory) observation of their existence can be confirmed by observing lack of fluorescence, very rapid (sub-picosecond) decay of electronically excited states and by rapid formation of products [29, 36-41]. Conical intersections are a common feature in most singlet photoreactions. Recently, by means of *ab initio* calculations, conical intersections have been located for a various organic photochemical reactions [29]. They play key mechanistic role in organic photochemistry; the validity of this statement has been established from the studies of different types of photochemical reactions like, ring-opening and ring-closure reactions [42,43], [1,2], [1,3]-sigmatropic shifts [44-46], di- π -methane rearrangement [47,48], valence isomerization of aromatics [44,49], cycloadditions reactions [50,51], *cis-trans* isomerization of polyenes [52-54], hydrogen transfer and charge transfer reactions [55], isomerization of nitrones to oxaziridine, etc. The central role of conical intersection in the decay channels associated with ultrafast radiationless deactivation of polyenes and PSBs [56-58], benzene [59,60], azulene [61-63] and fulvene [64,65] has also been reported.

1.4. Brief background of research based on literature survey

One of the significant studies involving the conical intersection which has been investigated thoroughly in recent times is the photoinduced *trans*→*cis* isomerization of polyenes which occurs through non-adiabatic reaction path. In this isomerization process, the initial photo-excitation is followed by the excited state intermediate decay to the ground state through a twisted molecular geometry. The ultrafast dynamics of the natural pigments like rhodopsin (light-sensitive vision protein) and bacteriorhodopsin (used by *Achaea* as a proton pump) has been the subject of interest in the recent years [66-69]. Bacteriorhodopsin contains all-*trans* retinal iminium ion connected to the lysine residue of a protein which consists of 248 amino acids. The all-*trans* retinal form isomerizes to 13-*cis* retinal (Figure 1-4-a) on photo-irradiation. This *trans-cis* isomerization triggers a series of events, which causes conformational change in the surrounding protein and eventually results in the proton pumping action of Bacteriorhodopsin [70,71]. On the other hand, in vision, primarily the retinal protonated Schiff base (RPSB) chromophore [72-74] of the visual protein rhodopsin is found in the 11-*cis* form. Here the photochemical 11-*cis* to all-*trans* isomerization includes a conformational change in the photoreceptor (Figure 1-4-b), and this isomerization is known to be one of the fastest photochemical reactions observed, so far [75,76]. In a sequence of processes, the photorhodopsin is the first photoproduct formed in 200 femtoseconds after photoirradiation, while the next one is bathorhodopsin which contains distorted all-*trans* bonds and forms within picoseconds after photorhodopsin.

Due to the very high computational costs, high level *ab initio* calculations are not practically possible on these systems. Instead, the protonated Schiff base, 2,4-pentadien-1-iminium cation, is usually chosen as the model compound of RPSB for the purpose of computational studies. Choice of this shorter conjugated chain length in the model system may quantitatively affect the spectroscopy and the energetic of the system and moreover, the lack of β -ionone ring (may be responsible for steric factors in the constrained environments) may deviate their properties from the actual system; however, it is a fact that the photochemical behavior of these model systems are found to be quite similar to that of RPSB, which justifies their choice as the model systems. The photoisomerizations of these systems are fast barrierless processes which primarily involve the central double bonds. The initial photo-excitation process in such systems leads to an excited singlet state (S_1) having charge transfer characteristics, which subsequently passes through a peaked S_1/S_0 conical intersection with a twisted central double bond

geometry. It must be mentioned here that there are three different types of conical intersections, the sloped intersection related to the comparatively slower dynamics and the two faster varieties of peaked intersections (Figure 1-5). In the peaked type conical intersections, the molecule on the excited state surface (through a barrier or without passing through any barrier) is funnelled towards the intersection point leading to highly efficient ultrafast non-radiative decay to ground state surface. On the other hand, in the sloped topography, the excited state goes towards the conical intersection point less effectively, where the excited state might be equilibrated and thus may result in a less efficient non-radiative process.

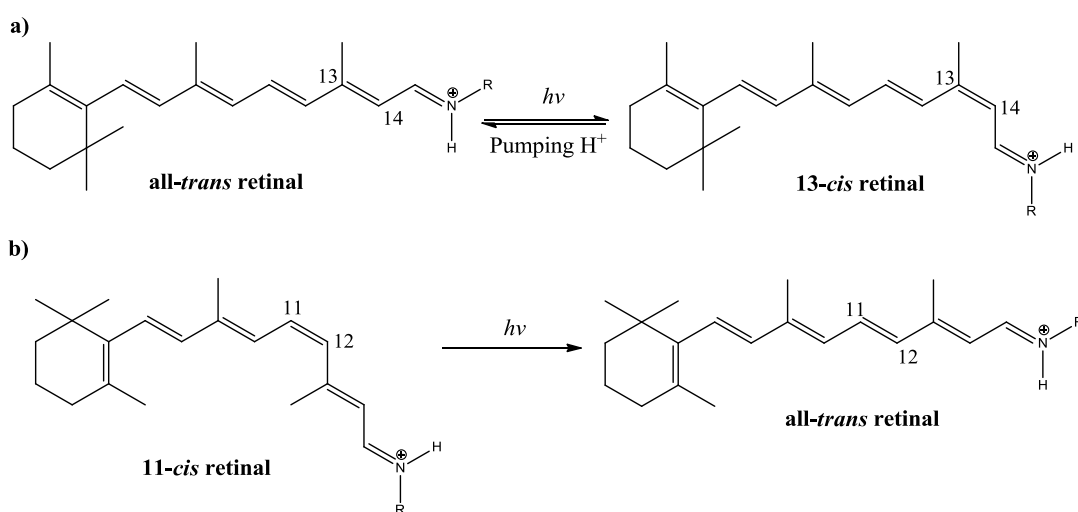


Figure 1-4: Photoisomerization of a) Bacteriorhodopsin chromophore and b) Rhodopsin chromophore

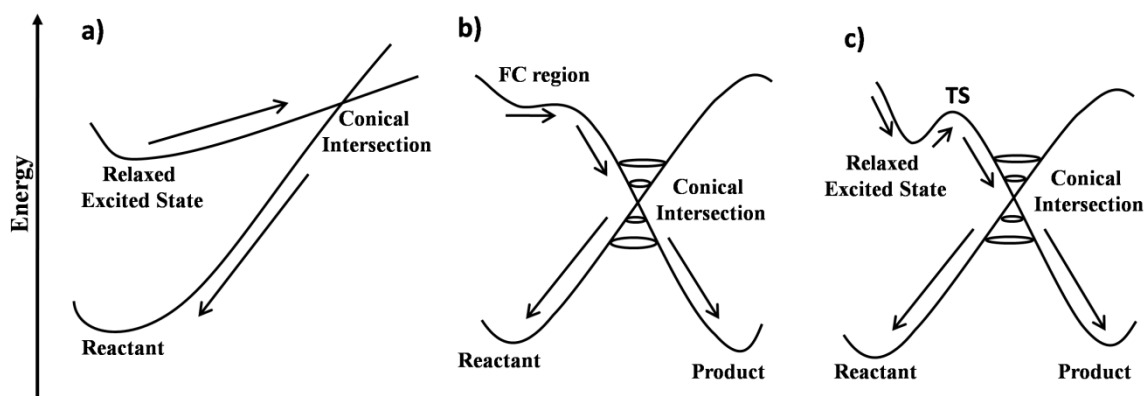


Figure 1-5: Different types of conical intersections where a) is sloped type conical intersection, b) and c) are peaked conical intersection

The strong effects of the types of substitutions (on nitrogen and conjugated chain) and counter ions on the photo-reactivity of the retinal chromophore model have been reported in recent times [77,78]. These affect the excited state lifetime and reaction rate

which consequently changes the photo-isomerization efficiency. The position of the counter charge introduced can be also used as an important tool to tune the photo-isomerization rate and efficiency. In fact, less efficient radiationless decay channels operate when negative counter ions are placed at the *N*-head position of the chromophore or certain groups are substituted on the nitrogen atom of the iminium ion [77-79]. This is related to the change of the conical intersection topography from peaked to sloped [79]. These reported studies on the retinyl iminium systems have dragged our attention towards the structurally similar retinyl nitrone systems. Almost thirty years back, a new class of retinoids, *N*-substituted retinyl nitrones, was (Figure 1-6) synthesized and characterized by Balogh-Nair et al. [80]. These open chain conjugated nitrones were found to be chemopreventive and effective in reversing the keratinization in hamster organ cultures. The *N*-alkyl-substituted varieties of these nitrones were found to be stable and under room light the *N*-methyl system was reported to give highly stable oxaziridine species. The formation of this terminal heterocyclic species under photo-excitation clearly indicates that the photochemical features of these compounds are quite different

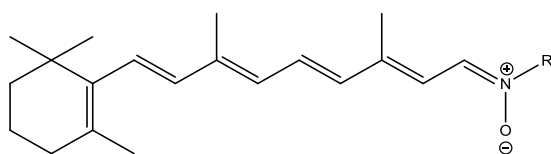


Figure 1-6: Structure of *N*-substituted retinyl nitrones

from that of the retinyl iminium systems. From the structural point of view, one can expect that the retinyl nitrone system with positively charged nitrogen linked to negatively charged oxygen is somewhat similar to the retinyl iminium compounds with a negative counter charge on the nitrogen. Consequently, it can be expected that the photochemistry of these nitrone systems might be having some sort of similarity with that of retinyl iminium systems with counter ions where comparatively slower non-radiative decay channel operates. It is a fact that in general (including the retinyl systems), nitrone ultrafast photo-dynamics has not been reported, so far, which supports the possible presence of slower non-radiative decay channels operating in these systems; moreover, this is also true that their nature of photoproducts are completely different in comparison to that of the structurally similar iminium ions. In fact, the photo-irradiation of any kind of acyclic nitrones usually leads to oxaziridine and/or amide as the primary photoproducts depending on the substitutions on the nitrogen or carbon.

These observations have initiated our interest in the unexplored field of nitrone photochemistry. We have attempted to put forward a proper mechanism of the photo-

chemical processes of nitrones through comprehensive analysis using high-level quantum mechanical investigations. Our targeted studies in this thesis include conjugated long-chain and short-chain nitrones, naphthyl nitrones etc. In this context we need to discuss few fundamental facts about nitrones before going to further discussions. Since last several decades, there has been considerable amount of studies done on several nitro-compounds including their photochemical investigations; however, it seems that relatively less attention has been paid on the photochemistry and excited state analysis of nitrone systems, so far. Nitrones are quite well-known versatile intermediates in organic synthesis [81]. Their stereoselective 1,3 dipolar cycloaddition reactions with alkenes are well-studied through which they form synthetically useful iso-oxazolidines [82,83]. It has already been discussed that nitrones are photosensitive; their photo-excitation usually leads to oxaziridine and subsequent photo-products, such as amide. In the last fifty years, nitrones have drawn huge attention of experimentalists due to their wide applications in synthetic chemistry. They are widely accepted as building blocks in synthesis of various natural and biologically active compounds [84]. There are quite a few nitrones known for their spin trapping abilities. These nitrones react with the transient free radicals to form more persistent paramagnetic species, known as spin adduct; these are used to detect the transient radicals in electron paramagnetic resonance (EPR) spectroscopy. The most commonly used spin-trapping agent in this category is the *N*-tert-butyl- α -phenyl nitrone (PBN) which along with its derivatives are known to inhibit fundamental pathogenic mechanisms and also used in the inflammation treatment. Nitrones are effective pharmacological agents against the oxidative stress mediated injuries. They are known for their potential activity against various age related diseases [85,86], such as Parkinson's disease, Alzheimer's disease [87] etc. Some nitrones are reported to be chemopreventive, as well [80]. There are numerous examples where nitrones play important roles against several other diseases too [88-94].

Experimental studies of the photo-irradiation process of nitrones and subsequent formation of oxaziridines with other photochemical products has been the subject of interest since last five decades. Experimental studies done by Splitter et al. [95,96] and Koyano et al. [97] in the last century are still considered to be the major experimental studies done on these systems. Usually the nitrones are found to be quite unstable and their photo-irradiation usually results in transient oxaziridine species which eventually gives amide (shown in Figure 1-7) and other products. However, depending on the substitutions, the oxaziridines can be of better stability, too. Nitrones having substitution

of alkyl groups on either or both the nitrogen and carbon atoms were found to give stable and experimentally isolable oxaziridines. On the other hand, presence of aryl groups on

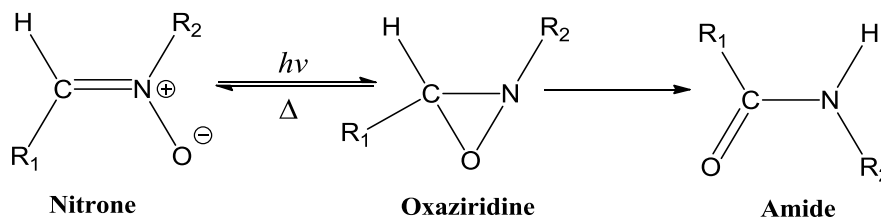


Figure 1-7: Nitron to amide conversion via oxaziridine

both of these atoms decreases the stability of this terminal heterocyclic species significantly. Photo-irradiation studies on *N*-methyl and *N*-*t*-butyl derivative of α -(2-naphthyl)-nitron were reported [98] to give stable and isolable oxaziridines, however, its *N*-(*p*-tolyl) derivative was found to be highly unstable. The previously discussed example of stable oxaziridine formation from *N*-methyl retinyl nitron also supports the same observation. The stereospecificity of the nitron-oxaziridine conversion was another topic which created some controversy in the last century. The Boyd group had doubted this stereospecificity due to the formation of both *cis* and *trans* oxaziridines from the *trans* isomer of methyl nitrones [99]; however, it was soon proposed by Splitter et al. [96] that this happens due to the thermal ring opening of the oxaziridine in two possible conrotatory modes which eventually results in a mixture of *cis* and *trans* isomers of nitron. Another important observation was the *cis-trans* isomerization reaction of α -Cyano- α -phenyl-*N*-phenylnitrones [97] which was found to occur thermally or in the presence of photosensitizers, such as uranine, eosine, iodine etc. This isomerization process was reported to involve the triplet excited states. On the other hand, the normal photoisomerization of nitrones to oxaziridines and other rearrangement products were confirmed to involve only singlet states.

In spite of numerous experimental investigations, only few theoretical studies were reported on the nitron systems, till recent times. However, these studies [100] are mostly related to the ground state processes only. No comprehensive photochemical studies were known which involve their excited state analysis. This thesis aims to provide a complete probable mechanism of photo-excitation processes of different types of nitron systems by revealing the nature of their unexplored low-lying excited electronic states. One major objective of this thesis is to investigate the exact photochemical processes happening during the nitron-oxaziridine conversion step and to analyze the possibility of other photoproducts in the subsequent stages. We have

carried out rigorous computational investigations based on high-level methods on various nitrene systems to establish the actual mechanism of their photochemical processes.

1.5. Gaps in existing research

Following are the gaps in the existing research work which has dragged our attention and made us interested in this field:

1. Lack of studies on the nitrene photoisomerization mechanism

To the best of our knowledge, the complete mechanism of the photo-excitation process of nitrene leading to the photoproduct formation was not well-established, till recent times. Probably, this was primarily due to the lack of enough information on their excited state characteristics. Almost fifty years back, it was predicted by Koyano et al. [97] that the photoproduct oxaziridine formation of nitrene probably involves the first excited singlet state. However, no comprehensive analysis on this photochemical path had been reported earlier. Theoretical studies on nitrenes were mostly related to their ground state investigations only.

Interestingly, the photo-excitations of nitrenes are known to give oxaziridines and/or amides as the primary photoproducts, however, the *cis-trans* photo-isomerization has not been reported, so far. In fact, some experimental studies have predicted that this isomerization in nitrenes probably takes place through a thermal process. For an example, we may compare the photochemistry of the long-chain conjugated retinyl nitrenes and that of structurally similar conjugated non-polar polyenes or conjugated polar iminium ions (protonated Schiff bases). The latter two systems are known to undergo isomerization through contrasting mechanisms. For a better understanding we may compare the photo-isomerization paths of 1,3,5-hexatriene and 2,5-pentadienyl iminium ion. Their ground states are having A_g (or A_g -like) symmetries; however, their S_1 (and S_2) states are exactly opposite in nature [56, 81]. The first excited state of conjugated polyene systems are biradical in nature with A_g symmetry while in the PSB systems, an ionic nature has been found for the same with B_u symmetry. In the former system $S_0 \rightarrow S_1$ is forbidden; the initial photo-excitation to S_2 is followed by an ultrafast relaxation to the S_1 state [101,102] which subsequently undergoes a conical intersection (S_0/S_1) with the ground state through a triangular kink-type structure [103], known as Kinked-CI. This process involves the so-called Hula twist (HT) type of motion which is a volume conserving process. On the other hand, in the protonated Schiff base, the

allowed $S_0 \rightarrow S_1$ transition is subsequently followed by an ultrafast barrierless process of one-bond flip (OBF) [57,78,79,104] around a single bond (C–C) in the S_1 state which was originally a double bond (C=C) in the ground state. As the rotation continues, the S_1 state becomes more stabilized, while the ground state energy increases. At a certain torsion angle (near 90°) a conical intersection (TICT-CI) between these two surfaces takes place; consequently, a radiationless transition occurs to the ground state resulting in an isomerization. It seems that in case of structurally similar nitron systems something else is happening as similar isomerization products are not reported after their photo-irradiations. The ground state of nitron system is a zwitterionic (dipolar) species and hence electrically neutral. A positive charge on nitrogen may indicate some similarity in their behavior with the polar iminium ions, however, being neutral in nature it may have some similarities with the neutral polyene systems. Eventually this may end up with a contrasting behavior which is neither similar to polyenes nor aligned with the characteristics of the iminium ions. The key lies in the analysis of the nature of the excited states which was missing in the literature, so far.

2. Oxaziridine stability depending on the substituents

One interesting fact about the photo-product oxaziridine is the stability of this species depending on the substituents present on the nitrogen atom of the C=N bond in the parent nitron. It has been noticed from the experimental results in past that alkyl groups on nitrogen favors stability of oxaziridine while phenyl groups on the same has opposite effect. The latter usually leads towards an amide as the photoproduct. The electron deficit oxaziridines with electron-withdrawing groups (sulfonyl, acyl, perfluorinated oxaziridines) on nitrogen are used as the source of electrophilic oxygen. Conversion of nitrones to these oxaziridines by photo-irradiations is not known experimentally. Usually oxidation of imines and electrophilic amination of ketones are known to be the popular methods for preparing such oxaziridines. This substituent effect on the stability of oxaziridines during the course of photo-excitation of nitrones probably requires a lot of attention and there is huge scope to reveal this completely unexplored field.

1.8. Objectives of the research:

To propose a mechanism for the photo-excitation and subsequent photo-chemical processes happening in some nitron systems through quantum mechanical studies. This will involve:

- Analysis of the un-explored low-lying electronic states of different nitron systems.
- Exploring the nitron-oxaziridine conversion mechanism and effects of electron-donating and electron-withdrawing groups on the oxaziridine formation.
- Investigations on the involvement of different non-radiative decay channels operating in these nitron systems.
- Identifying the types of conical intersections governing the non-radiative decay processes.

1.7. Thesis structure

Chapter 1: Introduction

In this chapter basic introduction to computational photochemistry is provided. Important points on the potential energy surfaces like equilibrium points (ground state and excited state), transition state, conical intersection etc, have been discussed. A brief background with extensive literature survey is given. In this chapter, the gap existing in the research, objective of the research done and thesis structure are also discussed. Finally, some fundamentals of the methodologies used have been provided at the end.

Chapter 2:

Spectroscopic features of the low-lying singlet states of some *N*-alkyl retinyl nitron model systems and their involvement in oxaziridine formation are discussed. In this chapter, thorough discussions have been done on the central key role played by the terminal CNO moiety in the photochemical oxaziridine conversion process of chemopreventive retinyl nitron systems; this was revealed through hybrid QM:QM and QM:MM ONIOM calculations.

Chapter 3:

This chapter provide details of the computational investigation of the photochemical oxaziridine and amide conversion process of open-chain conjugated nitron with substitution of electron-withdrawing trifluoromethyl group on nitrogen. The effect of electron withdrawing groups on nitron-oxaziridine conversion is compared with the effect of electron donating alkyl groups.

Chapter 4:

In this chapter a comprehensive spectroscopic investigation of α -(2-naphthyl)-*N*-methylnitrene and its isomer has been discussed, which includes computational study of their photochemical nitrene–oxaziridine conversion. A detailed study of their radiative properties and thermal *E–Z* isomerization are also explained.

Chapter 5:

A comprehensive spectroscopic investigation of some terminally phenyl-substituted small chain conjugated nitrenes has been discussed in this chapter, which includes computational study of their photochemical nitrene–oxaziridine conversion and the obtained results are compared with the experimental observations.

Chapter 6: Conclusion

The conclusions, future scopes of research work and appendixes have been presented.

1.8. A brief overview of some of the quantum chemical methods used to explore the photochemical reactions in this thesis.

1.8.1. Post-Hartree-Fock calculations and electron-correlation methods [105,106]

The Hartree-Fock (HF) method does not treat the electron correlation effect properly and the energy value obtained is usually too high than the real ground state energy:

$E_{Correlation} = E_0 - E_{HF}$, where E_0 is the exact ground state energy and E_{HF} is the Hartree-Fock energy for a given basis set & $E_{Correlation} < 0$

Hartree-Fock method uses a single Slater determinant wavefunction. In this method, the electron-electron interactions are treated in an average way and each electron (say, out of N electrons) feels the average Coulomb repulsion originating from the static distribution of the other $N-1$ electrons. Here the instantaneous electron-electron interactions are neglected and the Coulomb energy becomes very high. It should be mentioned here that it is not true that the HF theory completely neglects electron correlation. It includes some correlation effects (*exchange correlation*) of the motion of electrons with the same spin which arises by satisfying the antisymmetry requirement of the Pauli principle, but in this theory, electrons of opposite spin remains uncorrelated. To overcome this correlation problem, we need to include more than one determinant in the wavefunction. In the post-Hartree-Fock methods, the Hartree-Fock (HF) wave function is used as a starting point of calculation, and then the missing electron correlation is corrected by adding excited Slater determinants which makes the overall a multideterminant wavefunction. But the question arises here that from where do we get the other determinants in these methods? The simplest way of generating other Slater determinants is to promote electrons from the occupied orbitals to the virtual ones or in other words replacing the MOs which are occupied in the HF determinant by unoccupied MOs. If we consider a case of a closed shell calculation with N electrons and b basis functions, it will give us $N/2$ occupied and $b - N/2$ virtual orbitals. From these orbitals we can generate singly, doubly, triply (or more) excited determinants by promoting one, two, three electrons (or more), respectively, from the occupied orbitals to the virtual orbitals. Total number of the excited Slater determinants depends on the size of the basis set and in a given basis set, if all possible Slater determinants are included then the whole correlation energy will be recovered (Figure 1-8).

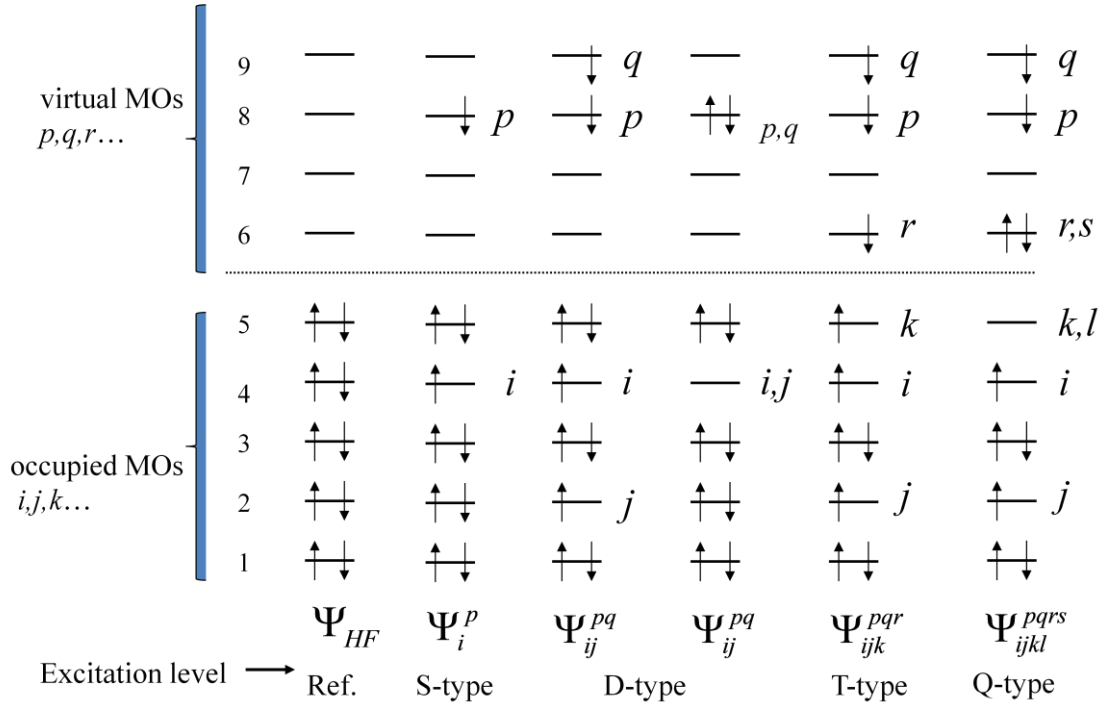


Figure 1-8: Excited Slater determinants can be generated by promoting electrons from the $N/2$ occupied to $b-N/2$ virtuals.

In the above shown figure (Figure 1-8), the HF ground state wavefunction (Ψ_{HF}) is termed as reference which is a single determinant. When one electron is promoted from an occupied orbital ‘ i ’ to a virtual orbital ‘ p ’, the corresponding wavefunction can be represented as a linear combination of Slater determinants with single excitations. Mathematically this wave function can be represented as:

$$\Phi^{(1)} = \sum_i^{occ} \sum_p^{vir} c_i^p \Psi_i^p$$

Similarly, doubly excited ones can be represented as:

$$\Phi^{(2)} = \sum_{ij}^{occ} \sum_{pq}^{vir} c_{ij}^{pq} \Psi_{ij}^{pq}$$

The configuration state function (CSF) is a symmetry-adapted linear combination of Slater determinants to produce the desired symmetry. Only CSFs that have the same multiplicity as the HF reference contribute to the correlation energy.

A. Configuration Interaction [5,107,108]

Configuration interaction optimizes the coefficients in the CSF expansion of the ‘exact’ wavefunction, using variational principle.

$$\Psi_{CI} = C_0 \Phi_{HF} + \Phi^{(1)} + \Phi^{(2)} + \Phi^{(3)} + \dots$$

In a Configuration Interaction calculation, we start with the set of basis functions, and do a SCF calculation to find SCF occupied and virtual Molecular Orbitals (MOs); subsequently these MOs are used to form configuration state functions. The linear combination of the configuration functions can be used to write the molecular wave function and finally variation principle can be used to find the coefficients of the configuration functions used in the linear combination. The number of possible determinants increases exponentially with the excitation, so there are huge number of possible configurations, even with moderately sized molecule and relatively small basis set. For n electrons and b basis functions, the number of configuration functions will be roughly proportional to b^n .

If the expansion includes all possible CSFs with the appropriate symmetry, then this will be termed as full *configuration interaction* (Full CI) procedure, which exactly solves the electronic Schrödinger equation within the limits of the finite basis set. This exponential growth of CSF's even for small molecules (small n) and small basis sets (small b) makes it practically impossible to solve the full CI. It is therefore important to truncate the CI-space (keeping in mind that which type of configuration functions are likely to make largest contributions to the wavefunction) to keep the problem practically manageable and also to save huge computational cost. For example, the method CID is limited to double excitations only and the method CISD is limited to single and double excitations.

$$\Psi_{CI} = C_0 \Phi_{HF} + \Phi^{(1)} + \Phi^{(2)}$$

Methods like CISDT, CISDTQ are also there; the latter gives energy close to full-CI but only applicable for small molecules and small basis sets. The only CI method which is usually feasible for a large variety of systems and recovers 80-90% of the available correlation energy is the CISD method. However, the effect of truncation causes an error due to the lack of handling the size-consistency problem. Size-consistency means the total energy of non-interacting particles must be equal to the sum of energies of the individual particles. This property is there in the full CI.

B. Multi-Configurational Self Consistent Field (MCSCF) [109-111]

In the MCSCF method, the molecular wave function is written as a linear combination of CSFs (Φ_i) and not only the expansion coefficients c_i in $\Psi = \sum_i c_i \Phi_i$ (where Ψ is the molecular wave function) are varied but also the molecular orbitals are varied by varying

the coefficients a_{ji} in $\Phi_i = \sum_{j=1}^b a_{ji} \chi_j$ (where χ_j represents one-electron basis functions). We can take an example of MCSCF calculation on Helium (He) ground state using the basis functions χ_1 and χ_2 , and including CSFs Φ_1 and Φ_2 . The MCSCF wave function can be written as:

$$\begin{aligned} \psi &= c_1 \Phi_1 + c_2 \Phi_2 \\ &= c_1 |\phi_1 \bar{\phi}_1| + c_2 |\phi_2 \bar{\phi}_2| \\ &= c_1 |(a_{11}\chi_1 + a_{21}\chi_2)(\overline{a_{11}\chi_1 + a_{21}\chi_2})| + c_2 |(a_{12}\chi_1 + a_{22}\chi_2)(\overline{a_{12}\chi_1 + a_{22}\chi_2})| \end{aligned}$$

As discussed, in MCSCF all these six coefficients ($c_1, c_2, a_{11}, a_{12}, a_{21}$ and a_{22}) are varied to minimize the variational integral. The optimized MCSCF orbitals are obtained through an iterative procedure like SCF. The most commonly used MCSCF method is the complete active space self consistent field (CASSCF) method.

C. Complete Active Space SCF (CASSCF) [112-118]

This multi-configurational approach divides the occupied orbital space into inactive (closed-shell) and active orbitals. For all the CSFs the inactive orbitals are doubly occupied. The remaining (active) electrons occupy the active orbitals. All possible occupied and virtual orbitals where active electrons can be present, forms the active space for CASSCF calculations. The active spaces are chosen according to the specific chemical problem we are studying. In CASSCF, the wave function is written as a linear combination of all CSFs arising out of all possible distributions of active electrons in the active orbitals those have the matching spin and symmetry eigenvalues as the state under consideration. The active space is often defined by two numbers (M, N), where M is the number of active electrons and N is number of active orbitals used in the calculation. CASSCF method is also known as full-optimized reaction space (**FORS-MCSCF**) as it includes all the possible CSFs in an active space.

Different active spaces may have different impact on the relative and absolute energy of the studied system. Usually, the active space should include all the valence orbitals and valence electrons, however, as we expand the active space, the computational cost increases rapidly [119]. Large active spaces give large number of CSFs. For an active space (M, N),

$$n_{CSF} = \frac{N!(N+1)!}{\left(\frac{M}{2}\right)!\left(\frac{M}{2}+1\right)!\left(N-\frac{M}{2}\right)!\left(N-\frac{M}{2}+1\right)!}$$

For example, a singlet CASSCF (12, 12) wavefunction, where 12 electrons and 12 orbitals are in active space, the numbers of Slater determinants and CSFs are 853,776 and 226,512, respectively. If we increase the active space to CASSCF (14, 14) for a singlet wavefunction, these numbers increase to 11,778,624 and 2,760,615, respectively [119]. Therefore in practice, we should only select the relevant orbitals and electrons whose occupations change during the studied chemical process, such as during excitation or relaxation to a different state. In other words, we should only include those electrons or orbitals in active space which actively participate in a chemical process. There is no correct single active space in a molecule; for the same molecule active space choice can be different depending on the chemical process under consideration [119].

D. Dynamic Correlation Methods (CASMP2 and CASPT2) [120-122]

The CASSCF method takes into account the static correlation effects, however, to get a better description of the system, dynamic correlation is required to be included. To incorporate both dynamic and nondynamic electron correlations, one needs to perform CI or perturbation calculations from multiple reference configurations. In these methods one does a CASSCF calculation first and then uses the resulting multideterminant wave function to provide reference configurations for the calculation of dynamic electron correlation. In recent times, a number of methodologies based on the multireference second-order perturbation theory have been reported. The complete active space with 2nd order perturbation techniques, such as CASMP2 and CASPT2, uses a second order perturbation to include dynamic correlation effects. In these methods, the standard approach is to run CASMP2(M,N)//CASSCF(M,N) or CASPT2(M,N)//CASSCF(M,N). We have extensively used these methodologies in this thesis through single point calculations on top of the CASSCF optimized geometries.

1.8.2. ONIOM [123-132]

It has been discussed earlier that the use of the CASSCF method and the other post-HF methods are limited by the size of the system. As the size of the system under investigation increases, the computational cost exponentially increases due to the large

number of atoms. To overcome this problem we use hybrid methods. These methods provide a solution to the scaling problem by dividing the system in different parts considering the fact that there is an active site which plays a major role in the reaction. In hybrid methods, different parts of the system are treated with different computational methods. A well-known hybrid method is ONIOM, where an expensive high level quantum mechanical method is combined with a low level quantum mechanical (QM:QM) or with a classical molecular mechanics (QM:MM) method.

The **ONIOM** (**O**ur own **N**-layered **I**ntegrated molecular **O**rbital and molecular **M**echanics) method takes advantage of the fact that specific regions of a system often play key roles in the chemical processes under investigation. This hybrid method treats the region of high-priority of the system which actively participates in a chemical process with an appropriate high-level of theory, while the remaining part of the system is treated with a lower level of theory. In this way, by doing an ONIOM calculation one can minimize the computational cost by giving less importance to the parts of the system which practically remains silent during that particular chemical process. In ONIOM up to three-layered calculations can be done by combining quantum mechanical methods and molecular mechanics. In the present thesis we have performed 2- layered ONIOM calculations which consists of Quantum Mechanical: Quantum Mechanical (QM: QM) type and Quantum Mechanical: Molecular Mechanics (QM: MM) type. The ONIOM energy of a system is obtained through an extrapolation scheme, and mathematically it can be expressed as shown below:

$$E^{ONIOM} = E^{high, model} + E^{low, real} - E^{low, model}$$

Here “real” refers to the full system while “model” is a small fragment of the whole system; “high” and “low” are levels of calculations performed. The high level method is always the better level of quantum mechanical (QM) method; the low-level method is the cheaper one in terms of computational cost. A low level of method can be a Molecular Mechanics (MM) method (eg. UFF), semiempirical method (for example AM1, PM3, etc.) or it can also be a cheaper QM method (like Hartree-Fock). The link atoms are used in ONIOM to saturate the dangling bonds, which together with the high level region forms the model system. Link atom should be placed far away from the region of the primary process under consideration, especially, in the cases where one is combining QM level with MM method. In case, if one is combining two very compatible level of

theories (e.g. QM: QM), the link atom can be close to the reaction center as the errors get cancelled in that process [132].

ONIOM method can be used to explain the excited state potential energy surfaces, as well; the high level of method in that case should be able to analyze the excited state surface (CASSCF used in this thesis). It should be mentioned here that to study the excited state surface by ONIOM, it is important that the excitation must be localized in the model system. The ONIOM excited state energy can be expressed as:

$$E^{*,ONIOM} = E^{*,high, model} + E^{*,low, real} - E^{*,low, model}$$

The excitation energy (ΔE^{ONIOM}) can be written as:

$$\begin{aligned} \Delta E^{ONIOM} &= E^{*,ONIOM} - E^{ONIOM} \\ &= (E^{*,high, model} + E^{*,low, real} - E^{*,low, model}) \\ &\quad - (E^{high, model} + E^{low, real} - E^{low, model}) \\ &= (E^{*,high, model} - E^{high, model}) + (E^{*,low, real} - E^{low, real}) + \\ &\quad (E^{*,low, model} - E^{low, model}) \\ &= \Delta E^{high, model} + \Delta E^{low, real} - \Delta E^{low, model} \end{aligned}$$

As we assumed that the excitation is localized in the model part, we can write $(E^{*,low, real} - E^{*,low, model}) \approx (E^{low, real} - E^{low, model})$. If we substitute this assumption in the above mentioned equation then ΔE^{ONIOM} can be approximated as $\Delta E^{high, model}$.

As already discussed that ONIOM treats different region of system with different level of theory, therefore it is very important to identify the parts where reaction center of the process lies. On the other hand, ONIOM method cannot be applied to those cases where the whole molecule participates in the reaction, as it is very difficult to identify a localized active site in that case. The active part of a system in ONIOM is always treated with an expensive high level method but it is also important that the low level method must be accurate enough to describe the substituent effects [132]. If the role of the low-level region in a process under consideration is purely steric, then a MM or a semi-empirical method can produce satisfactory results; whereas, an appropriate QM method should be used as low level when there are electronic effects between the regions. ONIOM (QM:QM') methods perform best when the two methods are close in hierarchy, for example ONIOM(MP2:HF). An important point should be kept in mind while using

ONIOM (QM:QM') method is that the high level method must be better than the low level method in every aspect. If we use a relatively better low level method then this will result in ONIOM extrapolation in a wrong direction.

Inclusion of electronic embedding scheme can incorporate the partial charges of the MM region into the quantum mechanical Hamiltonian. The electrostatic interaction between the QM and MM regions are considered in a better way by this method and allows the wave function to respond to the charge distribution of the MM region.

1.9. References

1. T. V.-T. Mai, M. v. Duong, X. T. Le, L. K. Huynh and A. Ratkiewicz, *Structural Chemistry*, 2014, **25**, 1495.
2. S. C. Tucker and D. G. Truhlar, *J. Phys. Chem.*, 1989, **93**, 8138.
3. M. A. Robb, M. Garavelli, M. Olivucci and F. Bernardi, *A Computational Strategy for Organic Photochemistry, in Reviews in Computational Chemistry*, Eds., K. B. Lipkowitz and D. B. Boyd, John Wiley & Sons, Inc., New Jersey, USA., 2000.
4. M. L. Mckee and M. Page, *Reviews in Computational Chemistry*, Eds., K. B. Lipkowitz, and D. B. Boyd, VCH Publishers, 1993.
5. J. B. Foresman, M. Head-Gordon, J. A. Pople and M. J. Frisch, *J. Phys. Chem.* 1992, **96**, 135
6. D. G. Truhlar, and M. S. Gordon, *Science*, 1990, **249**, 491.
7. F. Zhang, Y. Ai, Y. Luo and W. Fang, *J. Chem. Phys.*, 2009, **130**, 144315.
8. G. Cui, Y. Ai and W. Fang, *J. Phys. Chem. A*, 2010, **114**, 730.
9. W. Domcke and D. R. Yarkony, *Ann. Rev. Phys. Chem.*, 2012, **63**, 325.
10. T. Mori and T. J. Martínez, *J. Chem. Theo. Comput.*, 2013, **9**, 1155.
11. D. R. Yarkony, *Chem. Rev.*, 2012, **112**, 481.
12. A. H. Zewail, *J. Phys. Chem.*, 1996, **100**, 12701.
13. A. Lauer, A. L. Dobryakov, S. A. Kovalenko, H. Fidler and K. Heyne, *Phys. Chem. Chem. Phys.*, 2011, **13**, 8723.
14. S. Vyas et al., *J. Am. Chem. Soc.*, 2010, **132**, 16796.
15. R. Improta and V. Barone, *Top Curr. Chem.*, 2015, **355**, 329.
16. I. Szydłowska, A. Kyrychenko, A. Gorski, J. Waluk and J. Herbich, *Photochem. Photobiol. Sci.*, 2003, **2**, 187.
17. H. B. Schlegel, *J. Comput. Chem.*, 2003, **24**, 1514.

18. H. P. Hratchian and H. B. Schlegel, *Theory and Applications of Computational Chemistry: The First 40 Years*, Eds., C. E. Dykstra, G. Frenking, K. S. Kim and G. Scuseria, Elsevier, Amsterdam, 2005.
19. H. P. Hratchian and H. B. Schlegel, *J. Chem. Theory Comput.*, 2005, **1**, 61.
20. H. P. Hratchian and H. B. Schlegel, *J. Chem. Phys.*, 2004, **120**, 9918.
21. M. Born and J. R. Oppenheimer, *Annalen der Physik* (in German), 1927, **389**, 457.
22. M. Born and K. Huang, *Dynamic Theory of Crystal Lattice*, Oxford University Press, Oxford, 1954.
23. E. J. Teller, *Phys. Chem.*, 1937, **41**, 109.
24. M. O. Trulson and R. A. Mathies, *J. Phys. Chem.*, 1990, **94**, 5741.
25. S. Pullen, L. A. Walker II, B. Donovan and R. J. Sension, *Chem. Phys. Lett.*, 1995, **242**, 415.
26. P. J. Reid, S. J. Doig, S. D. Wickham and R. A. Mathies, *J. Am. Chem. Soc.*, 1993, **115**, 4754
27. D. R. Cyr and C. C. Hayden, *J. Chem. Phys.*, 1996, **104**, 771.
28. N. J. Turro, V. Ramamurthy and J. C. Scaiano, *Modern Molecular Photochemistry of Organic Molecules*, University Science Books, Sausalito, California, 2010.
29. M. Klessinger and J. Michl, *Excited States and Photochemistry of Organic Molecules*, VCH Publishers Inc., New York, 1995.
30. J. v. Neumann and E. P. Wigner, *Physikalische Zeitschrift*, 1929, **30**, 467.
31. G. Herzberg and H. C. Longuet-Higgins, *Discuss. Farad. Soc.*, 1963, **35**, 77.
32. G. J. Atchity, S. S. Xantheas and K. Ruedenberg, *J. Chem. Phys.*, 1991, **95**, 1862.
33. F. Bernardi, M. Olivucci and M. A. Robb, *Chem. Soc. Rev.*, 1996, **25**, 321.
34. G. Groenhof, M. Boggio-Pasqua, L. V. Schafer and M. A. Robb, *Advances in Quantum Chemistry*, Eds., E. S. Brandas and S. Canuto, Academic Press, San Diego, CA, USA, 2010.
35. A. H. Zewail, *J. Phys. Chem.*, 1996, **100**, 12701.
36. W. Fuß, S. Lochbrunner, A. M. Müller, T. Schikarski, W. E. Schmid and S.A. Trushin, *Chem. Phys.*, 1998, **232**, 161.
37. S. A. Trushin, W. Fuß and W. E. Schmid, *Chem. Phys.*, 2000, **259**, 313.
38. E. W. G. Diau, S. De Feyter and A. H. Zewail, *J. Chem. Phys.*, 1999, **110**, 9785.
39. M. Chachisvilis and A. H. Zewail, *J. Phys. Chem. A*, 1999, **103**, 7408.
40. D. Zhong, E. W. G. Diau, T. M. Bernhardt, S. De Feyter, J. D. Roberts and A. H. Zewail, *Chem. Phys. Lett.*, 1998, **298**, 129.

41. J. M. Metsdag, J. P. Visicot, M. Elhanine and B. Soep, *J. Chem. Phys.*, 2000, **113**, 237.
42. A. Nenov, W. J. Schreier, F. O. Koller, M. Braun, R. de Vivie-Riedle, W. Zinth and I. Pugliesi, *J. Phys. Chem. A.*, 2012, **116**, 10518.
43. B. C. Arruda and R. J. Sension, *Phys. Chem. Chem. Phys.*, 2014, **16**, 4439.
44. A. Migani and M. Olivucci, *Conical Intersections: Electronic Structure, Dynamics & Spectroscopy Advanced series in Physical Chemistry*, Eds., W. Domcke, D. R. Yarkony and H. Koppel, World Scientific Publishing Co.(P). Ltd, Singapore, 2004.
45. M. D. Su, *Chemistry*, 2007, **13**, 9957.
46. S. Wilsey and K. N. Houk, *J. Am. Chem. Soc.*, 2000, **122**, 2651.
47. M. Olivucci, F. Bernardi S. Ottani and M. A. Robb, *J. Am. Chem. Soc.*, 1994, **116**, 2034.
48. M. Reguero, F. Bernardi, H. Jones, M. Olivucci, I. N. Ragazos and M. A. Robb, *J. Am. Chem. Soc.*, 1993, **115**, 2073.
49. H. Jansen, J. C. Slootweg and K. Lammertsma, *Beilstein J. Org. Chem.*, 2011, **7**, 1713.
50. F. Bernardi, M. Olivucci, and M. A. Robb, *Acc. Chem. Res.*, 1990, **23**, 405.
51. J. J. Serrano-Pérez, M. J. Bearpark and M. A. Robb, *Molecular Physics*, 2012, **110**, 2493.
52. W. Fuß, *J. Photochem. Photobio. A: Chemistry*, 2012, **237**, 53.
53. D. S. Ruiz, A. Cembran, M. Garavelli, M. Olivucci, and W. Fuß, *Photochem. Photobio.*, 2002, **76**, 622.
54. M. Garavelli, B. R. Smith, M. J. Bearpark, F. Bernardi, M. Olivucci, and M. A. Robb, *J. Am. Chem. Soc.*, 2000, **122**, 5568.
55. O. Tishchenko, D. G. Truhlar, A. Ceulemans and M. T. Nguyen, *J. Am. Chem. Soc.*, 2008, **130**, 7000.
56. A. Chattopadhyay, *J. Chem. Sci.*, 2012, **124**, 985.
57. A. Cembran, F. Bernardi, M. Olivucci, and M. Garavelli, *Proc. Natl. Acad. Sci. USA*, 2005, **102**, 6255.
58. A. Sanchez-Galvez, P. Hunt, M. A. Robb, M. Olivucci, T. Vreven and H. B. Schlegel, *J. Am. Chem. Soc.*, 2000, **122**, 2911.
59. Q. Li, D. Mendive-Tapia, M. J. Paterson, A. Migani, M. J. Bearpark, M. A. Robb, and L. Blancafort, *Chem. Phys.*, 2010, **377**, 60.

-
60. I. J. Palmer, I. N. Ragazos, F. Bernardi, M. Olivucci and M. A. Robb, *J. Am. Chem. Soc.*, 1993, **115**, 673.
 61. M. J. Bearpark, F. Bernardi, S. Clifford, M. Olivucci, M. A. Robb, B. R. Smith and T. Vreven, *J. Am. Chem. Soc.*, 1996, **118**, 169.
 62. M. Boggio-Pasqua, M. J. Bearpark, P. A. Hunt, and M. A. Robb, *J. Am. Chem. Soc.*, 2002, **124**, 1456.
 63. P. Foggi, F. V. R. Neuwahl, L. Moroni and P. R. Salvi, *J. Phys. Chem. A*, 2003, **107**, 1689.
 64. O. Deeb, S. Cogan and S. Zilberg, *Chem. Phys.*, 2006, **325**, 251.
 65. Q. Li and L. Blancafort, *Chem. Comm.*, 2013, **49**, 5966.
 66. A. Yabushita, T. Kobayashi and M. Tsuda, *J. Phys. Chem. B*, 2012, **11**, 1920.
 67. D. P. Aalberts, F. L. J. Vos, and W. v. Saarloos, *Pure & App. Chem.*, 1997, **69**, 2099.
 68. P. J. M. Johnson, A. Halpin, T. Morizumi, L. S. Brown, V. I. Prokhorenko, O. P. Ernst and R. J. D. Miller, *Phys. Chem. Chem. Phys.*, 2014, **16**, 21310.
 69. S. Schenkl, F. v. Mourik, N. Friedman, M. Sheves, R. Schlesinger, S. Haacke and M. Chergui, *Proc. Natl. Acad. Sci. USA*, 2006, **103**, 4101.
 70. P. C. Mowery and W. Stoeckenius, *Biochemistry*, 1981, **20**, 2302.
 71. K. C. Hasson, F. Gai and P. A. Anfinrud, *Proc. Natl. Acad. Sci. USA*, 1996, **93**, 15124.
 72. D. Polli, and P. Altoè, *Nature*, 2010, **467**, 440.
 73. M. M. Huntress et al., *J. Phys. Chem. B*, 2013, **117**, 10053.
 74. J. P. Malhado, R. Spezia and J. T. Hynes, *Inter. J. Quant. Chem.*, 2013, **113**, 296.
 75. S. Gozem, M. Huntress, I. Schapiro, R. Lindh, A. Granovsky, C. Angeli, and M. Olivucci, *J. Chem. Theory Comput.*, 2013, **9**, 4495.
 76. S. Gozem, A. I. Krylov and M. Olivucci, *J. Chem. Theory Comput.*, 2013, **9**, 284.
 77. B. L. Vukovic, C. F. Burmeister, P. Kral and G. Groenhof, *J. Phys. Chem. Lett.*, 2013, **4**, 1005.
 78. I. Conti and M. Garavelli, *J. Photochem. Photobio. A: Chem.*, 2007, **190**, 258.
 79. M. Garavelli, *Theo. Chem. Acc.*, 2006, **116**, 87.
 80. V. Balogh-Nair and K. Nakanishi, *Pharm. Res.*, 1984, **1**, 93.
 81. H. Feuer, *Nitrile Oxides, Nitrones, and Nitronates in Organic Synthesis*, John Wiley & Sons, Inc., Hoboken, New Jersey. 2008.
 82. M. A. Saliva and J. M. Goodman, *Tetrahedron*, 2002, **58**, 3667.

-
83. K. V. Gothelf and K. A. Jørgensen, *Chem. Rev.*, 1998, **98**, 863.
 84. Z. Baoxiang, *Progress in Chemistry*, 2000, **12**, 77.
 85. R. A. Floyd, R. D. Kopke, C.-H. Choi, S. B. Foster, S. Doblas and R. A. Towner, *Free Radical Biol. Med.*, 2008, **15**, 1361.
 86. R. A. Floyd, K. Hensley, M. J. Forster, J. A. Kelleher-Anderson and P. L. Wood, *Mech. Ageing Dev.*, 2002, **123**, 1021.
 87. R. A. Floyd, H. C. C. F. Neto, G. A. Zimmerman, K. Hensley and R. A. Towner, *Free Radical Biol. Med.*, 2013, **62**, 145.
 88. A. Samadi et al., *Bioorg. Med. Chem.*, 2011, **19**, 951.
 89. M. Chioua et al., *J. Med. Chem.*, 2012, **55**, 153.
 90. R. A. Floyd et al., *Free Radical Res.*, 2010, **44**, 108.
 91. B. Guo, D. Xu, H. Duan, J. Du, Z. Zhang, S. M. Lee and Y. Wang, *Biol. Pharm. Bull.*, 2014, **37**, 274.
 92. R. A. Floyd, H. K. Chandru, T. He and R. Towner, *Anti-Cancer Agents Med. Chem.*, 2011, **11**, 373.
 93. P. Astolfi, P. Carloni, M. G. Marini, G. Mobbili, M. Pisani and P. Stipa, *RSC Adv.*, 2013, **3**, 22023.
 94. X. Song, Y. Qian, R. Ben, X. Lu, H.-L. Zhu, H. Chao and J. Zhao, *J. Med. Chem.*, 2013, **56**, 6531.
 95. J. S. Splitter and M. Calvin, *J. Am. Chem. Soc.*, 1965, **30**: 3427.
 96. J. S. Splitter, T.-M. Su, H. Ono and M. Calvin, *J. Am. Chem. Soc.*, 1971, **93**, 4075.
 97. K. Koyano and I. Tanaka, *J. Phys. Chem.* 1965, **69**, 2545.
 98. E. Lipczynska-Kochany and J. Kochany, *J. Photochem. Photobiol. A*, 1988, **45**, 65.
 99. D. R. Boyd, W. B. Jennings, R. Spratt and D. M. Jerina, *J. Chem. Soc. D: Chem. Comm.*, 1970, 745.
 100. R. M. Aminova and E. Ermakova, *Chem. Phys. Lett.*, 2002, **359**, 184.
 101. T. Arlt, S. Schmidt, W. Zinth, U. Haupts and D. Oesterhelt, *Chem, Phys. Lett.*, 1995, **241**, 559
 102. D. Xu, C. Martin and K. Schulten, *J. Biophys.*, 1996, **70**, 453
 103. J. E. Norton and K. N. Houk, *Mol. Phys.*, 2006, **104**, 993.
 104. I. Conti, F. Bernardi, G. Orlandi and M. Garavelli, *Mol. Phys.*, 2006, **104**, 915.
 105. C. J. Cramer, *Essentials of Computational Chemistry, Theories and Models*, John Wiley & Sons Ltd, England, 2004

-
106. F. Jensen, *Introduction to Computational Chemistry*, John Wiley & Sons Ltd, England, 1999.
 107. K. Raghavachari, H. B. Schlegel, and J. A. Pople, *J. Chem. Phys.*, 1980, **72**, 4654.
 108. K. Raghavachari and J. A. Pople, *Int. J. Quant. Chem.*, 1981, **20**, 1067.
 109. B. O. Roos, *Advances in Chemical Physics: Ab Initio Methods in Quantum Chemistry Part II*, Ed., K. P. Lawley, John Wiley & Sons, Inc., New Jersey, USA, 1987.
 110. A. Szabo and N. S. Ostlund, *Modern Quantum Chemistry: Introduction to Advanced Electronic Structure Theory*, Dover Publications Inc., Mineola, 1996.
 111. I. N. Levine, *Quantum Chemistry*, Pearson Education Inc., New Jersey, USA, 2014.
 112. P. E. M. Siegbahn, J. Almlöf, A. Heiberg and B. O. Roos, *J. Chem. Phys.*, 1981, **74**, 2384
 113. D. Hegarty and M. A. Robb, *Mol. Phys.* 1979, **38**, 1795.
 114. R. H. A. Eade and M. A. Robb, *Chem. Phys. Lett.*, 1981, **83**, 362.
 115. H. B. Schlegel and M. A. Robb, *Chem. Phys. Lett.*, 1982, **93**, 43.
 116. F. Bernardi, A. Bottini, J. J. W. McDougall, M. A. Robb and H. B. Schlegel, *Far. Symp. Chem. Soc.*, 1984, **19**, 137.
 117. M. J. Frisch, I. N. Ragazos, M. A. Robb and H. B. Schlegel, *Chem. Phys. Lett.*, 1992, **189**, 524.
 118. N. Yamamoto, T. Vreven, M. A. Robb, M. J. Frisch and H. B. Schlegel, *Chem. Phys. Lett.*, 1996, **250**, 373.
 119. M. J. Bearpark, F. Ogliaro, T. Vreven, M. Boggio-Pasqu, M. J. Frisch, S. M. Larkin, M. Morrison and M. A. Robb, *J. Photochem. Photobiol. A*, 2007, **190**, 207.
 120. J. F. Arenas, J. I. Marcos, J. C. Otero and A. Sanchez-Galvez, *J. Chem. Phys.*, 1999, **111**, 551.
 121. K. Andersson, P.-Å. Malmqvist, B. O. Roos, A. J. Sadlej, and K. Wolinski, *J. Phys. Chem.*, 1990, **94**, 5483.
 122. K. Andersson and B. O. Roos, *Int. J. Quant Chem.*, 1993, **45**, 591.
 123. S. Dapprich, I. Komáromi, K. S. Byun, K. Morokuma and M. J. Frisch, *Mol. Struct. (Theochem.)*, 1999, **462**, 1.
 124. T. Vreven, K. S. Byun, I. Komáromi, S. Dapprich, J. A. Montgomery Jr., K. Morokuma and M. J. Frisch, *J. Chem. Theory Comput.*, 2006, **2**, 815.
 125. T. Vreven and K. Morokuma, *Ann. Rep. Comput. Chem.*, 2006, **2**, 35.

126. T. Vreven, K. Morokuma, O. Farkas, H. B. Schlegel and M. J. Frisch, *J. Comput. Chem.*, 2003, **24**, 760.
127. M. J. Bearpark et al., *J. Photochem. Photobiol. A: Chem.*, 2007, **190**, 207.
128. M. J. Bearpark, S. M. Larkin and T. Vreven, *J. Phys. Chem. A*, 2008, **112**, 7286.
129. T. Vreven and K. Morokuma, *Theo. Chem. Acc.*, 2003, **109**, 125.
130. I. Geronimo and P. Paneth, *Phys. Chem. Chem. Phys.*, 2014, **16**, 13889.
131. A. Bhattacharya and E. R. Bernstein, *J. Phys. Chem. A*, 2011, **115**, 4135.
132. F. R. Clemente, T. Vreven and M. J. Frisch, *Quantum Biochemistry*, Ed., C. F. Matta, Wiley-VCH Verlag GmbH & Co. KGaA, Weinheim, Germany, 2010.

CHAPTER 2

A computational study of the photochemistry of some retinylnitrones and their model compounds with electron-donating groups on nitrogen**2. 1. Introduction**

The photo-irradiation process of nitrones has been the subject of interest since last several decades. The fundamental studies on *cis-trans* isomerizations [1, 2] of nitrones and their conversion to oxaziridines [3, 4] were carried out long back. It was found that the types of substituents present on nitrogen and carbon (of C=N) play a vital role in the stability of the oxaziridine ring and its nature of cleavage. In fact, it was found that experimentally isolable and stable oxaziridines contain alkyl groups on either or both nitrogen and carbon atoms. On the other hand, presence of aryl groups on both these atoms was found to decrease their stability significantly.

In past, several research groups [5-16] have reported structural and spectral aspects of various substituted nitrones through quantum mechanical [12-15] and molecular dynamics [16] studies. However, most of these studies were related to the ground state aspects of nitrone systems. To explore the properties of nitrone excited states and subsequently their photochemistry, we had started our work with some experimentally reported long chain conjugated nitrone systems those were known to give stable oxaziridines on photo-irradiation. These long-chain nitrones were synthesized and studied by Balogh-Nair et al. [17] in the last century. These synthesized retinoids with polar nitrone groups were found to be chemopreventive in nature. Their role in the reduction of neoplasia (caused due to the deficiency of vitamin A) and participation in controlling epithelial cell differentiation (*in vitro*) were observed. These retinylnitrones were reported to be effective in reversing the keratinisation in hamster tracheal organ cultures. The *N*-methyl derivative of retinylnitrone was found to be of highest activity, almost matching the activity of all-*trans* retinoic acid; at room temperature this methyl derivative was found to be stable in the dark. Its methanol solution was found to convert slowly to the corresponding oxaziridine when exposed to room light and reversibly back to the nitrone under dark (Figure 2-1). In fact, almost all *N*-substituted nitrones studied by them were light sensitive and more or less of similar nature. Unlike many other nitrones, the *N*-alkyl derivative of these nitrones and their oxaziridines were reported to be of better stabilities. The *N*-methyl retinyl nitrone was found to give [17] isolable

oxaziridine. It is quite obvious that, the low-lying electronic states are responsible for their light-sensitized properties. However, the spectroscopic features of the low-lying electronic states of such conjugated nitron systems were not studied previously.

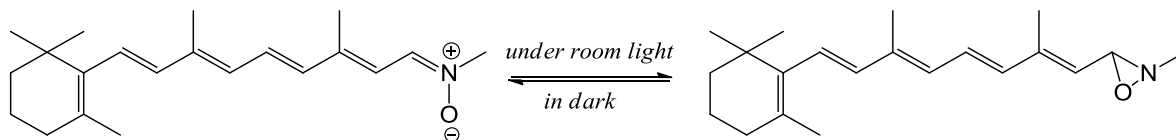


Figure 2-1: Photo-conversion of *N*-methyl retinyl nitron to oxaziridine and reverse conversion to the parent nitron in dark

The work presented in this chapter is a thorough investigation of the mechanism of the photo-excitation process of conjugated long-chain nitron systems by revealing the nature of their excited electronic states. In the first part of this chapter we have discussed the electronic properties of the model compounds of *N*-alkyl retinyl nitron systems, studied at high level of quantum mechanical theories (Figure 2-2a). In the latter part, we have discussed the ONIOM based QM:QM and QM:MM studies on the 13-*trans* and 13-*cis* isomers of *N*-alkyl retinyl nitrones (Figure 2-2b), which has revealed the active role of the terminal CNO moiety in their photochemical oxaziridine conversion process. Results described in the present chapter have been published [18, 19].

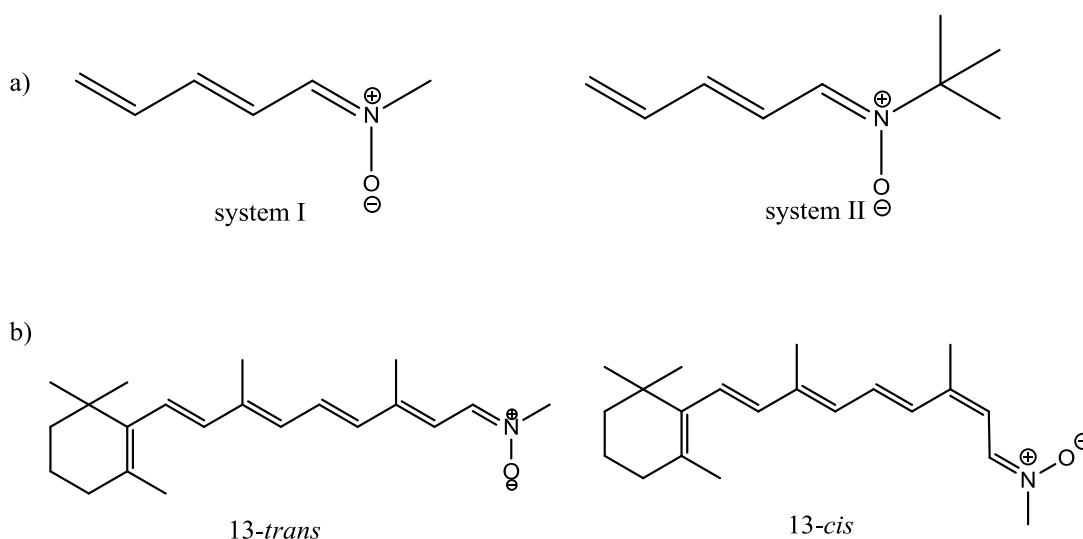


Figure 2-2: Structures of (a) studied model systems of methyl (system I) and isopropyl-substituted (system II) retinyl nitrones, (b) 13-*trans* and 13-*cis* isomer of *N*-methyl retinyl nitron studied at hybrid ONIOM methods.

The main objective of this part of our work was to explore the nitron-oxaziridine conversion mechanism of the above-mentioned alkyl-substituted nitron systems.

However, the expected outcome of this work may have far reaching consequences in terms of revealing the actual photo-excitation mechanism of several other nitron systems, too.

2. 2. Computational details

This present chapter reports computational studies of the low-lying electronic states of the above-mentioned retinyl nitron molecules and their model systems based on *ab initio*, semi-empirical and hybrid techniques. The calculations reported in this chapter were mostly carried out using the Gaussian 09 suite of programs [20] and for visualizing results, ChemCraft [21] and GaussView softwares had been used.

The ground and the first excited singlet states of the model systems were analyzed using the Complete Active Space Self-Consistent Field (CASSCF) method in Gaussian 09 and configuration interaction calculations with semiempirical-based PM3 Hamiltonian (PM3/CI) in MOPAC. The CASSCF method was employed for locating the minimum energy geometries, transition states and conical intersection points on the potential energy surfaces (PES). For optimizing the ground and excited state equilibrium geometries of the model systems (Figure 2-2a), CASSCF/6-31G* methods [22-31] with both (6,6) and (4,4) active space varieties had been used; however, for the conical intersections, transition states and oxaziridine geometry optimizations, the (4,4) active space was chosen. It is a well-known fact that there is no correct single active space in a molecule; for the same molecule active space choice can be different depending on the type of reaction we are studying [32]. In the present studies, this choice of smaller active space was done based on the chemical intuition looking at the reported experimental results of *N*-alkyl retinyl nitrones [17].

Along with the density functional theory (DFT) and restricted Hartree-Fock (RHF) theory, the 2-layer hybrid ONIOM calculations were used to optimize the ground state geometries of the two isomeric forms of retinyl nitron systems (Figure 2-2b). However, for optimizing the conical intersection geometries and the oxaziridine ground states, the hybrid method has been only employed. As discussed in detail in chapter 1, the basic idea behind ONIOM method is to treat the active zone of a system (where the chemical process is actually happening) with a better level of quantum mechanical (QM) theory, while the less important portions of the system can be treated with molecular mechanics (MM) or lower-level of QM (QM') theories. In the ONIOM extrapolation scheme the total energy can be expressed as:

$$E_{\text{ONIOM(QM:QM'/MM)}} = E^{\text{high(QM), model}} + E^{\text{low(QM'/MM), real}} - E^{\text{low(QM'/MM), model}}$$

where, real = the whole system, model = core region of interest.

The 2-layer ONIOM calculations [32-40] with both QM:QM' and QM:MM methodologies were used for studying retinyl nitrone systems, where the CASSCF/6-31G* was used as the higher level method and the lower level methods were varied. RHF method as the lower-level with STO-6G, STO-3G, 4-31G and 6-31G basis sets were used. For the lower-level, Moller-Plesset perturbation theory (MP2), density functional theory (B3LYP/6-311G*) and semiempirical methods (PM3, PM6, AM1) were also tested. The active region of these systems (Figure 2-3) were varied with the appropriately chosen corresponding active spaces, such as (8,8), (6,6) and (4,4). Keeping the higher level fixed to CASSCF (4,4) /6-31G* on the CNO model part, the QM:MM calculations were done. In this study the molecular mechanics (UFF) method using both with and without electronic embedding (EE) schemes were employed at the lower-level. The inclusion of EE scheme incorporates the partial charges of the MM region into the quantum mechanical region which gives better electrostatic interactions between the QM and MM regions, and this eventually had produced the similar nitrone-oxaziridine conversion path as predicted by the CASSCF:HF method (discussed in detail in latter portions).

For both the model systems and the actual retinyl nitrone systems, dynamic correlation effect of MP2 level was included through single point calculations on top of the CASSCF/6-31G* optimized points. The 'nocpmcscf' option was used for conical intersection (S_0/S_1) optimization, which excludes the orbital rotation derivative. For locating the transition states STQN-based QST2 methodology [41,42] and the normal TS techniques based on the Berny-algorithm [43] had been employed. Intrinsic reactions coordinate (IRC) calculations [44-46] were performed on optimized transition state structures to follow their minimum energy path.

Some semiempirical-based CI treatment has been also performed on the model systems where NDDO-based PM3 [47,48] Hamiltonian has been used in the multielectron configuration interaction technique (MECI). Considering the fact that the first excited singlet state (S_1) might be having both ionic and biradical contributions in these nitrones, the second CI root was analyzed by using both with and without biradical options as the keywords in the input file of PM3/CI calculations in MOPAC.

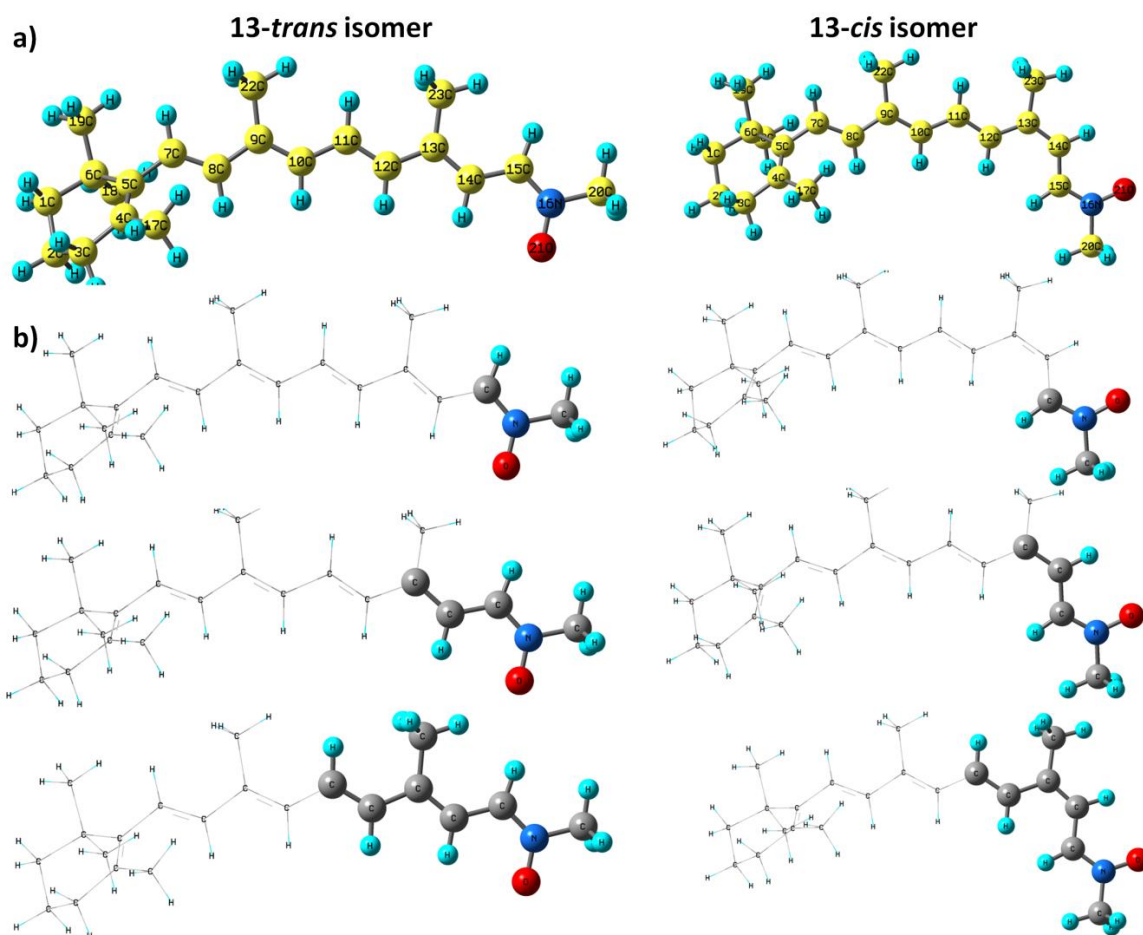


Figure 2-3: **a)** Structures of the studied nitrones (13-*trans* and 13-*cis* isomer) and **b)** the different high-level and low-level portions used in the ONIOM calculations. Portions on which high level calculations were carried out are shown in ball-and-stick and the low level regions are shown in wireframe.

In addition to these calculations, GUGA-based CISD technique had also been used for some other important calculations through the GAMESS [49-53] suite of programs. Based on this GUGA CI code, the radiative transition properties (transition moment, oscillator strength) [54-56] were calculated. Radiative lifetime of the first excited singlet state was determined from the Einstein's coefficient, A_{21} . Einstein's coefficient (A_{21}) and oscillator strength values were obtained from the output of the transition moment calculations. Electrostatic potential-based atomic charges had been calculated for the ground and excited state species using the Merz-Kollman [57,58] scheme in Gaussian 09.

2.3. SECTION 1: Model compounds of the *N*-alkyl retinylnitron

In this section we have discussed the possible oxaziridine photo-conversion mechanism of the model systems of *N*-alkyl retinylnitrones which has been explored through quantum mechanical investigations. The chosen conjugated nitron systems (shown in

Figure 2-2a) have methyl (system I) and isopropyl (system II) groups on the nitrogen. Choice of such shorter conjugated chain systems (without the extended conjugated part and the β -ionone ring) as the model for the retinyl systems is quite common for the photochemistry studies of retinyl iminium ions. Our choice of these small-chain conjugated nitrones as the model compounds has been justified by the similar results obtained from the photochemical investigations on these model systems and the whole retinyl nitron systems (discussed in next section of this chapter).

2.3.1. Results and discussion

A) Important points on the potential energy surface

a) Results of semiempirical-based Configuration Interaction calculations

The semiempirical-based Configuration Interaction (PM3/CI) calculations were done in the beginning to get a prior idea of the reaction path before exploring it through high level CASSCF method. It is quite obvious that semiempirical level of calculation is far from the reality; however, sufficient hint was given by these studies to make an initial guess of the photo-excitation processes of these unexplored systems, and helped us to finally clarify the results obtained from the CASSCF and CASMP2 level of theories.

The level of PM3/CI calculations employed were of 2×2 (2 pi electrons in 2 orbitals) type and as expected they predicted geometry of poor quality; however, they had given some interesting results.

- Two non-planar excited state geometries of ionic (**B₁**) and biradical (**B₂**) nature were obtained (Figure 2-4). These states were found to be more stable than the planar excited states.
- A lowering of negative charge on oxygen was noticed as we move from ground state to the planar excited state (Table 2-1), which continues in the stable non-planar forms.
- In case of the biradical (**B₂**) form, the ESP-derived charges indicate the presence of a lone pair on nitrogen, an odd electron on C5 and a reduced electronic cloud on oxygen.

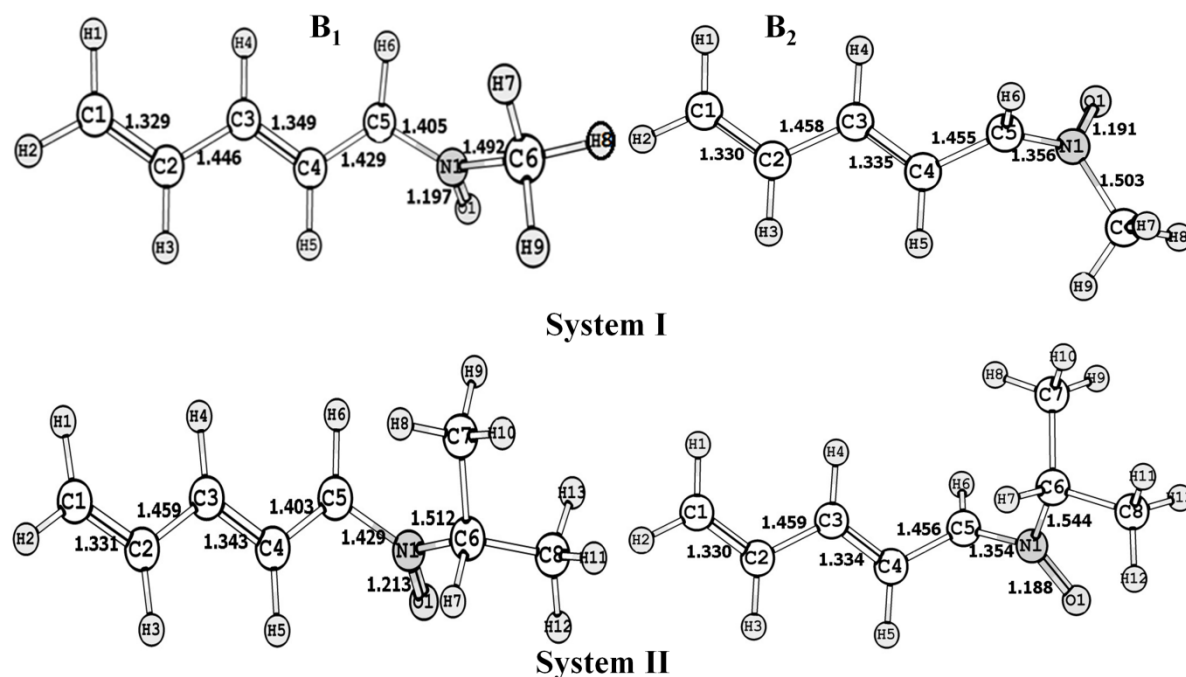


Figure 2-4: Non-planar excited state geometries (\mathbf{B}_1 and \mathbf{B}_2) of system I and II at the PM3/CI level of calculations.

Table 2-1: Atomic charges of important atoms determined from the electrostatic potential at PM3/CI level.

System	Atom	Ground State	Planar excited state	Non-planar \mathbf{B}_1 state	Non-planar \mathbf{B}_2 state
I	C(5)	-0.5363	-0.5731	-1.1853	-0.3221
	N	0.8584	0.8482	1.2114	0.5141
	C(7)	-0.4954	-0.5026	-0.6119	-0.3269
	O	-0.5248	-0.4695	-0.3691	-0.4458
II	C(5)	-0.5902	-0.6603	-1.1681	-0.3433
	N	0.7609	0.7853	1.1321	0.4731
	C(7)	-0.0173	-0.0558	-0.1660	-0.0093
	O	-0.4987	-0.4372	-0.3446	-0.4338

Interestingly, the deviations from the planarity of the \mathbf{B}_1 and \mathbf{B}_2 structures had some resemblance to the one-bond-flip (OBF) and the Hula-twist (HT) motions, respectively. The turn in \mathbf{B}_1 was similar to the ionic excited state rotation (OBF) of the protonated Schiff base (PSB) iminium systems, while the nature of the geometry of the \mathbf{B}_2 species resembled with the out-of-plane H-bridge-type (here oxygen-bridge) geometry, normally seen in the biradical excited state of the neutral conjugated polyene systems. During optimization of \mathbf{B}_1 , the movement of the *N*-terminal part of the C–N bond stopped at the geometry where the N–O bond was twisted to 90° from the initial plane without any significant movement of the *C*-terminal part and looks like TICT-CI geometry. On the

other hand, the twist in **B**₂ was found to be identical to the half-way HT motion. An initial electron transfer from oxygen to nitrogen (Table 2-1) was observed, and this feature was found to be responsible for triggering the whole photochemical process. These rough estimations of the photo-excitation process from semiempirical calculations had helped us enormously to progress further in our subsequent higher-level calculations based on CASSCF methodologies.

b) Results of *ab initio* calculation

i) Optimized ground states and first singlet excited states

There are five canonical forms of nitrene; three of them are ionic structures (I, II and III) (Figure 2-5) and two are non-ionic (IV and V) in nature. The zwitterionic form (I) dominates the ground states (S_0) of the studied nitrene systems and this is evidenced by their optimized ground state geometries (Table 2-2) from both *ab initio* and semi-empirical level of studies.

It was found that the HOMO² configuration dominates these states. On the other hand, the planar first excited singlet state was found to have minor contribution from the

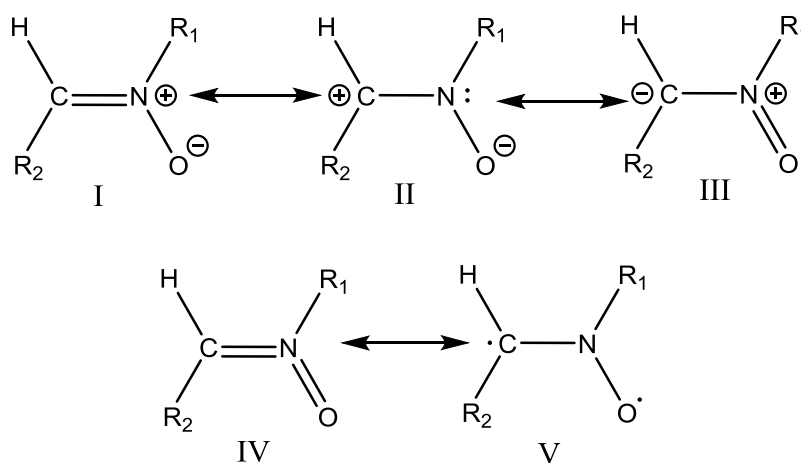


Figure. 2-5: Possible ionic (I-III) and non-ionic (IV-V) canonical forms of nitrene systems

zwitterionic form (I), which was confirmed by substantial increase in the C5–N bond length (Figure 2-6). A mixture of configurations primarily arising due to the HOMO-1 → LUMO and HOMO² → LUMO² excitations with a significantly leading contribution from the latter one was found in the planar first excited singlet state (S_1 state) (Figure 2-6). Some minor contributions of HOMO → LUMO and other configurations were also noticed in this state. It should be mentioned here that the nature of the ground state of nitrene systems were first predicted by Komaromi et al. [13] at the CASSCF level of study. However, the excited singlet state structures had not been analyzed much, except

for few studies [12]. Our detailed analysis [18] of the excited state topography (presented in the subsequent portions of this chapter) had clearly shown the possible involvement of the biradical form in the oxaziridine formation process.

Table 2-2: Structural parameters of the optimized ground state geometries of system I and II at various level of calculations. Reported bond lengths are in angstrom (Å).

System	Method	C3–C4	C4–C5	C5–N	N–O	N–C6
I	CASSCF/6-31G* ^a	1.330	1.451	1.276	1.265	1.459
	CASSCF/6-31G* ^b	1.330	1.451	1.309	1.253	1.461
	RHF /6-311G**	1.328	1.451	1.276	1.271	1.459
	PM3 /CI	1.347	1.436	1.351	1.245	1.501
II	CASSCF/6-31G* ^a	1.331	1.452	1.307	1.299	1.479
	CASSCF/6-31G* ^b	1.349	1.453	1.301	1.271	1.482
	RHF /6-311G**	1.328	1.450	1.275	1.271	1.503
	PM3 /CI	1.348	1.434	1.351	1.242	1.534

^a(4,4) and ^b(6,6) CASSCF level of theories

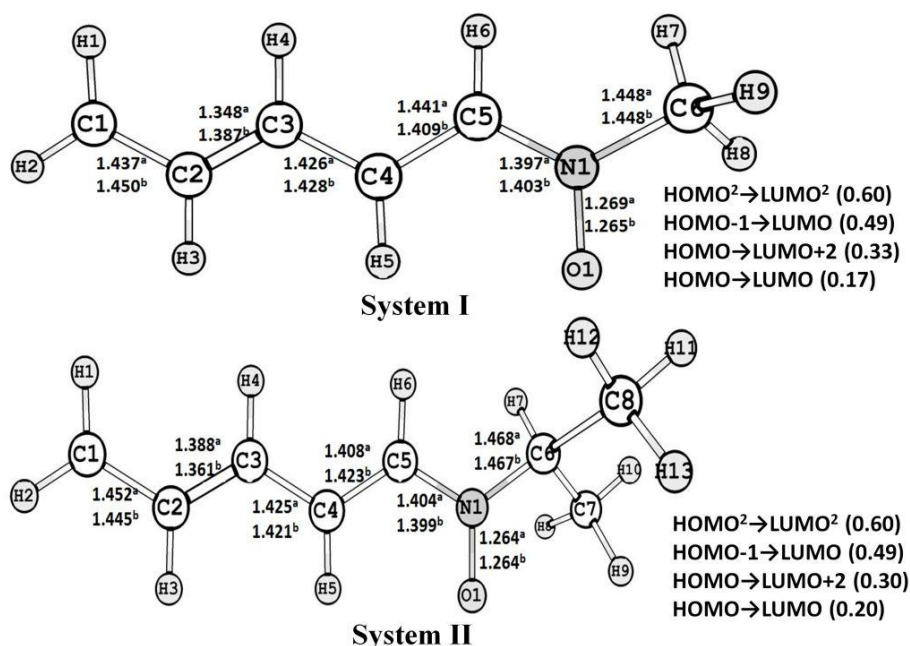


Figure 2-6: Optimized excited state geometries (A) of system I and II at the CASSCF/6-31G* ^a(4,4) and ^b(6,6) level of theories with dominant configurations at the respective geometries.

ii) Conical intersections at higher energies than planer excited state

Our preference for using the (4, 4) active space for this part of calculation is required to be discussed at this point. The choice of the relevant molecular orbitals in a CAS space requires some amount of prior knowledge of that particular system to be investigated. In

this present work, the choice of a (4,4) active space was influenced by the chemical intuition which was based on the observations from the experimental photochemical study done on the retinyl nitron systems. These experimental studies [17] had shown that the conjugated nitron system experiences a twist at the terminal CNO moiety to form oxaziridine with no effect on the conjugated chain part. A similar twist of the CNO moiety was also experienced by us, especially in the biradical \mathbf{B}_2 geometry, during the PM3/CI level of calculations (discussed in the previous section). Based on these experimental and PM3/CI results, the possible reaction path of this photochemical process can be predicted as shown in Figure 2-7.

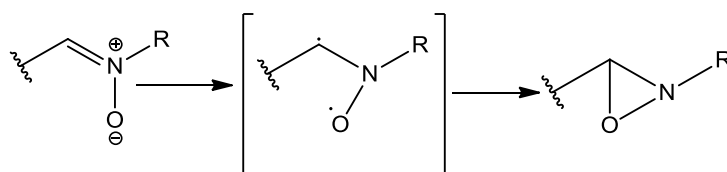


Figure 2-7: A possible scheme of nitron to oxaziridine conversion

The involvement of a C–N π bond (breaking of π bond) and p_z orbital (holding the negative charge on oxygen which is partly shifted towards N afterwards) seems to occur in the initial step of the photo-isomerization process, which results in a C–N σ bond and a possible C–O bond (probably through a transient biradical species) after photo-excitation; this finally leads to oxaziridine. Following this intuition we have chosen a possible appropriate active space of (4,4) size consisting of HOMO-1, HOMO, LUMO and LUMO+1 (Figure 2-8) orbitals. The HOMO (MO No. 30) consists of π symmetry on the CNO moiety while the LUMO (MO No. 31) is having the corresponding π^* symmetry. On the other hand, the HOMO-1 is of σ symmetry on the same moiety and the LUMO+1 has σ^* symmetry. So basically our process was biased towards the possible reaction path and we had tried to make an accurate minimal choice of the active space leaving out the less important extended conjugated side which probably has no role to play in the studied reaction. It is quite obvious that for some other process of these conjugated nitrons, this chosen active space may not be accurate; however, for the oxaziridine conversion process, this choice of smaller active space, centered on the CNO moiety was found to be quite satisfactory. The CASSCF and CASMP2 energy values calculated with the (4,4) active space for different geometries are reported in Table 2-3. It must be added here that higher active spaces were also tested for the whole process; however, they were unable to produce the oxaziridine type twist at the terminal CNO part which confirmed the fact that our initial intuition was correct.

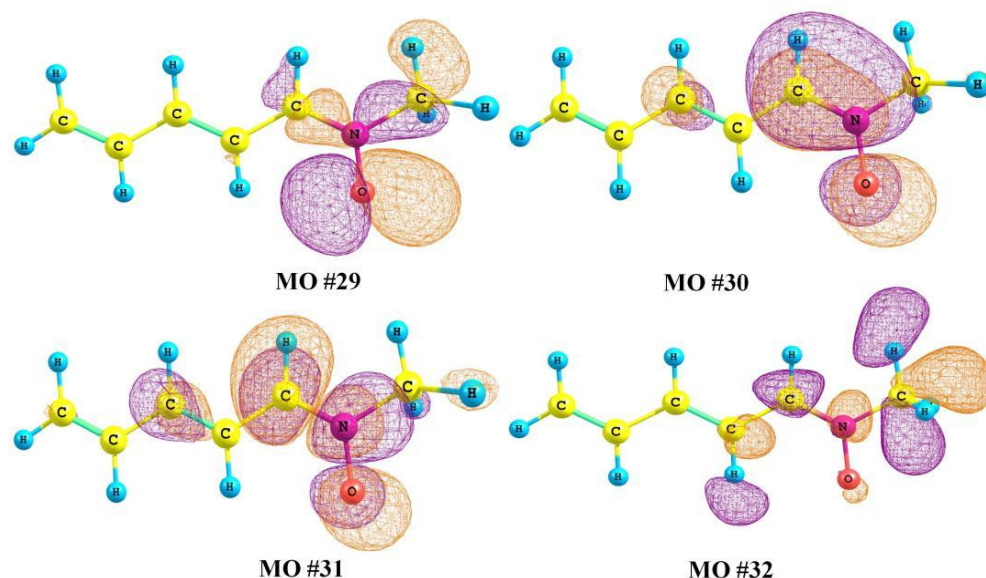


Figure 2-8: Molecular Orbitals involved in the CAS(4, 4) active space calculations for the methyl nitron (system I).

Table 2-3: Absolute energy values (E) in Hartree and relative energy values (ΔE) in kcal/mol (with respect to the planar excited states) at various important geometries on the potential energy surfaces

Molecular geometry	System I				System II			
	CASSCF		CASMP2		CASSCF		CASMP2	
	E	ΔE	E	ΔE	E	ΔE	E	ΔE
GS	-361.6645	-78.08	-362.7609	-97.28	-439.7373	-76.72	-441.1186	-101.39
ES	-361.5401	0	-362.6058	0	-439.6150	0	-440.9570	0
CI₁	-361.5322	4.95	-362.6013	2.88	-439.6059	5.71	-440.9521	3.10
CI₂	-361.5347	3.40	-362.6084	-1.59	-439.6072	4.91	-440.9586	-0.95
CI₃	-361.5337	4.02	-362.6063	-0.32	-439.6085	4.06	-440.9574	-0.21
CI₄	-361.5653	-15.81	-362.6299	-15.08	–	–	–	–
CI₅	-361.5692	-18.21	-362.6523	-29.15	–	–	–	–
Ox₁	-361.6440	-65.17	-362.7259	-75.36	–	–	–	–
Ox₂	-361.6408	-63.16	-362.7347	-80.36	–	–	–	–

The PM3/CI calculation-based optimized geometries (**B₁** and **B₂**) were taken as the initial guess structures for the conical intersection (CI) [59-61] optimization, considering the fact that probability of finding both OBF-type CI and Hula-twist-type CI were there in these systems. In each case, S_0/S_1 conical intersection points (**CI₁** and **CI₂**) were found at the CASSCF (4,4) /6-31G* level of theory (Figure 2-9a and 2-9b). A closer examination of the ESP-charges (Table 4) of the optimized excited state geometry (**A**) and the ground state gives enough reason for the existence of both these types of CIs. There is a clear indication of the biradical mode of charge separation in the excited states; however,

some ionic contribution is also present. This fact was further supported by the presence of mixed contributions from the ionic and biradical configurations in the planar excited states (Figure 2-6).

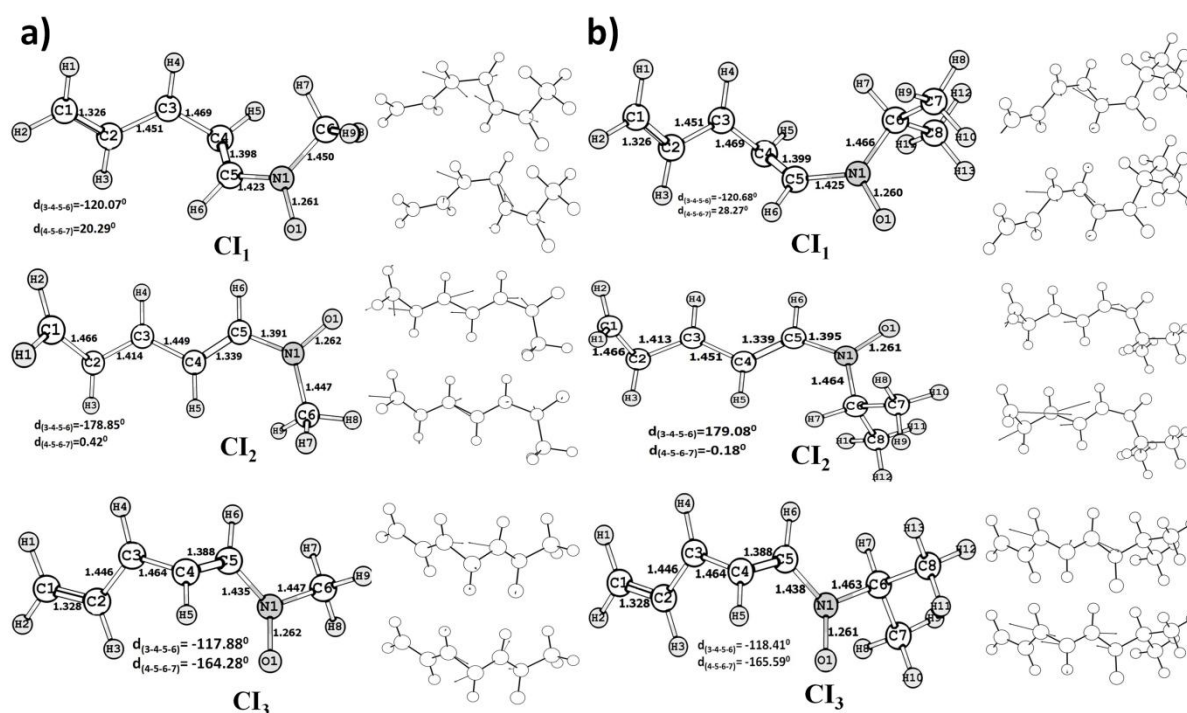


Figure 2-9: Optimized conical intersection geometries (CI_{1-3}) for three different types of motions of **a)** System I and **b)** System II at the CASSCF/6-31G* level with their respective gradient difference and derivative coupling vectors. [$d_{(3-4-5-6)}$ indicates $\langle C3-C4-C5-N$ torsion angle, $d_{(4-5-6-7)}$ indicates $\langle C4-C5-N-C6$ torsion angle]

It must be mentioned here that the ground state of these conjugated nitron systems are electrically neutral zwitterionic (dipolar) species and this may indicate their resemblance to the neutral conjugated polyene systems. On the other hand, the positive charge on nitrogen may bring some similarity with the polar conjugated iminium ions. Hence, these nitron systems can be roughly considered to be in between the two above mentioned conjugated systems. This fact also justifies the presence of a mixed contribution of biradical (similar to S_1 of polyene) and ionic (similar to S_1 of PSB) forms in the S_1 state of these nitrons. A thorough comparison with the photo-excitation processes of the nonpolar 1,3,5-hexatriene system and 2,5-pentadien-1-iminium cation are required to be discussed here (Figure 2-10a & 10b). Both these systems have covalent ground states (A_g) but their S_1 (and S_2) states are opposite in nature. The S_1 state of the conjugated hexatriene system has biradical characteristic (A_g symmetry), while this state is of ionic

nature with B_u -like symmetry in the PSB system. In the former system the initial photo-excitation populates the S_2 (B_u , ionic) state because the $S_0 \rightarrow S_1$ transition is forbidden; this is followed by an ultrafast relaxation to the S_1 state which is subsequently followed by a kinked S_0/S_1 conical intersection. On the other hand, in the PSB, the allowed $S_0 \rightarrow S_1$ transition is followed by an ultrafast non-radiative decay through a barrierless one-bond flip (OBF) process. During this OBF rotation, the S_1 state becomes stabilized, while the energy of S_0 increases. At a certain torsion angle ($\sim 90^\circ$) these two states become degenerate and a twisted-intramolecular charge transfer conical intersection (TICT-CI) results in a radiationless transition to the ground state.

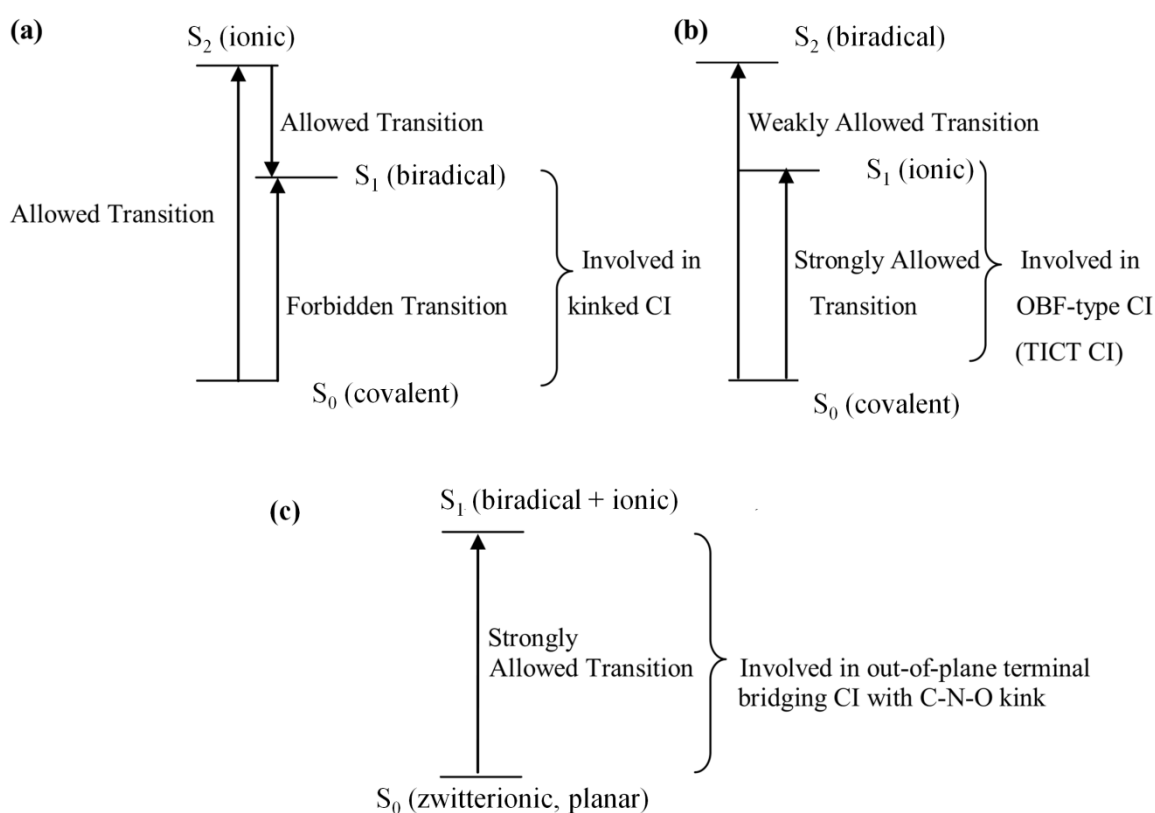


Figure 2-10: A schematic representation of the difference in ground and excited singlet state properties of **a)** non-polar conjugated hexatriene **b)** polar 2,5-pentadien-1-iminium cation and **c)** conjugated nitrone systems.

Coming back to our discussions on the nitrones, the mixed nature of the first excited state in nitrones probably drives the system towards two different types of motions. In CI_1 , the negative charge on C5 was found to be delocalized on the conjugated part and that's why the flip was found to take place with respect to the C3–C4 single bond (Figure 2-9a and 2-9b) which results in a one-bond-flip process. However, in the CI_2 conical

intersection, the rotation at the N-terminal part was found analogous to the one obtained at the semiempirical CI level and the reason for this is again related to the charge distribution in this species. An electron cloud seems to be there on the C5 atom (Table 2-4) which is not fully delocalized on the rest of the conjugated chain. The turn in the **CI**₂ is restricted in the terminal part only, probably due to the lack of charge distribution. This structure, somewhat looks like a C–N–O kink, which can be roughly compared to the H₁-bridging (here oxygen-bridging) conical intersection [62] reported in the terminal part of the non-polar conjugated polyene systems.

The oxygen atom holds an important role in the whole photo-excitation process. The analyses the ESP-charges reveal that the photo-excitation process is kicked off by the initial electronic transfer from the oxygen. This transfer is quite comparable to the well-established single electron transfer (SET) process reported for nitrones [63]; however, the difference lies in the fact that here it is intramolecular in nature. The C5–O bond length of **CI**₂ species is roughly 2.28 Å, and this is shorter than the same bond distance of **CI**₁ geometry (2.32 Å). At the CASSCF (4,4) level of calculation, the two above-mentioned conical intersection geometries were found to have slightly higher energies than the relaxed excited state structure (**A**) (Table 2-4).

The third high-energy conical intersection (**CI**₃) geometry was found to be of kinked nature and obtained from the conical intersection optimization run given on the optimized singlet excited state (**A**) geometry. At the CASSCF level, this geometry is situated at roughly 4 kcal/mol above the excited state geometry (**A**) in both *N*-methyl and *N*-isopropyl-substituted systems. The gradient-difference (GD) and the derivative coupling (DC) vectors corresponding to these conical intersection geometries are shown in Figure 2-9a and Figure 2-9b. Inclusion of dynamic correlation treatment on these optimized CI geometries at the CASMP2 level was found to lower their energies (Table 2-3).

Table 2-4: Atomic charges of various important geometries determined using Merz-Kollman scheme at the CASSCF/6-31G* level

System	Atom	Ground State	Planar excited state (A)	Conical Intersection CI ₁	Conical Intersection CI ₂	Conical Intersection CI ₃	Conical Intersection CI ₄	Conical Intersection CI ₅
I	C(1)	-0.3688	-0.3662	-0.5139	-0.2958	-0.4664	-0.4783	-0.4522
	C(2)	-0.0727	-0.0601	-0.0536	-0.1773	-0.1039	-0.0455	0.0349
	C(3)	-0.1406	-0.2888	-0.1862	-0.0965	-0.0657	-0.0246	-0.3501
	C(4)	-0.1790	-0.0874	-0.0925	-0.1622	-0.2255	-0.3986	0.0285
	C(5)	-0.1348	0.0347	-0.2037	-0.3303	-0.0967	0.3155	-0.0344
	N	0.5057	0.1880	0.4260	0.4537	0.2871	-0.1696	-0.1606
	C(7)	-0.4480	0.0770	-0.4471	-0.2812	-0.3348	-0.2795	-0.1923
	O	-0.6097	-0.3050	-0.3899	-0.4294	-0.4096	-0.2833	-0.1497
II	C(1)	-0.3606	-0.3425	-0.4626	-0.3058	-0.4619	–	–
	C(2)	-0.0830	-0.0496	-0.1076	-0.1698	-0.1035	–	–
	C(3)	-0.1558	-0.3240	-0.0940	-0.0572	-0.1008	–	–
	C(4)	-0.1207	0.0329	-0.1925	-0.2387	-0.2157	–	–
	C(5)	-0.1964	-0.0948	-0.0695	-0.2761	-0.0611	–	–
	N	0.4204	0.0845	0.1721	0.3247	0.1453	–	–
	C(7)	0.2588	0.2873	0.3934	0.3432	0.3295	–	–
	O	-0.5905	-0.2989	-0.4176	-0.4195	-0.3970	–	–

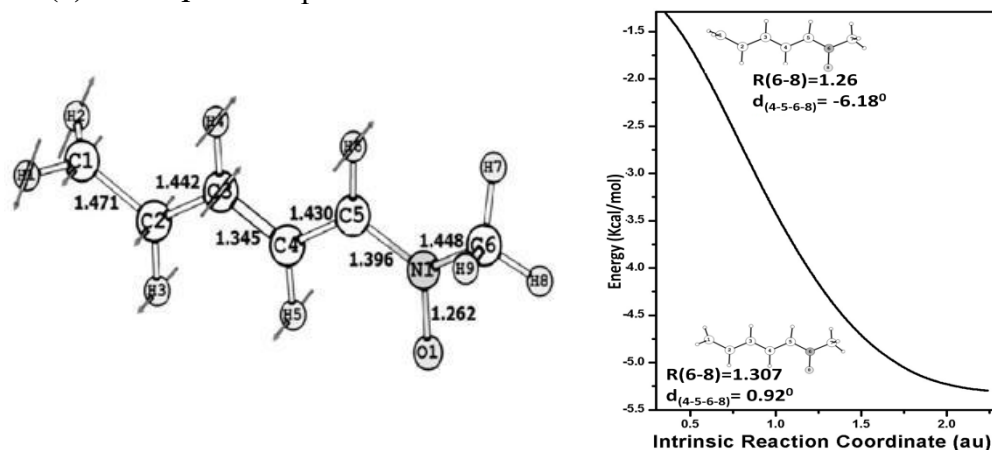
iii) Transition states (TS₁₋₃) at excited state surface

In the above section, we have discussed three important types of conical intersection geometries, two of them were found to be arising due to the twist around the central part of the molecule (CI₁ and CI₃) while the third one was of terminal out-of-plane bridging-type (CI₂). For detailed further analysis of the excited state potential energy surfaces, we had taken the *N*-methyl substituted nitron (system I) as the representative one. A transition state between the optimized excited state (A) and the CI₂ conical intersection geometry was obtained using the QST2 optimization technique. The geometry of this transition state (TS₁) almost resembles the optimized excited state geometry (Figure 2-11a). From the intrinsic reaction coordinate (IRC) calculation on TS₁ it was found that it goes towards the relaxed excited state geometry. The transition vector related to the imaginary frequency has been shown in Figure 2-11a which describes the initial motion of the transition state.

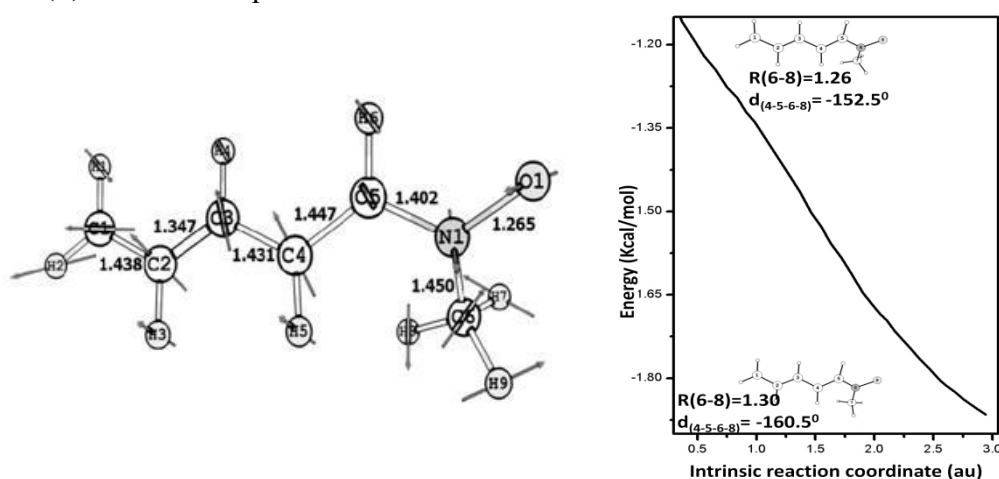
No optimized transition state was found between the relaxed excited state and the CI₁/CI₃ geometries using the QST2 method. Two more transition states, TS₂ and TS₃ (Figures 2-11b and 2-11c) were detected on the excited state surface, by using the normal TS optimization on a slightly non-planar guess geometry and the relaxed planar excited state geometry (A), respectively. At the CASSCF level, the barrier height from the excited state minimum (A) to TS₁ was 6.7 kcal/mol, whereas in TS₂, this was found to be

roughly 2.5 kcal/mol. The planar TS_3 was located very close (~ 0.5 kcal/mol) to the relaxed excited state (**A**) energy.

(a) TS_1 with displacement vectors and its IRC



(b) TS_2 with displacement vectors and its IRC



(c) TS_1 with displacement vectors and its IRC

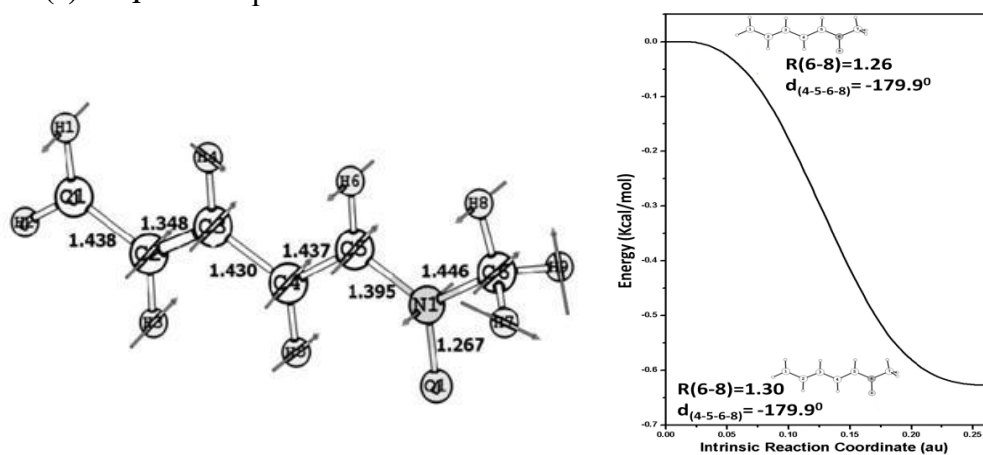


Figure 2-11: Transition states (a-c) TS_{1-3} on the excited state surface with the transition vectors corresponding to their imaginary frequencies and plots of minimum energy path along the intrinsic reaction coordinate (IRC) from these transition states.

iv) Conical intersections situated at lower energies

A lower-energy CI geometry (**CI₄**, shown in Figure 2-12a) was obtained from a conical intersection optimization run on **TS₃** geometry, situated around 15 kcal/mol below the **A** state. The lowest-energy conical intersection point (**CI₅**) had been optimized starting from a guess geometry with an elongated N–O bond. The geometry of this CI is characterized by an out-of-plane ($\sim 100^\circ$ away from the plane of the molecule) C4–C5–N–O torsion angle (Figure 2-12b) with a short C5–O bond (2.12 Å) and a highly stretched N–O bond distance (1.38 Å). At the CASSCF (4,4) level, **CI₅** was found to be situated at 60 kcal/mol above the ground state and 18 kcal/mol below the relaxed excited state. The CASMP2 calculations have predicted this CI point at a further 29 kcal/mol lower than the **A** state. The directions of the gradient difference vectors (Figure 2-12b) of this lowest-energy conical intersection point (**CI₅**) have indicated the possibility of oxaziridine formation with an out-of-plane C–N–O triangle. It must be added here that **CI₅** is expected to have a predominantly biradicaloid character (Table 2-4) unlike the relaxed excited state which has a mixed ionic-biradical nature. Possible presence of a lone pair on nitrogen was also noticed from the ESP-derived charges.

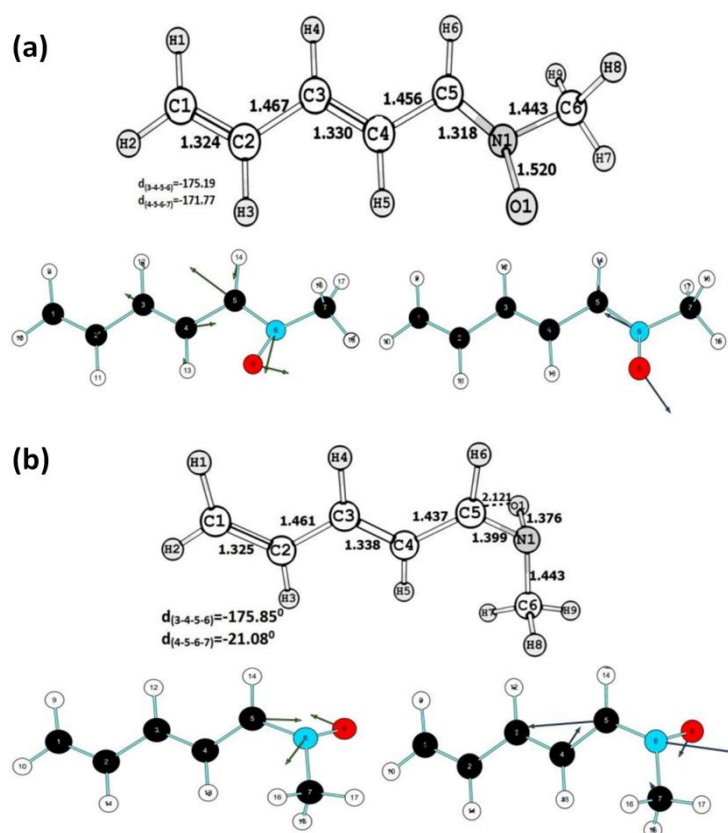


Figure 2-12: Optimized conical intersections (a) **CI₄** and (b) **CI₅** of system **I** with their gradient difference and derivative coupling vectors. [$d_{(3-4-5-6)}$ indicates \langle C3-C4-C5-N torsion angle, $d_{(4-5-6-7)}$ indicates \langle C4-C5-N-C6 torsion angle]

v) Optimized oxaziridine geometries

Following the gradient difference vectors of CI_5 (Figure 2-12b), oxaziridine ground state geometries were obtained. However, instead of minima, two second order saddle points (having two small imaginary frequencies) at ground state surface were found; one of them was a *trans* (Ox_1) isomer of oxaziridine while the other one was a *cis* (Ox_2) isomer. Both of them were geometrically similar ($R_{\text{C-O}}=1.38 \text{ \AA}$, $R_{\text{N-O}}=1.44 \text{ \AA}$, $R_{\text{C-N}}=1.41 \text{ \AA}$, $\angle\text{OCN} = 62.3^\circ$, $\angle\text{ONC} = 57.6^\circ$) with an out-of-plane C–N–O kink or oxygen-bridge (Figures 2-13a and 2-13b). These obtained parameters were in excellent agreement with the experimentally reported oxaziridine geometry [64], which has a C–N–O triangle with C–O and N–O bond lengths of 1.40 \AA and 1.50 \AA , respectively, while the C–N bond length was reported to be around 1.44 \AA . The two bond angles $\angle\text{OCN} = 63.7^\circ$ and $\angle\text{ONC} = 56.8^\circ$ were also in good agreement with the predicted ones. At the CASSCF (4,4) level of calculation the *trans* (Ox_1) species was found to be more stable than the *cis* oxaziridine (Ox_2) by roughly 2 kcal/mol. The latter geometry was calculated to be more stable than the Ox_1 geometry (by 5 kcal/mol) after inclusion of dynamic correlation effect. Analysis of the HOMO of these oxaziridine species (Figure 2-13) has indicated the formation of a bond between C5 and oxygen atom due to the overlap of orbitals on these respective atoms.

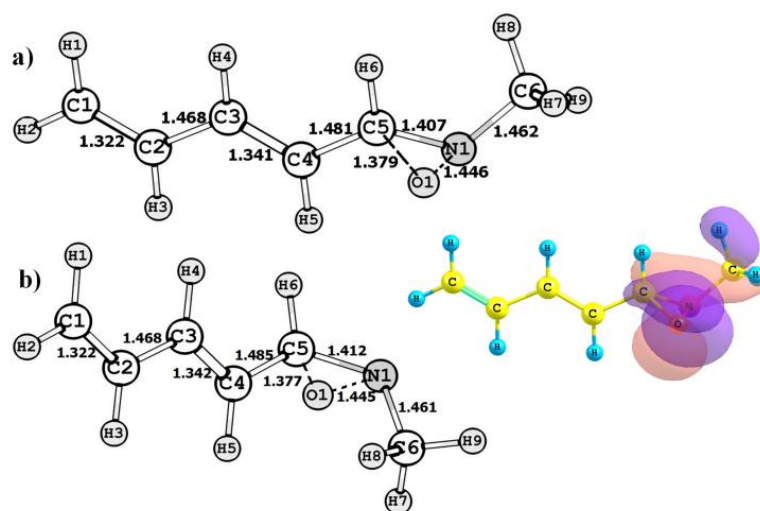


Figure 2-13: (a) *Trans* oxaziridine (Ox_1) geometry of system I with its HOMO (b) *cis* oxaziridine (Ox_2) geometry of system I.

B) Radiative transition properties and vertical excitation energies

Using the GUGA-CI code in GAMESS suite of program, the oscillator strengths, transition moments and Einstein's coefficient values of the lowest energy singlet-singlet transitions ($S_0 \rightarrow S_1$) were predicted (Table 2-5) at the optimized ground state geometries

of the two systems. The transition moment (TM) value of $S_0 \rightarrow S_1$ in system I was found to be higher than that of system II. A comparison with the conjugated iminium ion has revealed that the allowed transition moment values of the S_0-S_1 radiative transitions in these conjugated nitrones (4.75 D) are significantly lower than that of the PSB systems (7.50 D) [53]. The transition moment value of the $S_0 \rightarrow S_2$ radiative transition was found to be very low which resembles the nature of the iminium ion systems (discussed earlier). Radiative lifetime values (τ) of the first vertically excited states (S_1) for these two studied systems were found to be around 460 -525 ps, whereas it was below 250ps in the case of iminium ions.

In chapter 1, discussions about the sloped conical intersection and two varieties of peaked conical intersections were done. In the faster peaked types, the excited molecule is funnelled either from the Franck–Condon geometry or from the excited relaxed state geometry towards the point of intersection. In the latter case the excited state passes through a barrier which makes it a slower process; this probably happens in the nitrone systems before the oxaziridine geometry is reached through the CI_5 intersection point. A larger barrier here is expected to increase radiative lifetime of the excited state, as seen in several conjugated polyene systems. The vertical excitation energy (VEE) values of S_0-S_1 transitions were studied at different level of calculations. The PM3/CI and CASSCF values were found to be quite close (~ 4 eV). However, the CASMP2 has produced relatively higher values than the previously mentioned levels of calculations. Comparisons of vertical excitation energy at different level of chosen active spaces are shown in Table 2-5. It was found that at the CASMP2 level, there is negligible effect of the change of active spaces on the S_0-S_1 energy gap values.

Table 2-5: Vertical excitation energies (VEE) and radiative transition properties corresponding to the lowest vertical transition ($S_0 \rightarrow S_1$) at the ground state equilibrium geometry. The values in parentheses are the power to base 10.

System	VEE in eV	Transition Moment (in Debye) ^d				Oscillator Strength ^d		Einstein's Coefficient ^d	Radiative Lifetime (τ) in s
		μ	μ_x	μ_y	μ_z	f_L	f_V		
I	3.99 ^a 4.13 ^{b1} , 5.59 ^{b2} 3.99 ^{c1} , 5.65 ^{c2}	4.86	-4.68	-1.29	0.002	0.706	0.195	2.1472(+9)	525(-12)
II	3.99 ^a 3.93 ^{b1} , 5.75 ^{b2} 4.01 ^{c1} , 5.63 ^{c2}	4.69	4.45	-1.46	0.270	0.702	0.175	4.6046(+9)	466(-12)

^aVEE values reported at PM3/CI level

^bVEE values reported at ¹CASSCF/6-31G* and ²CASMP2/6-31G* level with (4,4) active space

^cVEE values reported at ¹CASSCF/6-31G* and ²CASMP2/6-31G* level with (6,6) active space

^dRadiative transition properties calculated between two CI wavefunctions using GUGA CI code

C) A complete possible scheme of whole photoisomerization process.

A possible scheme of the whole process is shown in Figure 2-14. The nitron-oxaziridine conversion process through the biradicaloid lowest-energy conical intersection geometry was found to have some similarity with the benzene-prefulvene photo-isomerization process, commonly known as the channel 3 decay [65-67]. The CI_5 geometry having an out-of-plane C–N–O kink with odd electrons on C5 and oxygen is quite comparable to the prefulvenic conical intersection which has a $-(CH)_3-$ kink with odd electrons on C1 and C5 atoms; on coupling this gives prefulvene intermediate, and ultimately leads to fulvene and other products. More interestingly similar to the oxaziridine geometries, following the lowest energy conical intersection, the prefulvene ground state was also reported to be a saddle point instead of a minimum, which was found to connect two prebenzvalene structures. We obtained quite similar results in our case, where the two obtained oxaziridine (Ox_1 and Ox_2) geometries were found to be saddle points. The kinked-CI (CI_3) in these nitrones with a conventional $-(CH)_3-$ kink in the middle-part of

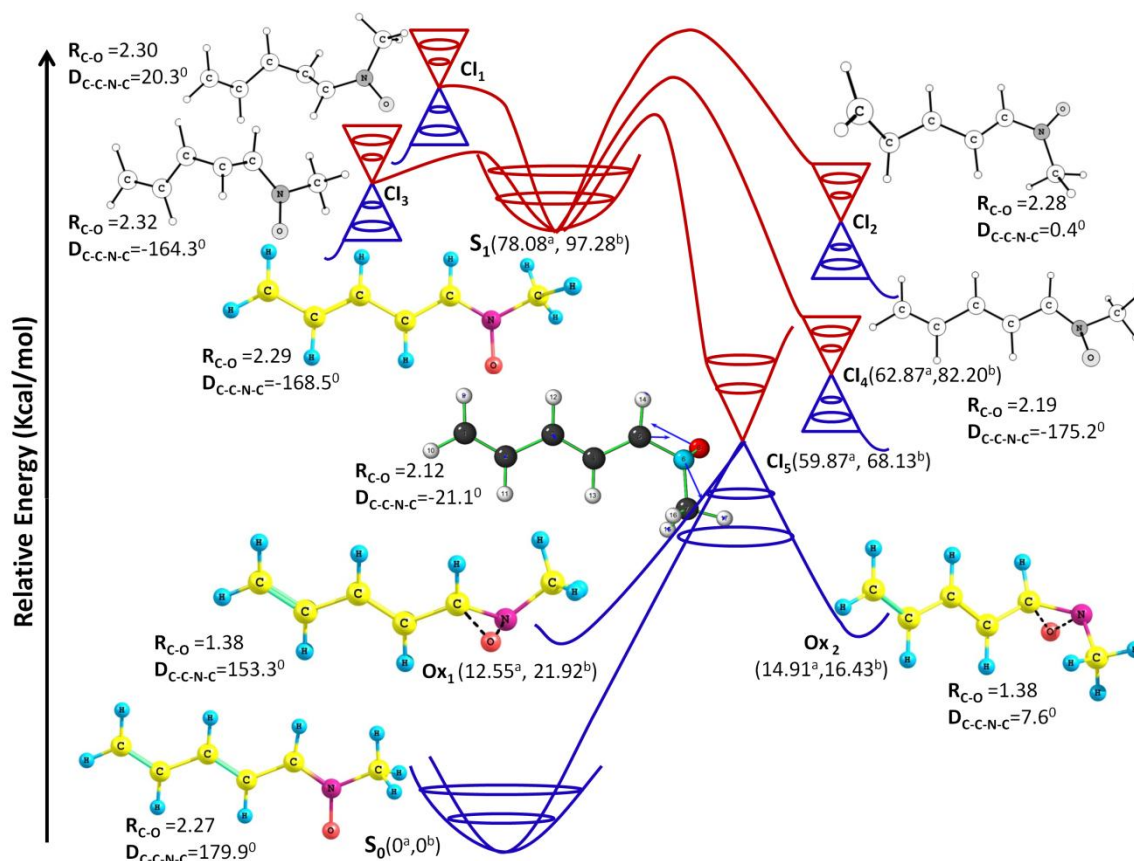


Figure 2-14: A schematic representation of the non-radiative decay processes involving different conical intersections in system I. (Relative energies in kcal/mol with respect to the optimized ground state energy at CASSCF^a and CASMP2^b levels are given in the parentheses)

the chain was located at higher energy than the relaxed excited state (A), and therefore, seems to be of less importance in these systems during their oxaziridine photo-conversion process.

In spite of some similarities as discussed above, a major difference was found between the CI_5 and the prefulvenic conical intersection geometries, as the latter being actually tetradicaloid in nature. In the CI_5 geometry, the nitrogen holds a lone pair of electron (Table 2-4), and odd electrons reside on C5 and oxygen atoms. This can be further justified by analyzing the products obtained from prefulvene, where benzvalene and fulvene are the two major possibilities. Formation of fulvene can be compared with the possibility of formation amide (as a photoproduct) in our studied systems. Though no amide has been reported from the *N*-methyl retinyl nitron system, it seems quite reasonable if we think of a possible route of amide formation from oxaziridine through the breaking of the N–O bond with simultaneous formation of the C5–O bond, followed by a [1,2-H] shift from C5 to nitrogen. This seems to be quite comparable to the prefulvene→fulvene conversion. However, unless two more odd electrons are there, no benzvalene-type product is expected to be obtained. In fact no such analogous product has been experimentally reported on photo-excitation of any kind of nitrones, so far which supports the possible existence of a lone pair on nitrogen in the oxaziridine system.

Our predicted results clearly indicate that oxaziridine and thereafter amide are probably the two expected photoproducts along with other numerous possibilities arising from the different relaxation paths. The high energy conical intersections with OBF-mode or Hula-twist-mode operating in the central part of the chain may lead to cis-isomer (with respect to the C3–C4 bond rotation) as a photoproduct, though experimental studies on the alkyl-retinyl nitrones have not reported this type of product. The geometry of the lowest-energy CI (CI_5) was found to be quite matching with the H₁-bridging (here oxygen-bridging) structure in HT1-mode described by Norton and Houk [62], which was reported to be an efficient volume conserving process. Experimentally obtained photochemical products (oxaziridine) of these nitrones indicate that this volume conserving mechanism of the terminal CNO-twisted mode dominates the photo-relaxation process. In fact, looking at the geometries in Figure 2-9a and 2-9b clearly indicates that the terminal C–N bond rotation requires less amount of space than the central C–C bond rotation, and therefore may be a more favourable process.

2.4. SECTION 2: N-methyl substituted retinylnitrones

In section 2.3, we have discussed our studies [18] on short chain conjugated model nitrone systems. These investigations have clearly established the importance of the first excited singlet states of nitrones in the oxaziridine formation through the lowest-energy conical intersection geometries having biradicaloid characteristics. This present section discusses our proposed mechanism of the experimentally reported oxaziridine formation process of the long-chain *N*-alkyl retinylnitronone systems [19]. The reported computational studies of the 13-*trans* and 13-*cis* retinylnitrones are mostly based on the 2-layer hybrid ONIOM methods [32-40]. The two studied retinylnitronone systems are having *N*-methyl substituents and isomeric in nature. The 13-*trans* isomer was reported to be of higher biological activity than the 13-*cis* form [17]. The former isomer was found to give a good yield of isolable oxaziridine under roomlight (Figure 2-1). The *Z*-form of 13-*trans* isomer was reported to be more stable than its *E*-form. This section also reports our computational investigation of thermal *E-Z* isomerisation path of the 13-*trans* isomer.

2.4.1. Purpose of studying extended conjugated *N*-methyl retinylnitronone system using ONIOM methodology

Though CASSCF [22-31] calculation is a highly accurate quantum mechanical technique to successfully explore the photochemistry of molecules, use of large active spaces in this method may be often troublesome and can lead to high computational costs. Reducing the active space size may not be a solution to this problem as doing this without any prior knowledge of the actual reaction path can introduce huge errors in the computational results. It is also a fact that use of a large active space in several reactions may take it away to some other directions instead of leading to the desired product. The use of hybrid methods, such as ONIOM gives an opportunity to emphasize more on the important part of the molecule (the core region of our desired photochemical reaction) by higher level of calculation through proper partitioning. The primary intension for carrying out this part of the work was to identify the proper active site in the ONIOM calculation for the extended conjugated *N*-methyl retinylnitronone system which can produce a successful nitronone-oxaziridine photo-conversion path as our CASSCF-predicted [18] one for the smaller model nitronone systems. We intended to check whether the presence of the long-conjugated chain and the β -ionone ring part (those were missing

in the model compounds) can influence the mechanism or not; probably the best possible computational way of doing this in a least expensive manner for such an extended conjugated system is to use a hybrid technique. A CASSCF calculation on the whole retinyl nitron system would have been too expensive; as conical intersection is likely to be responsible in the process, we have chosen CASSCF-based (as higher-level method) hybrid scheme. The low-level methods include both quantum mechanical level and molecular mechanics with electronic embedding (EE) calculations, and these are capable enough to influence the high-level part. Several possibilities of the high-level part were also explored by varying the size of the higher level part (CAS) in the ONIOM to identify the particular model part of the *N*-methyl retinyl nitron which is responsible for the oxaziridine formation process. (Table 2-6).

2.4.2 Results and discussions:

A) Optimized points on potential energy surface

a) Initial guess from semi-empirical calculations

We had performed the semiempirical calculations for the extended conjugated retinyl nitron systems in the beginning for a rough understanding of the whole photoexcitation process. Our previous knowledge on the CASSCF-based studies on the conjugated open-chain smaller nitrones had confirmed the dominance of the biradical contribution in the first excited singlet states along the oxaziridine formation path. Following this intuition, we have optimized the excited singlet state of the retinyl nitron system using both non-biradical and biradical options in PM3/CI, and in the latter case, a significant terminal twist of the CNO moiety (Figure 2-15) was noticed. These geometries from the PM3/CI calculations on the excited singlet states were used as starting guess geometries for the conical intersection optimizations, and they have successfully given the low-lying S_0/S_1 intersection points

b) Results of hybrid ONIOM calculations.

i) Optimized ground states geometries

The ground state geometrical parameters of the high-level portions (calculated at CASSCF with 6-31G* basis set) of the target systems reported at the respective hybrid ONIOM levels, were found to be almost identical to the values obtained at the B3LYP/6-31G* and RHF level of theories. A comparison of these parameters is shown in Table 2-6.

Table 2-6: Structural parameters of optimized ground states of 13-*trans* and 13-*cis* isomers at various level of calculations. Bond lengths are in Å and angles are in degrees.

Isomer	METHOD	C11-C12	C12-C13	C13-C14	C14-C15	C15-N	N-O	C15-O	N-C20	<CNO	D _{CNO}
13- <i>trans</i>	RHF/6-311G*	1.333	1.469	1.338	1.450	1.279	1.264	2.257	1.459	125.1	0.0
	B3LYP/6-311G*	1.361	1.443	1.368	1.421	1.328	1.268	2.304	1.476	125.1	0.0
	CASSCF(8,8)/6-31G* : HF/STO-6G	1.338	1.468	1.338	1.454	1.315	1.274	2.292	1.457	124.5	0.0
	CASSCF(8,8)/6-31G* : HF/4-31G	1.357	1.464	1.361	1.447	1.296	1.281	2.292	1.460	125.6	0.0
	CASSCF(8,8)/6-31G* : HF/ 6-31G	1.357	1.464	1.360	1.447	1.296	1.281	2.292	1.460	125.7	0.0
	CASSCF(6,6)/6-31G* : HF/STO-6G	-	-	1.371	1.441	1.297	1.280	2.292	1.460	125.6	0.0
	CASSCF(6,6)/6-31G* : HF/4-31G	-	-	1.364	1.444	1.296	1.282	2.293	1.459	125.6	0.0
	CASSCF(6,6)/6-31G* : HF/6-31G	-	-	1.365	1.444	1.296	1.282	2.293	1.460	125.6	0.0
	CASSCF(4,4)/6-31G* : HF/STO-3G	-	-	-	-	1.310	1.262	2.281	1.490	124.9	0.0
	CASSCF(4,4)/6-31G* : HF/STO-6G	-	-	-	-	1.310	1.262	2.281	1.490	125.0	0.0
	CASSCF(4,4)/6-31G* : HF/4-31G	-	-	-	-	1.302	1.273	2.282	1.488	124.9	0.0
	CASSCF(4,4)/6-31G* : HF/6-31G	-	-	-	-	1.302	1.273	2.283	1.488	125.0	0.0
	CASSCF(4,4)/6-31G* : PM3	-	-	-	-	1.287	1.258	2.271	1.463	126.3	0.0
	CASSCF(4,4)/6-31G* : PM6	-	-	-	-	1.303	1.270	2.290	1.496	125.7	0.2
	CASSCF(4,4)/6-31G* : AM1	-	-	-	-	1.313	1.260	2.291	1.493	125.8	0.0
	CASSCF(4,4)/6-31G* : UFF(with EE)	-	-	-	-	1.276	1.261	2.270	1.465	127.0	-0.9
	CASSCF(4,4)/6-31G* : B3LYP/ STO-6G	-	-	-	-	1.315	1.267	2.281	1.484	124.1	0.0
	CASSCF(4,4)/6-31G* :MP2/STO-6G	-	-	-	-	1.310	1.266	2.281	1.491	124.8	0.0
13- <i>cis</i>	RHF/6-311G*	1.333	1.469	1.338	1.452	1.279	1.264	2.258	1.459	125.2	0.0
	B3LYP/6-311G*	1.360	1.443	1.369	1.424	1.327	1.269	2.304	1.477	125.2	0.1
	CASSCF(8,8)/6-31G* : HF/STO-6G	1.362	1.462	1.364	1.449	1.295	1.281	2.292	1.460	125.7	0.0
	CASSCF(8,8)/6-31G* : HF/4-31G	1.358	1.464	1.361	1.449	1.295	1.281	2.292	1.460	125.7	0.0
	CASSCF(8,8)/6-31G* : HF/ 6-31G	1.358	1.464	1.361	1.449	1.296	1.281	2.293	1.460	125.7	0.0
	CASSCF(6,6)/6-31G* : HF/STO-6G	-	-	1.372	1.443	1.296	1.281	2.293	1.460	125.7	0.0
	CASSCF(6,6)/6-31G* : HF/4-31G	-	-	1.365	1.445	1.296	1.283	2.293	1.459	125.6	0.0
	CASSCF(6,6)/6-31G* : HF/6-31G	-	-	1.365	1.446	1.296	1.283	2.294	1.459	125.6	0.0
	CASSCF(4,4)/6-31G* : HF/STO-3G	-	-	-	-	1.310	1.262	2.281	1.490	125.0	0.0
	CASSCF(4,4)/6-31G* : HF/STO-6G	-	-	-	-	1.309	1.262	2.282	1.490	125.0	0.0
	CASSCF(4,4)/6-31G* : HF/4-31G	-	-	-	-	1.301	1.273	2.283	1.488	124.9	0.0
	CASSCF(4,4)/6-31G* : HF/6-31G	-	-	-	-	1.301	1.274	2.284	1.488	125.1	0.0
	CASSCF(4,4)/6-31G* : PM3	-	-	-	-	1.287	1.259	2.272	1.463	126.4	0.0
	CASSCF(4,4)/6-31G* : PM6	-	-	-	-	1.281	1.268	2.268	1.464	125.8	0.6
	CASSCF(4,4)/6-31G* : AM1	-	-	-	-	1.289	1.258	2.268	1.462	125.9	0.3
	CASSCF(4,4)/6-31G* : UFF(with EE)	-	-	-	-	1.276	1.262	2.271	1.465	127.0	-0.9
	CASSCF(4,4)/6-31G* : B3LYP/ STO-6G	-	-	-	-	1.315	1.267	2.280	1.484	124.2	0.0
	CASSCF(4,4)/6-31G* :MP2/STO-6G	-	-	-	-	1.310	1.265	2.281	1.491	124.7	0.0

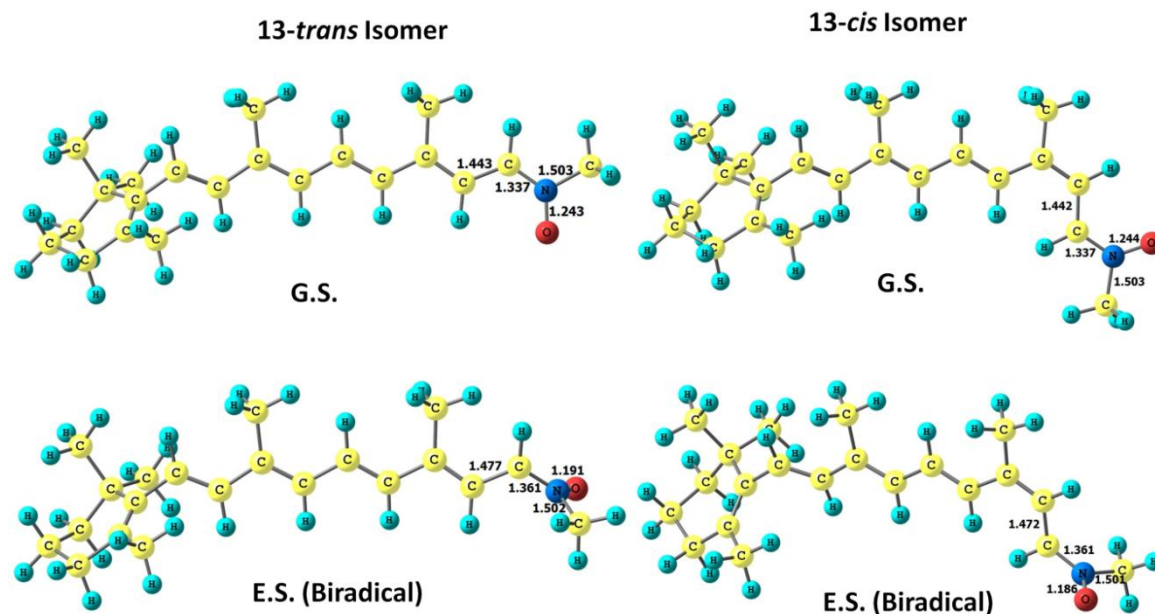


Figure 2-15: Planar ground state and non-planer biradical excited state geometries of 13-*trans* and 13-*cis* isomers obtained at semi-empirical PM3/CI level

The important molecular orbitals involved in the active spaces for the model part of these ONIOM calculations are shown in Figure 2-16.

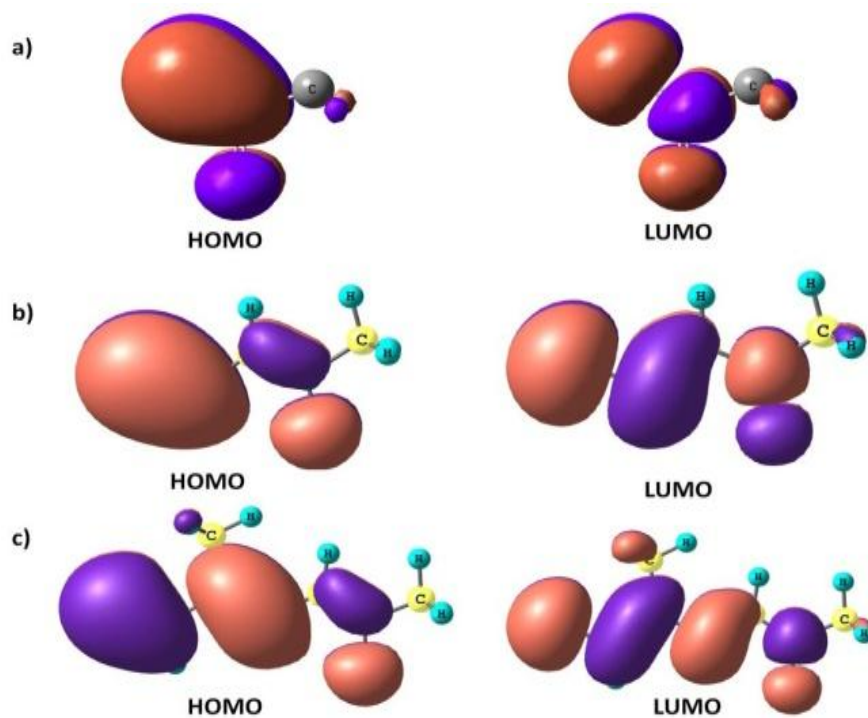


Figure 2-16: Important molecular orbitals involved in the active space for the model part of the a) ONIOM (CASSCF (4,4): QM'/MM), b) ONIOM (CASSCF (6,6): RHF) and c) ONIOM (CASSCF (8,8): RHF).

ii) Optimized conical intersection and oxaziridine geometries

Conical intersection optimization run on the guess structures obtained by PM3/ CI calculations have produced low lying conical intersection geometries (Figure 2-17). These optimized CI geometries were found to be situated at 65-70 kcal/mol above the ground state (Table 2-7). The gradient difference vectors (Figure 2-17 and Figure 2-18) of these conical intersections have given clear indications of the possibilities of 3-membered heterocyclic ring formations. Among the various hybrid calculations (shown in Table 2-6), only the CASSCF (4,4)/6-31G*: HF/STO-6G and CASSCF(4,4)/6-31G*: UFF(including electronic embedding) level of theories had produced the desired oxaziridine geometries through the low-lying conical intersections for both the isomers. In addition to the above mentioned calculations, the lower level treated at the HF/STO-3G for the 13-*trans* isomer had also produced similar low-lying conical intersection (Figure 2-19) (situated at 61 kcal/mol above the ground state) leading to the oxaziridine. Though this latter conical intersection was not completely optimized, the gradient difference (GD) vectors of the last step of the conical intersection optimization run had given clear indication of the possibility of an oxaziridine formation (Figure 2-20).

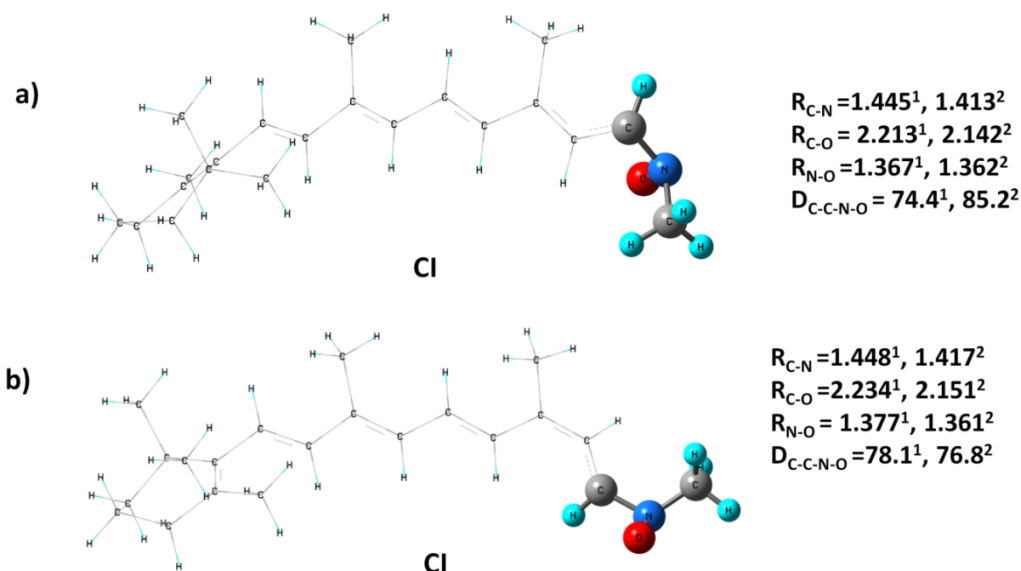


Figure 2-17: Conical intersection (CI) geometries of **a)** 13-*trans* isomer and **b)** 13-*cis* isomer at ¹CASSCF (4,4)/6-31G*:HF/STO-6G level and ²CASSCF(4,4)/6-31G*:UFF(with EE) level of calculations. Important bond lengths (in angstrom) and dihedral angles (in degrees) are also shown.

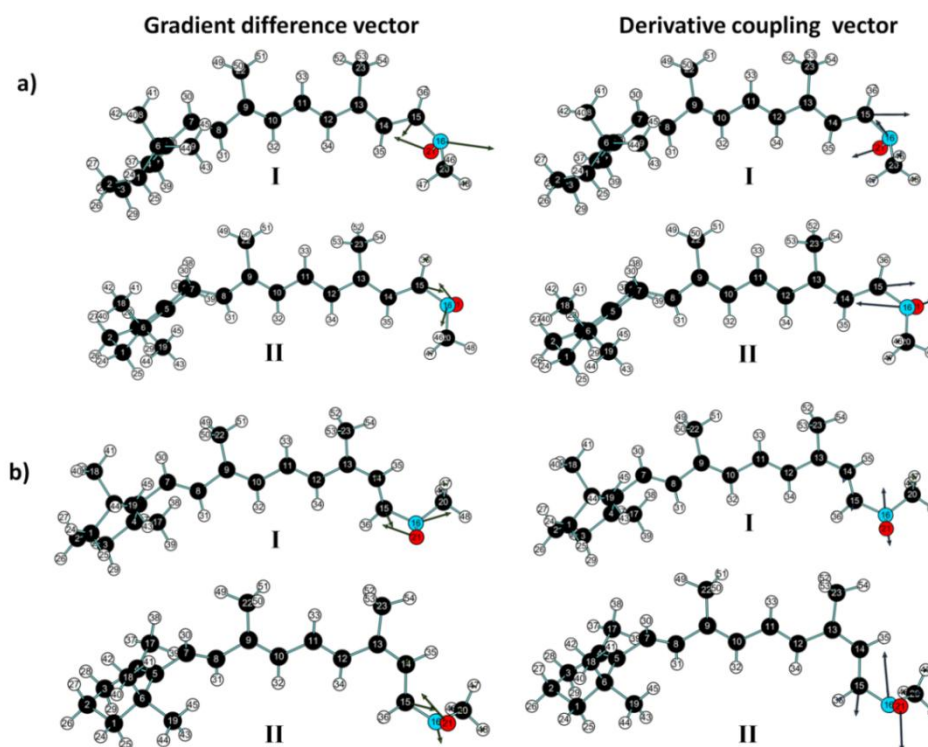


Figure 2-18: Gradient difference and derivative coupling vectors of conical intersection geometries of **a)** 13-*trans* and **b)** 13-*cis* isomer at **(I)** CASSCF(4,4)/6-31G*:RHF/STO-6G and **(II)** CASSCF(4,4)/6-31G*:RHF/UFF (with EE) level of ONIOM calculations.

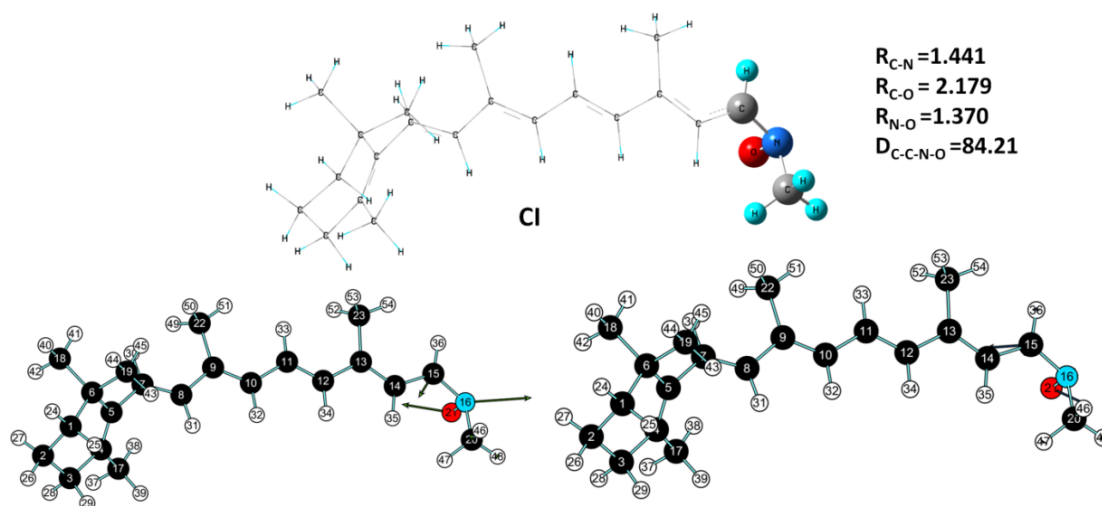


Figure 2-19: Conical intersection geometry of 13-*trans* isomer with their gradient difference and derivative coupling vectors at CASSCF (4,4)/6-31G*:RHF/STO-3G level of calculation. Important bond lengths (in angstrom) and dihedral angle (in degrees) are also shown.

Table 2-7: Relative energy values (ΔE) in kcal/mol of 13-*trans* and 13-*cis* isomers of *N*-methyl retinyl nitron using method I and method II, without using dynamic correlation ($\Delta E'$) and using dynamic correlation ($\Delta E''$) in the high-level calculations.

Method	Molecular geometry	13- <i>trans</i>		13- <i>cis</i>	
		$\Delta E'$	$\Delta E''$	$\Delta E'$	$\Delta E''$
I	GS	0	0	0	0
	VEE.	103.06	95.75	103.07	95.57
	CI	65.55	64.57	67.78	69.71
	Ox _I	5.54	23.09	5.37	22.90
	Ox _{II}	10.76	21.46	-1.19	19.95
II	GS	0	0	0	0
	VEE	99.51	96.51	105.27	96.57
	CI	69.64	63.44	67.62	65.51
	Ox _I	-6.60	17.50	-1.57	15.18
	Ox _{II}	-9.61	11.85	-8.59	12.73
III	GS	0	-	0	-
	VEE	103.07	-	103.08	-
	CI	61.33	-	-	-
	Ox _I	6.35	-	-	-
	Ox _{II}	5.00	-	-	-

Method I is CASSCF (4,4)/6-31G* : HF/STO-6G,
 Method II is CASSCF(4,4) / 6-31G*:UFF(with EE) and
 Method III is CASSCF (4,4)/6-31G* : HF/STO-3G

The optimized ground state structures of oxaziridines (**Ox_I** and **Ox_{II}**) (Figure 2-20) were obtained following the GD vector directions of these low-lying CI geometries (Figure 2-17 and 2-18). These oxaziridines were found to be situated around 55-60 kcal/mol below the conical intersection geometries (Table 2-7); in some cases (QM:MM) they were found below the ground state geometries. The inclusion of dynamic correlation (MP2) effect on the CASSCF high-level part had shifted the energies of the oxaziridine geometries at higher values. The reported geometrical parameters of these two species (**Ox_I** and **Ox_{II}**) (Table 2-8) closely resemble the experimentally reported value ($R_{C-O} = 1.40 \text{ \AA}$, $R_{N-O} = 1.50 \text{ \AA}$, $\angle OCN = 63.7^\circ$, $\angle ONC = 56.8^\circ$) of oxaziridine [64]. The directions of derivative coupling (DC) vectors indicated the possibilities of some other types of photoproducts; these products may be of some kind of isomeric species of the parent nitrones which can compete with the oxaziridine route. For both the isomers (13-*trans* and 13-*cis*), the relative energy values of the conical intersections and oxaziridine geometries with respect to the ground states were found to be almost similar (Table 2-7). It must be mentioned here that for the 13-*trans* isomer, these energy values at the CASSCF (4,4)/6-31G* : HF/STO-6G level were found to be almost comparable to the predicted CASSCF/6-31G* energy values of the *N*-methyl model nitron system (reported in previous section).

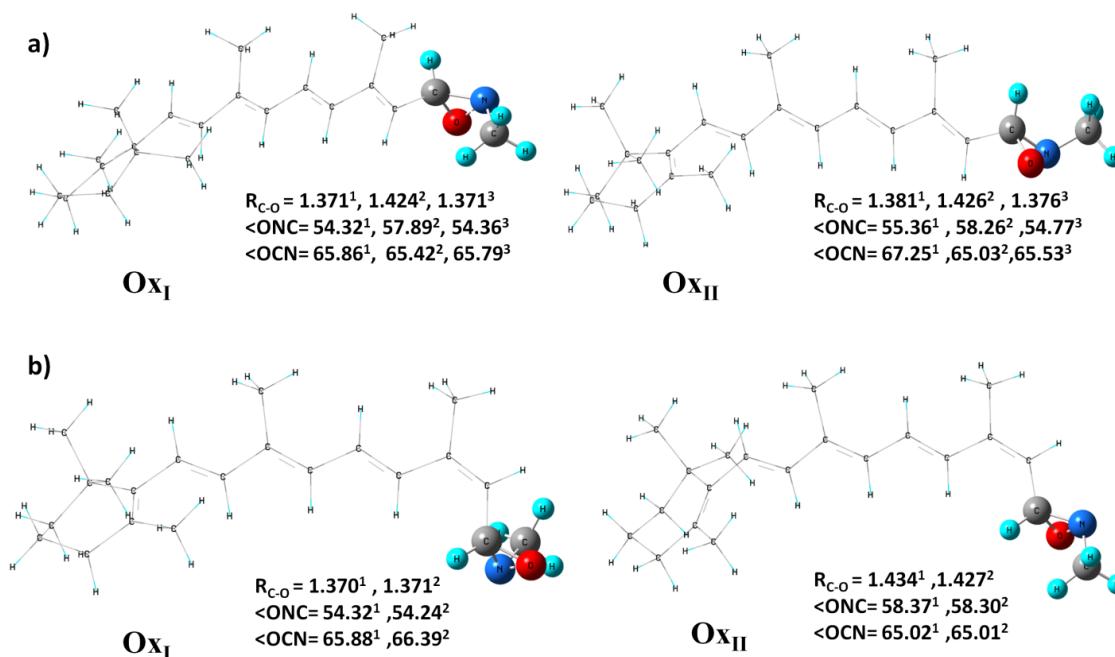


Figure 2-20: Optimized oxaziridine geometries **Ox_I** and **Ox_{II}** obtained from **a)** 13-*trans* isomer and **b)** 13-*cis* isomer at ¹CASSCF(4,4)/6-31G*:HF/STO-6G, ²CASSCF(4,4)/6-31G*:UFF(with EE) and ³CASSCF(4,4)/6-31G*:HF/STO-3G level of ONIOM calculations. Important bond lengths (in angstrom) and bond angles (in degrees) are also shown.

Table 2-8: Structural parameters of optimized oxaziridines of 13-*trans* and 13-*cis* isomers. Bond lengths are in Å and angles are in degrees.

Structural parameter	13- <i>trans</i>		13- <i>cis</i>	
	Ox _I	Ox _{II}	Ox _I	Ox _{II}
R_{C-C}	1.510 ^a / 1.479 ^b	1.504 ^a / 1.474 ^b	1.510 ^a / 1.488	1.500 ^a / 1.474 ^b
R_{C-N}	1.459 ^a / 1.405 ^b	1.414 ^a / 1.402 ^b	1.458 ^a / 1.448 ^b	1.406 ^a / 1.402 ^b
R_{N-O}	1.540 ^a / 1.529 ^b	1.548 ^a / 1.521 ^b	1.540 ^a / 1.545 ^b	1.527 ^a / 1.507 ^b
R_{N-C}	1.452 ^a / 1.451 ^b	1.449 ^a / 1.449 ^b	1.452 ^a / 1.453 ^b	1.449 ^a / 1.449 ^b
$\angle CNO$	54.32 ^a / 57.89 ^b	55.35 ^a / 58.26 ^b	54.32 ^a / 54.42 ^b	58.37 ^a / 58.30 ^b
$\angle CON$	59.80 ^a / 56.69 ^b	57.39 ^a / 56.07 ^b	59.78 ^a / 59.18 ^b	56.60 ^a / 56.68 ^b
D_{CCNO}	107.9 ^a / 108.2 ^b	-109.4 ^a / -109.2 ^b	107.8 ^a / 105.1 ^b	-108.1 ^a / -109.1 ^b
D_{CCNC}	13.6 ^a / 12.58 ^b	155.8 ^a / 153.9 ^b	13.54 ^a / 11.9 ^b	155.5 ^a / 154.1 ^b

^a CASSCF(4,4)/6-31G*: HF/STO-6G and ^b CASSCF(4,4)/6-31G*:HF/UFF(with EE)

Keeping the level of calculations same, the QM:QM partitioning was varied by using 3 conjugated and 2 conjugated double bonds (along with the non-bonded electrons on oxygen) as the high level part with (8,8) and (6,6) active space CASSCF calculations (Figure 2-21), respectively. No terminally twisted low-lying CI was obtained which can lead to oxaziridine. Both these calculations have produced a terminal CNO-kinked conical intersection, but their GD and DC vectors have shown no possibility of an oxaziridine formation as a possible photoproduct. The key involvement of the π -electron

cloud on the CNO moiety is clearly established from this during the oxaziridine formation process through the appropriate conical intersections. Incorporating the contributions from the remaining π -cloud in the higher-level part in these QM:QM methods has indicated the fact that the photochemical reaction will proceed to other directions resulting in different types of photoproducts. These tests avoid unnecessary computational costs by eliminating the portions those are not chemically important for a particular photochemical reaction.

Interestingly, no other combination of QM:QM was found to produce the desired reaction path. We had also tested better basis sets than STO-6G in the HF calculation (low level). The conical intersection calculation at CASSCF:HF/3-21G level didn't optimize completely; however, the directions shown by the GD vectors in the last step indicated some chance of oxaziridine formation. Use of HF/4-31G and HF/6-31G as the low-level had not produced any conical intersection with possibility of oxaziridine formation. Moreover, the conical intersection run at CASSCF:HF/6-31G calculation was found to produce distortion in the middle of the molecule which is not a characteristic of the experimentally reported oxaziridine structure.

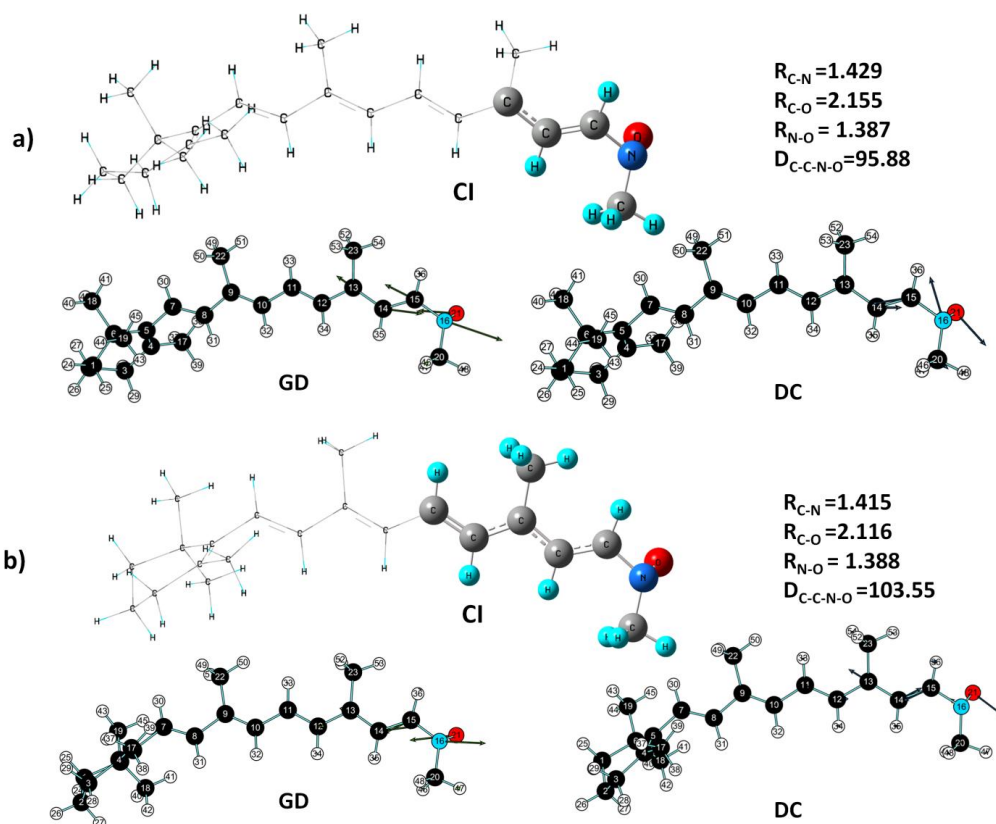


Figure 2-21: Conical intersection (CI) geometry of 13-*trans* isomer with their gradient difference (GD) and derivative coupling (DC) vectors at **a)** CASSCF (6,6)/6-31G*:RHF/STO-6G and **b)** CASSCF (8,8)/6-31G*:RHF/STO-6G level of ONIOM calculations.

The investigation of this reaction path was also carried out at other QM:QM ONIOM level of calculations like CASSCF:B3LYP and CASSCF:MP2, but the attempt was not successful. These calculations produced the lowest-energy conical intersection with a completely distorted structure. This is probably due to the fact that in ONIOM calculations the high-level method must be better than the low-level method in all possible ways [68]. In the above-mentioned two cases the dynamic correlation effects in the low-level part probably takes away the ONIOM extrapolation in a wrong direction. Another interesting observation was that in spite of using the CASSCF(4,4)/6-31G* as the higher level method for the CNO part, the QM:PM3 /PM6/ AM1 methods were unable to produce any conical intersection geometry which can lead towards an oxaziridine structure. This clearly indicates that the semiempirical methods as the lower level in ONIOM were unable to produce certain interactions with the core region (treated at a better level of calculation) those were essential to capture the desired reaction path towards oxaziridine.

Overall, these results indicate that a certain amount of optimal interaction from the lower-level part is required to produce the desired photochemical reaction. The success of some particular QM:QM (with lower level at HF/STO-6G or HF/STO-3G) and QM:MM (with electronic embedding) methods with better lower level of theories is due to the fact that more powerful electronic effects in these cases can cross the border. However, the failure of QM:QM methods with a similar lower level of theory with higher basis sets (such as HF/6-31G or 4-31G etc.) is probably due to the fact that this part interacts too heavily with the high level part. On the other hand very weak interactions from the lower level part (semiempirical level) and MM (without electronic embedding) were equally not capable to bring out the correct reaction path.

B) *E-Z* isomerization of the 13-*trans* retinyl nitron system

The *cis-trans* isomerizations of nitrones were earlier reported at the DFT level of calculation [69-70]. Our present study has revealed that the *E-Z* isomerizations of the retinyl nitrones are thermal in nature. We have analyzed the isomerization route of the 13-*trans* isomer using ONIOM calculations. At the B3LYP/6-311G* level the optimized ground state geometry of the *Z*-isomer of 13-*trans* compound was found to be more stable by 3.6 kcal/mol than its corresponding *E*-isomer; this gap was found to be roughly 3.1 kcal/mol at the CASSCF(4,4)/6-31G*: HF/STO-6G level. By using QST3 methodology at the same level of ONIOM calculation, a transition state was found on the

ground state surface [41,42]. The optimized transition state geometry was found at 30 kcal/mol (Figure 2-22) above the *E*-isomer with an imaginary frequency of $361i\text{ cm}^{-1}$; the transition vectors corresponding to this frequency have clearly indicated the possibility of the formation of the *Z*-isomer. A complete schematic representation of the possible mechanism of the photochemical nitron-oxaxiridine conversion process and thermal *E-Z* isomerization is shown in Figure 2-23.

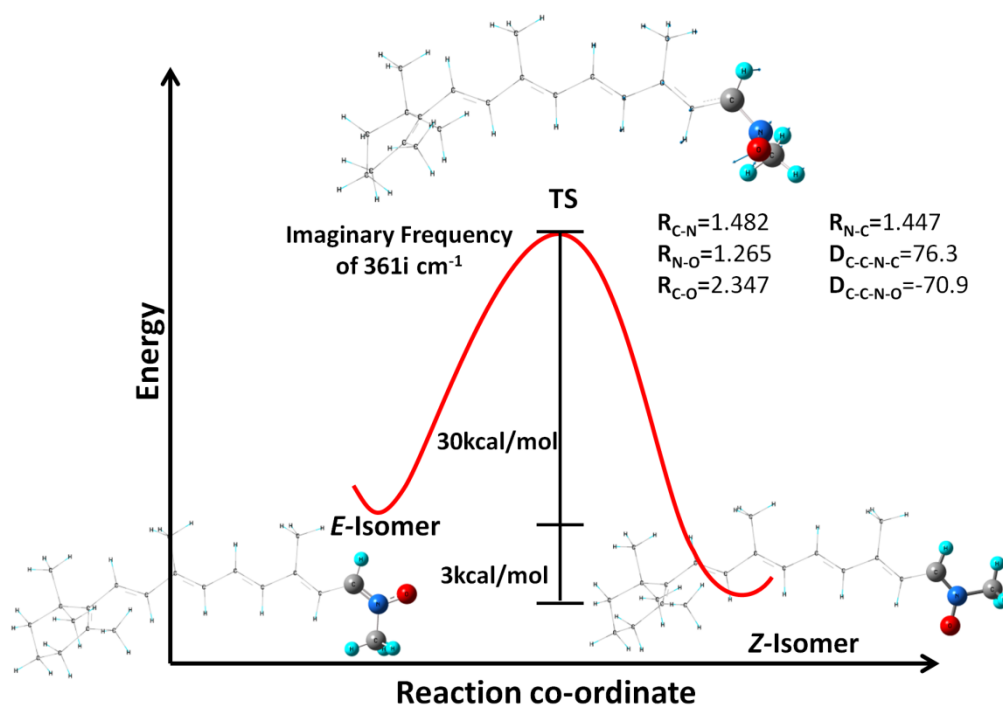


Figure 2- 22: A Schematic representation of *E-Z* isomerization of 13-*trans* *N*-Methyl retinyl nitron.

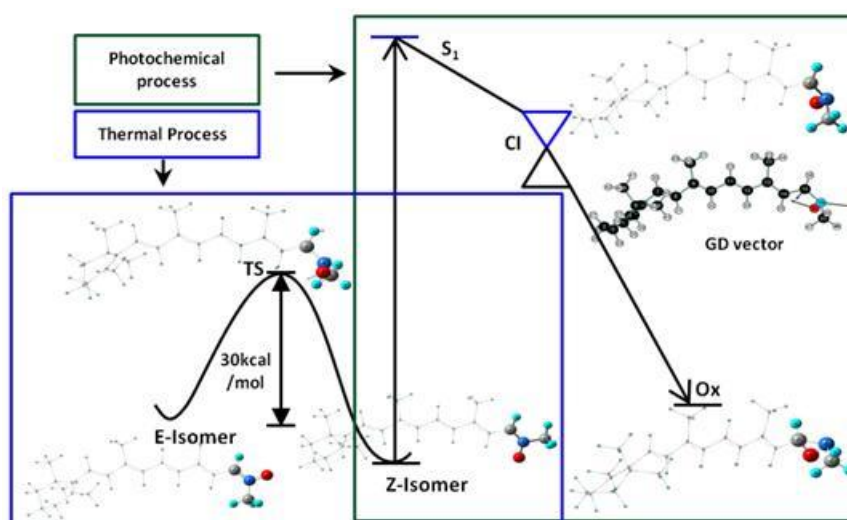


Figure 2-23: A possible scheme of thermal and photochemical processes occurring in *N*-Methyl retinyl nitron

2.5. Conclusions

The probable mechanism of the photo-excitation process of the *N*-alkyl-substituted retinyl nitrones has been proposed by a comprehensive study on their model systems and full extended conjugated systems. The predicted photochemical products of the studied nitron systems were matching with the experimentally reported results of the *N*-alkyl retinyl nitron molecules. The photo-excited first singlet state of the model nitron system was found to have a mixed biradical and ionic contribution. Rotations around the central C–C bond and the terminal C–N bond were characterized by their distinct conical intersection points which had made the excited state topography highly complicated. It can be concluded that the non-radiative decay path leading to the oxaziridine geometry is likely to pass through the lowest-energy intersection point. Nature of this conical intersection and its subsequent photoproduct was found analogous to the benzene→prefulvene conversion pathway through the prefulvenic intersection.

The ONIOM-based 2-layer hybrid calculations on 13-*trans* and 13-*cis* retinyl nitrones exposed the key of the terminal CNO part in their photo-conversion route to oxaziridines. Choosing this terminal moiety as the active site and employing higher level quantum mechanical method on this model part, we were able to track the targeted photoisomerization process. The reason behind the success of some particular QM:QM and QM:MM methodologies over the other level of ONIOM calculations have been discussed in detail. An optimal interaction from the low-level part is probably required to produce the desired photochemical route. In addition, this study has also supported the experimentally reported facts that the mutual conversion of stable *Z*-isomers of these retinyl nitrones to their unstable *E* varieties is not photochemical in nature.

The reported results in this chapter may stimulate rigorous experimental studies on conjugated nitron systems in future. Overall, the importance of this present study is not only restricted to the establishment of the probable mechanism of the photo-excitation process of conjugated long-chain nitron systems, but also it can have far reaching consequences in terms of the excited state properties of several other nitron systems, too. The proposed mechanism of these nitrones can reveal spectroscopic features of various structurally similar nitron systems, and tuning of photoproducts of nitrones can be done by proper choice of substituents on nitrogen.

2.6. References

1. K. Shinzawa and I. Tanaka, *J. Phys. Chem.*, 1964, **68**, 1205.
2. K. Koyano and I. Tanaka, *J. Phys. Chem.*, 1965, **69**, 2545.
3. J. S. Splitter and M. Calvin, *J. Am. Chem. Soc.*, 1965, **30**, 3427.
4. J. S. Splitter, T.-M. Su, H. Ono and M. Calvin, *J. Am. Chem. Soc.*, 1971, **93**, 4075.
5. G. G. Spence, E. C. Taylor and O. Buchard, *Chem. Rev.*, 1970, **70**, 231.
6. M. Nastasi and J. Streith, *Rearrangements in Ground and Excited States*, Ed., P. de Mayo, Academic Press, New York, 1980.
7. D. R. Boyd, K. M. McCombe, T. A. Hamor, W. B. Jennings and V. E. Wilson, *J. Chem. Soc. Perkin Trans II*, 1984, 95.
8. D. R. Boyd, P. B. Coulter, N. D. Sharma, V. B. Jennings and V. E. Wilson, *Tetrahedron Letters*, 1985, **26**, 1673.
9. S. Sivasubramanian, P. Manisankar, P. Jeyaram and N. Arumugam, *J. Pol. Chem.*, 1985, **59**, 367.
10. M. Iwamura, M. Katoh and H. Iwamura, *Org. Magn. Reson.*, 1980, **14**, 392.
11. J. R. Harbour, V. Chow and J. Bolton, *J. Can. Chem.*, 1974, **52**, 3552.
12. B. Bigot, D. Roux, A. Sevin and A. Devaquet, *J. Am. Chem. Soc.*, 1979, **101**, 2560.
13. I. Komeromi, M. Jean and J. Tronchet, *J. Mol. Struct. (Theochem)*, 1996, **366**, 147.
14. S. D. Kahn, W. J. Hehre and J. A. Pople, *J. Am. Chem. Soc.*, 1987, **109**, 1871.
15. K. N. Houk, J. Sims, R. E. Duke, R. W. Strozier and J. K. George, *J. Am. Chem. Soc.*, 1973, **95**, 7287.
16. R. M. Aminova and E. Ermakova, *Chem. Phys. Lett.*, 2002, **359**, 184.
17. V. Balogh-Nair and K. Nakanishi, *Pharm. Res.*, 1984, **1**, 93.
18. P. Saini and A. Chattopadhyay, *RSC Adv.*, 2014, **4**, 20466.
19. P. Saini and A. Chattopadhyay, *Chem. Phys. Lett.*, 2015, **633**, 6.
20. M. J. Frisch et al., *Gaussian 09*, Revision **B.01**, Gaussian, Inc., Wallingford CT, 2009.
21. Website of Chemcraft software: <http://www.chemcraftprog.com>.
22. D. Hegarty and M. A. Robb, *Mol. Phys.*, 1979, **38**, 1795.
23. R. H. A. Eade and M. A. Robb, *Chem. Phys. Lett.*, 1981, **83**, 362.
24. H. B. Schlegel and M. A. Robb, *Chem. Phys. Lett.*, 1982, **93**, 43.
25. F. Bernardi, A. Bottini, J. J. W. McDougall, M. A. Robb and H. B. Schlegel, *Far. Symp. Chem. Soc.*, 1984, **19**, 137.

26. M. J. Frisch, I. N. Ragazos, M. A. Robb and H. B. Schlegel, *Chem. Phys. Lett.*, 1992, **189**, 524.
27. N. Yamamoto, T. Vreven, M. A. Robb, M. J. Frisch and H. B. Schlegel, *Chem. Phys. Lett.*, 1996, **250**, 373.
28. P. Slavíček and T. J. Martínez, *J. Chem. Phys.*, 2010, **132**, 234102.
29. F. Bernardi, M. A. Robb and M. Olivucci, *Chem. Soc. Rev.*, 1996, **25**, 321.
30. M. J. Bearpark, M. A. Robb and H. B. Schlegel, *Chem. Phys. Lett.*, 1994, **223**, 269.
31. J. Olsen, *Int. J. Quant. Chem.*, 2011, **111**, 3267
32. M. J. Bearpark et al., *J. Photochem. Photobio. A: Chem.*, 2007, **190**, 207.
33. S. Dapprich, I. Komáromi, K.S. Byun, K. Morokuma and M. J. Frisch, *J. Mol. Struct. (Theochem)*, 1999, **462**, 1.
34. T. Vreven, K. S. Byun, I. Komáromi, S. Dapprich, J. A. Montgomery Jr., K. Morokuma and M. J. Frisch, *J. Chem. Theory Comput.*, 2006, **2**, 815.
35. T. Vreven and K. Morokuma, *Ann. Rep. Comput. Chem.*, 2006, **2**, 35.
36. T. Vreven, K. Morokuma, O. Farkas, H. B. Schlegel and M. J. Frisch, *J. Comput. Chem.*, 2003, **24**, 760.
37. M. J. Bearpark, S. M. Larkin and T. Vreven, *J. Phys. Chem. A*, 2008, **112**, 7286.
38. T. Vreven and K. Morokuma, *Theor. Chem. Acc.*, 2003, **109**, 125.
39. I. Geronimo and P. Paneth, *Phys. Chem. Chem. Phys.*, 2014, **16**, 13889.
40. A. Bhattacharya and E. R. Bernstein, *J. Phys. Chem. A*, 2011, **115**, 4135.
41. C. Peng, P. Y. Ayala, H. B. Schlegel and M. J. Frisch, *J. Comput. Chem.*, 1996, **17**, 49.
42. C. Peng and H. B. Schlegel, *Israel J. Chem.*, 1993, **33**, 449.
43. X. Li and M. J. Frisch, *J. Chem. Theory Comput.*, 2006, **2**, 835.
44. H. P. Hratchian and H. B. Schlegel, *Theory and Applications of Computational Chemistry: The First 40 Years*, Eds., C. E. Dykstra, G. Frenking, K. S. Kim and G. Scuseria, Elsevier, Amsterdam, 2005.
45. H. P. Hratchian and H. B. Schlegel, *J. Chem. Theory Comput.*, 2005, **1**, 61.
46. H. P. Hratchian and H. B. Schlegel, *J. Chem. Phys.*, 2004, **120**, 9918.
47. J. J. P. Stewart, *J. Comput. Chem.*, 1989, **10**, 209.
48. J. J. P. Stewart, *J. Comput. Chem.*, 1989, **10**, 221.
49. M. W. Schmidt et al., *J. Comput. Chem.*, 1993, **14**, 1347.
50. B. Brooks and H. F. Schaefer, *J. Chem. Phys.*, 1979, **70**, 5092.

51. B. Brooks, W. Laidig, P. Saxe, N. Handy and H. F. Schaefer, *Physica Scripta*, 1980, **21**, 312.
52. A. Chattopadhyay, *J. Phys. B: At. Mol. Opt. Phys.*, 2011, **44**, 165101.
53. A. Chattopadhyay, *J. Chem. Sci.*, 2012, **124**, 985.
54. F. Weinhold, *J. Chem. Phys.*, 1970, **54**, 1874.
55. C. W. Bauschlicher and S. R. Langhoff, *Theor. Chim. Act.*, 1991, **79**, 93.
56. S. Koseki and M. S. Gordon, *J. Mol. Spec.*, 1987, **123**, 392.
57. U. C. Singh and P. A. Kollman, *J. Comput. Chem.*, 1984, **5**, 129.
58. B. H. Besler, K. M. Merz Jr. and P. A. Kollman, *J. Comput. Chem.*, 1990, **11**, 431.
59. N. Ragazos, M. A. Robb, F. Bernardi and M. Olivucci, *Chem. Phys. Lett.*, 1992, **197**, 217.
60. M. J. Bearpark, M. A. Robb and H. B. Schlegel, *Chem. Phys. Lett.*, 1994, **223**, 269.
61. F. Bernardi, M. Olivucci and M. A. Robb, *Chem. Soc. Rev.*, 1996, **25**, 321.
62. J. E. Norton and K. N. Houk, *Mol. Phys.*, 2006, **104**, 993.
63. M. N. Khan, S. Bhattacharjee, H. Chandra and M. C. R Simons, *Spec. Chim. Acta. Part A*, 1998, **54**, 779.
64. S. S. Murphree, *Modern Heterocyclic Chemistry*, Eds., J. Alvarez-Builla, J. J. Vaquero and J. Barluenga, Wiley-VCH Verlag & Co. KGaA, Weinheim, Germany, 2011.
65. A. Migani and M. Olivucci, *Conical Intersections: Electronic Structure, Dynamics & Spectroscopy Advanced series in Physical Chemistry*, Eds., W. Domcke, D. R. Yarkony and H. Koppel, World Scientific Publishing Co. (P). Ltd, Singapore, 2004.
66. I. J. Palmer, I. N. Ragazos, F. Bernardi, M. Olivucci and M. A. Robb, *J. Am. Chem. Soc.*, 1993, **115**, 673.
67. J. Dreyer and M. Klessinger, *Chem. Eur. J.*, 1996, **2**, 335.
68. F. R. Clemente, T. Vreven and M. J. Frisch, *Quantum Biochemistry*, Ed., Chérif F. Matta, Wiley-VCH Verlag GmbH & Co. KGaA, Weinheim, Germany, 2010.
69. L. Meng, S. C. Wang, J. C. Fettinger, M. J. Kurth and D. J. Tantillo, *Eur. J. Org. Chem.*, 2009, 1578.
70. D. Roca-López, T. Tejero and P. Merino, *J. Org. Chem.*, 2014, **79**, 8358.

CHAPTER 3

A computational investigation of the photochemistry of open-chain conjugated nitrone systems with electron-withdrawing group on nitrogen

3.1. Introduction

As discussed in the previous chapter, the formation and stability of oxaziridines, produced on photo-irradiation of nitrones vary significantly depending on the types of substitutions [1-7]. It is now well-known from experimental studies that the presence of an alkyl group on nitrogen stabilizes oxaziridine; on the other hand, substitutions of *N*-aryl or electron-withdrawing groups (EWG) have an opposite effect. The presence of EWG was reported to destabilize the oxaziridine which usually converts to amide. This conversion was suspected to occur through a biradical mode [8] after the N–O bond cleavage.

The objective of the work discussed in this chapter is to investigate the possibility of oxaziridine formation on photo-irradiation of EWGs substituted acyclic nitrones. Oxaziridines are usually prepared by methods like photo-irradiation of nitrones, oxidation of imines and electrophilic amination of ketones; however, oxaziridines with EWGs, such as *N*-sulfonyl [9-11], *N*-acyl, perfluorinated oxaziridines [12] are known to be prepared by the latter two methods only. These types of oxaziridines are electron deficient and used as the source of electrophilic oxygen. Photo-conversions of nitrones to corresponding oxaziridines, having EWGs on nitrogen are not known, so far. Interestingly, nitrone photo-irradiation is not preferred for preparation of oxaziridine except for *N*-alkyl (and *N*-benzyl) substituted systems, as discussed previously. Appearance of a lone pair of electrons on the nitrogen atom (which initially contains a positive charge) and change in its hybridization from sp^2 to sp^3 (planar to pyramidal) is essential for the formation of an oxaziridine from nitrone. Probably the +I effect of electron donating groups (alkyl groups) on nitrogen can satisfy these requirements and hence facilitate the oxaziridine formation. In contrast, EWGs take away the electron cloud from the nitrogen atom and inhibit the formation of a proper oxaziridine. Experimental detection and isolation of such oxaziridines are probably very difficult in practice due to their lack of stability and might be the reason behind no experimental report on the detection of these terminal heterocyclic species from the photo-irradiation of corresponding nitrones, so far. It is also possible that EWG on nitrogen makes the

nitron highly unstable, and therefore unavailability of a stable nitron of this kind makes them a poor choice for oxaziridine preparation under photo-irradiation.

A conjugated nitron (system **I**) with EWG on nitrogen (can be considered as a model compound of the corresponding *N*-substituted retinyl nitron system) was chosen as the parent system, assuming that the conjugated bonds can bring some stability to the system (Figure 3-1), and maximum chance of oxaziridine formation can be expected from this species. We felt that this might eventually help us to conclude whether the unstable nature of nitron restricts the oxaziridine photo-conversion or is it truly not possible for some other reason. On the other hand, the studies on system **II** (unsubstituted system) were done primarily to have an idea that to what extent the EWG can affect the relative energy values, charges and geometrical parameters with respect to the unsubstituted species. Results presented in this chapter have been published [13].

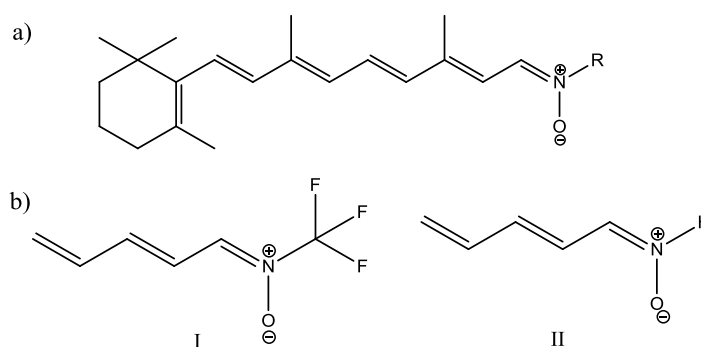


Figure 3-1: Structure of (a) *N*-substituted retinyl nitron and (b) studied *N*-trifluoromethyl-substituted (**I**) and unsubstituted (**II**) model nitron systems.

In this work, aryl nitron systems were not chosen as they were already known to produce unstable or no oxaziridines on photoirradiation. Another reason for studying the model 2,4-pentadiene-nitron system with *N*-EWG (system **I**) was to compare this nitron with our earlier discussed structurally similar nitron system having electron-donating *N*-alkyl substituents (chapter 2). The motive of choosing trifluoromethyl group as an EWG on nitrogen atom in this conjugated nitron system was based on the following reasons:

- Our primary objective was to include a strong EWG on nitrogen with a relatively smaller size. The chosen trifluoromethyl group is the simplest member of the perfluoroalkyl family, which has a van der Waals radius of 2.7 Å and a comparable electronegativity (3.5) as the oxygen atom [14].
- This small halomethyl group can be taken as a representative one for an EWG capable of involving the accumulated electronic charge on the nitrogen atom in π -

conjugation through its negative hyperconjugative effect [15,16] (discussed later on), and capable of taking away the lone pair cloud from nitrogen.

- A bulky group on the nitrogen atom is supposed to hinder the planar to pyramidal conversion step of nitrogen in the oxaziridine conversion process. Therefore, to avoid this steric factor we have used a relatively smaller group.

Overall, our choice of the studied nitrene system was basically related to provide a maximum possible chance of stable oxaziridine formation.

We have performed high-level quantum mechanical investigations to explore important points on the excited state surfaces, such as excited state minima, transition states and conical intersection points. The resulting photochemical pathway of the studied nitrene system was compared with our previously reported *N*-alkyl-substituted conjugated nitrene system [6]. The final results of this study on the *N*-trifluoromethyl-substituted nitrene have indicated that one of the possible photoproducts (amide) of the corresponding retinyl system may lie in the class of pharmacologically important compounds.

3. 2. Computational details

Using the Gaussian 09 suite of program [17], the CASSCF method [18-23] with 6-31G* basis set was employed to optimize the equilibrium ground and excited state geometries along with the other important points on the potential energy surfaces (i.e. conical intersection geometries, transition states etc). Different active spaces in CASSCF calculations, such as (4,4), (6,6) and (8,8), were employed for optimizing the ground and excited state geometries of the studied systems. However, for studies related to transition states and conical intersections, we have preferred to use a smaller active space with 4 active electrons in 4 active orbitals. As discussed in the previous chapter, some prior knowledge of a photochemical reaction path can provide certain intuitions which can be extremely helpful in choosing an accurate minimal active space by eliminating the less important orbitals for that particular reaction. The choice of CAS (4,4) active space in this work was based on prior experience of successful tracking of the nitrene-oxaziridine photoconversion path of our previously discussed (chapter 2) retinyl nitrene and their model compounds. The choice made in those studies were based on the chemical intuition by looking at their reported experimental photochemical results [4]. The studies done in the previous chapter clearly indicate that the ground state oxaziridine species is formed through lowest-energy conical intersection geometry which involves a terminal CNO twist, and this process was found to be perfectly captured by the CASSCF studies

using a proper (4,4) active space. The actual reaction path of this photochemical process is shown in Figure 3-2. This figure reveals the involvement of a C–N π bond and a p_z orbital on oxygen atom (holding the negative charge on oxygen) in the photoisomerization process, which after photo-excitation results in a C–N σ bond and a possible C–O bond (through a transient biradical species). The latter part of the conjugated chain was found to have no significant role to play in the whole conversion process.

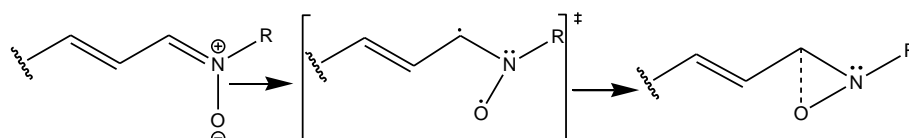


Figure 3-2: A possible route of nitron-oxaziridine conversion in conjugated *N*-alkyl nitrones

As the studied systems are structurally similar to our previously studied model *N*-alkyl conjugated retinyl nitrones, a similar result is expected to be true. Based on these intuitions we have chosen CAS(4,4) as a possible appropriate active space, where the chosen HOMO was of π symmetry on the CNO moiety while LUMO was of corresponding π^* symmetry. Molecular orbitals involved in the chosen (4,4) active space for tracking the photo-conversion path of system **I** are shown in Figure 3-3. It should be added here that, there is no single correct active space in a molecule [24]; the choice of active space depends on the particular process being carried out. It is a fact that the (4,4) active space chosen has correctly captured the photochemical conversion route of the conjugated *N*-substituted nitrones to oxaziridine; however, for some other processes of these nitrones this chosen active space may not be correct.

It must be mentioned here that we have also carried out calculations using higher active spaces, such as (6,6) and (8,8) to check whether they are capable to produce any terminally twisted oxaziridine geometry or not. However, these attempts with larger active spaces were unsuccessful. Their inability to track such reaction path have actually justified that our initial intuition behind choosing the smaller (4,4) active space was correct.

To include the dynamic correlation effect, single point Moller-Plesset perturbation (MP2) calculations were performed on top of the CASSCF/6-31G* optimized geometries. The transition states were located by employing normal TS technique based on the Berny-algorithm [25]. To follow minimum energy path from the transition state [26-28], intrinsic reaction coordinate (IRC) method was used. The GAMESS [29-33]

suite of programs was used for some important calculations using GUGA (Graphical Unitary Group Approach)-based configuration interaction singles and doubles (CISD) technique. In the CISD calculations, RHF/6-311G* method was used in the first step for self-consistent molecular orbital (SCFMO) calculation of the ground states, and these MOs were subsequently used for the configuration interaction steps. Based on this GUGA CISD code, the radiative transition [34-36] calculations were carried out between the two configuration interaction wavefunctions at ground state equilibrium geometry. Electrostatic potential-based atomic charges were calculated for the ground and excited state species using the Merz-Kollman [37,38] scheme. ChemCraft [39] and GaussView softwares were employed throughout this work for visualizing the output files.

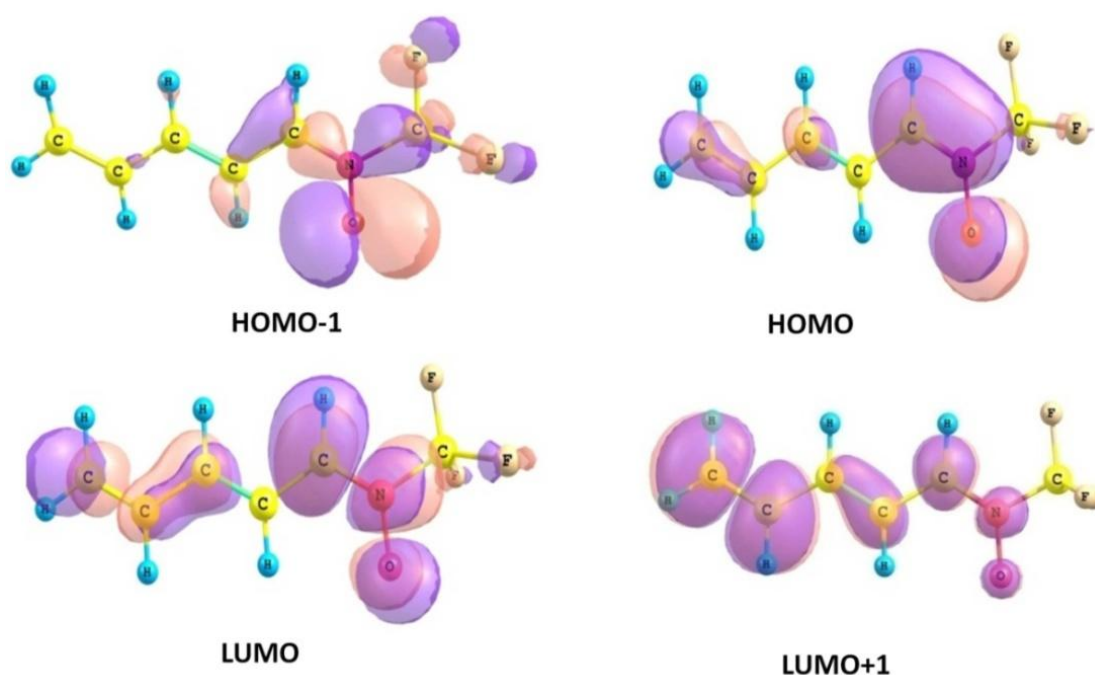


Figure 3-3: Molecular orbitals involved in the CASSCF (4, 4) active space calculations.

3. 3. Results and discussions

3. 3.1. Important optimized points on potential energy surfaces

A) Ground, vertically excited and optimized excited state geometries

Ground state geometries of both the systems (**I** and **II**) were optimized at RHF and CASSCF level of theories (Table 3-1). These optimized structures were found to be zwitterionic (positive charge on nitrogen and negative charge on oxygen) in nature, having planar geometries with alternate double and single bonds. The optimized first excited singlet states of both these systems are also found to be planar; however, unlike system **II** the excited state of system **I** have an elongated C5–N bond. The vertical excitation energy (VEE) values ($S_0 \rightarrow S_1$) of both the systems are reported in Table 3-2 at

different levels of calculations. At CASSCF (4,4) level, the VEE values of the trifluoromethyl-substituted system (**I**) and unsubstituted system (**II**) were found to be 4.94 eV (114 kcal/mol) and 5.09 eV (117 kcal/mol), respectively. Lower VEE values were found with increase in the size of the active spaces, whereas those calculated by CASMP2 were found slightly higher than the corresponding CASSCF values. The relaxed planar excited state of system **I** was optimized from the initial planar Franck-Condon geometry and this relaxed geometry results in a net stabilization of 28 kcal/mol. The above-mentioned stabilization was found to be ~30 kcal/mol after including the dynamical correlation effects (CASMP2). The energy gap of vertical and relaxed planar excited states for the unsubstituted system (**II**) was found to be in the similar range (26 kcal/mol at CASSCF level and 28.4 kcal/mol at CASMP2 level).

Table 3-1: Structural parameters of optimized ground state (GS) and excited state (ES) geometries at various level of calculations. The bond lengths are in Angstrom (Å).

System	State	Method	C1-C2	C2-C3	C3-C4	C4-C-5	C5-N	N-O	N-C6
I	GS	CASSCF(8,8)/6-31G*	1.322	1.465	1.350	1.449	1.317	1.273	1.455
		CASSCF(6,6)/6-31G*	1.341	1.463	1.330	1.452	1.311	1.253	1.456
		CASSCF(4,4)/6-31G*	1.343	1.464	1.330	1.451	1.312	1.254	1.456
		RHF /6-311G**	1.322	1.458	1.330	1.446	1.276	1.280	1.453
	ES	CASSCF(8,8)/6-31G*	1.447	1.388	1.423	1.412	1.434	1.266	1.423
		CASSCF(6,6)/6-31G*	1.434	1.356	1.418	1.433	1.406	1.273	1.423
CASSCF(4,4)/6-31G*		1.434	1.350	1.425	1.444	1.405	1.274	1.423	
II	GS	CASSCF(8,8)/6-31G*	1.345	1.460	1.352	1.449	1.315	1.265	–
		CASSCF(6,6)/6-31G*	1.343	1.465	1.330	1.448	1.292	1.275	–
		CASSCF(4,4)/6-31G*	1.343	1.465	1.329	1.452	1.308	1.247	–
		RHF /6-311G**	1.321	1.460	1.327	1.449	1.274	1.266	–
	ES	CASSCF(8,8)/6-31G*	1.452	1.387	1.427	1.404	1.420	1.258	–
		CASSCF(6,6)/6-31G*	1.451	1.387	1.426	1.407	1.395	1.265	–
CASSCF(4,4)/6-31G*		1.437	1.348	1.429	1.438	1.389	1.268	–	

On analyzing the atomic charges (Table 3-3), it was found that after the initial photo-excitation, an electronic transfer from oxygen to the nitrogen (or to the conjugated chain) takes place. This electronic transfer reduces the positive charge on nitrogen. Our previously studied *N*-alkyl-substituted systems (Chapter 2) had also produced similar results; however, the extent of electronic transfer from oxygen to nitrogen was much more pronounced in previously studied systems than the *N*-trifluoromethyl substituted system. The electron-withdrawing effect of the $-CF_3$ group in system **I** has taken away the excess negative charge accumulated on nitrogen (gained from the breaking of the C=N pi bond and electron transfer from oxygen), and consequently the positive charge on nitrogen has been relatively less affected in the excited state of this system. This was

further confirmed by the shorter N–CF₃ bond distance in the planar excited state (1.42 Å) in comparison to that of the ground state (1.45 Å). A negative hyperconjugative effect [40-42] can be the possible reason which happens due to the donation of electron density from the filled p-orbital of nitrogen to neighbouring σ^* -orbital of the carbon of CF₃ group (Figure 3-4) [14,15]; this indicates that the accumulated electron cloud on nitrogen will be not easily available and consequentially it stabilizes the planar excited state.

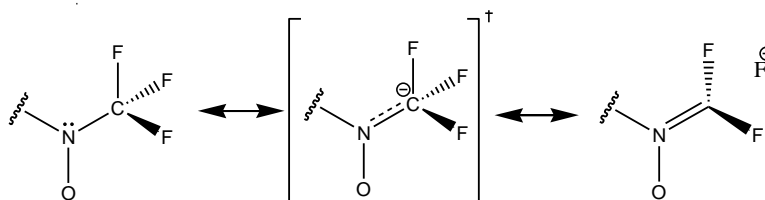


Figure 3-4: A schematic representation of the possible negative hyper-conjugative effect operating in the excited state (S_1) of the system **I**.

Table 3-2: Absolute (E) and relative (ΔE) energies of ground state (GS), vertically excited state (VEE), and optimized excited state (ES) of system **I** and **II** at different levels of calculations

Molecular State	System I				System II			
	CASSCF		CASMP2		CASSCF		CASMP2	
	E (hartree)	ΔE (kcal/mol)	E (hartree)	ΔE (kcal/mol)	E (hartree)	ΔE (kcal/mol)	E (hartree)	ΔE (kcal/mol)
GS	-658.2627 ^a	0 ^a	-659.8365 ^a	0 ^a	-322.6502 ^a	0 ^a	-323.5868 ^a	0 ^a
	-658.2912 ^b	0 ^b	-659.8154 ^b	0 ^b	-322.6812 ^b	0 ^b	-323.5528 ^b	0 ^b
	-658.2916 ^c	0 ^c	-659.8203 ^c	0 ^c	-322.7080 ^c	0 ^c	-323.5405 ^c	0 ^c
VEE	-658.0809 ^a	114.08 ^a	-659.6425 ^a	121.75 ^a	-322.4631 ^a	117.46 ^a	-323.3856 ^a	125.91 ^a
	-658.0891 ^b	127.10 ^b	-659.6549 ^b	100.17 ^b	-322.5103 ^b	107.23 ^b	-323.3789 ^b	109.08 ^b
	-658.1480 ^c	90.16 ^c	-659.6237 ^c	123.37 ^c	-322.5393 ^c	105.85 ^c	-323.3750 ^c	103.77 ^c
ES	-658.1254 ^a	86.11 ^a	-659.6907 ^a	91.48 ^a	-322.5059 ^a	90.68 ^a	-323.4312 ^a	97.63 ^a
	-658.1301 ^b	101.44 ^b	-659.6945 ^b	75.86 ^b	-322.5516 ^b	81.32 ^b	-323.4235 ^b	81.13 ^b
	-658.1901 ^c	63.75 ^c	-659.6580 ^c	101.84 ^c	-322.5707 ^c	86.21 ^c	-323.4020 ^c	86.97 ^c

Energy values at CASSCF/6-31G* and CASMP2/6-31G* level with ^a(4,4), ^b(6,6) and ^c(8,8) active spaces

B) Transition states and conical intersections

At the CASSCF (4,4) level, a transition state, **TS_{ex}** was detected on the excited state surface of system **I**. This geometry was found to be completely planar and was located only 1 kcal/mol above the relaxed singlet excited state. This low energy barrier on the excited state surface opened up an easily accessible route for the excited state. On the other hand, at the same level of calculation, the transition state (on the excited state surface) of the unsubstituted system (**II**) was found to have no difference in energy with the optimized excited state and found to have almost identical structural parameters.

Table 3-3: Atomic charges determined using Merz-Kollman scheme at the CASSCF/6-31G* level of calculation of trifluoromethyl and methyl- substituted model systems of retinyl nitrone

Atom	CF ₃ -substituted						CH ₃ -substituted			
	GS	ES	CI	TS _G	Ox ₁	Ox ₂	GS ^a	ES ^a	CI ^a	Ox
C(1)	-0.378	-0.375	-0.435	-0.422	-0.425	-0.427	-0.368	-0.366	-0.452	-0.437
C(2)	-0.125	-0.071	-0.062	-0.085	-0.111	-0.089	-0.072	-0.060	0.035	-0.125
C(3)	-0.102	-0.234	-0.098	-0.114	-0.017	-0.065	-0.141	-0.289	-0.350	-0.024
C(4)	-0.166	-0.091	-0.241	-0.085	-0.289	-0.288	-0.179	-0.087	0.028	-0.235
C(5)	-0.077	-0.137	0.051	-0.050	0.376	0.527	-0.135	0.035	-0.034	0.341
N	0.160	0.122	-0.238	-0.154	-0.374	-0.436	0.506	0.188	-0.161	-0.317
C(6)	0.589	0.650	0.642	0.597	0.758	0.783	-0.448	0.077	-0.192	0.071
O	-0.417	-0.337	-0.102	-0.146	-0.229	-0.257	-0.610	-0.305	-0.149	-0.285

^aReference [6]

In the last few decades, conical intersections have earned a lot of attention due to their key role in the mechanism of several important photochemical processes [43-58]. In chapter 2 we have discussed the significance of the lowest energy conical intersection (with terminal CNO twist) in the formation of ground state oxaziridine species. The studied photochemical path with biradicaloid lowest-energy conical intersection geometry was found to have some similarity with the benzene-prefulvene photoisomerization process, commonly known as the channel 3 decay [59-61]. The major aim of the work of this part was similar to chapter 2, i.e. to track the possible photochemical route of nitrone-oxaziridine conversion; therefore we had employed similar level of calculations, as discussed earlier. In the next section, the presence of non-radiative decay channels in the *N*-EWG substituted nitrone system (**I**) has been discussed.

a) Conical intersection geometries at CAS (4,4) level

During our investigations on the PESs of these studied systems (**I** and **II**), a number of interesting conical intersection geometries corresponding to different types of turns and twists, were obtained. In both the systems (**I** and **II**) the conical intersection geometries corresponding to hula twist motion and one-bond-flip twist were found to be situated above the optimized excited state structure. A central kinked type conical intersection was also found for system **I** with almost same energy as its planar excited state. For system **I**, along with the above mentioned conical intersection geometries, CAS (4,4) active space calculation has given the lowest energy conical intersection point (**CI**; shown in Figure 3-5), which arises due to a terminal twist in the C–N–O moiety. This intersection point (**CI**) was obtained by giving a conical intersection optimization [62-65] run on the planar excited state geometry. The resulting structure seems to form an out-of-plane CNO triangle, which resembles the oxaziridine structure. However, the

geometrical parameters of this **CI**, such as C5–O bond (~ 2.19 Å) and N–O bond (1.36 Å) were found to be substantially different from the reported values [66] of the terminal 3-membered heterocyclic species. To form an oxaziridine from this structure further stretching of N–O bond and shortening of C5–O bond is required. Interestingly, the opposite direction of the gradient difference vectors (-GD) of **CI** (Figure 3-5) showed a possibility of the C5–O bond shortening and on following these vectors an oxaziridine type structure was obtained. It should be mentioned here that the gradient difference (GD) and derivative coupling (DC) vectors of a conical intersection give the directions in which the degeneracy of the two states might be lifted to form possible relaxation channels leading to the photoproduct formation. This was discussed in detail in the earlier chapters.

On the other hand, conical intersection optimization run on the transition state (**TS_{ex}**) led to an intersection point (**CI'**), which was found to be the mirror-image of the **CI** geometry. The structural parameters, atomic charges and energy of this mirror-image geometry (**CI'**) were identical to the lowest energy intersection species (**CI**). At the CASSCF level these enantiomeric geometries were found to be situated around 27 kcal/mol (Table 3-4) below the planar excited state. A difference of 3.5 kcal/mol energy was found between these two conical intersection geometries after inclusion of dynamic correlation effect (CASMP2). The GD and DC vectors of these enantiomeric intersection geometries indicated that these conical intersections are heading towards completely different types of photoproducts at the end. In contrast to **CI**, no indication of oxaziridine formation was noticed from the vectors of the **CI'**.

Table 3-4: Absolute (E) and relative (ΔE) energy values of various important geometries of system **I** with respect to its relaxed planar excited state (ES).

Geometries on PES	CASSCF/6-31G*		CASMP2/6-31G*	
	E in hartree	ΔE in kcal/mol	E in hartree	ΔE in kcal/mol
ES	-658.1254	0	-659.6907	0
CI	-658.1685	-27.01	-659.7395	-30.66
CI'	-658.1683	-26.92	-659.7452	-34.24
TS_{ex}	-658.1237	1.07	-659.6900	0.43
TS_G	-658.2113	-53.88	-659.7527	-38.94
Ox₁	-658.2386	-71.04	-659.8469	-98.01
Ox₂	-658.2717	-91.81	-659.8410	-94.35

At CASSCF (4,4) level, the lowest energy conical intersection geometry of the unsubstituted system (system **II**) was found to be located around 25 kcal/mol below the relaxed excited state geometry. The GD and DC vectors of this intersection point were

found to be completely different from system I (Figure 3-6), and on following these vectors no indication of oxaziridine formation was noticed. Therefore, no further calculations were carried out on this system (II).

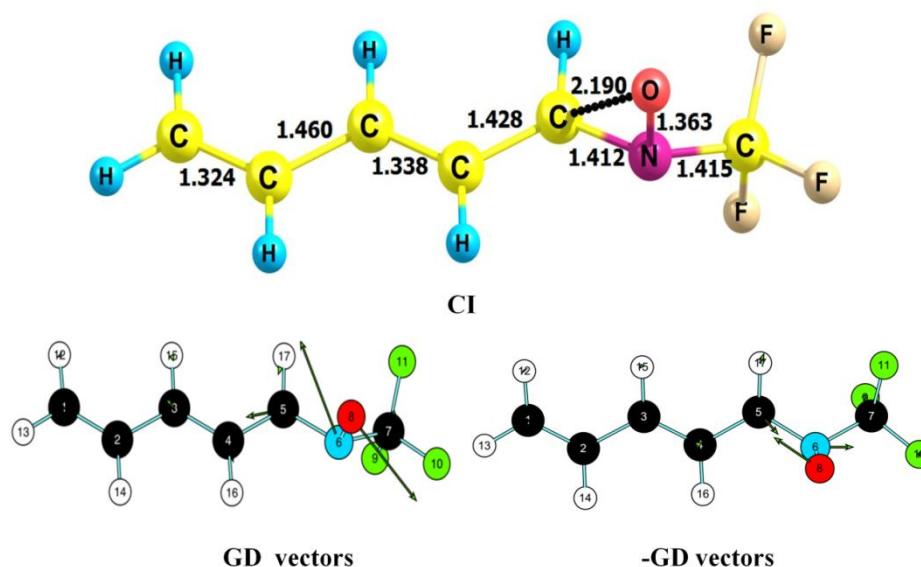


Figure 3-5: Optimized conical intersection (CI) geometry of system I at the CAS(4,4)/6-31G* level with its gradient difference (GD) and -GD vectors.

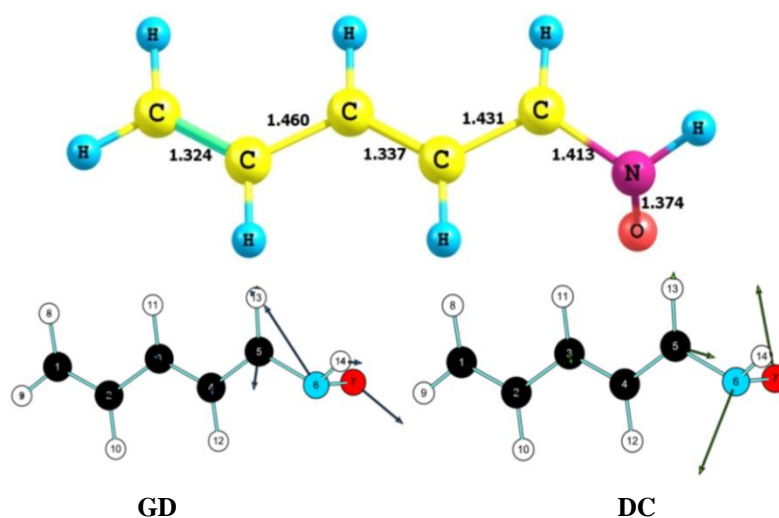


Figure 3-6: Optimized conical intersection geometry of system II at the CAS(4,4)/6-31G* level with its corresponding gradient difference (GD) and derivative coupling (DC) vectors.

b) Conical intersection geometries with larger active spaces

We had also performed CASSCF calculations with higher active spaces, but these calculations were not successful as they didn't approach any oxaziridine-type geometry. At CAS (6,6) active space, a terminally twisted conical intersection was approached initially; however, this conical intersection run didn't converge and the optimization was incomplete (Figure 3-7a). However, CAS (8,8) active space calculation was completely unable to produce any terminal C–N–O twist and it headed towards some other reaction

path. The (8,8) calculation had resulted in a centrally twisted kinked-type of conical intersection, which was located at higher energy than the optimized excited state (at the same level) (Figure 3-7b). The GD and DC vectors of this kinked-type conical intersection did not give any indication of oxaziridine formation. Therefore, we did not perform any further calculations using these active spaces.

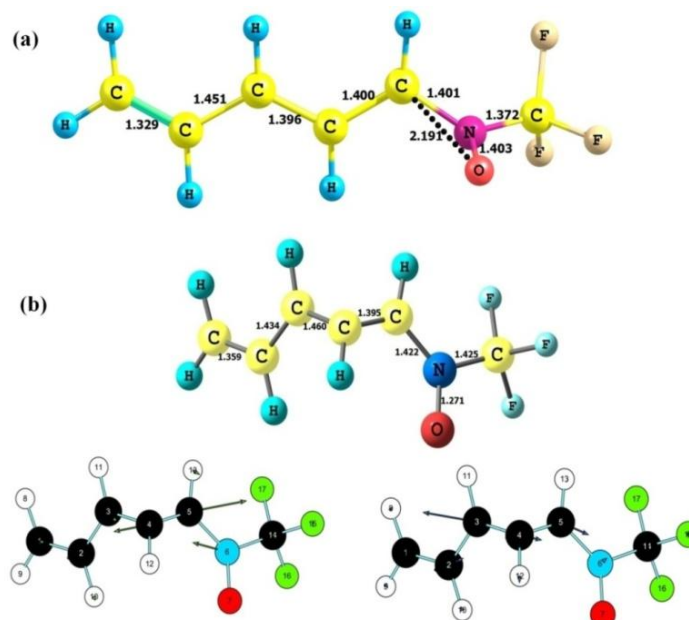


Figure 3-7: (a) Non-Optimized conical intersection geometry at CASSCF (6,6)/6-31G* level and (b) optimized conical intersection geometry at CASSCF (8,8)/6-31G* level with its GD and DC vectors.

C) Possible photoproducts of system I

As discussed in section 3.1, oxaziridines with EWG or π -conjugating substituents on nitrogen are known to be synthesized from oxidation of imines. To the best of our knowledge, photo-excitation of nitrones with *N*-EWG leading to corresponding oxaziridine has never been reported, so far. In this study, we have obtained an optimized oxaziridine geometry (Ox_1) following the opposite direction of the GD vectors ($-\text{GD}$) of **CI**. The geometrical parameters of this species resemble the experimentally reported structure of oxaziridine [66]. In addition to this, at CASSCF level, a transition state (TS_G) was detected on ground state surface at 32 kcal/mol (and 52 kcal/mol at CASMP2 level) above the ground-state nitron geometry. The transition vectors corresponding to the single imaginary frequency of TS_G have indicated a stretch of C5–O moiety (Figure 3-8) in forward direction, and this was found to be exactly parallel to the GD vectors of **CI**. This clearly indicated that TS_G is a continuation of the reaction path which passes through the **CI** point. Following the reverse direction of transition vectors of TS_G , an oxaziridine-type (Ox_2) geometry with an elongated N–O bond (1.52 Å) was obtained

(Figure 3-9). Comparison of Ox_1 and Ox_2 with the reported oxaziridine geometry revealed that Ox_2 is more towards an amide than an oxaziridine. The possibility of amide formation from oxaziridine with EWG on nitrogen was earlier suspected by Khoei and Memarian [8]. They proposed that this oxaziridine-amide conversion occurs through a biradical intermediate involving N–O bond cleavage. The electronic charge scheme described by them for oxaziridine (total 3-electrons on nitrogen, and an odd electron on oxygen) with *N*-EWG, is quite comparable to the atomic charges of the Ox_2 species (Table 3-3). The IRC calculation on TS_G geometry (Figure 3-8) has revealed that this transition state connects **P** and Ox_2 geometries on the ground state surface, where **P** is a product along the photochemical reaction path (Figures 3-8 and 3-10).

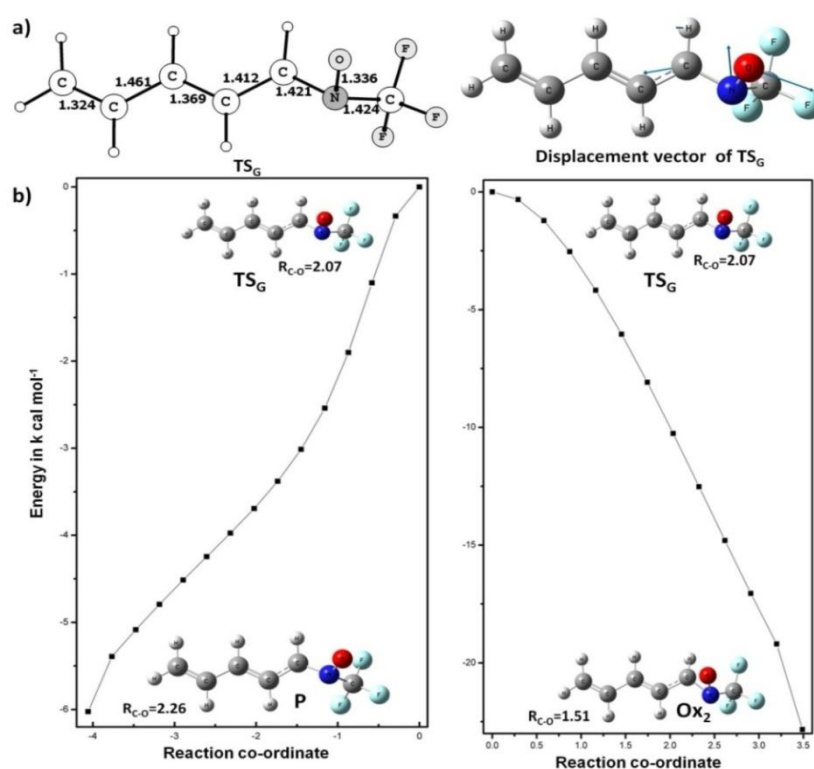


Figure 3-8: (a) Transition state (TS_G) with displacement vectors corresponding to its imaginary frequency (b) Forward and reverse intrinsic reaction coordinate (IRC) path of TS_G

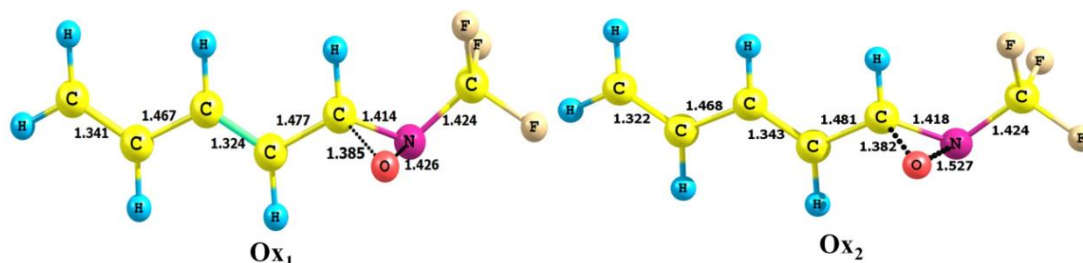


Figure 3-9: Optimized geometries of Ox_1 and Ox_2 with structural parameters at the CASSCF/6-31G* level of calculation.

3.3.2. A complete possible scheme of the photochemical path of system I

The photochemical process of system I (Figure 3-10) starts with the photo-excitation of the ground-state to its first singlet excited state which is followed by a non-radiative decay channel through the lowest energy conical intersection point, **CI**. This route subsequently leads to two important geometries; following the $-GD$ vectors, the normal oxaziridine (**Ox₁**) geometry was obtained, while through the ground state transition state (**TS_G**), the oxaziridine-type **Ox₂** species has been found along with the other photoproduct, **P**. The path towards **Ox₂** has a possibly broken N–O bond which may form amide on further [1,2-H] shift. A summary of the whole photochemical process is shown in Figure 3-11. This result shows an interesting fact that an amide may appear directly as a photoproduct from this kind of nitrones. A gradual increase in the N–O bond length (1.363 to 1.527 Å) and a decrease in the C–O bond length (2.19 to 1.382 Å) were observed in the path **CI-TS_G-Ox₂**. An opposite trend was noticed in the **CI-TS_G-P** conversion process. Overall, the predicted photoproducts are **Ox₁** and **Ox₂** (along with **P**), where the latter has an elongated (or broken) N–O bond which may eventually form amide.

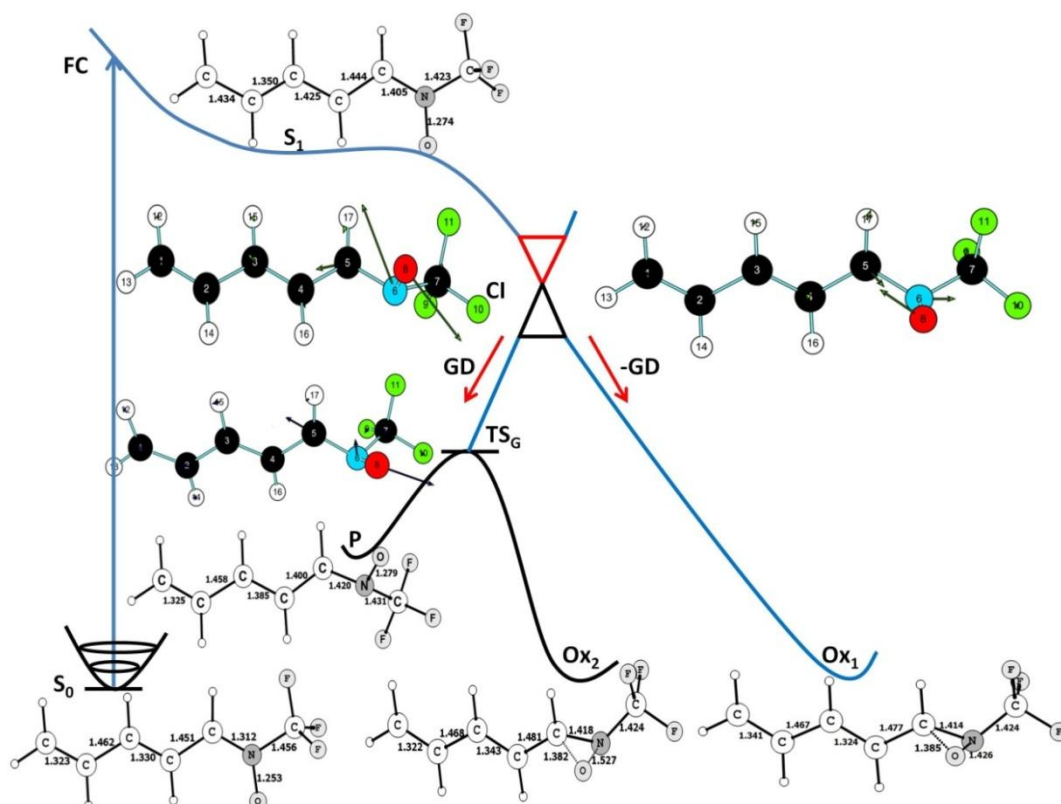


Figure 3-10. A Schematic representation of the non-radiative decay in system I

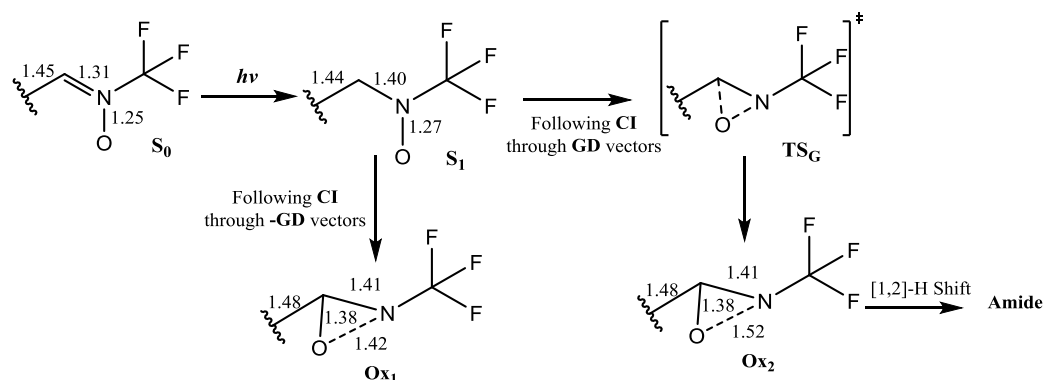


Figure 3-11. A summary of the whole photochemical process operating in system I.

3.3.3. Radiative transition properties

Using the GUGA-CISD code in GAMESS program, the radiative transition properties (oscillator strength and radiative transition moment) of the lowest energy ($S_0 \rightarrow S_1$) transitions were calculated for both the systems at their respective optimized ground state geometries. The transition moment values of these two systems were found to differ by 0.5 Debye. A comparison of transition parameters for the studied systems (**I** and **II**) with the *N*-methyl-substituted conjugated nitron is shown in Table 3-5. The values of these radiative transition parameters of trifluoromethyl-substituted nitron were found to be higher than the values observed for *N*-methyl-substituted nitron systems (Chapter 2).

Table 3-5: Radiative transition properties of the studied systems corresponding to the lowest energy ($S_0 \rightarrow S_1$) transitions at their respective ground state equilibrium geometry .

Systems	Radiative transition Moment in Debye				Oscillator Strength	
	μ	μ_x	μ_y	μ_z	f_L	f_V
<i>N</i> -trifluoromethyl-substituted model retinyl nitron (system I)	4.98	-4.589	-1.933	-0.002	1.049	0.123
Unsubstituted model retinyl nitron (system II)	4.49	-4.375	1.022	0.000	0.597	0.170
<i>N</i> -methyl-substituted model retinyl nitron system ^a	4.86	-4.684	-1.296	0.002	0.706	0.195

^aReference [6]

3.4. Possible practical significance of this work

The chemopreventive retinyl nitrones with electron-donating *N*-alkyl groups (discussed in the previous chapter) were reported to give stable oxaziridines [4] as the primary photoproduct which was confirmed by our theoretical studies on these nitrones and their model compounds [6]. In contrast, the presence of *N*-EWG substitution in these nitrones seems to produce an oxaziridine-type species with an elongated N–O bond along with a proper oxaziridine, both originating from the lowest-energy conical intersection geometry. The **Ox₁** geometry resembles (both geometrically and charge-wise) the

oxaziridine structure obtained from the analogous conjugated *N*-methyl nitronone system (Table 3-3). On the other hand, the possibility of **Ox₂** and thereafter an amide compound through a barrierless path on photo-excitation of nitronones could be an important finding, especially when the study on the model compound is extended to the corresponding retinyl nitronone system. In this type of nitronone system, the presence of EWG on nitrogen seems to open up a facile route for retinamide formation under photo-excitation. Retinamides [67-69] are reported to have chemo-preventive nature with low toxicity. They are known as potent drug candidates for the prevention of various chemically-induced cancers (i.e. skin, mammary gland and urinary bladder cancer). In addition, amide and their derivatives with *N*-trifluoromethyl group are reported to have antifungal [70] and anti-HIV [71,72] properties. Overall, the possibility of formation of the so far unexplored *N*-trifluoromethyl retinamide from the photo-excitation of their corresponding retinyl nitronone may lead to a significant route to form a highly pharmacologically active compound. In fact, substitution of other EWGs may also lead to their corresponding retinamide systems, through a similar mechanism.

3.5. Conclusions

The reported theoretical results in this work can contribute significantly to the oxaziridine and amide chemistry. The photo-excitation of the conjugated open-chain nitronone system with *N*-EWG substitution was found to result in two different types of oxaziridine species. The obtained results from this study have similarities with the experimentally reported observations on *N*-sulfonyl and *N*-aryl nitronones. This has indicated that the proposed mechanism for *N*-trifluoromethyl-substituted nitronone is equally applicable to any acyclic nitronone system having strong electron-pulling and π -conjugation (hyperconjugative group) on the nitrogen atom. The oxaziridines with EWG on nitrogen are usually known to be prepared from imine-oxidation or ketone amination, rather than the nitronone photo-excitation. This study reveals that in addition to a conventional oxaziridine (**Ox₁**), an oxaziridine-type look-alike species (**Ox₂**) appears in the photo-excitation process with a broken N–O bond, and a [1,2-H] shift may lead to an amide as the photoproduct. Both these processes were found to be barrierless and pass through the lowest energy conical intersection (CI) point having a terminal C–N–O twisted geometry. A continuous decrease in the C–O bond length and increase in the N–O bond length ultimately forms these two species through this low lying CI with a possible amide compound from one of them. This work has strongly justified the possibility reported almost a decade ago by other groups that the unstable oxaziridine-

type species obtained from nitrones with EWGs on nitrogen are likely to give N–O bond cleavage with three electrons on nitrogen and one electron on oxygen, which eventually leads to amide formation. The possibility of obtaining an amide as one of the photoproducts from a suitably substituted nitrone system through a barrierless photochemical route may provide useful information to the organic photochemists and there remains huge scope for the experimentalists to explore this field in future.

3.6. References

1. E. Lipczynska-Kochany and J. Kochany, *J. Photochem. Photobiol. A: Chem.*, 1988 **45**, 65.
2. J. S. Splitter and M. Calvin, *J. Am. Chem. Soc.*, 1965, **30**, 3427.
3. J. S. Splitter, T.-M. Su, H. Ono and M. Calvin, *J. Am. Chem. Soc.*, 1971, **93**, 4075.
4. V. Balogh-Nair and K. Nakanishi, *Pharm. Res.*, 1984, **1**, 93.
5. P. Saini and A. Chattopadhyay, *RSC. Adv.*, 2015, **5**, 22148.
6. P. Saini and A. Chattopadhyay, *RSC. Adv.*, 2014, **4**, 20466.
7. P. Saini and A. Chattopadhyay, *Chem. Phys. Lett.*, 2015, **633**, 6.
8. S. Khoei and H. R. Memarian, *J. Photochem. Photobiol. A, Chem.*, 2006, **177**, 276.
9. F. A. Davis and O. D. Stringer, *J. Org. Chem.*, 1982, **47**, 1774.
10. M. Bucciarelli, A. Forni, I. Moretti and G. Torre, *J. Chem. Soc., Perkin Trans.2*, 1983, 923.
11. W. B. Jennings, S. P. Watson and M. S. Tolley, *J. Am. Chem. Soc.*, 1987, **109**, 8099.
12. V. A. Petrov and G. Resnati, *Chem. Rev.*, 1996, **96**, 1809.
13. P. Saini and A. Chattopadhyay, *J. Chem. Sci.*, 2015, **127**, 1757.
14. J.-J. Yang, R. L. Kirchmeier and J. M. Shreeve, *J. Org. Chem.*, 1998, **63**, 2656.
15. O. Exner and S. Böhm, *New J. Chem.*, 2008, **32**, 1449.
16. M. C. Karni, F. Bernasconi and Z. Rappoport, *J. Org. Chem.*, 2008, **73**, 2980.
17. M. J. Frisch et al., *Gaussian 09*, **B.01**, Gaussian Inc., Wallingford, CT, 2010.
18. D. Hegarty and M. A. Robb, *Mol. Phys.*, 1979, **38**, 1795.
19. R. H. A. Eade and M. A. Robb, *Chem. Phys. Lett.*, 1981, **83**, 362.
20. H. B. Schlegel and M. A. Robb, *Chem. Phys. Lett.*, 1982, **93**, 43.
21. F. Bernardi, A. Bottini, J. J. W. McDougall, M. A. Robb and H. B. Schlegel, *Far. Symp. Chem. Soc.*, 1984, **19**, 137.

22. M. J. Frisch, I. N. Ragazos, M. A. Robb and H. B. Schlegel, *Chem. Phys. Lett.*, 1992, **189**, 524.
23. N. Yamamoto, T. Vreven, M. A. Robb, M. J. Frisch and H. B. Schlegel, *Chem. Phys. Lett.*, 1996, **250**, 373.
24. M. J. Bearpark et al., *J. Photochem. Photobio. A: Chem.*, 2007, **190**, 207.
25. X. Li and M. J. Frisch, *J. Chem. Theory Comput.*, 2006, **2**, 835.
26. H. P. Hratchian and H. B. Schlegel, *Theory and Applications of Computational Chemistry: The First 40 Years*, Eds., C. E. Dykstra, G. Frenking, K. S. Kim and G. Scuseria, Amsterdam, Elsevier, 2005
27. H. P. Hratchian and H. B. Schlegel, *J. Chem. Theory Comput.*, 2005, **1**, 61.
28. H. P. Hratchian and H. B. Schlegel, *J. Chem. Phys.*, 2004, **120**, 9918.
29. M. W. Schmidt et al., *J. Comput. Chem.*, 1993, **14**, 1347.
30. B. Brooks and H. F. Schaefer, *J. Chem. Phys.*, 1979, **70**, 5092.
31. B. Brooks, W. Laidig, P. Saxe, N. Handy and H. F. Schaefer, *Physica Scripta*, 1980, **21**, 312.
32. A. Chattopadhyay, *J. Phys. B: At. Mol. Opt. Phys.*, 2012, **45**, 035101.
33. A. Chattopadhyay, *J. Chem. Sci.*, 2012, **124**, 985.
34. F. Weinhold, *J. Chem. Phys.*, 1970, **54**, 1874,
35. C. W. Bauschlicher and S. R. Langhoff, *Theor. Chim. Act.*, 1991, **79**, 93.
36. S. Koseki and M. S. Gordon, *J. Mol. Spect.*, 1987, **123**, 392.
37. U. C. Singh and P. A. Kollman, *J. Comput. Chem.*, 1984, **5**, 129.
38. B. H. Besler, Jr. K. M. Merz and P. A. Kollman, *J. Comput. Chem.*, 1990, **11**, 431.
39. Website of Chemcraft software: <http://www.chemcraftprog.com>
40. I. V. Alabugin, M. Manoharam, M. Buck and R. J. Clark, *J. Mol. Struct. (Theochem)*, 2007, **813**, 21.
41. I. V. Alabugin, S. Bresch and M. Manoharam, *J. Phys. Chem. A*, 2014, **118**, 3663.
42. I. V. Alabugin, K. M. Gilmore and P. W. Peterson, *WIREs Comput. Mol. Sci.*, 2011, **1**, 109.
43. M. Garavelli, P. Celani, F. Bernardi, M. A. Robb and M. Olivucci, *J. Am. Chem. Soc.*, 1997, **119**, 6891.
44. J. E. Norton and K. N. Houk, *Mol. Phys.*, 2006, **104**, 993.
45. M. Olivucci, F. Bernardi, P. Celani, I. Ragazos and M. A. Robb, *J. Am. Chem. Soc.*, 1994, **116**, 1077.

46. P. Celani, M. Garavelli, S. Ottani, F. Bernardi, M. A. Robb and M. Olivucci, *J. Am. Chem. Soc.*, 1995, **117**, 11584.
47. A. Cembran, F. Bernardi, M. Olivucci and M. Garavelli, *Proc. Natl. Acad. Sci.*, 2005, **102**, 6255.
48. D. S. Ruiz, A. Cembran, M. Garavelli, M. Olivucci and W. Fuß, *Photochem. Photobiol.*, 2002, **76**, 622.
49. J. A. Dobado and M. Nonella, *J. Phys. Chem.*, 1996, **100**, 18282.
50. I. Conti, F. Bernardi, G. Orlandi and M. Garavelli, *Mol. Phys.*, 2006, **104**, 915.
51. I. Conti and M. Garavelli, *J. Photochem. Photobio. A: Chem.*, 2007, **190**, 258.
52. D. Polli et al., *Nature*, 2010, **467**, 440.
53. S. R. Reddy and S. Mahapatra, *J. Chem. Phys.*, 2014, **140**, 084311.
54. V. S. Reddy, S. N. Reddy and S. Mahapatra, *Theo. Chem. Acc.*, 2015, **134**, 39.
55. T. Mondal and S. Mahapatra, *J. Chem. Phys.*, 2010, **133**, 084304.
56. S. Mukherjee, S. Bandyopadhyay, A. K. Paul and S. Adhikari, *J. Phys. Chem. A*, 2013, **117**, 3475.
57. A. K. Paul, S. Ray, D. Mukhopadhyay and S. Adhikari, *J. Chem. Phys.*, 2011, **135**, 034107.
58. M. Araujo, B. Lasorne, M. J. Bearpark, and M. A. Robb, *J. Phys. Chem. A*, 2008, **112**, 7489.
59. A. Migani and M. Olivucci, *Conical Intersections: Electronic Structure, Dynamics & Spectroscopy Advanced series in Physical Chemistry*, World Scientific Publishing Co. (P). Ltd., Singapore, 2004
60. I. J. Palmer, I. N. Ragazos, F. Bernardi, M. Olivucci and M. A. Robb, *J. Am. Chem. Soc.*, 1993, **115**, 673.
61. J. Dreyer and M. Klessinger, *Chem. Eur. J.*, 1996, **2**, 335.
62. N. Ragazos, M. A. Robb, F. Bernardi and M. Olivucci, *Chem. Phys. Lett.*, 1992, **197**, 217.
63. M. J. Bearpark, M. A. Robb and H. B. Schlegel, *Chem. Phys. Lett.*, 1994, **223**, 269.
64. F. Bernardi, M. Olivucci and M. A. Robb, *Chem. Soc. Rev.*, 1996, **25**, 321.
65. F. Sicilia, L. Blancafort, M. J. Bearpark and M. A. Robb, *J. Chem. Theory Comput.*, 2008, **4**, 257.
66. S. S. Murphree, *Modern Heterocyclic Chemistry*, Eds., J. Alvarez-Builla, J. J. Vaquero and J. Barluenga, Wiley-VCH Verlag & Co. KGaA, Weinheim, Germany, 2011.

67. A. B. Barua and J. A. Olson, *J. Lipid Res.*, 1985, **26**, 258.
68. R. Kuefer et al., *Neoplasia*, 2007, **9**, 246.
69. S. Bruno et al., *Leukemia*, 2012, **26**, 2260.
70. Y. Hagooly, J. Gatenyo, A. Hagooly and S. Rozen, *J. Org. Chem.*, 2009, **74**, 8578.
71. K. K. Sahu, V. Ravichandran, V. K. Mourya and R. K. Agrawal, *Med. Chem. Res.*, 2007, **15**, 418.
72. J. Ren, J. Milton, K. L. Weaver, S. A. Short, D. I. Stuart and D. K. Stammers, *Structure*, 2000, **15**, 1089.

CHAPTER 4

A computational investigation of the photochemical nitrone-oxaziridine conversion and thermal *E-Z* isomerization processes of fluorescent α -(2-naphthyl)-*N*-methylnitronone**4.1. Introduction**

Nitrones are well known to have various pharmacological activities. They have neuroprotective, antiaging [1,2], anti-inflammatory characteristics and they are used in the treatment of degenerative age-related diseases, such as Alzheimer's disease [3]. They also act as important pharmacological agents in several other diseases [4-10], as well; one such example of pharmacologically active nitrone system is the chemopreventive *N*-alkyl retinylnitrones [11]. Computational studies [12,13] on these nitrone systems were done in chapter 2. Their photochemical nitrone to oxaziridine conversion mechanism was found to involve the lowest-energy biradicaloid conical intersection, which led to the 3-membered heterocyclic oxaziridine species as the primary photoproduct.

The photochemical studies of nitrones have been experimentally carried out by several groups in the last few decades [14,15]. The results of these studies can be summarized into two important observations; the conversion of nitrone to oxaziridines and other photo-products (such as amides) involve photo-excitation through singlet excited states while their *cis-trans* isomerization reactions occur thermally or through triplet excited states in presence of photosensitizers [16,17]. The other important feature of the nitrone-oxaziridine photoconversion was found to be the varying stability of oxaziridine, which depends on the type of substitution on nitrogen and/or α -carbon [12,18]. Experimental studies have shown that *N*-alkyl substituent increases their stability where as opposite effects were noticed in the presence of *N*-aryl or *N*-EWGs. Similar observations (regarding the properties photo-irradiation of nitrone systems) were noticed by our group (chapter 2 and 3) through CASSCF-based studies of retinylnitronone systems with *N*-alkyl and *N*-electron withdrawing group substituents [12,13,19]. The work discussed in this chapter is intended to reveal the unexplored mechanism of nitrone to oxaziridine conversion of experimentally studied fluorescent *N*-methyl substituted α -(2-naphthyl)-nitronone (Figure 4-1). This nitronone was reported to give a stable and isolable oxaziridine on photo-irradiation [18], whereas its *N*-(*p*-tolyl) derivative was not found to produce such photoproduct. An increase in the fluorescence intensity with fluctuations was

observed on photo-irradiation of neutral solution of *N*-methyl substituted nitron, which was predicted to be arising due to the formation of efficiently fluorescing oxaziridines.

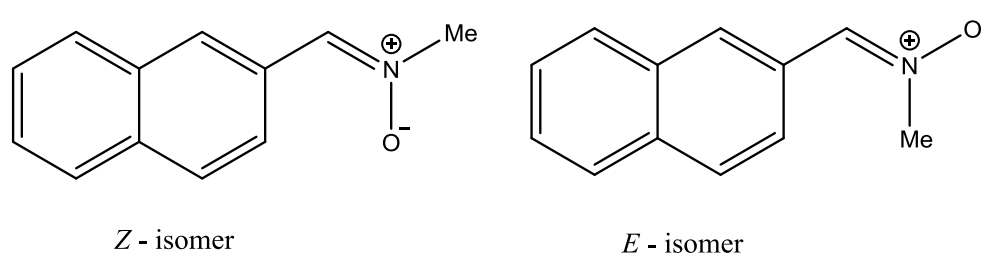


Figure 4-1: The studied *Z* and *E* isomers of the α -(2-naphthyl) *N*-methyl nitron system

The main objective of this work was to propose a proper theoretical background of the nitron-oxaziridine conversion and *E-Z* isomerization processes of the above-mentioned nitron system through high-level quantum mechanical investigations. A comprehensive analysis of the optimized ground state, relaxed excited state, conical intersections [20-24], transition states and other important geometries on the potential energy surfaces was performed for the same. From our studies on the *N*-alkyl retinyl nitrons and their model compounds (chapter 2), it was found that the terminally twisted (C–N–O kink) biradicaloid conical intersections (on the photochemical paths) play a key role in their photochemical conversion to oxaziridine and have some similarity with the prefulvenic conical intersection (in benzene), which appears during its channel-3 decay [24-26]. The present study was carried out to investigate whether our targeted naphthyl nitrons also follow similar conical intersection topography as the retinyl nitron during the oxaziridine conversion step or they differ in nature. In addition, their radiative transition properties were also investigated which led to some interesting results (discussed in latter sections). Computationally calculated UV-Vis peaks of these nitron systems were compared with the experimental values. In addition to all these photochemical and photophysical studies of α -(2-naphthyl)-*N*-methyl nitron, the probable mechanism of its *E-Z* isomerization process was also studied. Results obtained from these studies were published [27].

4.2. Computational methods

CASSCF [28,29] and ONIOM [30-36] based calculations were employed for locating the minimum energy geometries, transition states and conical intersection points on the potential energy surfaces (PES), using Gaussian 09 suite of programs [37]. In addition to these calculations, the ground state geometries of both the studied isomers were also

optimized at the Restricted Hatree-Fock (RHF), Density Functional Theory (DFT) and PM3/CI level of calculations. The excited state topographies were explored using highly accurate multi-configuration-based CASSCF [28,29,38] method. The dynamic correlation effects were treated at the CASMP2 [39,40] level on top of the CASSCF optimized geometries. It must be mentioned here that the choice of active space must be done in a proper way while using the CASSCF method. The use of large active space may be troublesome in several systems which can significantly increase the computational costs. Moreover, it may not be always true that use of a large active space leads to more accurate results; it may take the reaction to some other directions instead of leading to the desired product. On the other hand, reducing the active space size without any knowledge of the actual reaction path can certainly bring huge errors in the computational results. Therefore, some prior experimental knowledge of the studied reaction path is very important; it may help to choose an accurate minimal active space, leaving out the less important orbitals (for that particular reaction) from the calculations. The photochemical study of the model *N*-alkyl retinyl nitron system (discussed in chapter 2) has clearly indicated that these systems experience a twist at the terminal C–N–O region during the oxaziridine formation step without any significant change in the conjugated chain part. These studies also concluded that involvement of the orbitals having electronic cloud distributed over the portions of the molecule situated away from the CNO moiety in the active space does not lead to desired oxaziridine product. The same was expected to be true for the α -naphthyl *N*-methyl nitron, as experimental results indicated no change in the naphthyl part during the course of oxaziridine formation. This implies that the large active spaces in this present photochemical study are less likely to capture our desired nitron–oxaziridine photoconversion process. Therefore, we have chosen an accurate minimal active space leaving out the less important naphthyl part from it, and this method is completely biased towards the possible reaction path [34] using previous intuitions from our earlier work and the experimental findings of Kochany et al. [18]. In the discussed work, CASSCF method with 4 active electrons and 4 active orbitals (4,4) were used, where the chosen HOMO is of π symmetry on the CNO moiety and the LUMO is of corresponding π^* symmetry (Figure 4-2). It must be added that we had actually started our CASSCF calculations using a (14,12) active space size, but we were unable to find any oxaziridine type species on the photochemical path similar to the (4,4) active space calculation.

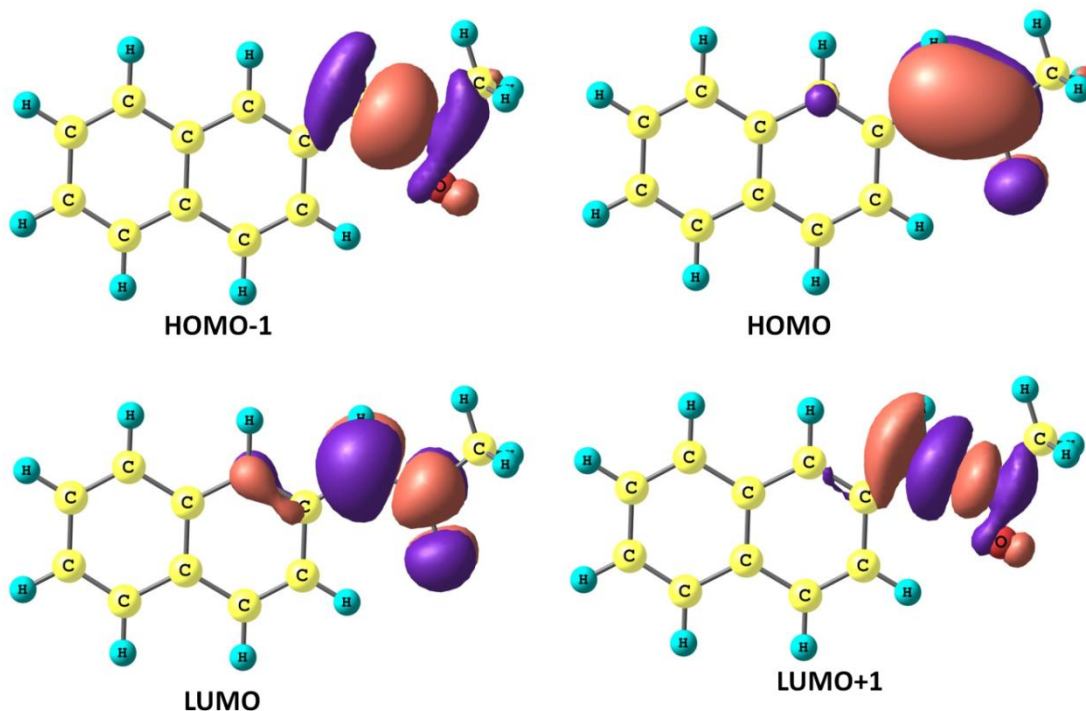


Figure 4-2: Molecular orbitals involved in the active space of CASSCF (4, 4) /6-31G* calculations for the α -(2-naphthyl)-*N*-methyl nitrene.

In addition to the CAS (4,4) and CAS (14,12) methods, in a separate level of calculation, the 2-layer hybrid ONIOM method had been employed for studying the photochemical path of these nitrene systems, as well. The theory of ONIOM methodology is discussed in detail in chapter 1. In ONIOM method, different regions of a system under investigation can be treated with a different level of theory. The region of our interest (the active site), where the chemical process is actually happening can be treated with a higher level of quantum mechanical (QM) theory, while the less important region can be treated with a lower-level QM theory (QM') or molecular mechanics (MM). Keeping this fact in mind that a similar photochemical path as the retinyl nitrene system is probably operating in the α -naphthyl nitrene systems too, we considered the terminal C–N–O moiety as the active site for the ONIOM calculations. We have employed CASSCF (4,4)/6-31G*:RHF/4-31G as a 2-layer QM:QM' method for studying the nitrene-oxaziridine conversion mechanism. The CASSCF-based method (higher level theory) was treated with 4 active electrons in 4 active orbitals, with the C–N–O moiety as the active region (model part), which included the C–N π bond and the p_z orbital on oxygen. Treatment of low level region was done with HF method considering the fact that it will give a better interaction with the model part as both are treated at quantum mechanical level [41].

Transition state optimizations on the potential energy surfaces were done using the normal TS techniques based on Berny-algorithm [42] and QST3 [43] methodologies. To follow the minimum energy path from transition state, intrinsic reaction coordinate (IRC) [44-46] have been used. To calculate electrostatic potential-based atomic charges of the optimized ground and excited state species, Merz-Kollman [47,48] scheme was employed using Gaussian 09 program. The GAMESS [49-53] suite of program was used for the GUGA CI code-based calculations of radiative transitions [54-56] at the ground state equilibrium geometries. Visualizations of the output files were done through ChemCraft [57] and GaussView softwares.

4.3. Results and discussions

4.3.1. Important points on the potential energy surfaces

A) Optimized ground and excited state geometries

The ground and excited state geometries of both the isomers of α -(2-naphthyl)-*N*-methyl nitrene were optimized at different level of calculations (Figure 4-3). A comparison of their structural parameters is shown in Table 4-1. Interestingly, the optimized ground state of the *Z*-isomer was found to be more stable than the experimentally studied [18] *E*-isomer (Table 4-2). Unlike the planar ground state of *Z*-isomer, the *E*-isomer was found to be non-planar, where the naphthyl part was found to be slightly tilted away from the plane to avoid steric interaction with the methyl group. The C–N double bond of this isomer becomes elongated in the optimized first singlet excited state by roughly 0.1 Å (Figure 4-3). The planarity of the optimized excited state of the *Z*-isomer was found to vary with the level of calculation employed; a non-planar structure (with \angle C–C–N–O dihedral angle value of 57°) for this isomer was predicted by CASSCF method whereas ONIOM calculation (Figure 4-3) resulted in a planar excited singlet state. The PM3/CI (4x4) calculations has predicted a non-planar excited state geometry (Figure 4-4) of *Z* isomer (similar to the CASSCF method) with approximately 43° value of the \angle C–C–N–O dihedral angle. However, the optimized geometries of the ground and the first excited singlet states of the *E*-isomer were found to be non-planar for all the studied methods (Table 4-1, Figure 4-3).

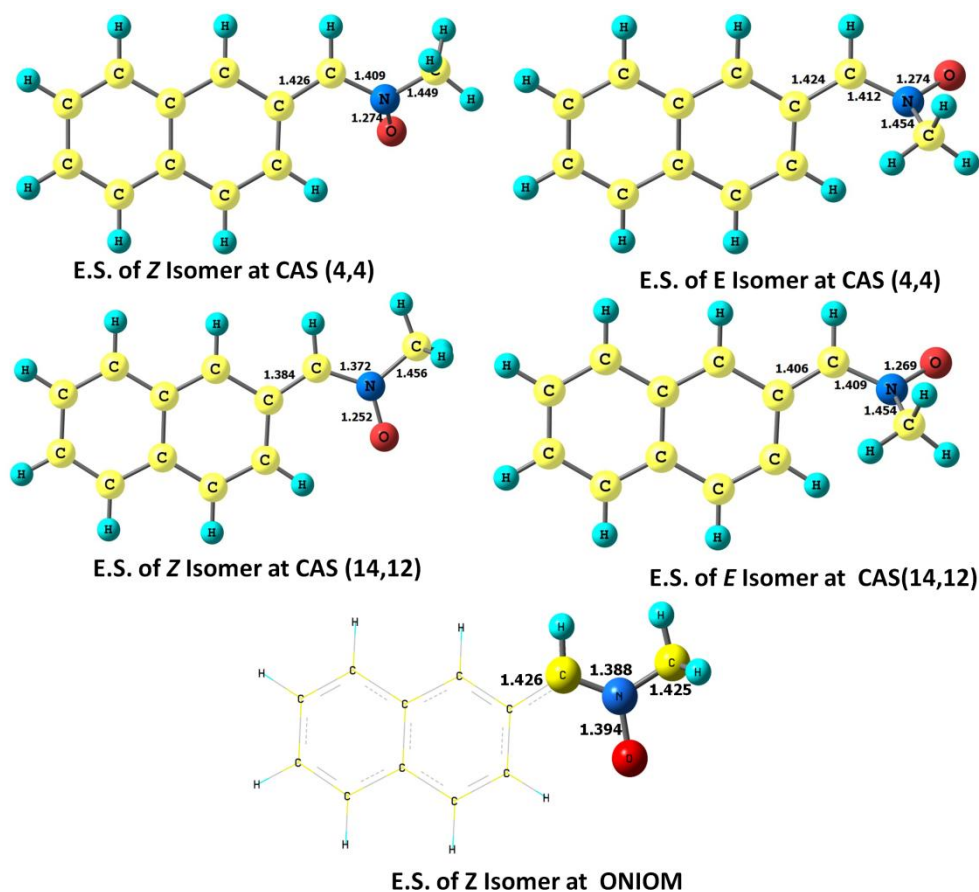


Figure 4-3: Optimized excited state geometries of *E* and *Z* isomers of α -(2-naphthyl)-*N*-methyl nitrene at CASSCF (4,4)/6-31G*, CASSCF(14,12)/6-31G* and ONIOM (QM:QM') level of calculations.

Table 4-1: Structural parameters of the optimized ground states (GS) of *Z* and *E* isomers at various level of calculations. Bond lengths are in Å and angles are in degree.

Molecular States	Level of calculation	C–C	C–N	N–O	N–C	D _{C-C-C-N}	D _{C-C-N-O}
GS of <i>Z</i> -Isomer	CASSCF (4,4)/ 6-31G*	1.469	1.311	1.276	1.459	0.0	0.0
	CASSCF (4,4)/6-31G*:RHF/4-31G	1.456	1.291	1.319	1.455	0.0	0.0
	CASSCF(14,12)/ 6-31G*	1.465	1.303	1.265	1.462	0.0	0.0
	RHF /6-311G **	1.465	1.276	1.265	1.462	0.0	0.0
	B3LYP/ 6-311G **	1.447	1.318	1.271	1.482	0.0	0.0
	PM3/CI	1.455	1.334	1.243	1.507	-24.2	0.1
GS of <i>E</i> -Isomer	CASSCF (4,4)/ 6-31G*	1.483	1.307	1.254	1.466	-60.0	176.6
	CASSCF (4,4)/6-31G*:RHF/4-31G	1.473	1.296	1.274	1.495	-50.5	176.8
	CASSCF(14,12)/ 6-31G*	1.481	1.307	1.254	1.466	-57.5	176.6
	RHF /6-311G **	1.481	1.274	1.265	1.465	-55.7	177.4
	B3LYP/ 6-311G **	1.458	1.318	1.270	1.483	-34.7	175.5
	PM3/CI	1.460	1.330	1.247	1.500	-49.1	-179.7

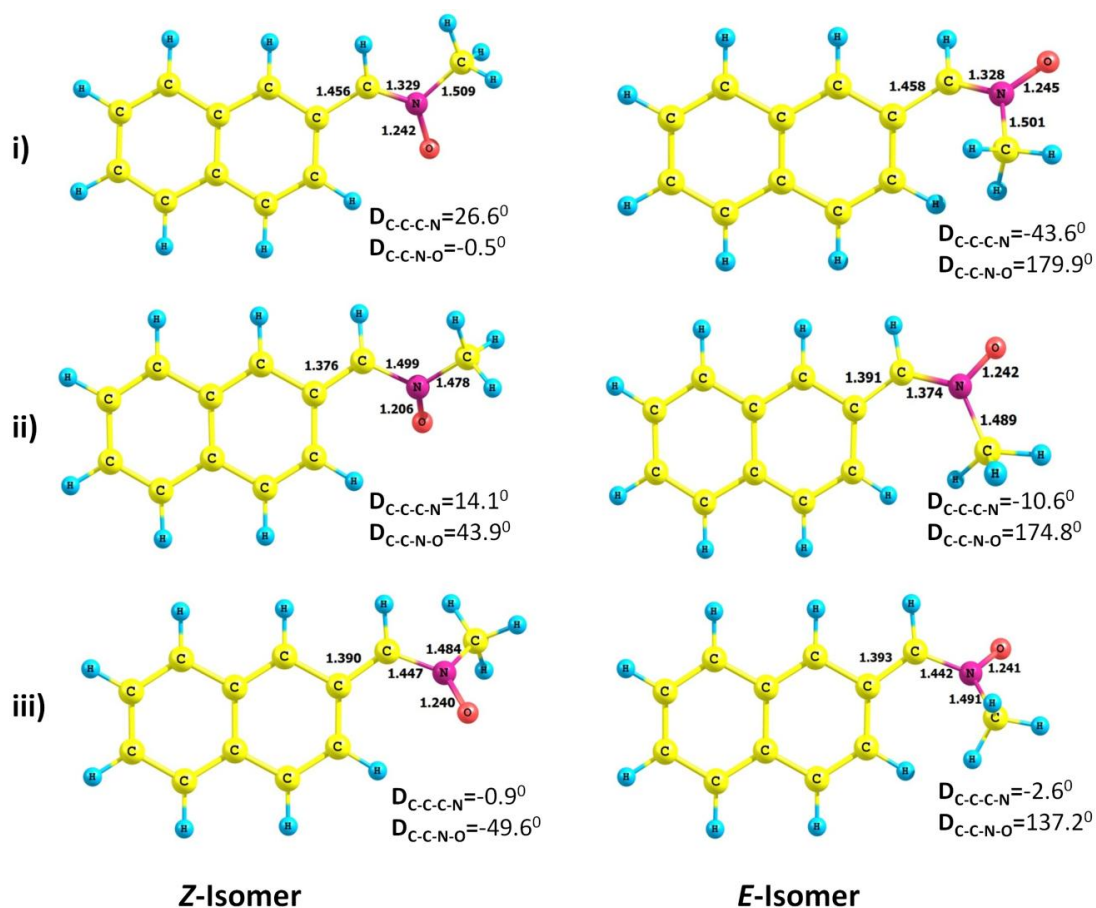


Figure 4-4: i) Ground state ii) Excited state and iii) Biradical excited state geometries of Z and E isomers with important structural parameters obtained at the PM3/CI level of calculations.

The vertical excitation energy (VEE) values of the Z-isomer were found to be 118 and 96 kcal/mol at the CAS(4,4) and CAS(14,12) level of theories, respectively (Table 4-2). Inclusion of dynamic correlation in CASSCF results (CASMP2 calculations) has changed this value to 110 kcal/mol, while the value predicted by 2-layer ONIOM method (98 kcal/mol) was found to be close to the CAS(14,12) predicted values. These latter values have predicted an absorption peak position close to 295 nm. However, the VEE values of the E-isomer calculated at CASSCF (91 kcal/mol, 315 nm) and CASMP2 (85 kcal/mol, 335 nm) level using (4,4) active space were found substantially lower than those predicted at CASSCF(14,12) and ONIOM level (102-103 kcal/mol). The experimental absorption peak position [18] of the E isomer is close to 325 nm. After initial photo-excitation, the vertically excited state of the Z-isomer relaxes by 8-12 kcal/mol to stable excited state equilibrium geometry. However, in the case of E-isomer this stabilization was quite smaller (1-2 kcal/mol). The ESP-based atomic charges (Table 4-3) of these nitrones were found to follow the same trend as our earlier studied long-chain conjugated nitron system (chapter 2). A clear indication of initial electronic

transfer from the oxygen atom can be observed after the photo-excitation; this electronic transfer was found to be responsible for triggering the subsequent photochemical processes.

Table 4-2: Relative energy values (ΔE) of important excited state geometries of *E* and *Z* isomers at different level of calculations; values in parentheses are in nm.

Molecular state	Level of calculation ^a	Z-Isomer ΔE in kcal/mol	E-Isomer ΔE in kcal/mol
Ground State	CASSCF (4,4)/6-31G*	0	0
	CASMP2 (4,4)/6-31G*	0	0
	CASSCF(4,4)/6-31G*:RHF/4-31G	0	0
	CASSCF(14,12)/6-31G*	0	0
Excited State	CASSCF (4,4)/6-31G*	110.68	88.62
	CASMP2 (4,4)/6-31G*	102.05	84.52
	CASSCF(4,4)/6-31G*:RHF/4-31G	86.62	-
	CASSCF(14,12)/6-31G*	84.38	82.70
Vertical excitation energy	CASSCF (4,4)/6-31G*	118.31 (241)	91.30 (313) ^a
	CASMP2 (4,4)/6-31G*	110.89 (257)	84.83 (337) ^a
	CASSCF(4,4)/6-31G*:RHF/4-31G	98.02 (291)	102.34 (279) ^a
	CASSCF(14,12)/6-31G*	95.83 (298)	103.49 (276) ^a

^aExperimental value is 327 nm; Reference [18]

Table 4-3: Atomic charges of optimized ground state (GS) and excited states (ES) of both the isomers, determined using Merz-Kollman scheme at CASSCF/6-31G*

Molecular geometries	C	N	C	O
GS (Z-Isomer)	-0.2204	0.4999	-0.3921	-0.6323
ES (Z-Isomer)	-0.1211	0.2019	-0.3243	-0.2847
GS (E-Isomer)	-0.2808	0.4702	-0.3237	-0.5731
ES (E-Isomer)	-0.2505	0.2395	-0.1331	-0.3243

B) Optimized conical intersections and oxaziridine geometries

The semi-empirical configuration interaction (PM3/CI) calculations were initially employed to have some rough idea of the photochemical processes happening in these systems. The optimized biradical excited state geometries (Figure 4-4 iii) of both the isomers were used as the starting guess structures for the conical intersection optimization run through the CASSCF and ONIOM level of calculations.

At the higher level of *ab initio* calculations (CASSCF and ONIOM), the initial guess geometry corresponding to the Z-isomer has led to two types of conical intersections due to different types of rotations around the C–C bond and C–N bond. The conical intersection point, **CI₁** was formed as a result of simultaneous change of C–C–C–N and

C–C–N–O dihedral angles (Table 4-4). It seems to be a consequence of the Hula twist (HT)-type motion, which is usually responsible for the kinked conical intersection in conjugated polyenes. On the other hand, a terminally-twisted intersection, **CI**₂ (Figure 4-5, Table 4-5) was found with an out-of-plane C–N–O kink (oxygen-bridge) structure; this is formed due to a rotation of the C–C–N–O dihedral angle. This **CI**₂ closely resembles the lowest-energy conical intersection geometries of the long-chain conjugated retinyl nitron systems. The ESP based atomic charges of both the intersection points were found to match the values reported for the lowest energy conical intersection geometries of the model retinyl nitron systems [12]. In other words, similar to the lowest energy conical intersections of the retinyl nitron systems, atomic charge analysis indicated that these CI points are also biradicaloid in nature with an odd electron on the α -C and a reduced electronic cloud on oxygen with a lone pair cloud residing on the nitrogen atom (Table 4-6). Though the geometries obtained from the CI optimization run using the two different methods (CASSCF and ONIOM) are apparently similar, the predicted C–C and C–N bond lengths differ by 0.05 Å. Energetically, the CASSCF and CASMP2 level of calculations detected these conical intersections around 33 and 38 kcal/mol below the optimized excited state; however, the hybrid ONIOM method has predicted their location between 20-26 kcal/mol (Table 4-5).

Table 4-4: Structural parameters of some important conical intersections and oxaziridine geometries at CASSCF (I) and 2-layered ONIOM (II) level of calculations

Molecular geometry	Level of calculation	R _{C-C}	R _{C-N}	R _{N-O}	R _{C-O}	R _{N-C}	D _{C-C-C-N}	D _{C-C-N-O}
CI ₁	I	1.453	1.392	1.360	2.125	1.445	176.0	-80.5
	II	1.392	1.474	1.366	2.355	1.461	-174.5	-116.5
CI ₂	I	1.464	1.389	1.387	2.128	1.444	17.2	-71.0
	II	1.413	1.446	1.385	2.227	1.446	-1.0	-79.2
CI ₃	I	1.376	1.466	1.257	2.340	1.450	-173.1	-168.8
	II	–	–	–	–	–	–	–
CI ₄	I	1.453	1.409	1.368	2.173	1.446	8.0	82.0
	II	1.428	1.428	1.406	2.206	1.448	3.0	78.1
Ox ₁	I	1.493	1.406	1.443	1.378	1.449	-125.1	-108.9
	II	1.486	1.405	1.425	1.529	1.450	-135.1	-109.6
Ox ₂	I	1.490	1.404	1.442	1.381	1.450	36.8	-108.8
	II	1.484	1.403	1.528	1.427	1.450	36.7	-109.5
Ox ₃	I	1.490	1.404	1.404	1.384	1.450	-36.7	108.8
	II	1.483	1.403	1.427	1.528	1.450	36.7	109.5

Table 4-5: Relative energy (ΔE) values with respect to the relaxed excited state (ES) energy of *Z*-isomer at various important geometries on the potential energy surfaces

Molecular Geometry	CASSCF ΔE in Kcal/mol	CASMP2 ΔE in Kcal/mol	ONIOM(CAS:RHF) ΔE in Kcal/ mol
ES (<i>Z</i> -isomer)	0	0	0
ES (<i>E</i> -isomer)	0.20	0.80	–
CI ₁	-35.49	-36.29	-20.34
CI ₂	-33.50	-37.68	-26.15
CI ₃	12.31	10.27	–
CI ₄	-41.52	-36.87	-27.23
Ox ₁	-81.49	-93.57	-91.27
Ox ₂	-82.68	-94.22	-92.20
Ox ₃	-96.96	-93.61	-92.20

The gradient difference (GD) vectors of the two conical intersections, **CI₁** and **CI₂** (Figure 4-5), indicated the possibility of a C–N–O triangle formation. Following these GD vectors, optimized ground state geometries (**Ox₁** and **Ox₂**) with CNO kink structures (Figure 4-6) were obtained in both the cases. The structural parameters of these optimized geometries (i.e. bond lengths and bond angles) were found to be in good agreement with the experimentally reported oxaziridine structure [58]. The geometrical parameters of **Ox₁** and **Ox₂** predicted at CASSCF level ($R_{C-O} = 1.38 \text{ \AA}$, $R_{N-O} = 1.44 \text{ \AA}$, $R_{C-N} = 1.40 \text{ \AA}$, $\angle OCN = 62^\circ$, $\angle ONC = 58^\circ$) were found to be very similar to the ONIOM-predicted values, with some exceptions in the C–O and N–O bond lengths. The experimentally reported oxaziridine geometry [58] has a C–N–O triangle with C–O and N–O bond lengths of 1.40 \AA and 1.50 \AA , respectively, and the C–N bond length is approximately 1.44 \AA ; the bond angles $\angle OCN = 63.7^\circ$ and $\angle ONC = 56.8^\circ$ were also close to our predicted results (Table 4-4). The energy values calculated by CASSCF and CASMP2 methods suggested that the **Ox₁** and **Ox₂** geometries are situated between the optimized ground and excited state geometries; however, the ONIOM study had located their position below the optimized ground state geometry. Molecular orbital analysis of both the structures had given a clear evidence of a three-centred C–O–N-type bond formation (Figure 4-6).

Following the guess structure provided by the semi-empirical PM3/CI calculation for the *E*-isomer, two conical intersection geometries, **CI₃** and **CI₄**, were obtained at both CASSCF and ONIOM level of calculations. The high-energy conical intersection **CI₃** was found to have a twist in the opposite direction of **CI₁**; on the other hand, the low-lying **CI₄** intersection point has a terminal C–N–O kink on the backside. The rotation of C–N bond in this intersection geometry was exactly in the reverse direction in

comparison to that of the **CI₂** geometry. The energy of **CI₄** was found to be close to the **CI₂** geometry at both level of calculations, though the CASSCF level has predicted this geometry (**CI₄**) as the lowest-energy conical intersection point. It was found to be situated at 60-69 kcal/mol (Table 4-5) above the optimized ground state of the *Z*-isomer. The CASSCF and ONIOM-based geometrical parameters of these conical intersection geometries were in close agreement with each other, while the ONIOM method has predicted **CI₄** at a higher energy value (51 kcal/mol) than CASSCF and CASMP2 reported values (47 kcal/mol) with respect to ground state geometry of *E*-isomer.

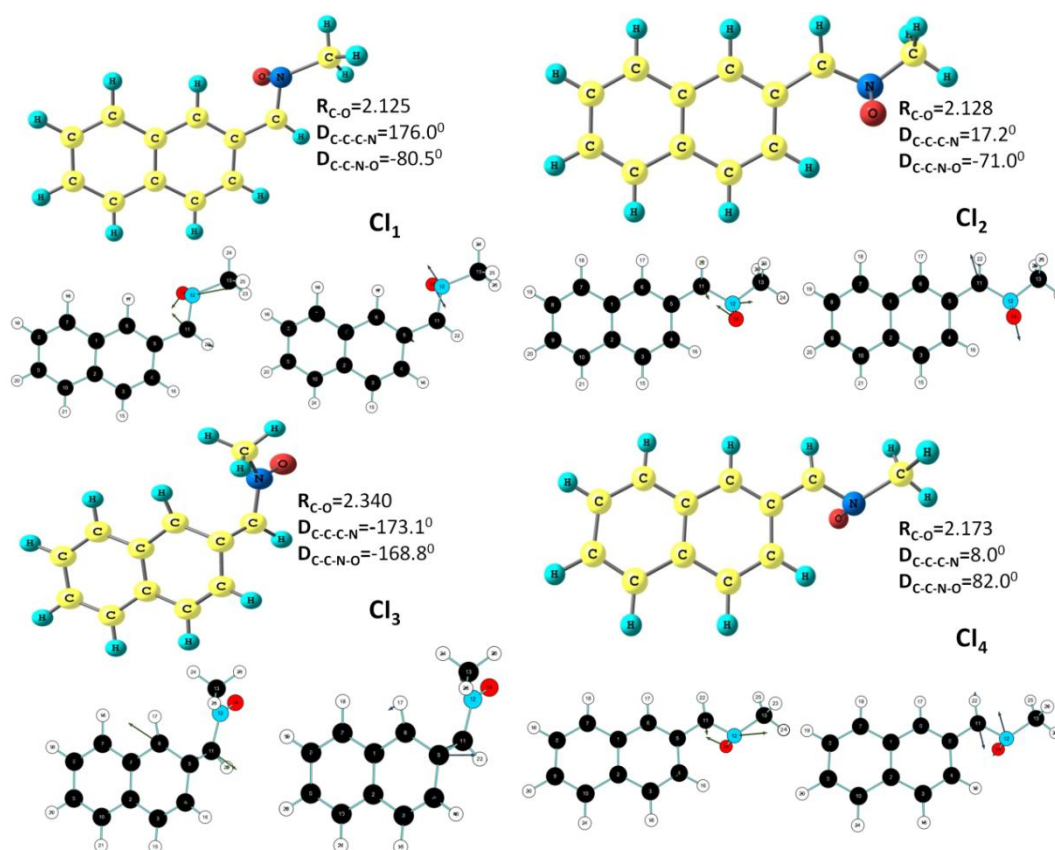


Figure 4-5: Optimized conical intersection geometries (**CI₁₋₄**) at the CASSCF/6-31G* level with their corresponding gradient difference and derivative coupling vectors.

The gradient difference vectors of **CI₄** also indicated a chance of C–N–O triangle formation through the shortening C–O bond distance; following these vectors, oxaziridine geometry (**Ox₃**) was optimized, which almost reproduced the experimentally reported geometrical parameters of this 3-membered heterocyclic species (Table 4-4). In contrast to the other two oxaziridine structures (**Ox₁** and **Ox₂**), the **Ox₃** species was found to be situated at 8.5-9.9 kcal/mol below the optimized ground state geometry of *E*-isomer at the CASSCF and CASMP2 level of studies, while the hybrid method predicted its

location at 13.7 kcal/mol below the ground state. Similar to the **Ox₁** and **Ox₂** geometries, the formation of a 3-centred C–O–N bond with a clear overlap of orbitals on carbon and oxygen was also noticed in the HOMO of **Ox₃** geometry. Though the **Ox₃** and the **Cl₄** geometries are mentioned to be arising from the *E*-isomer, based on the guess structures of rough semi-empirical calculations, it must be added that these two points may originate from the *Z*-isomer, as well. In fact, the back-side turn of the C–C–N–O dihedral angle (57.3°) in the optimized excited state of the *Z*-isomer is also quite consistent with the formation of the **Cl₄** geometry where the angle increases to 82°.

Table 4-6: Atomic charges of various important points on potential energy surfaces determined using Merz-Kollman scheme at CASSCF level.

Molecular geometries	C	N	C	O
TS_{ex1}	-0.3162	0.3314	-0.4135	-0.3065
TS_{ex2}	-0.2916	0.4270	-0.4595	0.3006
TS_{ex3}	-0.2554	0.3189	-0.3516	-0.3232
Cl₁	0.0744	-0.0598	-0.4078	-0.1587
Cl₂	0.0953	-0.1356	-0.3258	-0.1405
Cl₃	-0.0469	0.2364	-0.02011	-0.4317
Cl₄	0.0954	-0.1806	-0.1955	-0.1446
TS_{gs1}	-0.0386	0.2318	-0.3382	-0.2821
TS_{gs2}	0.2877	-0.1422	-0.2568	-0.3675
TS_{gs5}	-0.1523	0.3468	-0.3742	-0.3471
Ox₁	0.3959	-0.2920	-0.0552	-0.2945
Ox₁	0.2487	-0.2456	-0.2131	-0.2723
Ox₃	0.2503	-0.2513	-0.1328	-0.2774

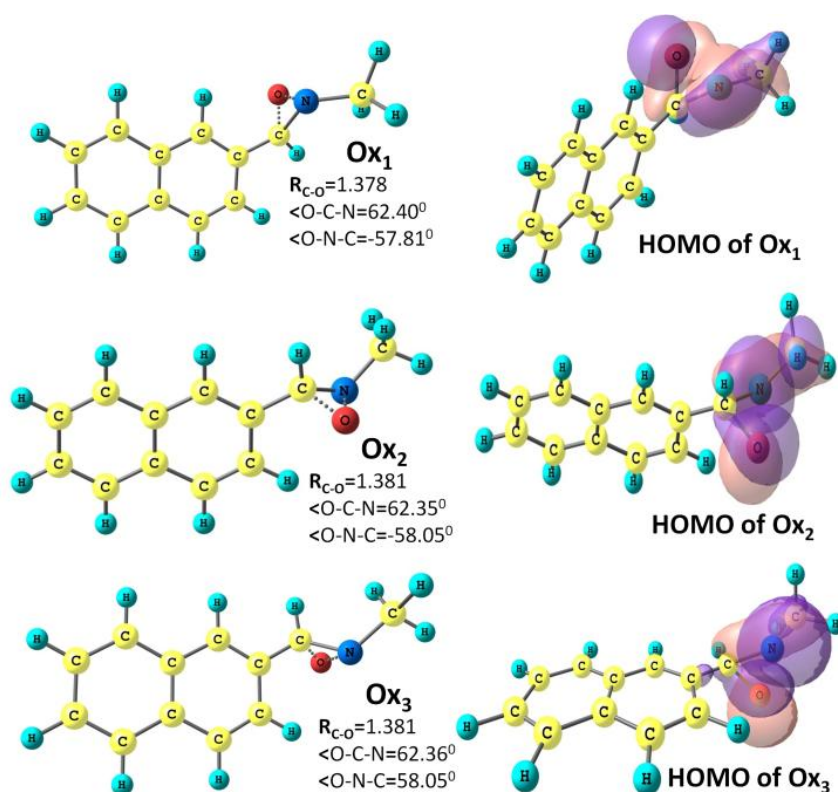


Figure 4-6: Optimized geometries of oxaziridines (Ox_{1-3}) at the CASSCF/6-31G* level. Their corresponding HOMOs are also shown.

C) Optimized transition states (TS)

a) TS geometries on the excited state surface

Two transition state geometries (TS_{ex1} and TS_{ex2}) were optimized on the excited state surface for the *Z*-isomer (Figure 4-7) at the CASSCF level of calculation. The TS_{ex2} was found to have a planar geometry and has an imaginary frequency of $126i \text{ cm}^{-1}$. The transition vectors corresponding to this frequency indicate a turn of the oxygen atom towards the front side. Following these vectors, it is possible to reach to the conical intersection geometry CI_2 which subsequently leads to Ox_2 . The other optimized TS geometry (TS_{ex1}) was found to have slightly higher imaginary frequency ($175i \text{ cm}^{-1}$), and it was observed that this transition point is not directly connected to the photochemical path under investigation. Another transition state (TS_{ex3}) having almost similar structural parameters as TS_{ex1} was also optimized on the excited state surface of the *E*-isomer with an opposite C–N–O twist; it has an imaginary frequency of $139i \text{ cm}^{-1}$. All these transition state geometries ($\text{TS}_{\text{ex1-3}}$) were located slightly (1-2 kcal/mol) above the optimized excited state.

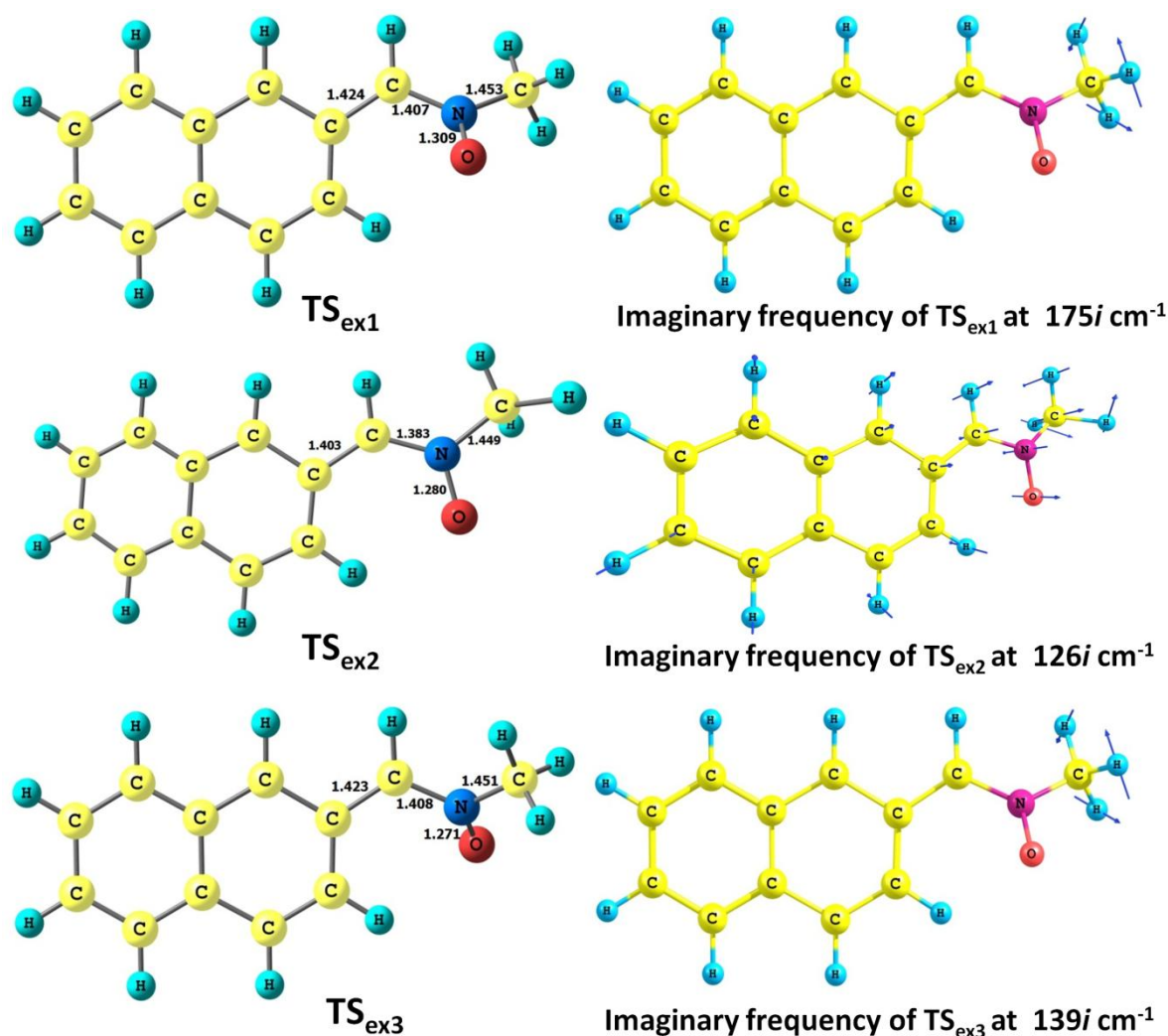


Figure 4-7: Optimized transition states ($\text{TS}_{\text{ex}1-3}$) on the excited state surface with their respective displacement vectors.

b) TS geometries on the ground state surface

A similar level of investigation of transition states on the ground state surface of the Z-isomer led to two transition state geometries ($\text{TS}_{\text{gs}1}$ and $\text{TS}_{\text{gs}2}$), while at the ONIOM level two different transition states ($\text{TS}_{\text{gs}3}$ and $\text{TS}_{\text{gs}4}$) were optimized (Figure 4-8). The imaginary frequency ($1305i \text{ cm}^{-1}$) of $\text{TS}_{\text{gs}2}$ geometry indicated the stretching and contracting of the C5–O bond. This was found to be consistent with the IR stretching frequency of the C–O bond and had given the indication that the C5–O bond will open up to give back the parent nitron passing through $\text{TS}_{\text{gs}2}$. Therefore, it was concluded that this transition state is a connecting link between the oxaziridine (Ox_2) and the Z-isomer of the nitron. The transition states $\text{TS}_{\text{gs}3}$ and $\text{TS}_{\text{gs}4}$ (predicted by ONIOM method) were characterized by imaginary frequencies of $332i \text{ cm}^{-1}$ and $323i \text{ cm}^{-1}$, respectively. In both the cases their transition vectors clearly indicated the possibility of

C–O bond formation. It must be mentioned here that the transition vectors corresponding to the imaginary frequencies of the two above-mentioned transition states, TS_{gs3} and TS_{gs4} , were found to be parallel to the gradient difference vectors of CI_1 and CI_2 , respectively, and both seemed to be leading towards their respective oxaziridine structures. Analysis of their energy values revealed that the TS_{gs3} lies 40 kcal/mol below the CI_1 intersection point and 30 kcal/mol above the Ox_1 geometry, while the TS_{gs4} was found to be situated half-way between the CI_2 and the Ox_2 geometries. Overall, it was concluded that both these TSs are situated on the nitron-oxaziridine photochemical conversion pathway.

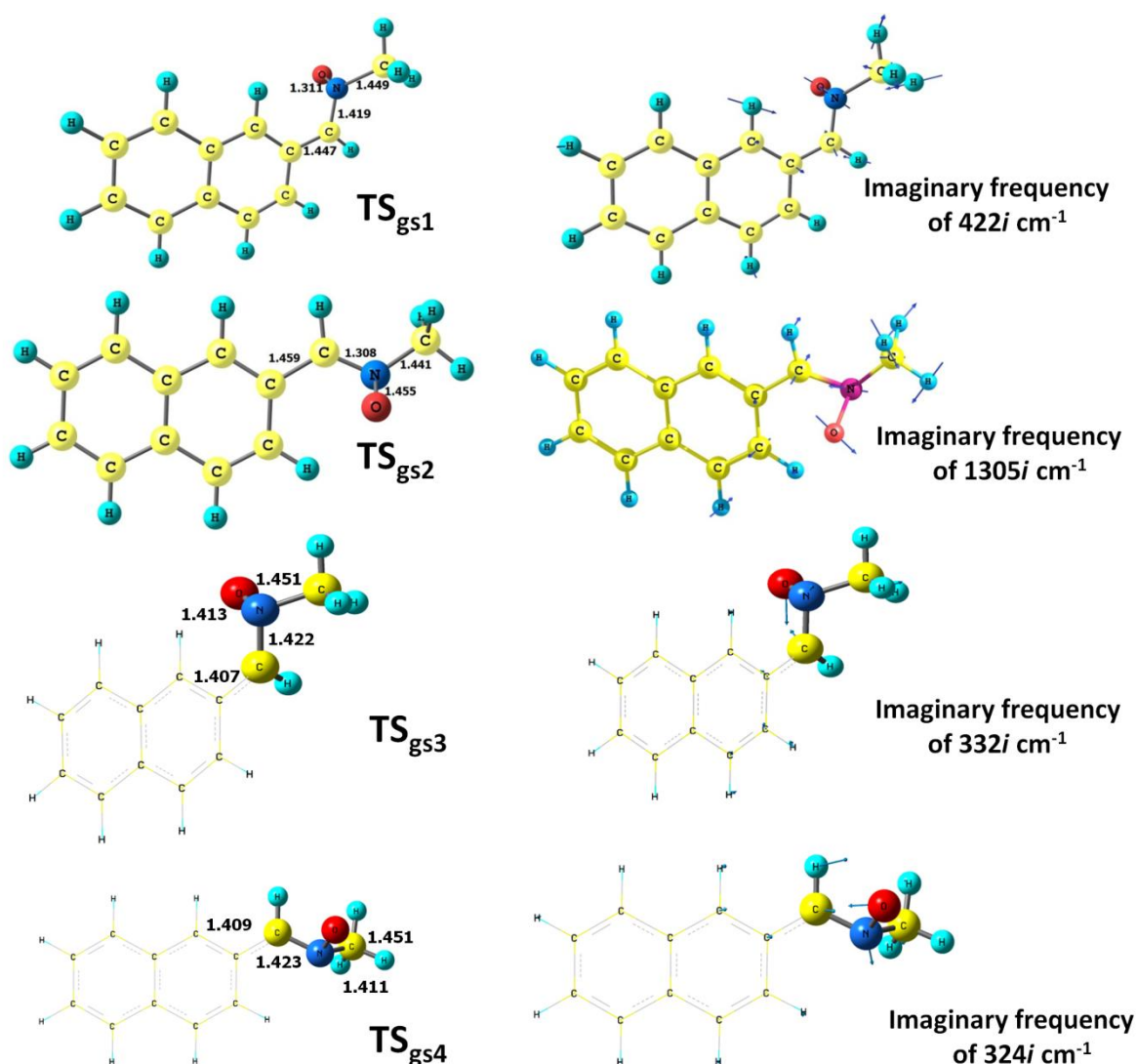


Figure 4-8: Optimized transition states ($\text{TS}_{\text{gs1-4}}$) on ground state surface with their respective displacement vectors

Table 4-7: Absolute (E) and relative energy values (ΔE) of various transition states geometries with respect to the relaxed excited states (ES). Imaginary frequencies of the corresponding transition states are also reported.

Molecular Geometry	Imaginary frequency in cm^{-1}	CASSCF		CASMP2		2-Layer ONIOM	
		E in hartree	ΔE in kcal/mol	E in hartree	ΔE in kcal/ mol	E in hartree	ΔE in kcal/mol
ES (Z-isomer)	–	-589.9443	0	-591.8003	0	-589.4371	0
ES (E-isomer)	–	-589.9440	0.20	-591.7990	0.80	–	–
TS _{ex1}	175 <i>i</i>	-589.9407	2.26	-591.7985	1.13	–	–
TS _{ex2}	126 <i>i</i>	-589.9425	1.14	-591.8007	-0.26	–	–
TS _{ex3}	139 <i>i</i>	-589.9425	1.15	-591.7999	0.28	–	–
TS _{gs1}	422 <i>i</i>	-590.0457	-63.61	-591.8674	-42.13	–	–
TS _{gs2}	1305 <i>i</i>	-590.0425	-61.60	-591.8740	-46.28	–	–
TS _{gs3}	332 <i>i</i>	–	–	–	–	-589.5324	-59.80
TS _{gs4}	323 <i>i</i>	–	–	–	–	-589.5305	-60.60
TS _{gs5}	350 <i>i</i>	-590.0474	-64.65	-591.8883	-55.21	–	–

4.3.2. E-Z isomerization mechanism of α -(2-naphthyl)-N-methylnitron

In recent times, computational studies on the *E-Z* isomerizations of different types of nitrones have been extensively reported at the DFT level of calculations by various groups [59,60]. At the CASSCF level, along with the above mentioned transition states, we have detected one more TS geometry (TS_{gs5}) on the ground state surface of α -(2-naphthyl)-N-methylnitron system. This transition state geometry was obtained by employing the QST3 methodology, where the *E*-isomer and the *Z*-isomer were specified as the reactant and the product, respectively. This optimized transition state (TS_{gs5}) was characterized by an imaginary frequency of 350*i* cm^{-1} , and it was found to connect the *E* and *Z* isomers (Figure 4-9B). On analyzing the entire process it was found that the unstable *E* isomer (situated at 22 kcal/mol above the stable *Z*-isomer) reaches TS_{gs5} by climbing a barrier of 23.7 kcal/mol. (Table 4-7), and subsequently following the imaginary frequency of TS_{gs5}, the *Z*-isomer is formed. The optimized ground state of the *Z*-isomer was detected at 46 kcal/ mol below the TS_{gs5} geometry. An IRC run was given on this transition state in both forward and reverse directions to further confirm the fate of TS_{gs5}. The corresponding IRC plot is illustrated in Figure 4-9A.

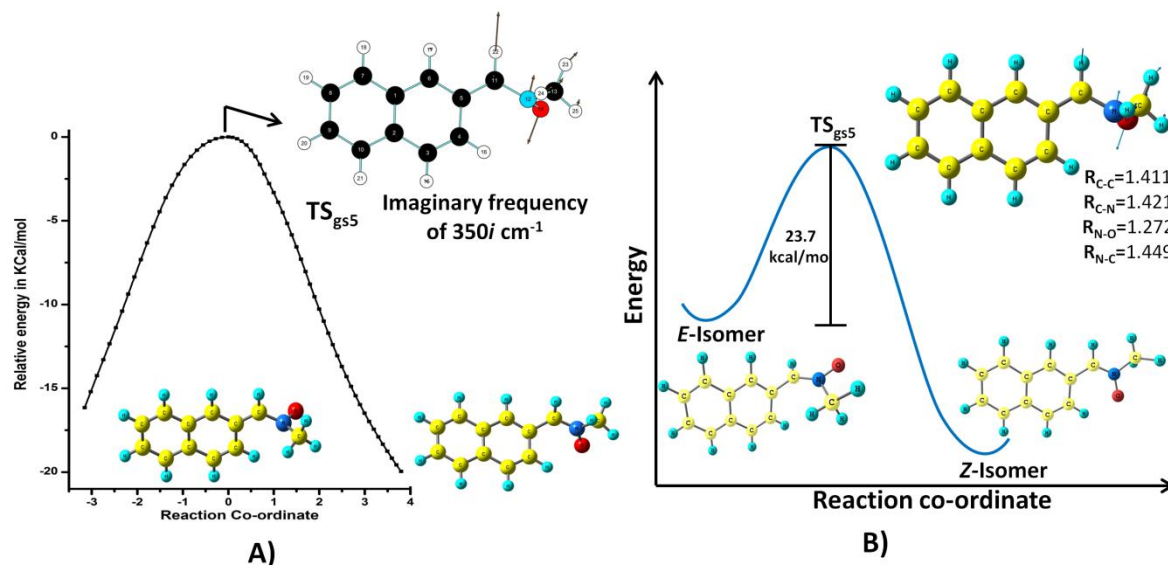
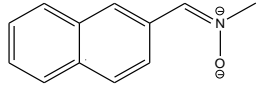
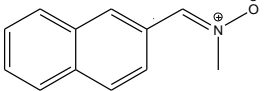
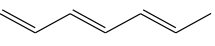
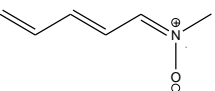
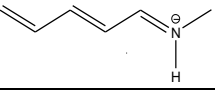


Figure 4-9: A) Intrinsic reaction coordinate (IRC) path of TS_{gs5} along forward and reverse directions. B) Schematic representation of *E-Z* isomerization of α -(2-naphthyl)-*N*-methyl nitrene through TS_{gs5} .

4.3.3. Radiative transition studies

Unlike the retinyl nitrenes (reported in chapter 2), the α -naphthyl *N*-methyl nitrene systems were reported to give fluorescence emission [18]. The radiative transition properties of the low-lying S_0-S_1 , S_0-S_2 and S_2-S_1 transitions were analyzed at the optimized ground state geometry using the GUGA CISD code in GAMESS program. These studies have revealed that for both the isomers the transition from ground state (S_0) to the first excited singlet state (S_1) is very weak. The transition moment (TM) value of S_0-S_1 transition was found to be 0.30 Debye for the *Z*-isomer and 0.37 Debye for the *E*-isomer with low oscillator strength values, and their corresponding Einstein coefficients (A) were found to be in the order of 10^7 (Table 4-8). The radiative lifetime values of the S_1 states are expected to be in the order of nanoseconds (roughly 35-60 ns) for these isomers. In contrast, higher TM values for S_0-S_2 transitions were obtained for both *Z*-isomer (5.61 Debye) and *E*-isomer (3.86 Debye) with high oscillator strength values. The Einstein coefficients corresponding to the S_0-S_2 transitions were found to be in the order of 10^9 which corresponds to radiative lifetime values in pico second order (roughly 140-275 ps). The S_2-S_1 transition moments are also moderately strong with TM values of 2.0 Debye with oscillator strengths of 0.01.

Table 4-8: A comparison of radiative transition properties at ground state equilibrium geometries of different systems. The values in parentheses are the powers to base 10.

Systems	Transition moment in Debye			Oscillator strength			Einstein's coefficient in sec ⁻¹		
	S ₀ -S ₁	S ₀ -S ₂	S ₂ -S ₁	S ₀ -S ₁	S ₀ -S ₂	S ₂ -S ₁	S ₀ -S ₁	S ₀ -S ₂	S ₂ -S ₁
	0.304	5.616	2.099	0.003	1.322	0.010	1.7280 (+7)	7.0138 (+9)	1.8008 (+5)
	0.371	3.862	1.890	0.005	0.644	0.010	2.7374 (+7)	3.6303 (+9)	2.5472 (+5)
	0.961	7.764	4.303	0.028	1.861	0.010	7.7773 (+7)	5.3540 (+9)	9.1551 (+3)
	4.861	0.112	0.069	0.706	0.000	0.000	2.1472 (+9)	1.0559 (+6)	1.2264 (+0)
	7.543	1.891	1.935	1.695	0.109	0.019	4.5380 (+9)	3.1182 (+8)	1.5590 (+6)

The obtained radiative transition properties of these naphthyl systems are quite different from our previously studied long-chain conjugated *N*-alkyl substituted nitrones. In the latter ones, the S₀-S₁ transitions were found to be the strongest while their S₀-S₂ transitions were very weakly allowed with low transition moment values. As discussed in chapter 2, the radiative properties of these conjugated retinyl nitrones were more towards the conjugated iminium ions. However, results of α -(2-naphthyl)-*N*-methylnitrone systems indicate their similarity with the conjugated methyl-substituted hexatriene system (Figure 4-10). The S₀-S₁ transition in this conjugated non-polar polyene (TM value 0.97 Debye) is weakly allowed, whereas the S₀-S₂ and S₂-S₁ transitions are strongly allowed. In these types of systems, the initial transition to S₂ (ionic) state has been reported to be followed by a quick downward transition to the S₁ (biradical) state before reaching the ground state (S₀) which eventually gets involved in a kinked conical intersection with this S₀ state through a Hula-twist motion. A similar low-lying kinked conical intersection (CI₁) was also observed in α -naphthyl *N*-methyl nitron system; however, the less volume demanding terminally-twisted conical intersections were found at lower energy level leading to the oxaziridine geometries.

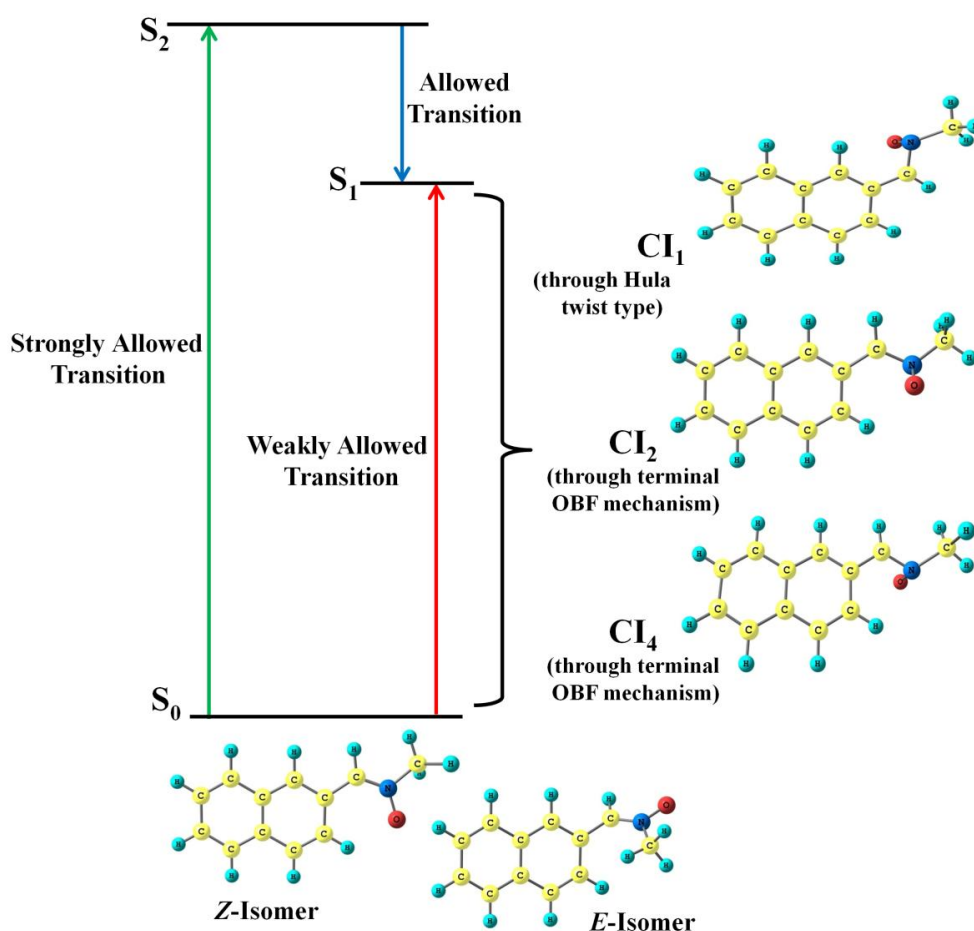
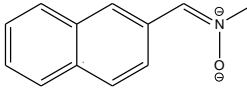
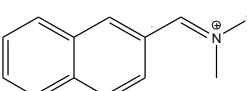
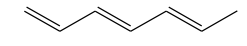
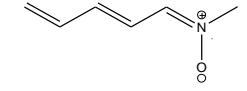
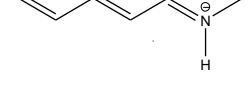


Figure 4-10: A schematic representation of the low-lying singlet-singlet transitions and involvement of some important conical intersections (S_0/S_1) in α -(2-naphthyl)-*N*-methylnitrone system.

A comparative study of dominant configurations of the four above-mentioned systems has been presented in Table 4-9. This analysis has revealed that the vertically excited S₁ state (FC geometry) of the conjugated *N*-methyl nitrone system is partly dominated by the configuration arising due to the HOMO→LUMO excitation, whereas in 2,4-pentadien-1-iminium ion, this configuration completely dominates in FC region. On the other hand, in 1,3,5-hexatriene system and α -naphthyl *N*-methyl nitrone, this configuration dominates in the S₂ state. The S₁ states of the latter systems were found to be mostly contributed by configurations arising due to the HOMO→LUMO+1 and HOMO-1→LUMO excitations at the above-mentioned geometries. The conjugated polyene has also a major contribution from the HOMO²→LUMO² configuration for its first vertically excited singlet state (FC geometry). Interestingly, unlike in the iminium ion, this doubly excited configuration becomes a key player in the S₁ state of the nitrones and the polyenes as the optimized geometry of this state is approached. This optimized excited state in the α -naphthyl *N*-methyl nitrone is almost equally contributed by

configurations due to $\text{HOMO}^2 \rightarrow \text{LUMO}^2$, $\text{HOMO} \rightarrow \text{LUMO}+1$ and $\text{HOMO}-1 \rightarrow \text{LUMO}$ excitations (Table 4-9).

Table 4-9: A comparison of dominant configurations of S_1 and S_2 states at Frank Condon (FC) geometries and at optimized S_1 states of different systems

Systems	At FC geometry		At optimized S_1 state geometry	
	S_1 state	S_2 state	S_1 state	S_2 state
	H \rightarrow L+1 (0.66) H-1 \rightarrow L (0.56) H \rightarrow L(0.15)	H \rightarrow L(0.87) H-1 \rightarrow L (0.20)	H-1 \rightarrow L (0.48) H \rightarrow L+1 (0.47) H $^2 \rightarrow$ L 2 (0.45)	H \rightarrow L(0.60) H-4 \rightarrow L (0.58) H \rightarrow L+1 (0.15)
	H \rightarrow L+1 (0.57) H-1 \rightarrow L (0.56) H-2 \rightarrow L (0.33)	H \rightarrow L(0.84) H \rightarrow L+1 (0.19)	H-1 \rightarrow L (0.46) H \rightarrow L+1 (0.48) H $^2 \rightarrow$ L 2 (0.47)	H-4 \rightarrow L (0.64) H \rightarrow L(0.52) H \rightarrow L+1 (0.18)
	H $^2 \rightarrow$ L 2 (0.53) H \rightarrow L+1 (0.52) H \rightarrow L+4 (0.45)	H \rightarrow L(0.96)	H $^2 \rightarrow$ L 2 (0.60) H \rightarrow L+1 (0.47) H \rightarrow L+4 (0.40)	H \rightarrow L(0.94)
	H \rightarrow L(0.65) H-1 \rightarrow L(0.43) H $^2 \rightarrow$ L 2 (0.38)	H-2 \rightarrow L(0.88)	H $^2 \rightarrow$ L 2 (0.60) H-1 \rightarrow L (0.49) H \rightarrow L+2 (0.33) H \rightarrow L(0.17)	H-2 \rightarrow L(0.86)
	H \rightarrow L(0.92)	H-1 \rightarrow L (0.64) H $^2 \rightarrow$ L 2 (0.46) H \rightarrow L+4 (0.28)	H \rightarrow L(0.87) H $^2 \rightarrow$ L 2 (0.29)	H-1 \rightarrow L(0.55) H \rightarrow L+1 (0.46) H $^2 \rightarrow$ L 2 (0.42) H \rightarrow L(0.24)

From the reported experimental studies on α -naphthyl nitro systems it is found that the photoproduct oxaziridines (formed during their photo-irradiation) are also fluorescent in nature which results in increase and fluctuation of fluorescence intensity. The radiative transition properties of the ground state oxaziridine systems were also analysed using GUGA CISD code in GAMESS program. The results of these studies (Table 4-10) were found to be quite similar to those of parent nitro systems. The S_0 - S_1 transitions were found weaker than the S_0 - S_2 and S_2 - S_1 transitions; however, the transition moment and oscillator strength values of the latter-mentioned transitions were significantly lower in comparison to those values of nitrones. On the other hand, these parameters of the lowest-energy transition (S_0 - S_1) were found to decrease slightly in oxaziridines.

Table 4-10: Important radiative transition properties of the oxaziridine geometries at their respective ground state equilibrium geometries

Systems	Transition moment (Debye)			Oscillator strength		
	S_0 - S_1	S_0 - S_2	S_2 - S_1	S_0 - S_1	S_0 - S_2	S_2 - S_1
Ox₁	0.151	1.615	0.405	0.000	0.115	0.000
Ox₂	0.203	1.554	0.333	0.001	0.107	0.000
Ox₃	0.207	1.568	0.330	0.001	0.108	0.000

4.4. Conclusions

A comprehensive computational study of the photochemistry of fluorescent α -(2-naphthyl)-*N*-methylnitronone system has been carried out. Biradicaloid conical intersection geometries through terminal one-bond flip and low-lying hula-twist type motions were found to play key role in the photochemical nitronone-oxaziridine conversion process. Following the directions of the gradient difference vectors of these conical intersections, the optimized geometries of the corresponding three-membered heterocyclic systems (oxaziridine) were obtained. These oxaziridine geometries were found to have a 3-centred molecular orbital and have a close resemblance with the experimentally reported geometry of this terminally twisted species. A transition state on the ground state potential energy surface was found to be responsible for the thermal *E-Z* isomerization of this nitronone. In addition to these, the radiative transition studies of this nitronone have revealed that in contrast to our previously reported model compounds of *N*-alkyl retinylnitronones, the vertical transition to the first excited singlet state is weakly allowed here. This resembles the nature of non-polar conjugated polyene systems, and similar to these systems, the first excited singlet state of naphthyl nitronone borrows population from the S_2 state from its downward transition and then eventually gets involved in the S_0/S_1 conical intersection to produce oxaziridine and other photoproducts. On the other hand, the transition properties of our previously studied model compounds of retinylnitronones were found to be somewhat close to that of the structurally similar iminium ion systems. The computed absorption peak position of the *E*-isomer had almost reproduced its experimentally reported value, and the excited singlet state, which was reported to give fluorescence, was found to have a radiative lifetime of nanosecond order. Overall, these computed results at various level of quantum mechanical calculations are expected to contribute significantly to the properties of the α -(2-naphthyl)-*N*-methylnitronone system. However, it must be concluded that the importance of this work is not only restricted to this particular type of nitronone system, rather it can have far reaching consequences in terms of understanding the details of the photochemistry and isomerization processes of several other structurally similar nitronone systems, too.

4.5. References

1. R. A. Floyd, R. D. Kopke, C-H Choi, S. B. Foster, S. Doblbas and R. A. Towner, *Free Radic. Biol. Med.*, 2008, **15**, 1361.

2. R. A. Floyd, K. Hensley, M. J. Forster, J. A. Kelleher-Anderson and P. L. Wood, *Mech. Ageing Dev.*, 2002, **123**, 1021.
3. R. A. Floyd, H. C. C. F. Neto, G. A. Zimmerman, K. Hensley and R. A. Towner, *Free Radic. Biol. Med.*, 2013, **62**, 145.
4. A. Samadi et al., *Bioorg. Med. Chem.*, 2011, **19**, 951.
5. M. Chioua et al., *J. Med. Chem.*, 2012, **55**, 153.
6. R. A. Floyd et al., *Free Radic. Res.*, 2010, **44**, 108.
7. B. Guo, D. Xu, H. Duan, J. Du, Z. Zhang, S. M. Lee and Y. Wang, *Biol. Pharm. Bull.*, 2014, **37**, 274.
8. R. A. Floyd, H. K. Chandru, T. He and R. Towner, *Anti-cancer Agents Med. Chem.*, 2011, **11**, 373.
9. P. Astolfi, P. Carloni, M. G. Marini, G. Mobbili, M. Pisani and P. Stipa, *RSC Adv.*, 2013, **3**, 22023.
10. X. Song, Y. Qian, R. Ben, X. Lu, H.-L. Zhu, H. Chao and J. Zhao, *J. Med. Chem.*, 2013, **56**, 6531.
11. V. Balogh-Nair and K. Nakanishi, *Pharm. Res.*, 1984, **1**, 93.
12. P. Saini and A. Chattopadhyay, *RSC Adv.*, 2014, **4**, 20466.
13. P. Saini and A. Chattopadhyay, *Chem. Phys. Lett.*, 2015, **633**, 6
14. J. S. Splitter and M. Calvin, *J. Am. Chem. Soc.*, 1965, **30**, 3427.
15. J. S. Splitter, T.-M. Su, H. Ono and M. Calvin, *J. Am. Chem. Soc.*, 1971, **93**, 4075.
16. K. Shinzawa and I. Tanaka, *J. Phys. Chem.*, 1964, **68**, 1205.
17. K. Koyano and I. Tanaka, *J. Phys. Chem.*, 1965, **69**, 2545.
18. E. Lipczynska-Kochany and J. Kochany, *J. Photochem. Photobiol. A: Chem.*, 1988, **45**, 65.
19. P. Saini and A. Chattopadhyay, *J. Chem. Sci.*, 2015, **127**, 1757.
20. S. Gozem, E. Mirzakułova, I. Schapiro, F. Melaccio, K. D. Glusac and M. Olivucci, *Angew. Chem. Int. Ed.*, 2014, **53**, 9870.
21. H. Timmers, Z. Li, N. Shivaram, R. Santra, O. Vendrell and A. Sandhu, *Phys. Rev. Lett.*, 2014, **113**, 113003.
22. T. Mori and T. J. Martínez, *J. Chem. Theory Comput.*, 2013, **9**, 1155.
23. D. R. Yarkony, *Chemical Reviews*, 2012, **112**, 481.
24. A. Migani and M. Olivucci, *Conical Intersections: Electronic Structure, Dynamics & Spectroscopy Advanced series in Physical Chemistry*, Eds., W. Domcke, D. R. Yarkony and H. Koppel, World Scientific Publishing Co. (P). Ltd, Singapore, 2004.

25. I. J. Palmer, I. N. Ragazos, F. Bernardi, M. Olivucci and M. A. Robb, *J. Am. Chem. Soc.*, 1993, **115**, 673.
26. J. Dreyer and M. Klessinger, *Chem. Eur. J.*, 1996, **2**, 335.
27. P. Saini and A. Chattopadhyay, *RSC Adv.*, 2015, **5**, 22148.
28. N. Yamamoto, T. Vreven, M. A. Robb, M. J. Frisch and H. B. Schlegel, *Chem. Phys. Lett.*, 1996, **250**, 373.
29. M. J. Frisch, I. N. Ragazos, M. A. Robb and H. B. Schlegel, *Chem. Phys. Lett.*, 1992, **189**, 524.
30. S. Dapprich, I. Komáromi, K. S. Byun, K. Morokuma and M. J. Frisch, *J. Mol. Struct. (Theochem)*, 1999, **462**, 1.
31. T. Vreven, K. S. Byun, I. Komáromi, S. Dapprich, J. A. Montgomery Jr., K. Morokuma and M. J. Frisch, *J. Chem. Theory Comput.*, 2006, **2**, 815.
32. T. Vreven and K. Morokuma, *Ann. Rep. Comput. Chem.*, 2006, **2**, 35.
33. T. Vreven, K. Morokuma, O. Farkas, H. B. Schlegel and M. J. Frisch, *J. Comput. Chem.*, 2003, **24**, 760.
34. M. J. Bearpark et al., *J. Photochem. Photobio. A: Chem.*, 2007, **190**, 207.
35. M. J. Bearpark, S. M. Larkin and T. Vreven, *J. Phys. Chem. A*, 2008, **112**, 7286.
36. A. Bhattacharya and E. R. Bernstein, *J. Phys. Chem. A*, 2011, **115**, 4135.
37. M. J. Frisch et al., *Gaussian 09*, Revision **B.01**, Gaussian Inc., Wallingford CT, 2010.
38. P. Slavíček, and T. J. Martínez, *J. Chem. Phys.*, 2010, **132**, 234102.
39. J. J.W. McDouall, K. Peasley and M. A. Robb, *Chem. Phys. Lett.*, 1988, **148**, 183.
40. J. F. Arenas, J. I. Marcos, J. C. Otero and A. Sanchez-Galvez, *J. Chem. Phys.*, 1999, **111**, 551.
41. M. Lundberg, *J. Comput. Chem.*, 2012, **33**, 406.
42. X. Li and M. J. Frisch, *J. Chem. Theory and Comput.*, 2006, **2**, 835.
43. C. Peng and H. B. Schlegel, *Israel J. Chem.*, 1993, **33**, 449.
44. H. P. Hratchian and H. B. Schlegel, *Theory and Applications of Computational Chemistry: The First 40 Years*, Eds., C. E. Dykstra, G. Frenking, K. S. Kim and G. Scuseria, Elsevier, Amsterdam, 2005.
45. H. P. Hratchian and H. B. Schlegel, *J. Chem. Theory Comput.*, 2005, **1**, 61.
46. H. P. Hratchian and H. B. Schlegel, *J. Chem. Phys.*, 2004, **120**, 9918.
47. U. C. Singh and P. A. Kollman, *J. Comput. Chem.*, 1984, **5**, 129.
48. B. H. Besler, K. M. Merz Jr. and P. A. Kollman, *J. Comput. Chem.*, 1990, **11**, 431.

-
49. M. W. Schmidt et al, *J. Comput. Chem.*, 1993, **14**, 1347.
 50. B. Brooks and H. F. Schaefer, *J. Chem. Phys.*, 1979, **70**, 5092.
 51. B. Brooks, W. Laidig, P. Saxe, N. Handy and H. F. Schaefer, *Physica Scripta*, 1980, **21**, 312.
 52. A. Chattopadhyay, *J. Phys. B: At. Mol. Opt. Phys.*, 2012, **45**, 165101.
 53. A. Chattopadhyay, *J. Chem. Sci.*, 2012, **124**, 985.
 54. F. Weinhold, *J. Chem. Phys.*, 1970, **54**, 1874.
 55. C. W. Bauschlicher and S. R. Langhoff, *Theor. Chim. Act.*, 1991, **79**, 93.
 56. S. Koseki and M. S. Gordon, *J. Mol. Spect.*, 1987, **123**, 392.
 57. Website of Chemcraft software: <http://www.chemcraftprog.com>.
 58. S. S. Murphree, *Modern Heterocyclic Chemistry*, Eds., J. Alvarez-Builla, J. J. Vaquero and J. Barluenga, Wiley-VCH Verlag & Co. KGaA, Weinheim, Germany, 2011.
 59. L. Meng, S. C. Wang, J. C. Fettinger, M. J. Kurth and D. J. Tantillo, *Eur. J. Org. Chem.*, 2009, 1578.
 60. D. Roca-López, T. Tejero and P. Merino, *J. Org. Chem.*, 2014, **79**, 8358.

CHAPTER 5

A computational investigation of the photochemical reaction paths of C-terminal aryl substituted small-chain conjugated nitrones**5.1. Introduction**

In the present chapter, we have discussed the results of our studies on two different types of nitron systems, one having α -styryl group (**nitron A**) and the other with 1,1-diphenylethylene group (**nitron B**) substitutions on the C-terminal part of the C=N bond (Figure 5-1a and 5-1b). Photo-irradiations of these terminally phenyl and biphenyl-substituted nitrones had led to some interesting observations. Earlier, it was discussed that the transition properties of our previously studied nitrones had shown contrasting behavior and they were either inclined more towards the non-polar conjugated polyenes or the iminium ions (protonated Schiff bases) [1]. The studied model compounds of retinyl nitrones (with two conjugated C=C bonds and without any C-terminal substitutions) were found to have strongly allowed S_0-S_1 and almost forbidden S_0-S_2 transitions, which resemble the transition properties of the protonated Schiff bases (chapter 2). On the other hand presence of naphthyl substitution at the C-terminal end of the C=N bond (chapter 4) showed a strongly allowed S_0-S_2 transition and an almost forbidden S_0-S_1 transition [2] which is similar to the non-polar conjugated polyenes. These dissimilar transition properties led to their slightly different oxaziridine formation routes. From these observations we have concluded that substituting an α -aryl moiety at the C-terminal position of a nitron can give contrasting transition properties from that of conjugated chain substituted nitron systems. However, it is quite possible that if aryl substitution is done at the C-terminal end of the conjugated chain, the transition properties may vary from a normal open-chain and terminally unsubstituted conjugated

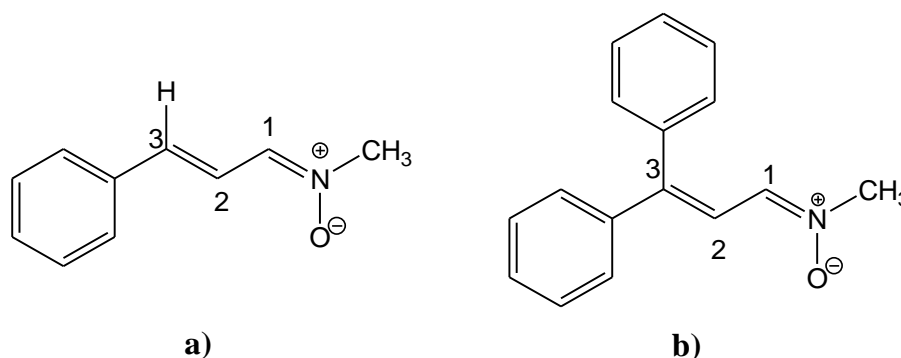


Figure 5-1: Structures of a) **nitron A** and b) **nitron B**

nitron, and therefore, depending on these transition properties the nitron-oxaziridine photochemical conversion route may vary significantly from our previously studied nitron systems. In addition, the presence of one phenyl group and two phenyl groups at the terminal position of the small conjugated chain nitrons may not have comparable effects on this photochemical path and their nitron-oxaziridine photo-conversion path may deviate from each other. The system is expected to be planar in the presence of one phenyl group, while the nitron system with two phenyl groups are supposed to be non-planar due to the steric repulsion created by the rings. This difference in planarity may affect their photochemical reaction path and the nature of the final photoproducts may be different.

In this present work, we have synthesized (not discussed in this thesis) and performed a comprehensive photochemical investigation on the two above-mentioned phenyl-substituted nitron systems (Figure 5-1a and 5-1b). The photochemical studies include their characterization through spectroscopic analysis and complete computational investigation of their photochemical reaction paths. The experimentally observed findings were validated by theoretically predicted results, and finally, the overall mechanisms of these photochemical processes were proposed from the computational studies. The obtained results of this work were published [3]. The experimental portion of work carried out for the present study is beyond the scope of this thesis, hence not discussed in detail in this chapter. The combined (computational and experimental) approach used for investigation, revealed the fact that these two studied systems follow completely different photochemical paths and have striking dissimilarities in their oxaziridine formation routes.

5.2. Computational methods

The low-lying electronic states of the above-mentioned nitrons were studied computationally using Gaussian 09 [4] suite of program. Important points on the potential energy surfaces (PES), such as minimum energy geometries, transition states and conical intersection points were located using the CASSCF [5-10] level of calculations. To optimize ground state geometries, RHF and DFT (B3LYP) methods with 6-311G** basis sets were also employed in addition to the CASSCF method. For locating the transition states on the PES, the normal TS technique based on the Berny-algorithm [11] was used. The CASMP2 [12-14] level of calculations (using Gaussian 09) and the CASPT2 [15-17] calculations (using MOLPRO program [18]) were employed to

introduce dynamic correlation corrections through single point calculations on top of the CASSCF-optimized geometries. The CASSCF calculations were performed using three different active space sizes, these include, (4,4), (6,6) and (12,12). Similar to our previous observations (presented in earlier chapters), here also we have found that the properly chosen CAS (4,4) active space was successful to track the oxaziridine photo-conversion path for both the studied nitrone systems. The success of the (4,4) active space in tracking the photo-isomerization path may be due to the same reason as mentioned in the previous chapters (chapter 2-4). These CAS (4,4) active space calculations have confirmed that in both the systems an oxaziridine species is formed through the lowest-energy conical intersection geometry with a terminal CNO kink.

To investigate the radiative transition properties [19-20] of these nitrones, GUGA CI [21-24] studies had been carried out through the GAMESS [25] program. Electrostatic potential-based atomic charges were calculated for all the important geometries through the Merz-Kollman scheme [26-27] using Gaussian 09 program. Time dependent density functional theory (TD-DFT) [28-29] was employed to calculate the absorption peaks, and these were compared with the experimentally obtained peak positions of the photoproduct formed on photo-irradiation of these nitrones. We have analyzed the output files using the Chemcraft [30], GaussView and Chemission visualization softwares.

5.3. Results and discussions

5.3.1. Photo-irradiation of studied nitrone systems

For both the nitrones (**nitrone A** and **nitrone B**), the intense absorption peaks in the ultraviolet spectra were found to arise near 330 nm while the weaker peaks were around 240 nm (Figure 5-2). On continued photo-irradiation of both the nitrones, changes in their spectra were observed, which indicated the formation of the photoproducts. However, the decay of the longer wavelength peak and the formation of the photoproduct absorption band were not quite similar in the two systems. The 326 nm peak of **nitrone A** decays at a much faster rate (in 25 minutes) than the 334 nm peak of **nitrone B** (90 minutes). In both the cases, on prolonged irradiation, the longer wavelength bands had totally disappeared, indicating complete conversion to the photoproducts and the newly formed bands on the blue side were found to have characteristic of oxaziridine. A comparative analysis of some sample photoproduct absorption peaks studied from photo-irradiation of some separate categories of nitrones

carried out by other groups [31,32] with that of ours had given clear indications that the produced photoproducts in our present study are probably oxaziridines. However, this was further confirmed by the FT-IR (not discussed in this thesis) [3] and computational studies.

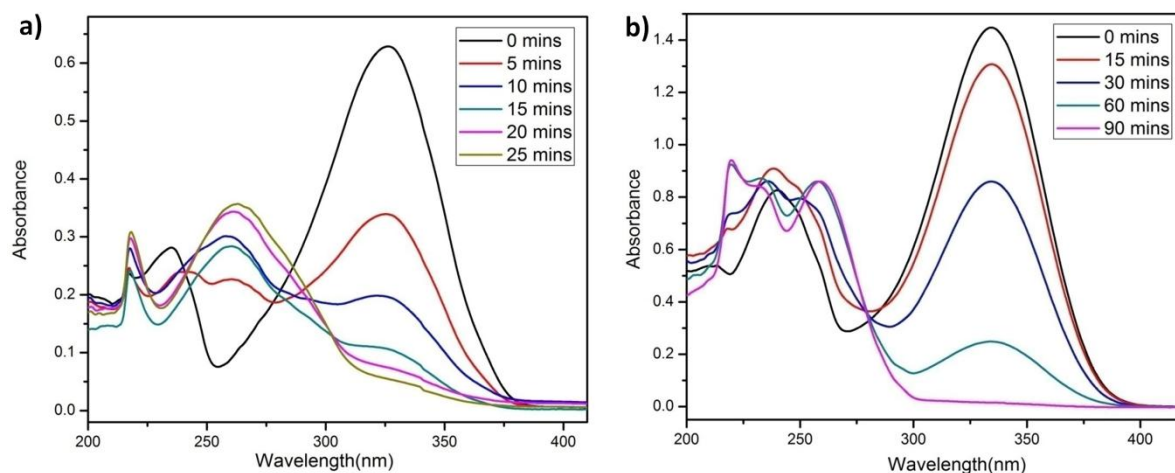


Figure 5-2: Photo-irradiation of a) **nitrone A** and b) **nitrone B**.

5.3.2. Important points on the potential energy surface

A) Ground and excited singlet states

To optimize the ground state geometries, the restricted Hartree-Fock (RHF) method and density functional theory (DFT) calculations were performed using the 6-311G* basis sets. On the other hand, 6-31G* basis sets were used for CASSCF level of calculations, performed with (4,4), (6,6) and (12,12) active spaces. A comparison of the structural parameters of the ground state geometries of both the nitrones, optimized at different level of calculations, is shown in Table 5-1. This table shows that the geometries optimized at different level of calculations have almost similar structural parameters, though slight deviations were noticed in the case of DFT calculated values. The optimized ground state geometry of **nitrone A** was found to be planar; however, the two phenyl rings in **nitrone B** were found to be non-planar with respect to the remaining portions of the molecule. The latter one is non-planar to avoid strong interactions between the ortho-hydrogens of the two phenyl moieties. A planar arrangement of the phenyl rings would have brought the two above-mentioned hydrogens very close (0.62 Å) and could have created a huge strain in the molecule, while in the actual optimized non-planar ground state these hydrogens were found to be 3.48 Å apart. This geometry

also releases the possible repulsion at the other two ortho-hydrogens of the two rings, one with the hydrogen on α -carbon and the other on the carbon atom of the C=N bond.

Table 5-1: Structural parameters of optimized ground and excited states of **nitrone A** and **nitrone B** at various levels of calculation

System	Geometry	Method	R _{C-C}	R _{C-C}	R _{C-N}	R _{N-O}	R _{C-O}	R _{N-C}	D _{C-C-N}	D _{C-C-N-C}	D _{C-C-N-O}		
nitrone A	GS_A	I	1.329	1.451	1.277	1.265	2.253	1.459	180.0	180.0	0.0		
		II	1.353	1.427	1.323	1.269	2.300	1.477	180.0	180.0	0.0		
		III	1.329	1.454	1.302	1.267	2.274	1.459	179.9	179.9	0.0		
		IV	1.328	1.454	1.301	1.266	2.272	1.459	180.0	180.0	0.0		
		V	1.329	1.454	1.302	1.266	2.287	1.459	180.0	180.0	0.0		
	ES_A	III	1.463	1.441	1.395	1.272	2.282	1.449	170.8	165.2	10.9		
		IV	1.429	1.405	1.401	1.266	2.295	1.448	177.1	165.9	5.9		
		V	1.430	1.402	1.388	1.309	2.308	1.447	176.7	163.2	9.0		
		nitrone B	GS_B	I	1.335	1.453	1.278	1.265	2.256	1.459	176.8	178.1	-1.8
				II	1.362	1.427	1.324	1.269	2.303	1.477	177.8	177.1	-2.5
III	1.334			1.457	1.304	1.265	2.276	1.460	176.8	177.9	-2.0		
IV	1.335			1.456	1.303	1.265	2.276	1.460	176.9	178.0	-2.0		
ES_B	III		1.453	1.332	1.406	1.393	2.295	1.458	175.6	129.1	10.3		
IV	1.452	1.332	1.405	1.393	2.295	1.457	175.6	129.1	10.2				

Where, **I**= RHF/ 6-311G*, **II**= B3LYP/ 6-311G*, **III**= CASSCF (4,4)/ 6-31G*, **IV**= CASSCF(6,6)/ 6-31G* and **V**= CASSCF(12,12)/ 6-31G*

The excited states of these nitrones were optimized at the CASSCF level of calculation with (4,4), (6,6) and (12,12) active spaces. The first excited singlet state (**ES_B**) of **nitrone B** was found to have an interesting feature; an increase in N–O bond distance and decrease in C1–C2 bond distance were noticed by almost similar margin (0.12 Å) with respect to its optimized ground state (**GS_B**) geometry. Unlike the excited state of **nitrone A** (discussed later on) and all other previously studied nitrones [1-2], the excited state of **nitrone B** (**ES_B**) was remarkably different due to the alternation of the single and double bonds in the C–C–C–N region and the stretching of the N–O bond length. Energetically (Table 5-2), this excited state (**ES_B**) geometry was found approximately 60 kcal/mol above the optimized ground state geometry (**GS_B**) and 25 kcal/mol below the vertically excited state point (**FC_B**) at the CASSCF level. On the other hand, the optimized excited singlet state of **nitrone A** (**ES_A**), was found to be situated around 80 kcal/mol above the ground state optimized geometry (**GS_A**) and 8 kcal/mol below the vertical excitation

point (\mathbf{FC}_A). The corresponding CASMP2 (in Gaussian 09) and CASPT2 (in MOLPRO) energy values of ground and excited state geometries are shown in Table 5-2.

Table 5-2: Absolute (E ; in Hartree) and relative (ΔE ; in kcal/mol) energy values at CASSCF level and with dynamic correlation corrections on the optimized structures of ground and excited states.

System	Mol. States	CASSCF/6-31G*				With dynamic correlation correction (CASMP2 ^a and CASPT2 ^b)			
		(4,4)		(6,6)		(4,4)		(6,6)	
		E	ΔE	E	ΔE	E	ΔE	E	ΔE
nitrone A	\mathbf{GS}_A	-514.3267	0	-514.3449	0	-515.9523 ^a	0 ^a	-515.9297	0 ^a
	\mathbf{FC}_A	-514.1893	88.03	-514.1875	98.77	-515.8886 ^b	0 ^b	-515.7412 ^a	118.28 ^a
	\mathbf{ES}_A	-514.2004	79.25	-514.2283	73.17	-515.7396 ^b	93.49 ^b	-515.7731 ^a	98.27 ^a
nitrone B	\mathbf{GS}_B	-743.8729	0	-743.8904	0	-746.2934 ^a	0 ^a	-746.2588 ^a	0 ^a
	\mathbf{FC}_B	-743.7360	85.90	-743.7296	100.90	-746.1911 ^b	0 ^b	-746.0755 ^a	115.02 ^a
	\mathbf{ES}_B	-743.7764	60.55	-743.7909	62.43	-746.1316 ^a	101.53 ^a	-746.0406 ^b	94.41 ^b
						-746.1781 ^a	72.35 ^a	-746.1724 ^a	54.21 ^a
						-746.0642 ^b	79.60 ^b		

Some interesting facts were revealed on analyzing the radiative transition properties of these two nitrone systems at their optimized ground state geometries. It was found that the transition properties of **nitrone A** are similar to our previously reported nitrone systems [1-2]. The S_0-S_1 transition in **nitrone A** is significantly stronger (with TM value 6.92 Debye) than the S_0-S_2 transition (TM value 0.68 Debye) at the ground state geometry. On the other hand, both S_0-S_1 and S_0-S_2 transitions in **nitrone B** are almost equally strong (~5 Debye) with high oscillator strength values (Table 5-3). A leading contribution of HOMO→LUMO, HOMO²→LUMO² and HOMO-4→LUMO configurations (with dominance of the first one) were found in both the vertically excited S_1 and S_2 states of **nitrone B**, though in the S_2 state, the dominance of the HOMO→LUMO excitation was comparatively lower. In the \mathbf{ES}_B geometry of **nitrone B**, the S_1 state is still found to be dominated by these three above-mentioned configurations in almost similar manner. On the other hand, the dominance of HOMO²→LUMO² increases significantly from the vertically excited geometry of

nitrone A (FC_A) to its optimized S_1 geometry (ES_A) and becomes almost equally contributing as the HOMO \rightarrow LUMO configuration.

Table 5-3: Radiative transition properties of **nitrone A** and **nitrone B** at their optimized ground state geometries. The values in parentheses are the power to base 10.

System	Transitions	Transition moment (Debye)	Oscillator Strength	Einstein coefficient A (1/sec)
nitrone A	S_0 - S_1	6.92	1.9320	9.47 (+09)
	S_0 - S_2	0.68	0.0202	1.10(+05)
	S_1 - S_2	0.20	0.0001	1.64 (+03)
nitrone B	S_0 - S_1	5.22	0.7980	2.05(+09)
	S_0 - S_2	4.47	0.6207	1.80(+09)
	S_1 - S_2	1.77	0.0055	5.14(+04)

To investigate further differences in the characteristics of these two nitrones, we have performed the Merz-Kollman (MK) charge analysis at their ground and excited state geometries (Table 5-4). In **nitrone A**, our earlier proposed electron transfer theory [1], i.e. the transfer of an electron from oxygen to nitrogen in the beginning of the photo-excitation process was found to hold good. In contrast, in the biphenyl system (**nitrone B**), a huge shift of oxygen lone pair cloud was observed, which consequently creates a lone pair cloud or negative charge on the nitrogen in its relaxed excited state geometry (ES_B). This feature supports the structural differences observed in the ES_B geometry (i.e. stretching of N–O bond). In our previously studied nitrone systems [1-2], a smaller amount of electron cloud transfer from oxygen orbital to an antibonding π^* orbital decreases the N–O bond order marginally, which results in the slight increase of this bond length in the excited state geometry, whereas in **nitrone B** we found a huge transfer of electron cloud from oxygen which results in a substantial increase of N–O bond length. The planarity of the C–C–N–O part of the ES_B geometry is lost due to the presence of lone pair cloud on nitrogen which converts it into a pyramidal or sp^3 hybridized centre. The huge deviation of the C–C–N–C dihedral angle from 180° also supports the formation of the pyramidal nitrogen. This lack of planarity of this part may well be the reason for the shorter central C1–C2 bond; as soon as the C–N π bond breaks, the adjacent C–C bond becomes a double bond. However, as the nitrogen with the negative charge now favors the tetrahedral structure (sp^3 hybridized nitrogen) it twists instantly and any further delocalization in the C–C–C–N moiety gets disrupted.

Table 5-4: ESP-based atomic charges determined using Merz-Kollmen scheme of various important geometries on potential energy surface

System	Point on PES	C1	N	O	C(of methyl)
nitrone A	GS_A	-0.1609	0.4675	-0.5961	-0.3958
	ES_A	-0.0997	0.1634	-0.3064	-0.3070
	TS_A	-0.2470	0.3155	-0.3577	-0.2549
	CI_A	0.0555	-0.0741	-0.1578	-0.3195
	OX_A	0.4106	-0.3094	-0.2995	-0.0295
nitrone B	GS_B	-0.1349	0.4705	-0.5978	-0.4193
	ES_B	-0.1355	-0.2229	-0.0899	-0.1835
	SP	-0.3013	0.3552	-0.3624	-0.2736
	TS_{B1}	0.1258	-0.2710	-0.1297	-0.1510
	TS_{B2}	-0.2496	0.3234	-0.3569	-0.2520
	CI_{B1}	0.2160	-0.2712	-0.1416	-0.2191
	CI_{B2}	0.0381	-0.1823	-0.0748	-0.3693
	OX_B	0.4329	-0.2829	-0.3127	-0.1623

B) Saddle points and transition states

At CASSCF level of calculations, few important saddle point and transition state geometries were identified on the first excited state surfaces (S_1) of both the nitrones (Figure 5-3). In **nitrone A**, a transition state (**TS_A**) with an imaginary frequency of $156i$ cm^{-1} was found to be situated at only 1 kcal/mol above the **ES_A** geometry and its gap with the vertically excited geometry (**FC_A**) was found to be 7 kcal/mol. On the other hand, in **nitrone B**, a second order saddle point (**SP_B**) with two imaginary frequencies was identified on its S_1 surface which lies around 6-7 kcal/mol (at CASSCF level) above the vertically excited geometry (**FC_B**) of this state (Table 5-5). However, at the CASPT2 level this geometry was found to be situated slightly below the **FC_B** geometry. Interestingly, this important saddle point **SP_B** had been detected only at the CASSCF (4, 4) level of calculations. Using the **SP_B** structure as an initial geometry, a transition state (**TS_{B1}**) with an imaginary frequency of $51i$ cm^{-1} was optimized. This transition state (**TS_{B1}**) was found to have a twist in the CNO region (quite similar to the twist shown by the transition vectors of $31i$ cm^{-1} frequency of **SP_B**). From our extensive studies (discussed in the latter sections), we have found that these geometries play a central role in the oxaziridine formation from **nitrone B**. Another transition state (**TS_{B2}**) was detected on the S_1 surface of **nitrone B** which was found to be situated approx 25 kcal/mol above the vertically excited point (**FC_B**) at the CASSCF level.

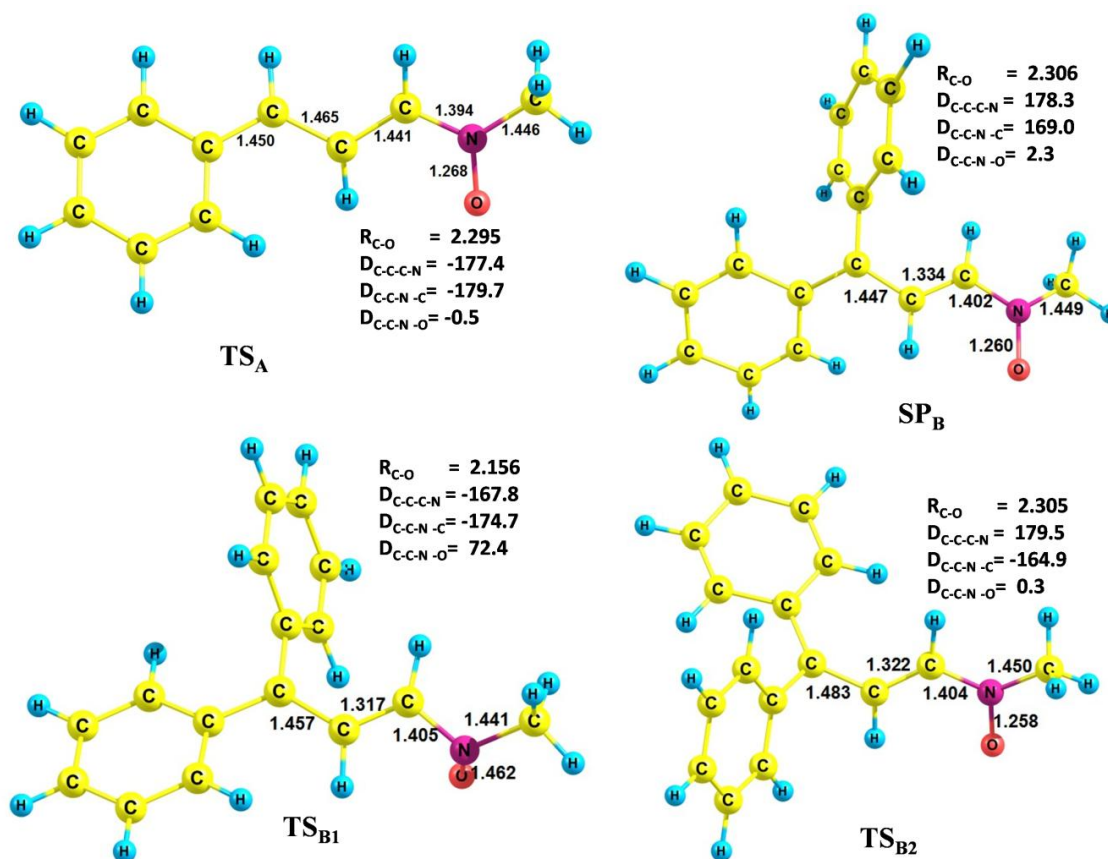


Figure 5-3: Optimized saddle point (SP_B) and transition states (TS_A, TS_{B1} and TS_{B2}) with structural parameters.

C) Optimized conical intersections and oxaziridines

Similar to our previously studied nitron systems [1-2], the lowest energy conical intersection (S_0/S_1) geometries (Figure 5-4a and 5-4b) of both the nitrones were found to have a terminally twisted CNO moiety. At CASSCF (4,4) level, the conical intersection point of **nitron A** (CI_A) was found to be situated approx 23-29 kcal/mol below the ES_A geometry. The gradient difference (GD) vectors of this intersection point (Figure 5-4a) had clearly indicated the possibility of oxaziridine formation with an out of plane C–N–O triangle. On following the GD vector directions, we have obtained the oxaziridine geometry **OX_A** (Figure 5-5a) below (38 kcal/mol at CASSCF and 45-69 kcal/mol on including dynamic correlations) the intersection geometry (Table 5-5). On the other hand, for **nitron B**, the lowest-energy conical intersection point with the terminal twist (CI_{B1}) was detected around 5 kcal/mol below the optimized excited state (ES_B) geometry. Following its GD vectors (Figure 5-4b), optimized oxaziridine **OX_B** (Figure 5-5b) geometry with 3-membered heterocyclic ring was obtained below (47 kcal/mol at CASSCF and 52-58 kcal/mol using dynamic correlation correction) the conical intersection point. The oxaziridine geometries obtained from both the nitrones (Figure 5-

5a and 5-5b) were found to be structurally similar (with a slight difference of 10° in their C–C–C–N dihedral angle) and resembled the geometrical parameters of the experimentally known [33] oxaziridine structures ($R_{C-O} = 1.40\text{\AA}$, $R_{N-O} = 1.50\text{\AA}$, $\angle OCN = 63.7^\circ$, $\angle ONC = 56.8^\circ$). We have also attempted conical intersection optimizations with higher active spaces. At CAS (6,6) level of calculation, terminally twisted conical intersection geometries (Figure 5-6) were found for both the nitrones, but neither the GD nor the DC vectors of these conical intersections gave any indications of oxaziridine formation. Therefore, these higher active spaces were not used further for studying the nitron-oxaziridine photo-conversion path.

Table 5-5: Absolute and relative energy values at CASSCF (4,4) level and with dynamic correlation corrections on the optimized transition states, conical intersection points and oxaziridine structures.

System	Molecular States	CASSCF(4,4)		With dynamic correlation correction (CASMP2 ^a and CASPT2 ^b)	
		E (Hartree)	ΔE (Kcal/mol)	E (Hartree)	ΔE (Kcal/mol)
nitrone A	TS _A	-514.1991	80.15	-515.7792 ^a	108.62 ^a
				-515.7455 ^b	89.79 ^b
	CI _A	-514.2431	52.45	-515.8257 ^a	79.44 ^a
				-515.7974 ^b	57.22 ^b
	OX _A	-514.3030	14.87	-515.9367 ^a	9.78 ^a
			-515.8673 ^b	13.36 ^b	
nitrone B	SP	-743.7241	93.37	-746.1111 ^a	114.39 ^a
				-746.0467 ^b	90.61 ^b
	TS _{B1}	-743.7702	64.44	-746.1487 ^a	90.80 ^a
				-746.0579 ^b	83.58 ^b
	TS _{B2}	-743.7121	100.90	-746.0932 ^a	125.62 ^a
				-746.0205 ^b	107.05 ^b
	CI _{B1}	-743.7865	54.21	-746.1707 ^a	76.99 ^a
				-746.0724 ^b	74.46 ^b
	CI _{B2}	-743.7402	83.27	-746.1375 ^a	97.78 ^a
			-746.0508 ^b	88.04 ^b	
OX _B	-743.8586	8.97	-746.2665 ^a	16.88 ^a	
			-746.1656 ^b	16.01 ^b	

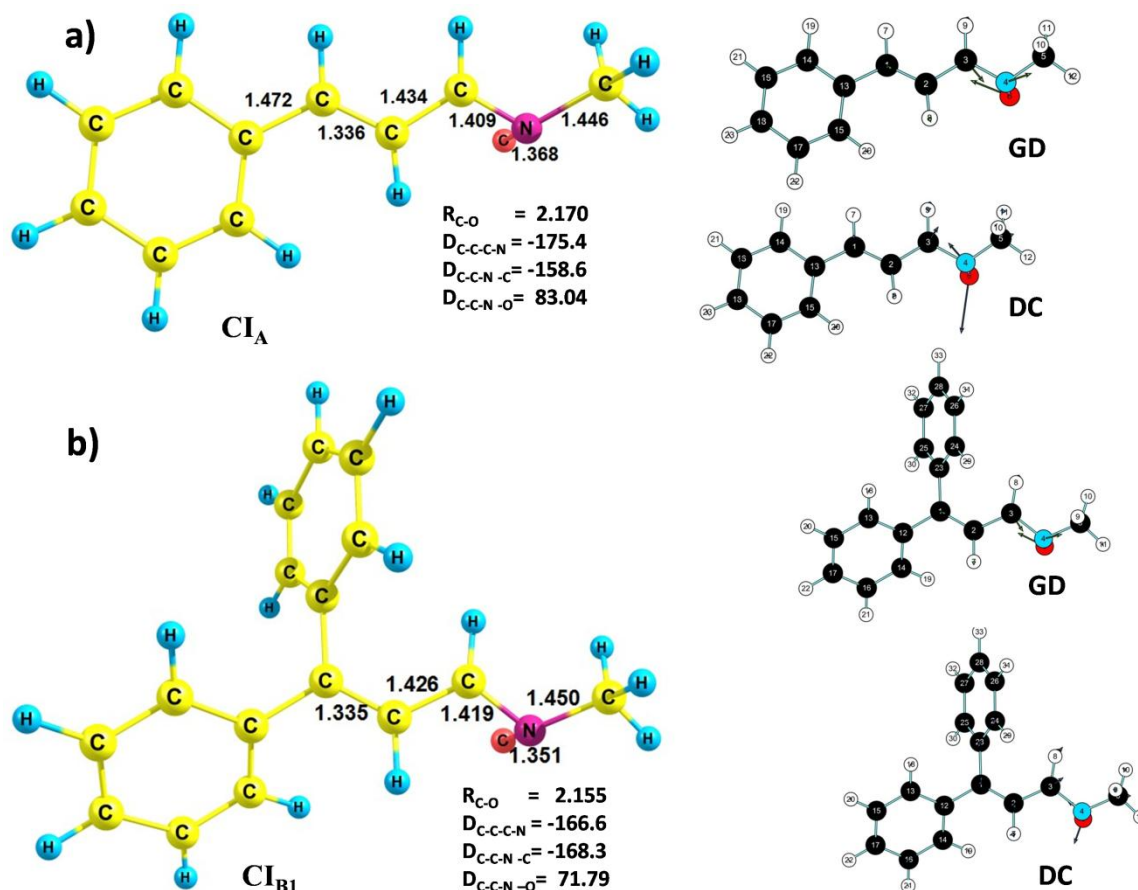


Figure 5-4: Optimized lowest-energy conical intersection geometries of **a) nitrone A** and **b) nitrone B** with their gradient difference (GD) and derivative coupling (DC) vectors at CASSCF (4,4) level of calculation.

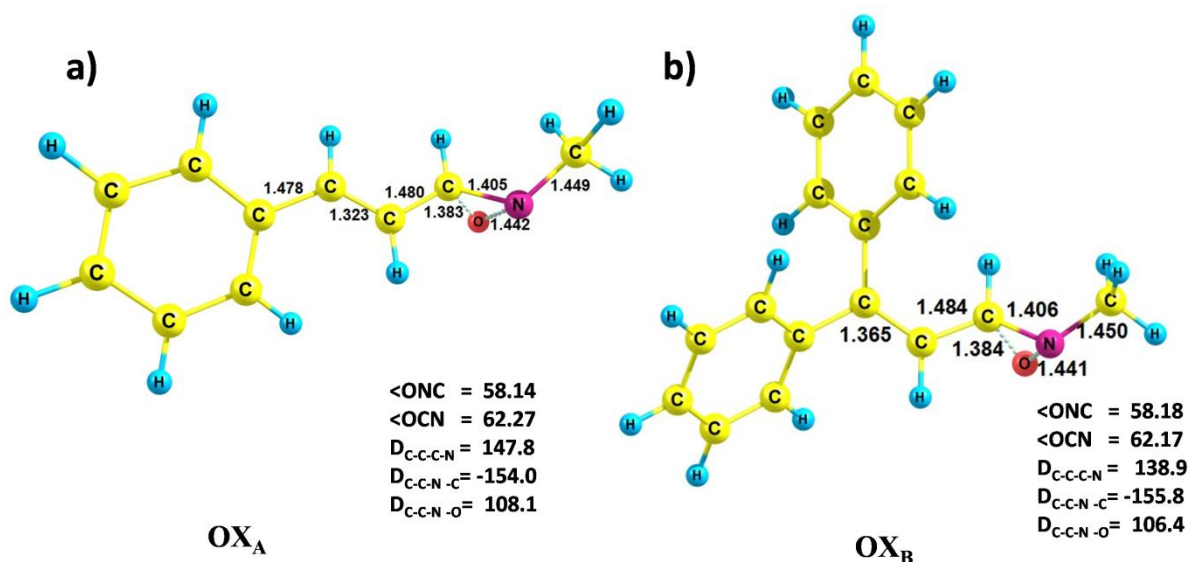


Figure 5-5: Optimized oxaziridine geometries of **a) nitrone A** and **b) nitrone B** with structural parameters at CASSCF (4,4) level of calculation.

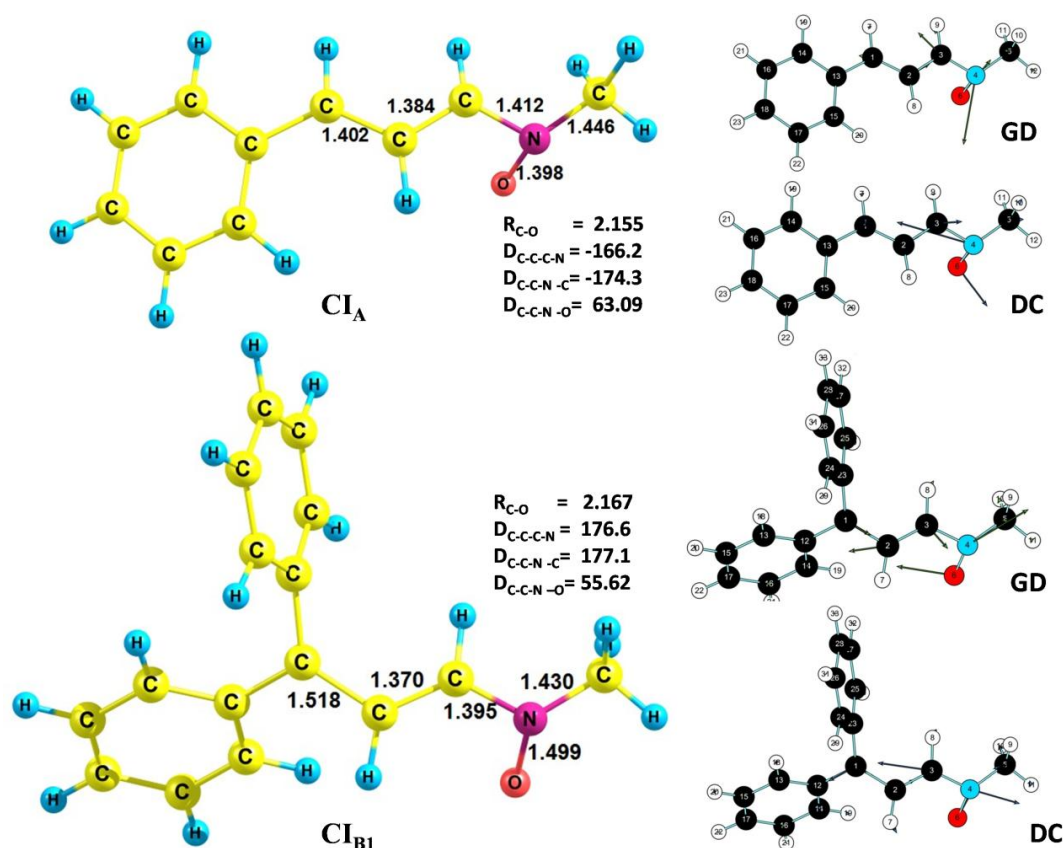


Figure 5-6: Conical intersection geometries of **nitrone A** and **nitrone B** at CASSCF (6,6) level of calculations with their gradient difference (GD) and derivative coupling (DC) vectors.

For **nitrone A**, the photo-chemical reaction path leading towards the oxaziridine (**OX_A**) was found to be quite analogous to the reaction path of our previously studied nitrone systems (discussed in chapters 2 and 4). The excitation of single electron from oxygen to nitrogen of **nitrone A** kick starts the photo-excitation process leading to the **ES_A** geometry (and thereafter possibly to the transition state, **TS_A**) which passes through the lowest energy conical intersection point (**CI_A**) with a CNO-kink and this eventually forms the photoproduct (**OX_A**). However, the photochemical path followed by **nitrone B** was not as simple as that of **nitrone A**. For this nitrone, a saddle point (**SP_B**) on its S_1 surface was detected; the S_1 - S_2 energy gap at this geometry was found to be considerably lower (~11 kcal/mol) in comparison to this gap at the vertically excited geometry (~31 kcal/mol). This observation indicated that this saddle point might be a result of an avoided crossing between the second and third singlet roots. The vertically excited S_2 state probably brings **SP_B** point into the photo-chemical reaction path. This geometry was found to have a good contribution from the $HOMO^2 \rightarrow LUMO^2$ excitation. The ESP based atomic charge analysis (Table 5-4) of this point shows that it follows the single electron transfer property, as seen in our earlier discussed nitrone systems. The

charges on the carbon, nitrogen and oxygen atoms suggest a continuity of the **SP-TS_{B1}-CI_{B1}** route during the passage towards **OX_B**, where the negative charge on nitrogen increases along this path. These observations gave enough evidence to confirm the existence of this saddle point on the reaction path of the nitron-oxaziridine conversion route.

One more conical intersection point (**CI_{B2}**) between the S_0 and S_1 states was detected (Figure 5-7) above the **ES_B** geometry of **nitron B**. This geometry (**CI_{B2}**) was found approximately at 22 kcal/mol above the **ES_B** at the CASSCF level of calculation. Unlike the peaked topography of the **CI_{B1}**, the sloped nature of this intersection indicates that the decay through **CI_{B2}** to the ground state will be very slow. In fact, the substantial value of ΔE (**CI_{B2}-ES_B**) may well indicate that the molecule along this path will equilibrate in the excited state. Our experimental results [3] showed that the 330 nm absorption peak (corresponding to the nitron moiety) of **nitron A** decays much faster than the similar peak for **nitron B**. The comparatively slower degradation of the latter nitron may have a direct correlation with the sloped topography of **CI_{B2}** which was reached after relaxation to **ES_B** following the initial photo-excitation to **FC_B**. Overall, it can be concluded that the oxaziridine formation in **nitron B** is occurring through the peaked **CI_{B1}**, which takes place through the slightly less populated S_2 state and requires an initial relaxation to S_1 surface.

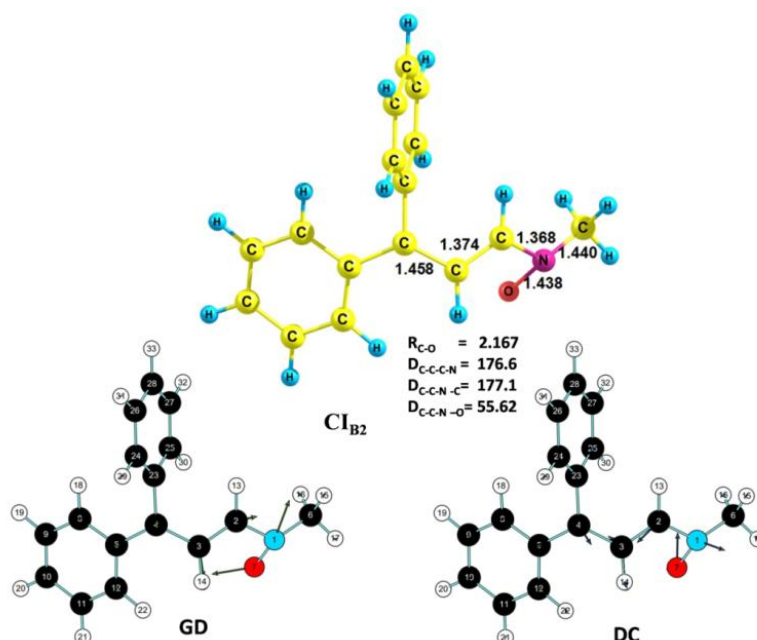


Figure 5-7: Conical intersection geometry (**CI_{B2}**) with its gradient difference (GD) and derivative coupling (DC) vectors.

5.3.3. Oxaziridine absorption peaks

The TDDFT/B3LYP level with 6-311G** basis sets was used to analyze the absorption peak positions (Figure 5-8a and 5-8b) of the oxaziridines formed during the photo-irradiation of both the nitrones. For **nitrone A**, the major experimentally observed peak (which rises along with the decay of the 330 nm peak) was observed near 263 nm, while the peak position from the theoretical calculations of oxaziridine (**OX_A**) was found at 252 nm. In the biphenyl system the predicted position of **OX_B** peak was 263 nm which was in good agreement with the experimentally observed 261 nm peak, developed during the course of photo-irradiation of **nitrone B** and decay of nitrone peak. These TDDFT calculations had shown that for both the systems strong S_0 - S_2 transitions with high oscillator strength (~ 0.20) values are responsible for these oxaziridine peaks (**OX_A** and **OX_B**). Primarily, the HOMO \rightarrow LUMO excitations play central role in these strong UV transitions. Our TDDFT level of calculations had also predicted the experimentally observed second peak (near 220 nm) with slight deviation in its position. This close matching of the theoretically derived peak positions of oxaziridines with the experimentally observed ones helped us to confirm that the photoproduct formed on photo-irradiation of both the nitrones are oxaziridines.

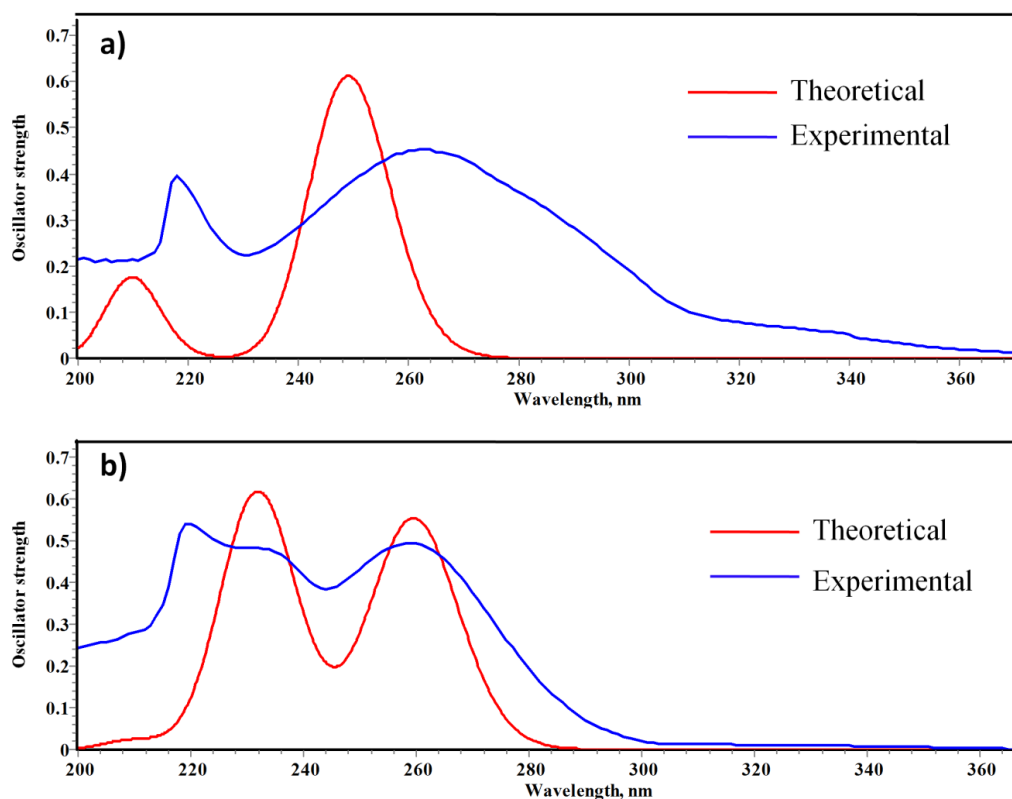


Figure 5-8: Comparison of theoretically obtained UV-Visible spectrum with the experimental peaks of a) **OX_A** and b) **OX_B**.

5.3.4. Summary of the overall photochemical path

Figures 5-9a and 5-9b summarize the whole photochemical conversion process operating in the two systems. The photochemistry of **nitrone A** (Figure 5-9a) is similar to our previously reported alkyl substituted conjugated nitrone systems. On photo-excitation, the initial transfer of single electron from oxygen to nitrogen takes place which takes the system to a relaxed excited state geometry. The transition property calculation results revealed that here only the vertical excitation to the S_1 state is allowed and the transition to the S_2 state is completely forbidden. The relaxed excited state then goes towards the lowest-energy CNO-kinked CI (CI_A) after crossing a small barrier of 1 kcal/mol which finally leads towards the oxaziridine geometry.

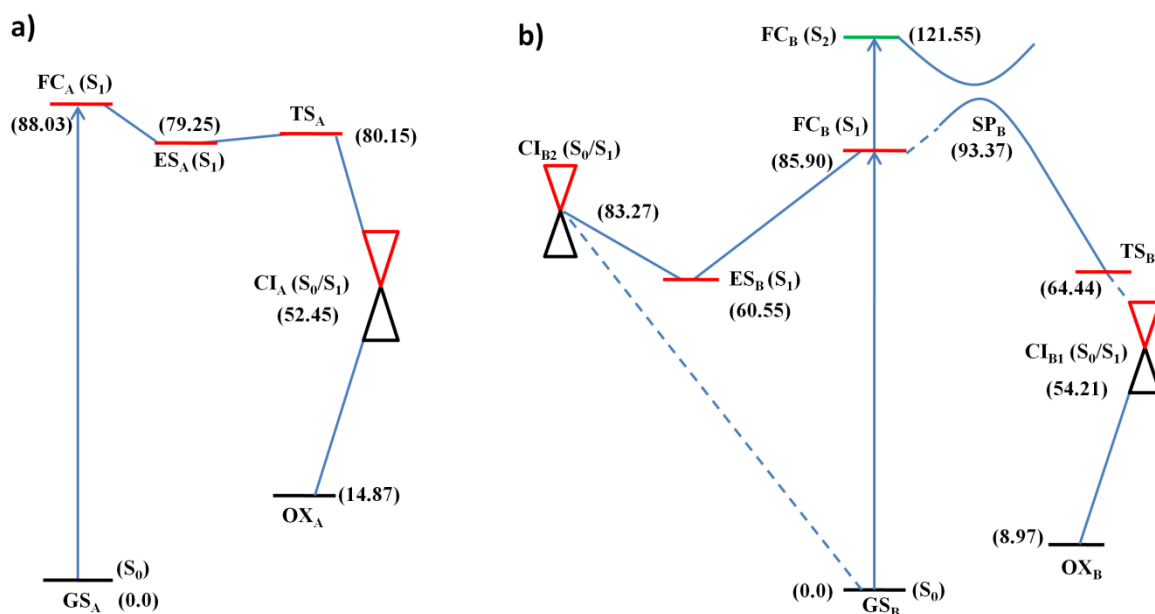


Figure 5-9: Schematic representation of the entire photo-conversion process of **a) nitrone A** and **b) nitrone B**. Energy values are shown in parentheses (in kcal/mol) with respect to the optimized ground state geometries of the respective nitrones.

On the other hand, in **nitrone B** (Figure 5-9 a), transition from non-planar ground state to both S_1 and S_2 states are allowed with high transition moment and oscillator strength values. On photo-excitation, the S_1 state relaxes to a stable excited state geometry which involves a considerable amount of charge transfer from the oxygen to the nitrogen (or conjugated part) with an elongation of the N–O bond. A sloped S_0/S_1 conical intersection (CI_{B2}) was identified above the stable excited state geometry (ES_B), which can be related to the slow decay of the nitrone (330 nm) peak. However, the oxaziridine formation route in this nitrone does not lie along this path. It was found to arise through a different

trajectory; the well-populated S_2 state decays to the S_1 state and proceed towards the S_0/S_1 lowest-energy conical intersection (CI_{B1}) point which eventually forms oxaziridine. This path seems to involve SP_B geometry (probably due to an avoided crossing with S_2) on the S_1 surface. Analysis of atomic charges revealed that this path is quite consistent with the single electron transfer mechanism which triggers the oxaziridine formation process, as described earlier.

5.4. Conclusions

Experimentally observed photochemical features of both the studied nitrones were justified and properly explained by the high-level quantum mechanical computational studies. Their contrasting behavior on photo-excitation was revealed computationally by exploring their reaction mechanisms. In both the cases, a comparison of the theoretically predicted TDDFT peak positions with the gradually developed UV peaks near 260 nm led to the conclusion that the final photoproduct was a terminal 3-membered heterocyclic species, oxaziridine. The photo-irradiation of the styryl nitron (**nitron A**) was found quite similar to our previously investigated open-chain conjugated nitrones. Here a single non-radiative decay route was followed by the first excited singlet state which passes through a low-barrier transition state followed by the lowest-energy conical intersection with a CNO-kink and goes toward the photoproduct oxaziridine. On the other hand, the nitron-oxaziridine formation route of **nitron B** has been predicted to involve two well-populated S_1 and S_2 states which leads to two different reaction paths. The reaction path from the S_1 state goes towards a stable optimized excited state with a sloped conical intersection at substantial height from its minimum energy geometry; this has indicated the possibility that the molecule might equilibrate at this excited state and consequently may not decay very quickly from here. This observation can be correlated with the slower decay of the absorption band of this nitron. The other route involves a relaxation of the S_2 state to the S_1 state which eventually forms the photoproduct oxaziridine through the lowest-energy conical intersection geometry (S_0/S_1). For both the nitrones, following the GD vectors of their lowest energy conical intersections, oxaziridine was obtained as the photoproduct. Finally, it can be concluded that the two-way decay channel of the **nitron B** with two different conical intersection topographies has made the photochemical behavior of this system significantly different from that of the planar conjugated phenyl system (**nitron A**).

5.5. References

1. P. Saini and A. Chattopadhyay, *RSC. Adv.*, 2014, **4**, 20466.
2. P. Saini and A. Chattopadhyay, *RSC. Adv.*, 2015, **5**, 22148.
3. P. Saini, M. Banerjee and A. Chattopadhyay, *J. Phys. Chem. A*, 2016, **120**, 396.
4. M. J. Frisch et al., *Gaussian 09*, revision B.01, Gaussian, Inc., Wallingford, CT, 2010.
5. D. Hegarty and M. A. Robb, *Mol. Phys.*, 1979, **38**, 1795.
6. R. H. A. Eade and M. A. Robb, *Chem. Phys. Lett.*, 1981, **83**, 362.
7. H. B. Schlegel and M. A. Robb, *Chem. Phys. Lett.*, 1982, **93**, 43.
8. F. Bernardi, A. Bottini, J. J. W. McDougall, M. A. Robb and H. B. Schlegel, *Far. Symp. Chem. Soc.*, 1984, **19**, 137.
9. M. J. Frisch, I. N. Ragazos, M. A. Robb and H. B. Schlegel, *Chem. Phys. Lett.*, 1992, **189**, 524.
10. N. Yamamoto, T. Vreven, M. A. Robb, M. J. Frisch and H. B. Schlegel, *Chem. Phys. Lett.*, 1996, **250**, 373.
11. X. Li and M. J. Frisch, *J. Chem. Theory Comput.*, 2006, **2**, 835.
12. I. Palmer, M. Olivucci, F. Bernardi and M. A. Robb, *J. Org. Chem.*, 1992, **57**, 5081.
13. J. J. W. McDougall, K. Peasley and M. A. Robb, *Chem. Phys. Lett.*, 1988, **148**, 183.
14. J. F. Arenas, J. I. Marcos, J. C. Otero, A. Sanchez-Galvezand and J. Soto, *J. Chem. Phys.*, 1999, **111**, 551.
15. C. R. Kemnitz, G. B. Ellison, W. L. Karney and W. T. Borden, *J. Am. Chem. Soc.*, 2000, **122**, 1098.
16. M.-X. Song, Z.-X. Zhao, F.-Q. Bai, Y.-J. Liu, H.-X. Zhang and C.-c. Sun, *J. Phys. Chem. A*, 2010, **114**, 7173.
17. T. Shiozaki, C. Woywod and H.-J. Werner, *Phys. Chem. Chem. Phys.*, 2013, **15**, 262.
18. H.-J. Werner et al., MOLPRO, version 2012.1, A package of *ab initio* programs, Cardiff, U.K., 2012.
19. F. Weinhold, *J. Chem. Phys.*, 1970, **54**, 1874.
20. C. W. Bauschlicher and S. R. Langhoff, *Theo. Chim. Act.*, 1991, **79**, 93.
21. B. Brooks and H. F. J. Schaefer, *Chem. Phys.*, 1979, **70**, 5092.
22. B. Brooks, W. Laidig, P. Saxe, N. Handy and H. F. Schaefer, *Phys. Scr.*, 1980, **21**, 312.
23. A. Chattopadhyay, *J. Phys. B: At. Mol. Opt. Phys.*, 2012, **45**, 035101.

24. A. Chattopadhyay, *J. Chem. Sci.*, 2012, **124**, 985.
25. M. W. Schmidt et al., *J. Comput. Chem.*, 1993, **14**, 1347.
26. U. C. Singh and P. A. Kollman, *J. Comput. Chem.*, 1984, **5**, 129.
27. B. H. Besler, K. M. Merz Jr. and P. A. Kollman, *J. Comput. Chem.*, 1990, **11**, 431.
28. E. Runge and E. K. U. Gross, *Phys. Rev. Lett.*, 1984, **52**, 997.
29. C. Ullrich, *Time-Dependent Density-Functional Theory: Concepts and Applications*, Oxford University Press, Oxford, U. K., 2012.
30. Website of Chemcraft software: <http://www.chemcraftprog.com>.
31. K. Shinzawa and I. Tanaka, *J. Phys. Chem.*, 1964, **68**, 1205.
32. K. Koyano, and I. Tanaka, *J. Phys. Chem.*, 1965, **69**, 2545.
33. S. S. Murphree, *Modern Heterocyclic Chemistry*, Eds., J. Alvarez-Builla, J. J. Vaquero and J. Barluenga, Wiley-VCH Verlag & Co. KGaA, Weinheim, Germany, 2011.

CHAPTER 6

Conclusions and Future Scope

This thesis has focused on the theoretical investigations of the unexplored low-lying electronic states of various nitrone systems with different substitutions on the alpha carbon and nitrogen atoms, to reveal their light induced properties. We have carried out rigorous quantum mechanical calculations using *ab initio*, semi-empirical and hybrid methods to explore the photo-chemical and thermal isomerization processes of these nitrone systems. These studies have successfully established the nitrone-oxaziridine photo-conversion mechanism. Starting from the photochemical features of the chemopreventive retinyl nitrones, we have explored our investigations to nitrones of other categories, as well.

Several similarities were observed in their overall photochemical behavior. The initial electronic transfer from oxygen to nitrogen triggers the subsequent nitrone-oxaziridine conversion process. The transition properties and the nature of the low-lying singlet excited states of nitrones are found to be somewhat in between the non-polar polyenes and polar protonated Schiff base (PSB) systems. Their first excited singlet states are found to have mixed ionic-biradical nature while for non-polar polyenes it is biradicaloid in nature and in PSB systems it is ionic. The non-radiative decay path leading to the oxaziridine geometry passes through the lowest-energy S_0/S_1 conical intersection point. This latter geometry is characterized by a terminal CNO-kink or oxygen-bridge structure and it is biradicaloid in nature in several nitrone systems, such as in long-chain conjugated ones. This photo-chemical path has some kind of similarity with the well-known channel-3 decay of benzene which passes through a biradicaloid prefulvenic conical intersection.

In contrast to many other structurally similar systems, the *cis-trans* isomerization of nitrone was suspected to follow a thermal route which is confirmed by our present studies. The 13-*trans* isomer of *N*-methyl retinyl nitrone was found to follow a ground state *E-Z* isomerization path (Chapter 2). Quite similar to this long-chain nitrone system, a transition state on the ground potential energy surface with single imaginary frequency was found responsible for the *E-Z* isomerization of the α -naphthyl *N*-methyl nitrone (Chapter 4).

Some contrasting behavior in their photochemical properties were observed, depending on the nature of substitutions on either sides of the C=N bond. The formation and stability of oxaziridines formed by photo-irradiation of nitrones vary significantly with the type of these substituents. Nitrones substituted with *N*-electron donating groups were found to give oxaziridines as the major photoproduct, while in case of electron withdrawing group on nitrogen, a weaker N–O bond indicated an unstable oxaziridine-type species which probably leads towards amide (Chapter 3). Both these observations justified their experimental findings, reported previously by other groups.

Radiative transition properties of some nitrones are found to be closer to the neutral polyenes while some of them are more towards the iminium ions. These properties of α -naphthyl *N*-methyl nitrones are comparable to that of non-polar conjugated polyenes where the vertical transition to the first excited singlet state is weakly allowed, and this state gets populated by downward transition from the second excited singlet state; this state is subsequently involved in S_0/S_1 conical intersections to produce photoproduct, oxaziridine (Chapter 4). On the other hand, conjugated long-chain systems, like *N*-alkyl retinyl nitrones have a strongly allowed transition to the first excited singlet state which resembles the characteristic of the conjugated protonated Schiff base systems (Chapter 2).

An interesting observation was the remarkable difference in the photo-excitation and subsequent photochemical paths of *N*-methyl nitrones with one (α -styryl) and two phenyl (1,1-diphenylethylene) groups at the *C*-terminal positions. Completely different photo-excitation pathways were identified for these two nitrones. The nitrone–oxaziridine route of the styryl nitrone is found to be quite similar to the conjugated long chain nitrones, where a single non radiative decay path is followed from the first excited singlet state which produces oxaziridine as the photoproduct. In contrast, the photo-irradiation of biphenyl substituted nitrone involves two well-populated (first and second) singlet excited states, which leads to different reaction pathways (Chapter 5). In this latter nitrone, the first excited singlet state goes towards a sloped S_0/S_1 conical intersection, which indicate the possibility that the system might equilibrate at this excited state and this observation was supported by the slower decay of the UV peak of this nitrone (observed by experimental results). On the other hand, relaxation of the second excited state to the first one led to the photoproduct oxaziridine through the lowest-energy S_0/S_1 conical intersection geometry (Chapter 5).

Finally, we can conclude that this thesis work has revealed several unexplored portions of the nitrene photochemistry. It is quite interesting that in spite of numerous experimental studies on nitrenes over the last five decades, the exact mechanism of their photochemistry was not known. To the best of our knowledge, this was the first attempt to reveal the nitrene-oxaziridine photoconversion mechanism which includes the involvement of non-radiative decay channels through low-lying terminally twisted conical intersections. Our high-level computational studies have successfully cleared most of the doubts related to the isomerization processes of acyclic nitrene systems and the previous experimental findings have been justified. Obviously, there remains huge scope in future to explore the photochemical features of several other categories of nitrenes and to investigate whether they follow similar trend or not. The results of this work can help experimentalists to tune the formation of the photoproducts of nitrenes by proper choice of substituents on *C*-terminal and *N*-terminal ends of the C=N bond. In addition to the results which predicted the formation of stable oxaziridines from *N*-alkyl nitrenes, the possibility of an oxaziridine-type species leading to amides from electron-withdrawing group substituted systems is an equally important observation. The latter may open up a facile route of amide formation from a properly substituted nitrene system. The two-way decay mechanism of the biphenyl nitrene system with two different types of topographies of conical intersection is an important observation, as well. Overall, we feel that this present study can have far reaching consequences and may immensely help the organic chemists to understand the nitrene photochemistry in a better way in future.

APPENDIX-I**List of Publications****List of Publications (Part of this thesis)**

1. P. Saini, M. Banerjee and A. Chattopadhyay, A Computational Investigation of the Photochemical Reaction Path of some Synthesized and Experimentally Analyzed Small-Chain Conjugated Nitrones, *The Journal of Physical Chemistry: A*, 2016, **120**, 396.
2. P. Saini and A. Chattopadhyay, Revealing the Active Role of the Terminal CNO Moiety in the Photochemical Oxaziridine Conversion Process of Some Chemopreventive Retinylnitrones through Hybrid QM: QM and QM: MM ONIOM Calculations, *Chemical Physics Letters*, 2015, **633**, 6.
3. P. Saini and A. Chattopadhyay, A Comprehensive Spectroscopic Investigation of α -(2-naphthyl)-*N*-methylnitron: A Computational Study on Photochemical Nitron–Oxaziridine Conversion and Thermal *E–Z* Isomerization Processes, *RSC Advances*, 2015, **5**, 22148.
4. P. Saini and A. Chattopadhyay, A Computational Investigation of the Photochemical Oxaziridine and Amide Conversion Process of Open-chain Conjugated Nitron with Electron-withdrawing Trifluoromethyl Group on Nitrogen, *Journal of Chemical Sciences*, 2015, **127**, 1757.
5. P. Saini and A. Chattopadhyay, Spectroscopic Features of the Low-lying Singlet States of Some *N*-alkyl Retinylnitron Model Systems and Their Involvement in Oxaziridine Formation, *RSC Advances*, 2014, **4**, 20466.

Other Publications (not part of this thesis)

6. S. Banerjee, A. Chattopadhyay, A. Banerjee, M. Haridas, P. Saini, M. Das, M. S. Majik and Y. K. Maurya, Synthesis and Photophysical Characterization of Quasi push–pull Dicyano-dibenzodioxins and their Anti-tumor Activity against Glioma Cell line C6, *Bioorganic & Medicinal Chemistry Letters*, 2015, **25**, 753.
 7. A. Chatterjee, D. G. Khandare, P. Saini, A. Chattopadhyay, M. S. Majik and M. Banerjee, Amine Functionalized Tetraphenylethylene: A Novel Aggregation-Induced
-

Emission based Fluorescent Chemodosimeter for Nitrite and Nitrate ions, *RSC Advances*, 2015, **5**, 31479.

8. S. Banerjee, A. Chattopadhyay, P. Saini and K. S. Singh. Synthesis and Optical Properties of 1,4- and 1,2-Dicyanodibenzodioxins Possessing Donor- π -Acceptor Architecture, *Synthetic letters*, 2015, **27**, A-F.
9. H. Kumar, A. Chattopadhyay, P. Rangaraj, V. Devaraji, R. Joshi, P. Bhavana, P. Saini and S. K. Ghosh, Design, Synthesis, Physicochemical Studies, Solvation, and DNA Damage of Quinoline-Appended Chalcone Derivative: Comprehensive Spectroscopic Approach toward Drug Discovery, *The Journal of Physical Chemistry: B*, 2014, **118**, 7257.

Conferences and workshop attended

1. Presented poster in Advanced Materials and Their Applications In Nanotechnology (*AMAN 2016*) at BITS Pilani, KK Birla Goa Campus, **2016**. Title: "Photochemical oxaziridine conversion and thermal *E-Z* isomerization processes of fluorescent α -(2-naphthyl)-*N*-methylnitron: A Computational Study"
 2. Presented poster in New Frontiers in Chemistry- from Fundamentals to Applications (*NFCFA 2015*) at BITS Pilani, KK Birla Goa Campus, **2015**. Title: "Computational investigations on the photochemical oxaziridine conversion and thermal *E-Z* isomerization processes of *N*-methyl retinyl nitron"
 3. Presented poster in 17th *CRSI* National Symposium in Chemistry (*NSC-17*) at NCL Pune, **2015**. Title: "Effects of electron-donating and electron-withdrawing groups on the photochemistry of conjugated *N*-substituted open-chain nitrones"
 4. Presented poster in 16th *CRSI* National Symposium in Chemistry (*NSC-16*) at IIT Mumbai **2014**. Title: "A comparative study of the non-radiative decay channels in conjugated long-chain iminium ions and nitrones"
 5. Attended workshop on "*Introduction to Gaussian: Theory and Practice*", at New Delhi, Organized by Gaussian and Scube Scientific Software Solutions (P) Ltd, **2014**.
-

APPENDIX-II

Brief Biography of the Candidate

Personal Details

Name: Praveen Saini
Date of birth: 17 June 1987
Education: M. S. (Pharm.), NIPER, Kolkata, 2011
B. Pharmacy, Kurukshetra University, 2009
E mail ID praveensaini17@gmail.com

Academic Achievements:

- i) Qualified **GATE- 2011** (Life sciences).
- ii) Qualified **GATE–2009** (Pharmaceutical sciences).
- iii) Qualified **NIPER JEE – 2009**.

Professional Experience:

1. **Senior Research Fellow** in a CSIR funded project at Department of Chemistry, BITS PILANI- K. K. Birla Goa Campus; from Jan 2013 to Nov 2015.
2. **Assistant Professor (Pharmaceutical Chemistry)** in Shri Ram College of Pharmacy, Karnal; from Nov 2011 to June 2012.

Research Publications

09 publications in peer reviewed international journals (Listed in Appendix-I)

Conferences/workshop attended during PhD

04 conferences and 01 workshop (Listed in Appendix-I)

APPENDIX-III

Brief Biography of the Supervisor

- Name:** Dr. Anjan Chattopadhyay
- Date of birth:** 02 Oct 1975
- Current Designation:** Associate Professor & Head, Department of Chemistry
BITS, Pilani-K. K. Birla Goa Campus
- Education:** Ph.D (Science), Jadavpur University, 2004
M.Sc (Physical Chemistry), Calcutta University, 1998
B.Sc. (Chemistry), Calcutta University, 1996
- E mail ID:** anjan_chattopadhyay@yahoo.com,
anjan@goa.bits-pilani.ac.in
- Web Page:** <http://universe.bits-pilani.ac.in/goa/anjan/Profile>
- Areas of Research:** Theoretical & Computational Chemistry
- Photochemistry of organic and bio-inorganic systems
 - Exciplex Laser systems
 - Excited state analysis of molecular rotor systems

No. of Sponsored Research Projects:

As PI: 02, completed (CSIR, DST); As Co-PI: 01 completed (CSIR)

Research Publications:

25 publications in peer reviewed international journals

Conferences attended in recent years: 10

Awards and Achievements:

- Prof. Sadhan Basu Memorial Award (Calcutta University, Kolkata)
 - Cunningham Memorial Award (Presidency College, Kolkata)
 - Sir Upendranath Bramachary Memorial Award (Presidency College, Kolkata)
 - Sandip Shome Memorial Award (Presidency college, Kolkata)
 - NET (2000), GATE (2001)
 - University Immersion, BITS-Pilani: Visited Institute of Physical Chemistry, Theoretical Chemistry group, University of Heidelberg, Germany, as a visiting researcher for some collaborative research work with Prof. Dr. Horst Köppel
-